

CONTENTS

CONTENTS	i
EDITORIAL BOARD	iii
PREFACE	iv
Inorganic Geochemistry of Coal from Patappa Village, Bone District, and Masenrengpulu Village, Barru District, South Sulawesi Province Using XRF Method	211–228
<i>Anshariah, Alam Budiman Thamsi, Mohammad Tholib</i>	
Characterization The Flavonoids Extract of <i>Tridax Procumbens</i> l. Leaves and Betel Lime as Materials for Open Wound Analgesic Ointment	229–240
<i>Muhammad Zainullah, Mina Devika Setiana, Vera Nur Fatimah, Ilma Fitriana, Robi Kurniawan</i>	
Density Functional Theory Investigation on The Electronic Structure, Properties and IR Spectra of 9,10-Iphenylanthracene	241–266
<i>Owolabi J. Adeyemi, Hassan Gambo, Onimisi M. Yusuf, Gidado S. Abdulkadir, Ali Haruna, Bankole J. Akinade, Akusu C. Onma, Muhammed L. Madugu, Sakinat L. Usman</i>	
An Analysis of Principals' Digital Literacy Capabilities as Instructional Leaders in Indonesia	267–276
<i>Jaja, Dwiniasih, Jajo Firman Raharjo</i>	
Laws of Gravitation and Motion in the Ancient Indian Texts	277–290
<i>Jumisree Sarmah Pathak</i>	
Red Wine Classification Using SVM and RBF Kernel	291–300
<i>Kevin Silvanus Hutabarat, Rosalia Arum Kumalasanti</i>	
Recent Developments in The Influencing Variables of Hydrodistillation for Enhancing Essential Oil Yields in Indonesia: A Brief Review	301–320
<i>Awaly Ilham Dewantoro, Alvita Rahma Alifia, Tanti Handini, Latifah Zainul Qolbi, Dita Amelia Ihsani, Desy Nurliasari</i>	
Automated Detection of Spine Deformities: Advancing Orthopedic Care with Convolutional Neural Networks	321–336
<i>Deepesh Pratap, Saran Sinha, A. Charan Kumari, K. Srinivas</i>	

Essay Answer Detection System Uses Cosine Similarity and Similarity Scoring in Sentences	337–348
<i>Diah Hidayatul Ula, Siti Yuliyanti</i>	
Comparative Analysis of Three Solid Waste Management Systems Towards Full Automation	349-366
<i>A.D. Omiyale, L.F. Ogunwolu, O.O. Ajibola</i>	
The Effect of Gamma Irradiation as A Food Preservation Technology on The Shelf Life and Quality of Fresh-cut Watermelon	367-378
<i>Rieka Arkaninto Adeska, Nur Octaviany, Renaldy Bernardo Saragih, Retno Andrianti, Ridho, Harum Azizah Darojati, Dhita Ariyanti</i>	
Evaluation of Tartrazine Solution as a Potential Gamma Dosimeter Material	379-392
<i>Farhansyah Yunandani Arumbifa, Deni Kurniawan, Desalsa Anggoro Diani, Dika Bhakti Praja, Fauziah Ulfah Ajri, Ariyani Kusuma Dewi, Dhita Ariyanti</i>	
Prediction of Life Expectancy in Indonesia by Implementing Website-Based Lagrange Polynomial Interpolation	393-406
<i>Syamsul Maarip, Aam Hermansyah, Sopi Nuryani Hadraeni, Salman Miqdad, Ardhan Dimas Nuryadin, Siti Yuliyanti</i>	
Quantitative Analysis of Magnetohydrodynamic Sustained Convective Flow via Vertical Plate	407-416
<i>D. R. Kirubaharan, A. D Subhashini, NVN. Babu, G. Murali</i>	
Evaluating the Performance of DWT-DCT Feature Extraction in Guitar Chord Recognition	417-428
<i>Linggo Sumarno</i>	
The Study of 3D Simulation on Heat Transfer Enhancement on Fin Tube Heat Exchanger Using Delta Wing and Winglet Vortex Generators	429-442
<i>Stefan mardikus, Claudia Agata Putri, Michael Seen, Rines, Y.B. Lukiyanto, Doddy Purwadianto, Heryoga Winarbawa, Gilang Argya Dyaksa, Wibowo Kusbandono</i>	
AUTHOR GUIDELINES	443-444

EDITORIAL BOARD

Editor in Chief

Dr. I Made Wicaksana Ekaputra (*Sanata Dharma University, Yogyakarta, Indonesia*)
Email: made@usd.ac.id

Associate Editor

Dr. Pham Nhu Viet Ha (*Vietnam Atomic Energy Institute, Hanoi, Vietnam*)
Dr. Hendra Gunawan Harno (*Gyeongsang National University, Jinju, The Republic of Korea*)
Dr. Mukesh Jewariya (*National Physical Laboratory, New Delhi, India*)
Dr. Mongkolserj Lin (*Institute of Technology of Cambodia, Phnom Penh, Cambodia*)
Dr. Yohanes Baptista Lukiyanto (*Sanata Dharma University, Yogyakarta, Indonesia*)
Dr. Apichate Maneewong (*Thailand Institute of Nuclear Technology, Bangkok, Thailand*)
Prof. Dr. Sudi Mungkasi (*Sanata Dharma University, Yogyakarta, Indonesia*)
Dr. Pranowo (*Universitas Atma Jaya Yogyakarta, Yogyakarta, Indonesia*)
Dr. Monica Cahyaning Ratri (*Sanata Dharma University, Yogyakarta, Indonesia*)
Dr. Mahardhika Pratama (*Nanyang Technological University, Singapore*)
Prof. Dr. Leo Hari Wiryanto (*Bandung Institute of Technology, Bandung, Indonesia*)
Dr. Ranggo Tungga Dewa (*Universitas Pertahanan, Bogor, Indonesia*)

Editorial Assistant

Rosalia Arum Kumalasanti, M.T. (*Sanata Dharma University, Yogyakarta, Indonesia*)
Vittalis Ayu, M.Cs. (*Sanata Dharma University, Yogyakarta, Indonesia*)

Contact us

International Journal of Applied Sciences and Smart Technologies
Faculty of Science and Technology
Universitas Sanata Dharma
Kampus III Paingan, Maguwoharjo, Depok, Sleman
Yogyakarta, 55282
Phone : +62 274883037 ext. 523110, 52320
Fax : +62 272886529
Email : editorial.ijasst@usd.ac.id
Website : <http://e-journal.usd.ac.id/index.php/IJASST>

IJASST is an open-access peer-reviewed journal that mediates the dissemination of research and studies conducted by academicians, researchers, and practitioners in science, engineering, and technology.

PREFACE

Dear readers, we are delighted to serve you Volume 6, Issue 1 of *International Journal of Applied Sciences and Smart Technologies* (IJASST), which is managed and published by the Faculty of Science and Technology, Universitas Sanata Dharma. IJASST is an open-access peer-reviewed journal that mediates the dissemination of research and studies conducted by academicians, researchers, and practitioners in science, engineering, and technology. Its scope also includes basic sciences which relate to technology, such as applied mathematics, physics, and chemistry.

In this edition, we have fourteen papers authored by researchers from Indonesia, Africa, and India. Submitted papers are reviewed fairly using the open journal system (OJS) of IJASST. After the review process, accepted papers of the journal are publicly available for free at the website of IJASST. For future issues, we are looking forward to your contributions to IJASST.

Dr. I Made Wicaksana Ekaputra
Editor in Chief
IJASST

Inorganic Geochemistry of Coal from Patappa Village, Bone District, and Masenrengpulu Village, Barru District, South Sulawesi Province Using XRF Method

Anshariah¹, Alam Budiman Thamsi^{1*}, Moh. Talib¹,

¹Faculty of Industrial Technology,
Universitas Muslim Indonesia, 455696, Indonesia
*Author Correspondence: alambudiman.thamsi@umi.ac.id

(Received 07-09-2023; Revised 19-01-2024; Accepted 29-02-2024)

Abstract

The chemical composition of coal is almost the same as that of plant tissue, containing the main elements of elements C, H, O, N, S, and P. An in-depth study of coal inorganic compounds is needed because coal inorganic compounds are the primary variable in ash formation during coal combustion. This study uses the X-ray fluorescence method to reveal the differences and similarities in inorganic chemical composition contained in coal in Bone Regency and Barru Regency. Coal in Masenrengpulu Village has the Al_2O_3 compound as the most dominant compound, while coal in Patappa Village has the SiO_2 compound as the most prevalent compound. The concentration of inorganic sulfide minerals in the village of Masenrengpulu was influenced by igneous rock intrusion and deposition processes. In contrast, the deposition process only affected the inorganic sulfide minerals of coal in Patappa village. The significant elements found in coal in the Masenrengpulu and Patappa Villages are Si, Al, Fe, S, Ca, K, and Ti. Coal inorganic sulfide minerals in Masenrengpulu Village with Patappa Village have high concentrations in the bottom channel of the coal seam and a low concentration in the middle channel and top of the seam. Coal inorganic sulfide minerals in Masenrengpulu Village and Patappa Village have high concentrations in the coal seam's lower channel and low concentrations in the middle and upper channels.

Keywords: Coal Comparison, Mallawa Formation, XRF, Inorganic Geochemistry.

1 Introduction

Coal has been one of the most important fossil fuels for centuries [1,2]. The consumption of coal resources accounts for more than 32% of the total consumption of fossil fuels in 2021, and coal is the most abundant distributed fossil fuel in the world [3,4].



The depositional environment is a characteristic of a geomorphic setting where physical, chemical, and biological processes produce a specific type of sediment [5,6]. The chemical composition of coal is almost the same as the chemical composition of plant tissue; both contain the main elements of C, H, O, N, S, and P [7,8]. An in-depth study of coal inorganic compounds is needed because coal inorganic compounds are the primary variable in ash (dust) formation during coal combustion [9,10].

Research on Mallawa Formation coal has been carried out regarding the study of coal depositional facies based on maceral composition in Barru Regency, South Sulawesi [11,12]. Improving the quality of sub-bituminous coal to bituminous coal by Brotowati and Sofia 2018 [13]. Analysis of the resistivity of Barru coal, Palluda Hamlet, Barru Regency, South Sulawesi Province by Umar, 2017 [14] Coal quality analysis based on proximate and ultimate test result in Masenreng Pulu Village, Lamuru District, Bone Regency by Bakri, 2022 [15].

Coal deposits in the Mallawa Formation are inserts in the middle Eocene age's shale, clay, and sandstone sequences. Mallawa Formation coal is thought to be associated with depositional environments near the coast or lagoons that influence the rise and fall of seawater [16]. The relatively high sulfur content reflects that the Mallawa Formation occurred in brackish water conditions [17]. Widodo *et al.*, 2022 carried out in-depth research on the inorganic geochemistry of Mallawa Formation coal using X-ray diffraction, which revealed the characteristics of the pyrite mineral in coal based on the results of microscope, proximate, all sulfur and X-ray diffraction analysis to determine the potential for air formation mine acid [18].

To find out in-depth about the inorganic geochemistry of Mallawa Formation coal, conducting an in-depth study of the mineral elements contained in Mallawa Formation coal is necessary. X-ray fluorescence analysis of coal inorganic geochemistry can illustrate the comparison and synchronization of mineral elements contained in Mallawa Formation coal in the Bone Regency and Barru Babupaten areas, South Sulawesi Province.

2 Methods

Initial Stages of Research

The research will be conducted in Maenreng Pulu Village, Lamuru District, Bone District, Patappa Village, Pujananting District, and Barru District, South Sulawesi Province.

- a. The administrative stage begins with preparing a research permit to obtain permission from the local area so that data legality and personal safety are better maintained when conducting research sampling. The research application letter issued by the industrial technology faculty is submitted to the investment office, then the investment office gives the research permit.
- b. Literature study as a basic guideline for research activities and determination of steps that are sourced from references and also some information available at the research location that is appropriate to the subject matter.
- c. Field orientation carried out overall observations regarding the location of the research area in Masenrengpulu Village, Lamuru District, Barru Regency, South Sulawesi Province.
- d. Field observations carry out direct observations at activity locations in the research area.

Data Retrieval Stages

The data taken is in the form of primary data or data taken directly at the research location:

- a. Collecting primary data at the research location in the form of coal position data, slope, coal flanking rock data, coordinate points, documentation, and coal samples [19].
- b. Coal samples were taken using the channel sampling method by taking the upper and lower parts of the coal seam. Before taking samples using a sampling channel, the coal seam to be channeled is first cleaned of weathered coal to obtain coal that is still in fresh condition and so that it is protected from contamination of the flanking rocks. The coal taken is approximately 10 cm from the flanking rocks. After the coal seam has been made into a clean channel, the coal collection starts from the bottom channel

to make it easier to collect the coal and avoid contamination of the flanking rocks. Approximately 2 kg of coal is taken in each channel.

Sample Preparation Stages

The following stages of analysis of coal sample preparation are depicted in Fig. 1. The stages are:

- The stage of reducing the size of the coal sample was carried out using a jaw crusher, then continued using a double roll crusher to obtain a maximum size before being put into the grinding tool [20], [21].
- The grinding stage is the stage of reducing the size of the coal sample to obtain a coal sample with a length of -200 mesh. The tool used to grind coal to get a size of -200 mesh is a ball mill, and you can also use other grinding tools.
- Sifting was carried out using a 200 mesh sieve to obtain a homogeneous size.
- The stage for packaging the test sample is by packing it in a sample bag that has been labeled at ± 50 gr, and the backup sample is packed in a sample bag that has been marked at ± 300 gr.

Sample Analysis Stages

The following stages of the XRF analyst are shown in Fig. 2.

- The ignition stage is the stage of converting coal samples measuring -200 mesh into ash samples. This is done because the tool XRF spectrometer cannot detect mineral elements in coal, which, in fact, dominantly has elements derived from organic

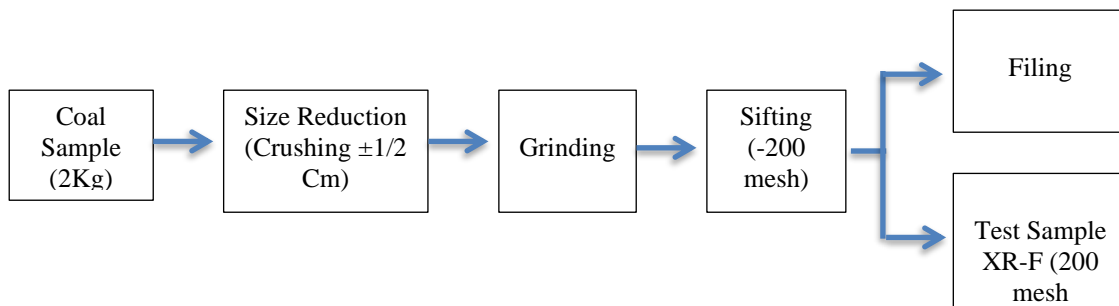


Figure 1. Flow of Sample Preparation Activities.

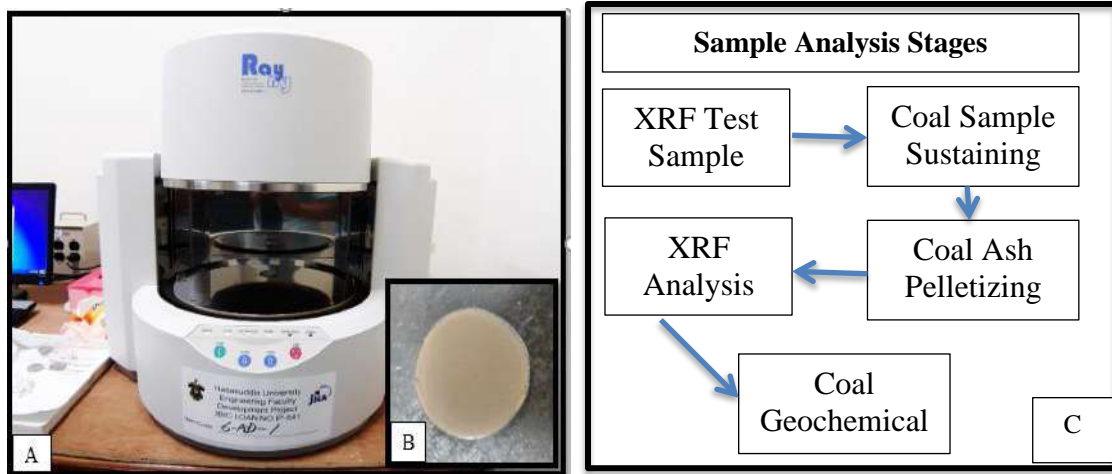


Figure 2. A. XRF spectrometer, B. Petete and C. Stages of Sample Analysis.

matter [10], [18], [22]. XRF analysis was conducted at the Laboratory of Hasanuddin University. The XRF tool brand is Shimadzu, EDX-720/800HS type.

- b. Stages of converting ash samples into pellets. The finished pellet sample is inserted into the XRF Spectrometer tool for approximately 15 minutes.

Data Processing Stages

XRF analysis data processing is processed using Mc Excel to get an overview of the relationship between coal inorganic chemical composition for each coal channel and a comparison of the coal inorganic chemical composition of the Bone Regency area with the Barru Regency area [23-25].

Stages of Report Preparation

The preparation of the report begins with outlining the research, then proceeds with making an introduction including background using seven references, two of which are to describe the study in general as much as one paragraph and five references are used to provide information about previous researchers in the research area as much as two paragraphs as presented in Fig. 3. The background is closed with a novelte or overview of the feasibility of this research.

- a. After the preparation of the Introduction is complete, it is continued with the preparation of research stages and methods to describe the flow of research activities from the beginning to the conclusion.
- b. After the preparation of the stages and methods of research is complete, it is continued by compiling the data processing results into scientific reporting forms equipped with clear and systematic explanations.
- c. After the preparation of the results and discussion is complete, it is continued with a closing that contains conclusions that synchronization of research objectives and suggestions for future researchers.
- d. After the preparation of the cover is complete, continue by making a summary and abstract that explains the essence of the research, followed by the preparation of the authorization letter, preface, table of contents, list of figures, and table list.

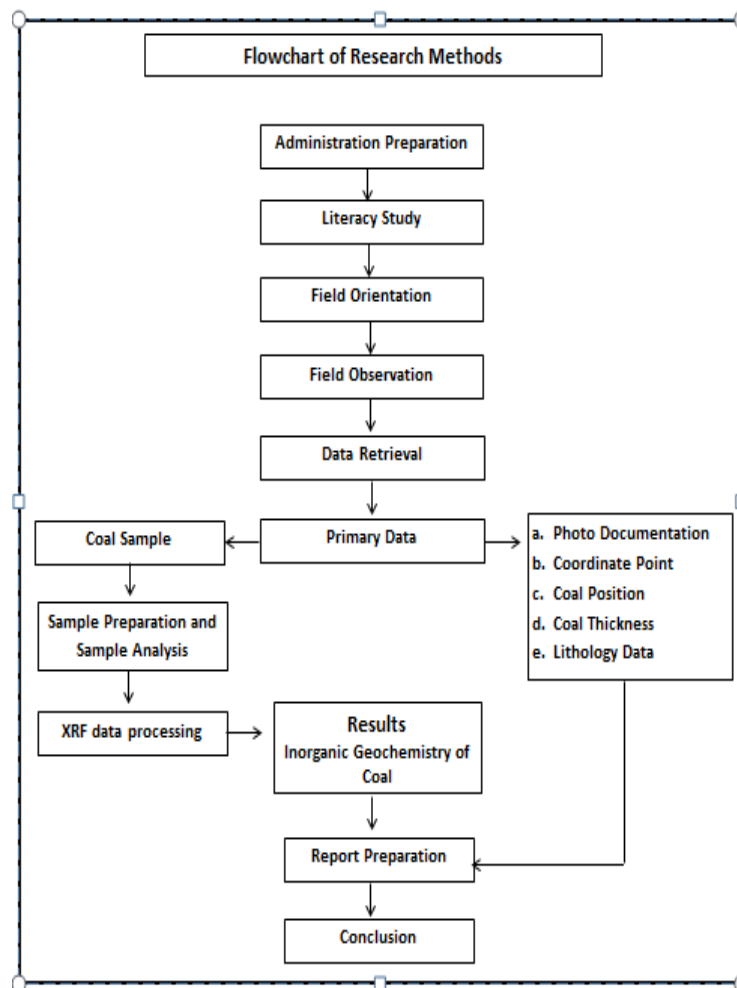


Figure 3. Flowchart of Research Methods.

3 Results and Discussions

Lokasi Penelitian Batubara

a. Bone Regency Coal

The coal at the research location is in Masenrengpulu Village, Lamuru Subdistrict, Bone Regency, South Sulawesi Province, with coordinates $119^{\circ} 56' 26.8''$ N and $4^{\circ} 41' 11.7''$ E (see Fig. 4). The coal at this location has a position of N 265°E/18° with a thickness of 165 cm and a slope of 60°. The coal in this location has a position of N 265°E/18° with a thickness of 165 cm and a slope of 60°. The roof rock in Masenrengpulu Village is silica sandstone, while the floor rock is andesite igneous rock in the form of sills.

b. Barru Regency Coal

Coal in the research location, Patappa Village, Pujananting Subdistrict, Barru Regency, South Sulawesi Province, has a position of N 275°E/12° with a thickness of 110 cm and a slope of 65° (see Fig. 5) The roof rock in Patappa Village is passive mudstone, while the floor is mudstone.

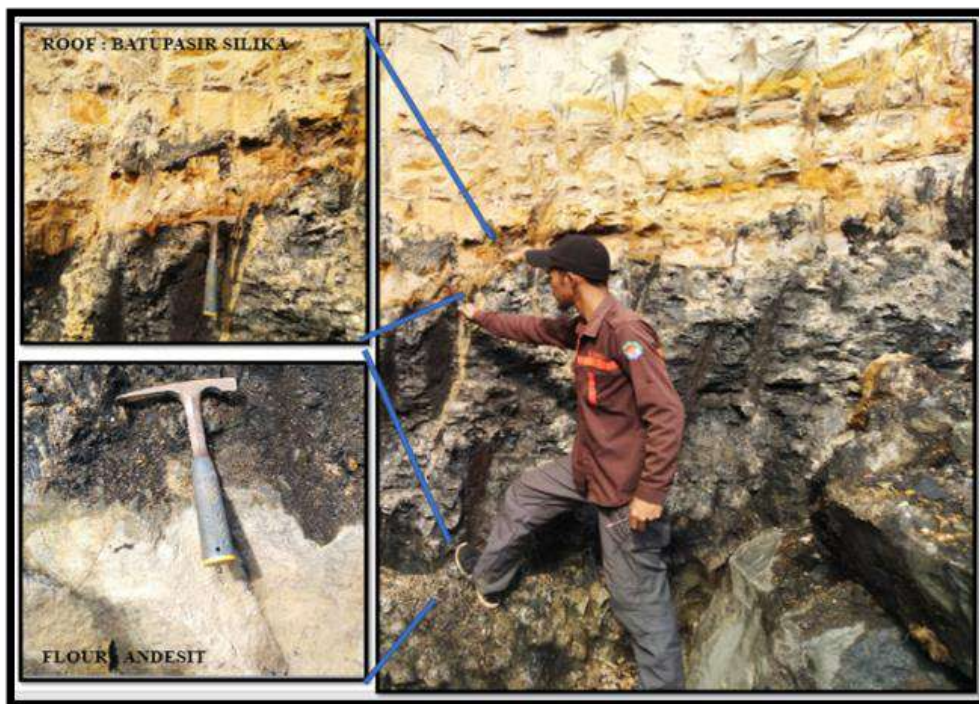


Figure 4. Coal of Masenrengpulu Village, Bone Regency.

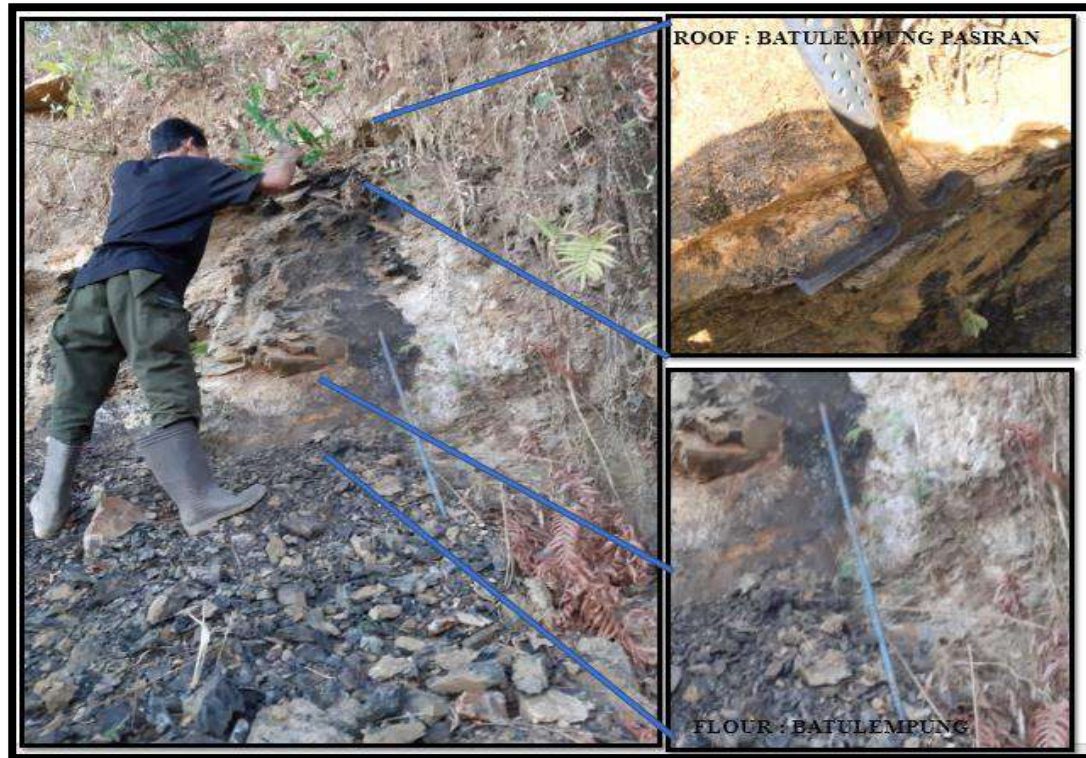


Figure 5. Coal of Patappa Village, Barru Regency.

Coal Inorganic Geochemistry

a. Regional Coal of Bone Regency

The Table 1 illustrates the concentration of the chemical composition of coal minerals in Masenrengpulu Village, Lamuru Sub-district, Bone Regency, South Sulawesi Province. In general, coal at the research location has the most dominant concentration of Al_2O_3 compounds, followed by SiO_2 , Fe_2O_3 , SO_3 , CaO , K_2O , TiO , SrO , MnO , V_2O_5 , Cr_2O_3 , NiO , CuO , ZrO_2 , Y_2O_3 , ZnO , and MoO_3 (see Fig. 6).

Table 1. Comparison of Mineral Compounds in Bone Regency Coal

No	Chemical Composition	Channel 1	Channel 2	Channel 3	Rata-Rata
1	SiO_2 (MM)	28.95%	35.90%	27.60%	30.82%
2	SiO_2 (MS)	33.10%	60.02%	61.50%	51.54%
3	Al_2O_3 (MM)	36.22%	45.82%	37.02%	39.69%
4	Al_2O_3 (MS)	26.05%	30.64%	32.60%	29.76%

5	Fe ₂ O ₃ (MM)	25.47%	12.28%	29.73%	22.49%
6	Fe ₂ O ₃ (MS)	22.70%	5.03%	3.21%	10.31%
7	SO ₃ (MM)	5.84%	2.59%	2.59%	3.67%
8	SO ₃ (MS)	9.78%	1.44%	0.47%	3.90%
9	CaO (MM)	1.88%	1.63%	1.41%	1.64%
10	CaO (MS)	6.78%	0.91%	0.56%	2.75%
11	K ₂ O (MM)	0.78%	0.93%	0.88%	0.86%
12	K ₂ O (MS)	0.63%	1.14%	0.97%	0.92%
13	TiO ₂ (MM)	0.39%	0.62%	0.56%	0.52%
14	TiO ₂ (MS)	0.58%	0.71%	0.63%	0.64%

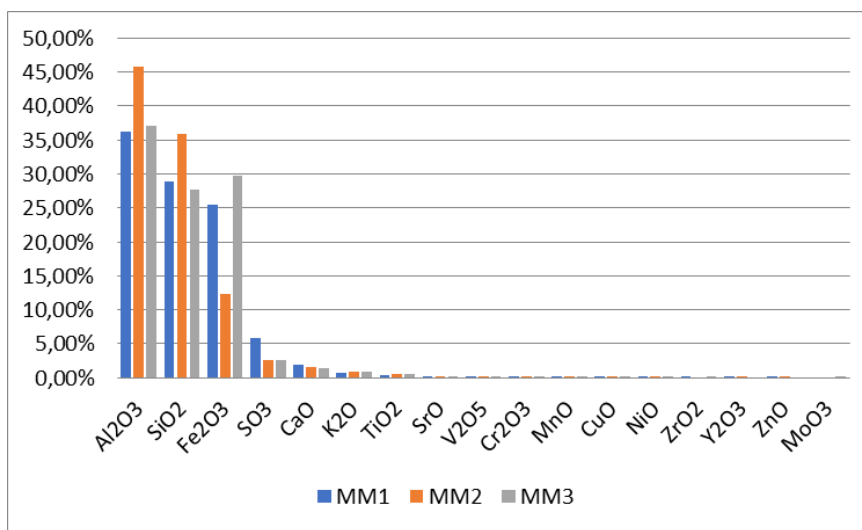


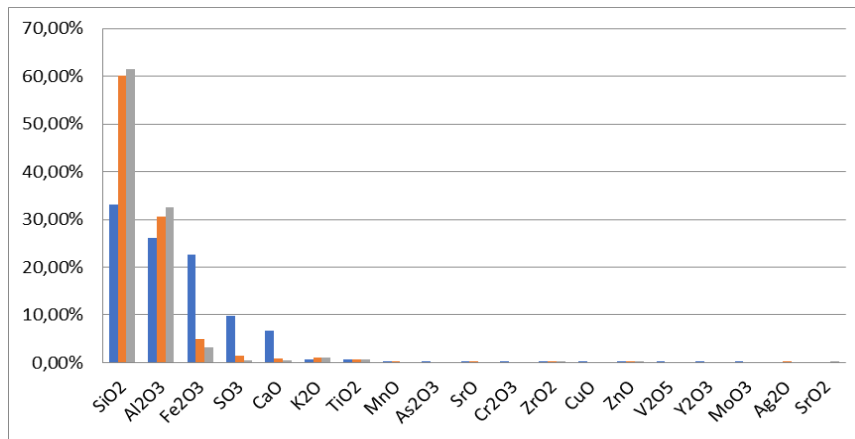
Figure 6. Comparison Chart of Bone Regency Coal Mineral Compounds.

b. Regional Coal of Barru Regency

The Table 2 illustrates the concentration of the chemical composition of coal minerals in Patappa Village, Pujananting Subdistrict, Barru Regency, South Sulawesi Province. In general, coal at the research location has the most dominant concentration of SiO₂ compounds, followed by Al₂O₃, Fe₂O₃, SO₃, CaO, K₂O, TiO, SrO, MnO, V₂O₅, Cr₂O₃, NiO, CuO, ZrO₂, Y₂O₃, ZnO, and MoO₃ (see Fig. 7).

Table 2 Comparison of Coal Mineral Compounds of Barru Regency.

No	Komposisi Kimia	MS1	MS2	MS3	Rata-Rata
1	SiO ₂	33.10%	60.02%	61.50%	51.54%
2	Al ₂ O ₃	26.05%	30.64%	32.60%	29.76%
3	Fe ₂ O ₃	22.70%	5.03%	3.21%	10.31%
4	SO ₃	9.78%	1.44%	0.47%	3.90%
5	CaO	6.78%	0.91%	0.56%	2.75%
6	K ₂ O	0.63%	1.14%	0.97%	0.92%
7	TiO ₂	0.58%	0.71%	0.63%	0.64%
8	MnO	0.12%	0.02%	0.00%	0.04%
9	As ₂ O ₃	0.06%	0.00%	0.00%	0.02%
10	SrO	0.06%	0.02%	0.00%	0.03%
11	Cr ₂ O ₃	0.05%	0.00%	0.00%	0.02%
12	ZrO ₂	0.02%	0.04%	0.04%	0.04%
13	CuO	0.02%	0.00%	0.00%	0.01%
14	ZnO	0.02%	0.01%	0.01%	0.01%
15	V ₂ O ₅	0.02%	0.00%	0.00%	0.00%
16	Y ₂ O ₃	0.01%	0.00%	0.00%	0.00%
17	MoO ₃	0.01%	0.00%	0.00%	0.00%
18	Ag ₂ O	0.00%	0.02%	0.00%	0.01%
19	SrO ₂	0.00%	0.00%	0.01%	0.00%

**Figure 7.** Comparison Chart of Coal Mineral Compounds of Barru Regency.

Coal Inorganic Chemical Composition Comparison

Figs. 8-11 illustrates the comparison of the concentration of the chemical composition of coal minerals in Masenrengpulu Village, Lamuru Subdistrict, Bone Regency, and Patappa Village, Pujananting Subdistrict, Barru Regency, South Sulawesi Province.

Coal in Patappa Village has a higher concentration of SiO_2 compounds, while coal in Masenrengpulu Village has a higher concentration of Al_2O_3 compounds. Coal in Patappa Village has a SiO_2 compound concentration of 51.54%, while coal in Masenrengpulu Village has a SiO_2 concentration of 30,816%. Coal in Patappa Village has a concentration of Al_2O_3 compounds of 29.761%, while coal in Masenrengpulu Village has a SiO_2 concentration of 39.688%.

Coal in Masenrengpulu Village has a higher concentration of Fe_2O_3 compounds than coal in Patappa Village. Coal in Masenrengpulu Village has a Fe_2O_3 compound concentration of 22.491%, while coal in Patappa Village has a Fe_2O_3 concentration of 10.31%. Coal in Masenrengpulu Village has similarities in deposition patterns from the beginning to the middle of the deposition process. The deposition pattern changes from the middle to the end of the deposition. From the beginning of deposition until the middle of the coal deposition process, Fe_2O_3 compounds together decreased. Still, in the middle to the end of the deposition, Fe_2O_3 coal compounds in Masenrengpulu Village increased while Fe_2O_3 coal in Patappa Village was relatively stable.

The pattern of deposition of SO_3 compounds in Masenreng Pula Village and Patappa Village is relatively similar. Where at the beginning to the middle of the SO_3 compound deposition process decreases, then in the middle to the end of the deposition process, the SO_3 compound is relatively stable. The deposition of CaO compounds in coal in Masenrengpulu Village is challenging from the beginning to the end of the deposition process. The deposition of CaO compounds in Patappa Village coal has decreased from the beginning to the middle of the deposition process. In contrast, in the middle to the end of the deposition process the CaO compounds are relatively stable. The deposition of K_2O compounds in Masenrengpulu Village and Patappa Village is relatively stable from the beginning to the end of the deposition process. The deposition of Ti_2O compounds in Masenrengpulu Village and Patappa Village from the beginning to the end of the deposition process is relatively stable.

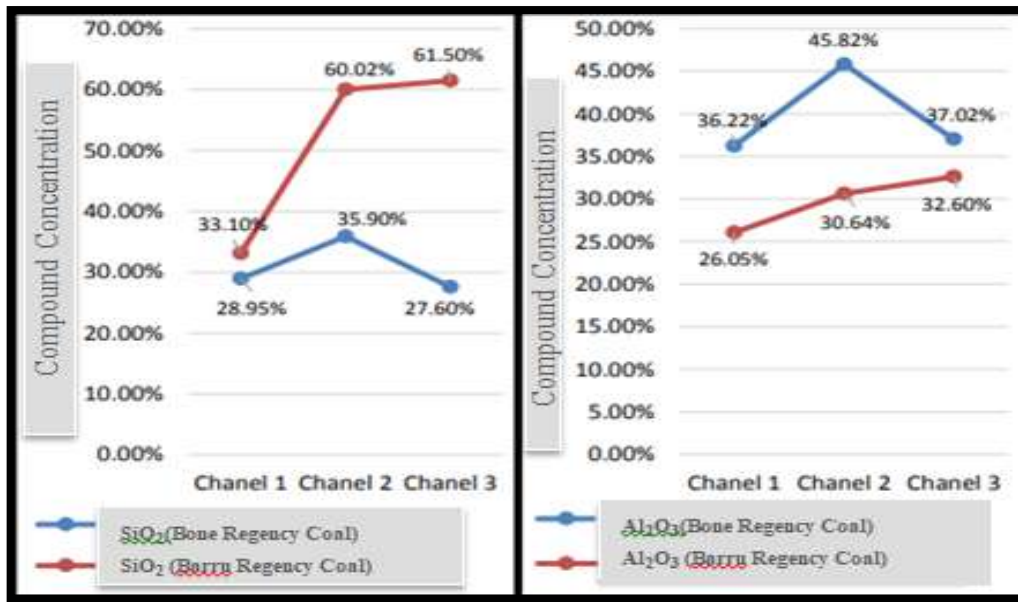


Figure 8. Comparison Chart of SiO₂ Compounds in Bone Regency and Barru Regency on the Left and Al₂O₃ compounds in Patappa Village and Masenrengpulu Village on the Right.

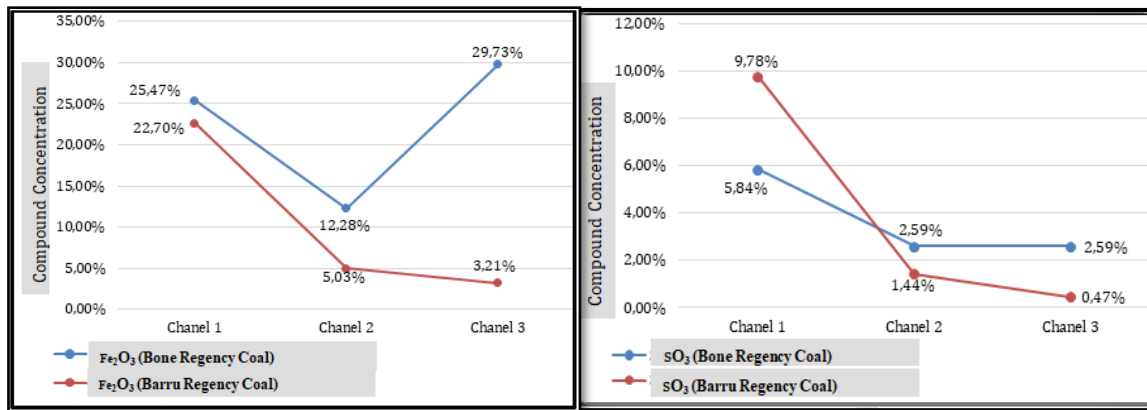


Figure 9. Comparison Chart of Fe₂O₃ and SO₃ Compounds in Coal in Bone Regency and Barru Regency.

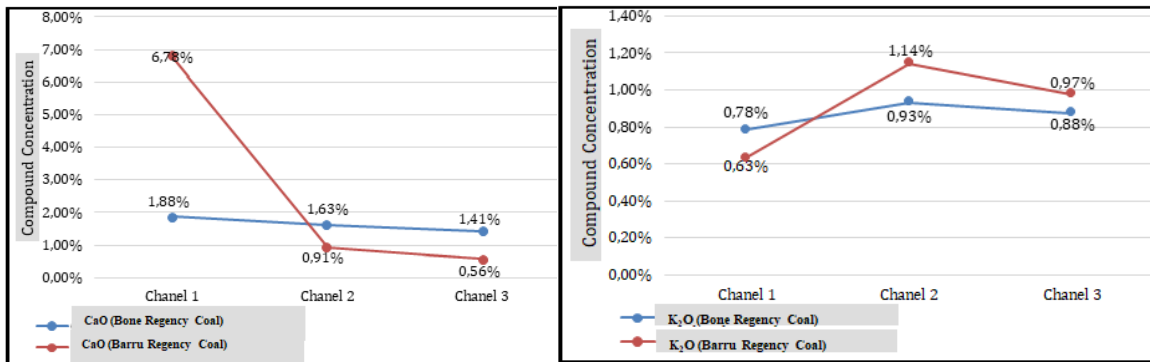


Figure 10. Comparison Chart of CaO and K₂O Compounds in Coal in Bone Regency and Barru Regency.

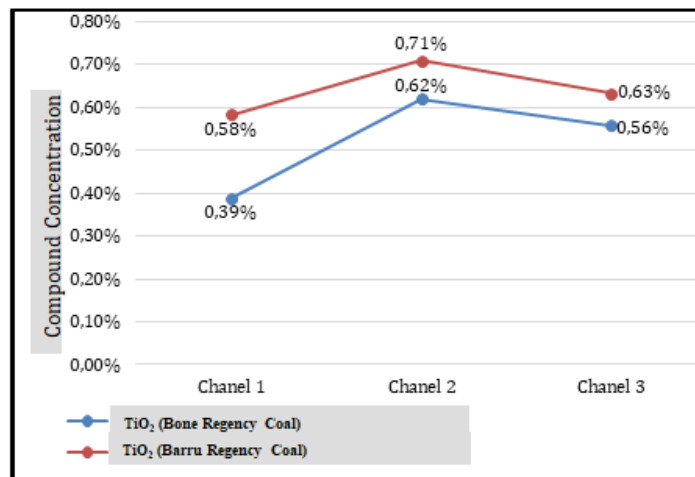


Figure 11. Comparison Chart of TiO₂ Compounds in Coal in Bone Regency and Barru Regency.

4 Conclusions

The difference in the inorganic geochemical composition of coal in Masenrengpulu Village and Patappa Village is in the Al₂O₃ and SiO₂ compounds. Coal in Masenrengpulu Village has Al₂O₃ as the inorganic compound with the highest concentration, while coal in Patappa Village has SiO₂ as the inorganic compound with the highest concentration. The concentration of coal inorganic sulfide minerals in Masenrengpulu Village is influenced by igneous intrusion and precipitation processes. In contrast, the precipitation process only affects coal inorganic sulfide minerals in Patappa Village. The similarity of the inorganic geochemical composition of coal in

Masenrengpulu Village with Patappa Village is that both have significant elements of Si, Al, Fe, S, Ca, K, and Ti. Coal inorganic sulfide minerals in Masenrengpulu Village and Patappa Village have high concentrations in the coal seam's lower channel and low concentrations in the middle and upper channels.

Acknowledgments

The researcher would like to thank the Mining Materials Processing Laboratory, Department of Mining Engineering, Muslim University of Indonesia, and the Geochemistry and Mineral Laboratory, Faculty of Engineering, Hasanuddin University, for providing the opportunity to test the research samples and my beloved parents who always sincerely provide endless prayer support, enthusiasm, and advice.

References

- [1] Z. Zamani, H. Rahimpour-Bonab, and R. Littke, "Coal petrology, sedimentology and depositional environment of the Parvadeh coals in the Upper Triassic, Tabas Block of Central-East Iran," *Int J Coal Sci Technol*, vol. 10, no. 1, pp. 1–20, Dec. 2023, doi: 10.1007/S40789-023-00600-W/FIGURES/9.
- [2] S. I. Arbuzov, "Geochemistry, mineralogy and genesis of rare metal (Nb-Ta-Zr-Hf-Y-REE-Ga) coals of the seam XI in the south of Kuznetsk Basin, Russia," *Ore Geol Rev*, vol. 113, 2019, doi: 10.1016/j.oregeorev.2019.103073.
- [3] H. Zhang *et al.*, "Development of an in-situ gel from CO₂-captured complex solution and inhibiting coal spontaneous combustion: A case study in thermal engineering," *Case Studies in Thermal Engineering*, vol. 50, p. 103423, 2023, doi: 10.1016/j.csite.2023.103423.
- [4] T. Rinder, "Geochemistry of coal mine drainage, groundwater, and brines from the Ibbenbüren mine, Germany: A coupled elemental-isotopic approach," *Applied Geochemistry*, vol. 121, 2020, doi: 10.1016/j.apgeochem.2020.104693.
- [5] M. I. Juradi *et al.*, "Identifikasi Clay Bands Pada Endapan Batubara Berdasarkan Data Well Logging Di Daerah Nunukan Provinsi Kalimantan Utara," *Jurnal Geomine*, vol. 9, no. 1, pp. 17–24, 2021, doi: 10.33536/jg.v9i1.812.

-
- [6] E. M. E. Malaidji, A. Anshariah, and A. A. B. A. A. Budiman, “Analisis Proksimat, Sulfur, Dan Nilai Kalor Dalam Penentuan Kualitas Batubara Di Desa Pattappa Kecamatan Pujananting Kabupaten Barru Provinsi Sulawesi Selatan,” *Jurnal Geomine*, vol. 6, no. 3, pp. 131–137, Dec. 2018, doi: 10.33536/JG.V6I3.244.
- [7] N. Jafar, F. Ridwan, and A. B. Thamsi, “Identification of Rare Earth Metal Content in Fly Ash and Bottom Ash Coal Combustion of PT Bosowa Energi PLTU Jeneponto Regency,” *International Journal of Engineering and Science Applications*, vol. 9, no. 2, pp. 78–83, Dec. 2022, Accessed: Dec. 30, 2022. [Online]. Available: <http://pasca.unhas.ac.id/ojs/index.php/ijesca/article/view/4244>
- [8] Y. Qi, “Organic matter provenance and depositional environment of marine-to-continental mudstones and coals in eastern Ordos Basin, China—Evidence from molecular geochemistry and petrology,” *Int J Coal Geol*, vol. 217, 2020, doi: 10.1016/j.coal.2019.103345.
- [9] U. Kleinhaus, C. Wieland, F. J. Frandsen, and H. Spliethoff, “Ash formation and deposition in coal and biomass fired combustion systems: Progress and challenges in the field of ash particle sticking and rebound behavior,” *Prog Energy Combust Sci*, vol. 68, pp. 65–168, Sep. 2018, doi: 10.1016/J.PECS.2018.02.001.
- [10] B. Liu, “Geochemistry of Carboniferous coals from the Laoyaogou mine, Ningwu coalfield, Shanxi Province, northern China: Emphasis on the enrichment of valuable elements,” *Fuel*, vol. 279, 2020, doi: 10.1016/j.fuel.2020.118414.
- [11] S. Widodo, S. Sufriadin, A. Imai, and K. Anggayana, “Characterization of Some Coal Deposits Quality by Use of Proximate and Sulfur Analysis in the Southern Arm Sulawesi, Indonesia,” *International Journal of Engineering and Science Applications*, vol. 3, no. 2, pp. 137–143, Apr. 2017, Accessed: Jan. 19, 2024. [Online]. Available: <http://pasca.unhas.ac.id/ojs/index.php/ijesca/article/view/1085>
- [12] A. Artiningsih, S. Widodo, and A. Firmansyah, “Studi Penentuan Kandungan Sulfur (Sulphur Analysis) Dalam Batubara Pada PT Geoservices Samarinda Kalimantan Timur,” *Jurnal Geomine*, vol. 2, no. 1, Aug. 2015, doi: 10.33536/JG.V2I1.25.

-
- [13] S. Brotowati, "Peningkatan Kualitas Batubara Subbituminus Mallawa Menjadi Batubara Bituminus," *INTEK: Jurnal Penelitian*, vol. 5, no. 1, p. 34, Apr. 2018, doi: 10.31963/INTEK.V5I1.197.
- [14] E. P. Umar and A. Nawir, "Analisis Resistivitas Batu Bara Barru Dusun Palluda Kabupaten Barru Provinsi Sulawesi Selatan," *Jurnal Geomine*, vol. 5, no. 1, Apr. 2017, doi: 10.33536/JG.V5I1.98.
- [15] S. Bakri, J. Jefri, and S. Widodo, "Coal Quality Analysis Based on Proximate and Ultimate Test Results in Massenreng Pulu Village, Lamuru District, Bone Regency," *Journal of Geology and Exploration*, vol. 1, no. 2, pp. 36–40, Dec. 2022, doi: 10.58227/JGE.V1I2.7.
- [16] . H., A. B. Thamsi, . F., I. Nur, A. Maulana, and A. F. Heriansyah, "Geokimia Endapan Bijih Besi Daerah Pakke Kecamatan Bontocani, Kabupaten Bone, Sulawesi Selatan," *Jurnal Pertambangan*, vol. 6, no. 4, pp. 161–164, Jan. 2022, doi: 10.36706/JP.V6I4.1212.
- [17] Ittong, A. Maulana, and U. R. Irfan, "Characteristic of Alteration and Mineralization of Sulfide Deposits at Sasak area, Tana Toraja, Indonesia," *IOP Conf Ser Earth Environ Sci*, vol. 1272, no. 1, p. 012029, Dec. 2023, doi: 10.1088/1755-1315/1272/1/012029.
- [18] S. Widodo, Sufriadin, M. Thamrin, and K. Alif, "Reduction of Sulfur and Ash Content on Mallawa's Coal using Flotation Column Method," *AIP Conf Proc*, vol. 2543, Nov. 2022, doi: 10.1063/5.0095362.
- [19] M. Zhou, "Mineralogy and geochemistry of the Late Triassic coal from the Caotang mine, northeastern Sichuan Basin, China, with emphasis on the enrichment of the critical element lithium," *Ore Geol Rev*, vol. 139, 2021, doi: 10.1016/j.oregeorev.2021.104582.
- [20] J. Li, "First insights into mineralogy, geochemistry, and isotopic signatures of the Upper Triassic high-sulfur coals from the Thai Nguyen Coal field, NE Vietnam," *Int J Coal Geol*, vol. 261, 2022, doi: 10.1016/j.coal.2022.104097.
- [21] B. Sun, "Geochemistry of two high-lithium content coal seams, Shanxi Province, China," *Int J Coal Geol*, vol. 260, 2022, doi: 10.1016/j.coal.2022.104059.

- [22] A. I. Karayigit, “The geology, mineralogy, petrography, and geochemistry of the Miocene Dursunbey coal within fluvio-lacustrine deposits, Balikesir (Western Turkey),” *Int J Coal Geol*, vol. 228, 2020, doi: 10.1016/j.coal.2020.103548.
- [23] T. U. Taliding, S. Widodo, and A. Ilyas, “Proximate and Microscopy Analysis of Coal in Tamalea Village, Bonehau District, Mamuju Regency, West Sulawesi Province, Indonesia,” *IOP Conf Ser Earth Environ Sci*, vol. 1134, no. 1, 2023, doi: 10.1088/1755-1315/1134/1/012028.
- [24] H. Schweitzer, “Changes in microbial communities and associated water and gas geochemistry across a sulfate gradient in coal beds: Powder River Basin, USA,” *Geochim Cosmochim Acta*, vol. 245, pp. 495–513, 2019, doi: 10.1016/j.gca.2018.11.009.
- [25] S. I. Arbuzov, “Comments on the geochemistry of rare-earth elements (La, Ce, Sm, Eu, Tb, Yb, Lu) with examples from coals of north Asia (Siberia, Russian far East, North China, Mongolia, and Kazakhstan),” *Int J Coal Geol*, vol. 206, pp. 106–120, 2019, doi: 10.1016/j.coal.2018.10.013.

This page intentionally left blank

Characterization The Flavonoids Extract of *Tridax Procumbens* L. Leaves and Betel Lime as Materials for Open Wound Analgesic Ointment

Muhammad Zainullah¹, Mina Devika Setiana¹, Vera Nur

Fatimah¹, Ilma Fitriana¹, Robi Kurniawan^{1*}

¹Faculty of Mathematics and Natural Sciences,
Universitas Negeri Malang, Malang, 65114, Indonesia
*Corresponding Author: robi.kurniawan.fmipa@um.ac.id

(Received 07-09-2023; Revised 19-01-2024; Accepted 29-02-2024)

Abstract

Tridax procumbens L. has quite high flavonoid content (6.51%). Flavonoids have antimicrobial effects that can fight bacteria. Besides that, the flavonoid content of *T. procumbens* leaves as an analgesic inhibits has the potential to be used as an analgesic ointment material for open wounds. Betel lime (CaCO₃) also helps speed up the healing of open wounds. This research aims to optimize a mixture of *T. procumbens* leaves and betel lime to make a material-based herbal ointment that effective in healing open wounds. This research uses quantitative and qualitative approaches. The dependent variables used are the results of FTIR characterization, SEM-EDX, and antibacterial tests. Research results show that the 1:1 ointment sample has the highest homogeneity with an average particle size distribution of 11.95 nm. The weight and total atomic weight of carbon and calcium elements fluctuated with increasing leaf extract concentration, but the 2:1 ointment sample showed a higher calcium element content than the other samples because the amount of whitening was greater than the leaf extract. Flavonoid functional groups were successfully detected, O-H, C-H, and C-O-C. In *S. aureus*, it was shown that the 1:1 ointment sample was able to inhibit bacterial growth with an inhibition zone diameter of 0.062 to 1.510 cm. In addition, the contents of stigmaterol, β -sitosterol, and n-hexadecanoic acid are the main components that play a role in the inhibitory activity of bacteria.

Keywords: Analgesic ointment, flavonoids, open wounds

1 Introduction

Open wounds are damaged structures and anatomical functions of the skin, so proper treatment is required to avoid infection due to contamination by germs or bacteria.



There are various types of open wounds, such as punching, lasering, cracking, injection, abrasion, and excision wounds [1]. Excision and incision wounds are caused by sharp scratches, excision wounds accompanied by epidermal tissue cuts while incision injury is not [2]. In 2013, the number of incision injuries reached 23.2 per cent and in 2018 it increased to 25.4 percent [3]–[5].

Open wound healing consists of phases of hemostasis, inflammation, proliferation, and remodelling. This phase can occur naturally, but if the treatment and maintenance is not optimal it will cause wider tissue damage [6]. Most of the treatments for wound healing are with the administration of ointment. There are many kinds of special wound ointments, this variation depends on the composition of the ingredients and the price. Regularly marketed ointments often contain the chemical povidon iodine that has irritating side effects on the skin [7]. On the other hand, continuous use of antibiotic ointment can cause resistance if its use is not based on proper instructions [8].

Indonesia has a variety of plants that can be used in the treatment of open wounds, one of which is the leaves of *T. procumbens* L. [9]. The contents of these plant compounds include the alkaloids aquamidine, voacangine, flavonoids procumbentin, luteolin, quercetin, isokuersetin, phenol, and saponins [10]. Based on the contents, the plant *T. procumbens* is potentially used as antimicrobial and antioxidant, anti-inflammatory, anticancer, antidiabetic, antihypertensive, immunomodulator, and hepatoprotector [10], [11]. Based on research by [12] it also shows that the plant has antimicrobial effect that is capable of fighting gram-positive and gram-negative bacteria so that it can heal wounds. Therefore, based on the properties and content of *T. procumbens* leaves potentially used as one of the materials of open wound analgesic ointment. However, the research has a weakness, namely that there are no substances that help wounds dry quickly, such as turnip. Turnip consists of calcium carbonate (CaCO_3) that helps accelerate open wound healing [13]. Based on a study by [14] that combines turnips and turnip extract with a ratio of 2:1 more rapidly heals wounds and inhibits inflammation than 1:1 and 1:2. The research aims to optimize the mixture of *T. procumbens* leaves and turnip for making nanomaterial-based herbal ointments so that they can be effective in healing open wounds.

2 Material and Methods

The Place and Time

Research was carried out in July until November at the Laboratory of Material Physics, Integrated Laboratory for Biology of Faculty Mathematics and Natural Sciences, the Central Laboratory on Minerals and Advanced Materials of the Universitas Negeri Malang.

Equipment and Materials

The materials used in this research include *T. procumbens* leaves, betel lime, ethanol, 70% alcohol, aquades, water, DI water, CMC (carboxy methyl cellulose), vaseline flavum, adeps lanae, propylene glycol, Methyl paraben, paraben propyl, BHT (butylated hydroxytoluene), spiritus, lisol, and medium Na. For the equipment used include glass, filter paper, pH paper indicator, aluminium foil, handcuffs, analytical weights, ovens, hot plates, magnetic stirrer, blenders, pipettes, stopwatches, glass glasses, erlenmeyer, paper disks, and OSE needles.

Research Variable

The free variable used is the dose of *T. procumbens* leaf extract. The controlled variables used are the dosage of calcium, the amount of vaseline flavum and adeps lanae, the duration of drying, and the rate of decomposition. The bound variables used are the results of the characterization tests FTIR, SEM-EDX, and antibacterial tests.

This research uses a combination of quantitative methods by conducting experiments in the laboratory and qualitative with library studies. The technique is intended to make an analgesic ointment medication from extracts of *T. procumbens* leaves and betel lime.

Characterization Techniques and Data Analysis

The characterization techniques carried out are FTIR, SEM-EDX characterization, antibacterial testing, and effectiveness (analgesic strength) and antibacteria strength. Data analysis to determine the effect of the comparison of extracts with betel lime using Oneway ANOVA with further testing using the Duncan test with a degree of significance of 5%. Data analyzed using SPSS 25.

3 Results and Discussions

The Material of The Analgesic Ointment

In this research consists of extracts of *T. procumbens* leaves, betel lime, CMC, DI water, BHT, vaseline flavum, adeps lanae, methyl paraben, propyl parabens, and propylene glycol. *T. procumbens* leaf extract acts as an active substance in the healing of open wounds because it contains flavonoids that are analgesic [15]. It also acts as an active ingredient because it contains calcium carbonate (CaCO_3) which can also help speed up the healing of open wounds [13]. This analgesic ointment is made in three variations with a comparison of the composition of *T. procumbens* leaf extract and betel lime 1:2, 1:1, and 2:1.

CMC serves as a gel base for ointments and DI water as an extract solvent. Meanwhile, BHT acts as an antioxidant to prevent damage to the ointment mixture due to oxidation [16]. Further, there is a vaseline flavum acting as a base of hydrocarbon ointment which has the advantage of being able to last on the skin for a long time, while adeps lanae as a basis of water-absorbing ointments has good softening properties (emolien) on skin [17]. Paraben and methyl parabens function as preservatives, making the ointment last longer and have good antibacterial properties. Propylene glycol itself acts as a humectant which means it can repair and maintain the stability of the ointment over a long period of time [16]. Overall, the final formulation of ointments can be seen in Table 1 below.

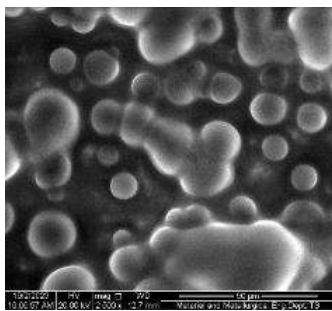
Table 1. Final Formulation of Ointments

No	Mixed Type	Material	Function	Variation		
				1:2	1:1	2:1
1	Type A	Leaves extract (g)	Active substance	12	12	12
		CMC (g)	Gel base	1	1	1
		DI water (mL)	Solvent	100	100	100
Total (g)				-	-	-
2	Type B	Type A (g)	Active substance	2,5	5	10
		Betel lime (g)		5	5	5
Total (g)				7,5	7,5	7,5

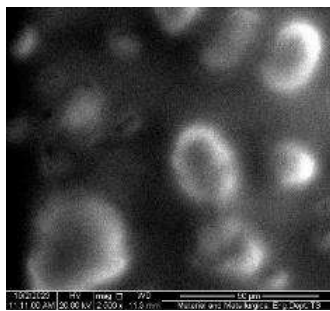
3	Type C	Campuran B (g)	Active substance	2,67	2,67	2,67
		BHT (g)	Antioxidant	0,1	0,1	0,1
4	Type D	Adeps lanae (g)	Ointment	8	8	8
		Vaseline flavum (g)	base	8	8	8
5	Type E	Propil paraben (g)	Preservative	0,05	0,05	0,05
		Metil paraben (g)		0,18	0,18	0,18
		Propilen glikol (g)	Humectant	1	1	1
Total (g)				12	12	12

Morphology, Size, Distribution, and Content of Analgesic Ointment Elements

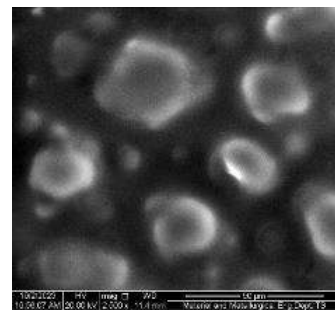
The surface area and bioactivity of the synthetic material are largely influenced by its size and shape. The results of SEM characterization of analgesic ointments 1:2, 1:1, and 2:1 show that the surface morphology is dominantly round, longitudinal, and has no crystalline structure as shown in Figs. 1 (a)-(c). Figs 2 (a)-(c) shows the distribution of the nanoparticles of the analgesical ointment has varying sizes. Ointments with a composition of 1:1 have high homogeneity with a particle size distribution of 11.95 nm, smaller than 1:2 and 2:1 with values of 22.97 nm and 24.74 nm. This is due to molecular clotting on 1:2 and 2:1 due to too thick polishing on the prepared glass. The effectiveness of analgesic ointment compared to reverse particle size. The smaller the particle size, the higher the surface area and the better its penetration so it's easier to penetrate the layer of the epidermis as well as interact with the wound cells and increase the rate of drug release. A homogeneous ointment is characterized by the absence of clumps on the treatment result, a smooth structure and a uniform colour from the starting point to the end point of the treatment [18].



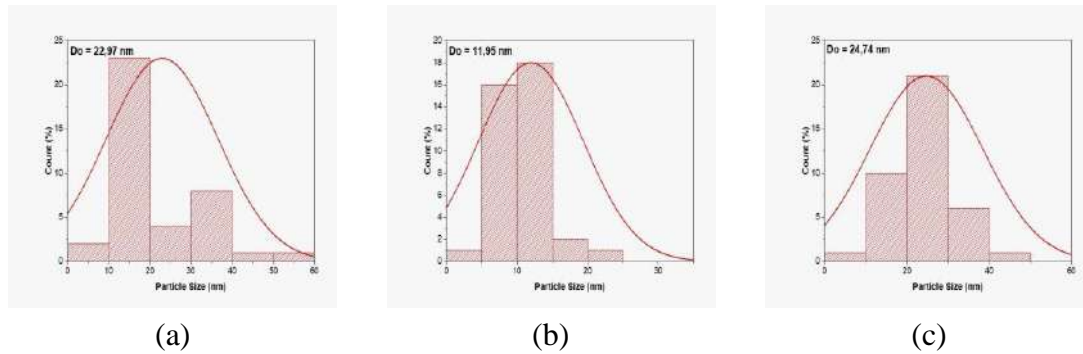
(a)



(b)



(c)

Figure 1. SEM Characterization Results of Analgesic Ointment**Figure 2.** Results of Analysis of Distribution and Particle Size of Analgesic Ointment

EDX analysis with mapping is used to identify elements in analgesic ointments 1:2, 1:1, and 2:1. The presence of the elements that make up the active ingredients of the ointment such as carbon, oxygen, and calcium in all the pure ointments samples has been identified. There is a predicted contaminant such as silicone (Si) originating from the glass preparation used in the SEM-EDX characterization. The total atomic weight of the carbon and calcium elements increased as the concentration of the leaf extracts increased, but in 1:2 the calcium element content was higher than in the other samples because the number of betel lime was more than in leaf extract. Table 2 shows the different weight and atomic proportions of the elements 1:2, 1:1, and 2:1 synthesized. Although there are differences in the element content of each sample of the ointment, the differences are not very significant due to the substance content of almost the same active substance. The research also concluded that the process of combining and making the ointment produces a high and effective purity.

Table 2. Chemical Element Composition of Analgesic Ointment

Element	1:2		1:1		2:1	
	Wt%	At%	Wt%	At%	Wt%	At%
C	83,89	89,32	86,98	90,68	84,35	89,48
O	11,19	8,94	10,84	8,48	10,72	8,54
Si	1,27	0,58	1,18	0,53	3,06	1,39
Ca	3,65	1,16	1,00	0,31	1,87	0,59
Total (%)	100	100	100	100	100	100

FTIR Spectrum Analgesic Ointment Function Group of analgesic ointment is shown by Fig. 3. The extension of the O-H function cluster of the phenol function was detected at the wave number 3644-3233 cm^{-1} . C=O aryl ketone stretching was detected at 1684-1682 cm^{-1} . The C=C aromatic ring stretching tape was visible at 1615-1520 cm^{-1} . The C-H sliding tape in aromatic hydrocarbons was detected at 2965-2859 cm^{-1} and 1393 cm^{-1} . Tires at 1180, 1163, and 1285-1002 cm^{-1} were caused by the C-O stretching of the aryl ether ring, the C-O stretch of the phenol, and the C = O-C stretching in each of the ketones. The C-C stretch tape was successfully detected on 1652-1650 cm^{-1} , whereas the =C-O-H tape was detected in 1385-1336. Tires of the C-O-C were also detected in 1285-1163 and 831-824 cm^{-1} . These functional groups are a functional group of flavonoids such as quercetin and kaempferol that act as analgesic materials. The function group values are also fairly consistent as by [19], [20] (Tabel 3).

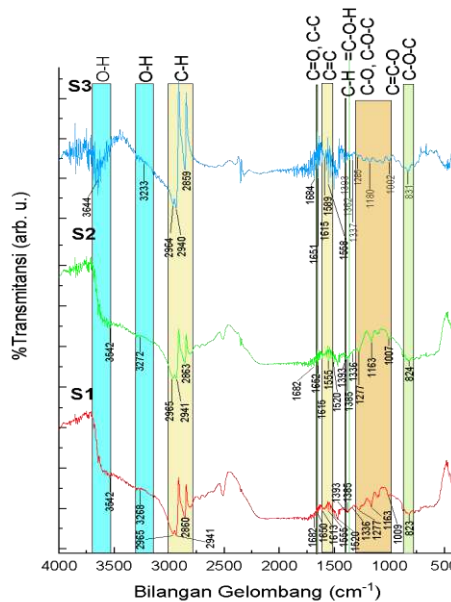


Figure 3. FTIR Test Results of Analgesic Ointment.

Tabel 3. Results of FTIR Analysis of Analgesic Ointment.

QUERCETIN				
Functional Groups	Wave Number (cm^{-1})			Reference
	1:2	1:1	2:1	
O-H	3542 – 3268	3542 – 3272	3644 – 3233	[19]
C-H	2965, 2941, 2860	2965, 2941, 2863	2964, 2940, 2859	
C=O	1682	1682	1684	

C=C	1613, 1555, 1520	1615, 1555, 1520	1615, 1589, 1558	
=C-O-H	1385, 1336	1385, 1336	1362, 1337	
C-O-C	1277, 1163, 824	1277, 1163, 824	1285, 1180, 831	
C=C-O	1277, 1007	1277, 1009	1285, 1002	
KAEMPFEROL				
Functional Groups	Wave Number (cm ⁻¹)			Reference
	1:2	1:1	2:1	
O-H	3542 – 3268	3542 – 3272	3644 – 3233	[20]
C=O	1682	1682	1684	
C-C	1650	1652	1651	
C-H	1393	1393	1393	
C-O	1163	1163	1180	

Table 4. Antibacterial Inhibitory Power of Analgesic Ointments

Bacteria	Inhibition Zone Diameter (cm) ± St. Dev		
	1:2	1:1	2:1
<i>Escherichia coli</i>	1,033 ± 0,005 ^a	1,503 ± 0,015 ^b	1,046 ± 0,232 ^a
<i>Staphylococcus aureus</i>	0,386 ± 0,557 ^a	1,406 ± 0,020 ^b	1,073 ± 0,015 ^b

Description: A number followed by the same letter in the same column, no real difference based on the Duncan test with a 5% significance rate (average ± stdev).

Bacterial Resistance

Here is the result of the analysis of the bacterial resistance of the base of the ointment with the main ingredient of the extract of the *T. procumbens* leaf with the purple betel lime (Table 4).

On a sample of *S. aureus* bacteria, a preparation of ointment with an extract ratio of 1:1 between *T. procumbens* leaves and lime can inhibit the growth of bacteria with a barrier zone diameter of 0.062-1,510 cm. In addition, there is a barrier zone that has been formed but has been rebuilt by bacteria. This can be caused by the concentration of bacteria and the number of the bacteria [21]. *E. coli* is one of the normal organisms that can cause infection [22]. This bacterium has a barrier zone of 1,029-1,520 cm. Comparing

the preparation of the ointment to a 1:1 ratio indicates a wider barrier zone compared to a 1:2 and a 2:1. It is believed to result from the release of Ca^{2+} and K^{+} ions from inside the bacterial cell membranes, resulting in cell leakage and changes in the morphology of *E. coli* cells. In addition, stigmasterol, β -sitosterol, and n-hexadecanoic acid are major components that play a role in the barrier activity of gram-positive (*S. aureus*) and gram-negative (*E. coli*) bacteria [9]. The compound spreads the spectrum of antibacterial activity on bacteria [23].

4 Conclusions

The ointment from the extracts of *T. procumbens* leaves and betel lime has the characteristics of surface morphology that are dominant round, longish, and have no crystalline structure and have high purity properties. The distribution and size of the ointment also varies where 1:1 samples have the highest homogeneity with a particle size distribution of 11.95 nm. Flavonoid function groups (curcetin and kaempferol) have been successfully identified, indicating that the ointment is analgesic so it is effective for healing open wounds. The ointment has fairly good antibacterial properties, where 1:1 samples have the best antibacteric properties with an average barrier zone diameter of $1,406 \pm 0,020b$ for gram-positive bacteria (*S. aureus*) and $1,503 \pm 0.015b$ for Gram-negative bacteria (*E. coli*).

Acknowledgements

We would like to thank the Directorate General and Higher Education (Ditjen Dikti), the Ministry of Culture, Research and Technology, and Universitas Negeri Malang for supporting this research.

References

- [1] A. L. King, M. S. Finnin, and C. M. Kramer, "Significance of Open Wounds Potentially Caused by Non-Lethal Weapons," no. June, pp. 1–75, 2019.
- [2] P. O. Samirana, L. M. Sudimartini, I. W. J. Sumadi, and P. D. Wilantari, "Efek Pemberian Sediaan Salep Ekstrak Daun Binahong secara Dermal pada Luka Insisi," *Bul. Vet. Udayana*, no. 158, p. 185, 2022, doi:

- 10.24843/bulvet.2022.v14.i02.p16.
- [3] Riskesdas, “National Health Survey.” Departemen Kesehatan RI, Jakarta, 2013. doi: 10.1126/science.127.3309.1275.
- [4] Riskesdas, “Laporan Riskesdas 2018 Nasional,” *Lembaga Penerbit Balitbangkes*. Jakarta, 2018.
- [5] I Komang Ary Werdhi Widnyana, Windah Anugrah Subaidah, and Nisa Isneni Hanifa, “Optimasi Formula Stick Balm Minyak Atsiri Daun Sereh (*Cymbopogon citratus*),” *J. Penelit. Farm. Indones.*, vol. 10, no. 2, pp. 16–24, 2021, doi: 10.51887/jpfi.v10i2.1417.
- [6] R. B. Diller and A. J. Tabor, “The Role of the Extracellular Matrix (ECM) in Wound Healing: A Review,” *Biomimetics*, vol. 7, no. 3, pp. 14–16, 2022, doi: 10.3390/biomimetics7030087.
- [7] M. A. O. Khan, R. Ramadugu, T. K. Suvvari, V. M., and V. Thomas, “Irritant contact dermatitis due to povidone-iodine following a surgical intervention: An unusual case report,” *SAGE Open Med. Case Reports*, vol. 11, pp. 10–12, 2023, doi: 10.1177/2050313X231185620.
- [8] M. A. Cahyadi, B. R. Sidharta, and N. To’bungan, “Karakteristik dan Efektivitas Salep Madu Klanceng dari Lebah *Trigona* sp. Sebagai Antibakteri dan Penyembuh Luka Sayat,” *Biota J. Ilm. Ilmu-Ilmu Hayati*, vol. 4, no. 3, pp. 104–109, 2019, doi: 10.24002/biota.v4i3.2520.
- [9] Y. Andriana, T. D. Xuan, T. N. Quy, T. N. Minh, T. M. Van, and T. D. Viet, “Antihyperuricemia, Antioxidant, and Antibacterial Activities of *Tridax procumbens* L.,” *Foods*, vol. 8, no. 1, pp. 1–12, 2019, doi: 10.3390/foods8010021.
- [10] E. Uzuegbu, J. C. Mordi, and S. I. Ovuakporay, “Effects of aqueous and ethanolic extracts of *Tridax procumbens* leaves on gastrointestinal motility and castor oil-induced diarrhoea in wistar rats,” *Biokemistri*, vol. 27, no. 1, pp. 26–32, 2015.
- [11] V. V. Ingole, P. C. Mhaske, and S. R. Katade, “Phytochemistry and pharmacological aspects of *Tridax procumbens* (L.): A systematic and comprehensive review,” *Phytomedicine Plus*, vol. 2, no. 1, p. 100199, 2022, doi: 10.1016/j.phyplu.2021.100199.
- [12] S. Debeturu, S. Tulandi, V. Paat, and G. Tiwow, “Uji Aktivitas Analgesik Ekstrak

- Etanol Daun Songgolangit (*Tridax procumbens* L.) Terhadap Tikus Putih (*Rattus norvegicus*),” *Biofarmasetikal Trop.*, vol. 5, no. 1, pp. 66–72, 2022, doi: 10.55724/jbiofartrop.v5i1.371.
- [13] Q. Zhou *et al.*, “Differentially Expressed Proteins Identified by TMT Proteomics Analysis in Bone Marrow Microenvironment of Osteoporotic Patients,” pp. 1089–1098, 2019, doi: <https://doi.org/10.1007/s00198-019-04884-0>.
- [14] Y. Susanto, F. A. Solehah, A. Fadya, and K. Khaerati, “Potensi Kombinasi Ekstrak Rimpang Kunyit (*Curcuma longa* L.) dan Kapur Sirih Sebagai Anti Inflamasi dan Penyembuh Luka Sayat,” *JPSCR J. Pharm. Sci. Clin. Res.*, vol. 8, no. 1, p. 32, 2023, doi: 10.20961/jpscr.v8i1.60314.
- [15] Departemen Kesehatan RI, “Materia Medika Indonesia,” *Direktorat Jenderal Pengawasan Obat dan Makanan*, vol. 4. Jakarta, pp. 333–337, 1995.
- [16] A. Febriani, I. M. Kusuma, S. Sianturi, and R. Choirunnisa’, *Pemanfaatan Bahan Alam Sebagai Obat, Kosmetik, dan Pangan Fungsional*. 2019.
- [17] A. N. Carabelly, I. W. A. K. Firdaus, P. C. Nurmardina, D. A. Putri, and M. L. Apriasari, “The Effect of Topical Toman Fish (*Channa micropeltes*) Extract on Macrophages and Lymphocytes in Diabetes Mellitus Wound Healing,” *J. Phys. Conf. Ser.*, vol. 1374, no. 1, 2019, doi: 10.1088/1742-6596/1374/1/012028.
- [18] A. Nagaraj *et al.*, “Biomimetic of hydroxyapatite with *Tridax procumbens* leaf extract and investigation of antibiofilm potential in *Staphylococcus aureus* and *Escherichia coli*,” *Indian J. Biochem. Biophys.*, vol. 59, no. 7, pp. 755–766, 2022, doi: 10.56042/ijbb.v59i7.61218.
- [19] A. Masek, A. Plota, J. Chrzastowska, and M. Piotrowska, “Novel hybrid polymer composites based on anthraquinone and eco-friendly dyes with potential for use in intelligent packaging materials,” *Int. J. Mol. Sci.*, vol. 22, no. 22, 2021, doi: 10.3390/ijms222212524.
- [20] Y. S. Qian, S. Ramamurthy, M. Candasamy, S. Md, R. H. Kumar, and V. S. Meka, “Production, Characterization and Evaluation of Kaempferol Nanosuspension for Improving Oral Bioavailability,” *Curr. Pharm. Biotechnol.*, vol. 17, no. 6, pp. 549–555, 2016, doi: 10.2174/1389201017666160127110609.
- [21] Holifah, Y. Ambari, A. W. Ningsih, B. Sinaga, and I. H. Nurrosyidah, “Efektifitas

- Antiseptik Gel Hand Sanitizer Ekstrak Etanol Pelepah Pisang Kepok (*Musa paradisiaca* L.) Terhadap Bakteri *Staphylococcus aureus* dan *Escherichia coli*,” vol. 6, no. 2, 2020.
- [22] N. Mufti, E. Bahar, and D. Arisanti, “Uji Daya Hambat Ekstrak Daun Sawo terhadap Bakteri *Escherichia coli* secara In Vitro,” *J. Kesehat. Andalas*, vol. 6, no. 2, p. 289, 2017, doi: 10.25077/jka.v6.i2.p289-294.2017.
- [23] T. Stefani, E. Garza-González, V. M. Rivas-Galindo, M. Y. Rios, L. Alvarez, and M. D. R. Camacho-Corona, “*Hechtia glomerata* Zucc: Phytochemistry and Activity of its Extracts and Major Constituents Against Resistant Bacteria,” *Molecules*, vol. 24, no. 19, pp. 1–14, 2019, doi: 10.3390/molecules24193434.

Density Functional Theory Investigation on The Electronic Structure, Properties and IR Spectra of 9,10-Iphenylanthracene

Owolabi J Adeyemi^{1*}, Hassan Gambo¹, Onimisi M Yusuf¹,
Gidado S Abdulkadir², Ali Haruna¹, Bankole J Akinade³, Akusu
C Onma⁴, Muhammed L Madugu¹, Sakinat L Usman¹

¹*Department of Physics Nigerian Defence Academy, Kaduna, Nigeria*

²*Department of Physics Bayero University Kano, Nigeria*

³*Department of Physics Federal University Iafia, Nigeria*

⁴*Department of Physics Gombe State University Gombe, Nigeria*

*Corresponding Author: jaowolabi@nda.edu.ng

(Received 18-05-2024; Revised 09-07-2024; Accepted 22-07-2024)

Abstract

9,10-Diphenylanthracene belongs to a class of polymer-based materials featuring a π -bonded molecules (organic semiconductors). We conducted a theoretical investigation into 9,10-DPA in both neutral and ionic states using Density Functional Theory (DFT) implemented in the Gaussian 09 package. The calculations employed B3LYP/6-31+G(d) and B3LYP/6-311++G(d,p) basis sets. The study focused on evaluating structural properties, electronic properties, global chemical reactivity descriptors and IR spectra of 9,10-DPA. These assessments aimed to elucidate the reactivity, stability, and conductivity of this molecule. The results reveal that charging influences the structural, electronic, and global index of the molecule. The analysis of bond lengths and angles emphasized that the following bond length R(C7-H18), R(C8-H19), R(C12-H26) and R(C13-H27) exhibits greater bond energy and strength in both neutral and ionic states because of having shorter bond length than the remaining regardless of the chosen basis set. In the case of energy gap, the anionic alpha molecular orbital exhibits lower stability of having the lowest energy gap of 1.3679eV, indicating higher reactivity and conductivity among the entire MO and is supported by a higher softness value (1.15eV) and higher chemical potential (1.39eV). The cationic beta molecule exhibited stronger electron-attracting power because of having higher electronegativity (9.00eV), lower chemical potential (-9.00eV) and higher electrophilicity index (36.81eV). The vibrational analysis shows that the anionic molecular state possessed the highest IR absorption which occurred at the frequency of 1346.96cm⁻¹. Overall, the findings underscore the importance of charge state in enhancing the electronic properties and the reactivity of these molecules for various applications in the field of organic electronics.



Keywords: 9,10-Diphenylanthracene, ionization potential, electron affinity, global chemical index, infrared spectra, density of state

1 Introduction

There has been a lot of interest in entirely organic technologies during the past few decades. Organic transistors and discrete OLED displays have the potential to produce devices with enhanced properties over liquid crystal display technology, including lower power consumption, better resolution, more mechanical flexibility, and lower production costs. To create novel materials with enhanced device performance, it is necessary to comprehend the connection between molecular structural and electrical properties [1].

Organic semiconductor materials have found vast application in light-emitting diodes; photovoltaic cells. This development is because of the strong optical absorption, mechanical flexibility, low cost and solubility these materials exhibit [2].

To be more precise, organic semiconductor devices are less expensive than traditional inorganic semiconductor electronic technologies since they are simpler to manufacture and does not need sophisticated photolithographic processes or high vacuum deposition procedures [3].

Organic semiconductors (OSCs) are solids made of π -bonded molecules or polymers that frequently include carbon and hydrogen atoms as well as heteroatoms like nitrogen, sulphur, and oxygen. They can be found as molecular crystals or amorphous thin films. By nature, they are electrical insulators, but when charges are added using appropriate electrodes during doping or photoexcitation, they become semiconductors [4]. The benefits of organic semiconductors for the production of electronic devices include their low cost, suitability for roll-to-roll processing, ease of fabrication at low temperatures, printable nature, flexible and large area applications due to their mechanical flexibility, and active matrix display backplanes. Additionally, these benefits served as the motivation for using these organic semiconductors [5]. Organic semiconductors, which combined the desirable qualities of metals and polymers with solubility, mechanical strength, and adjustable physicochemical properties, enabled the development of novel devices. However, a lot more cutting-edge studies and

advancements in manufacturing technology are still needed to realize all conductive macromolecules' potential applications [6].

Anthracenes and their derivatives hold a significant place in fundamental physics research among organic materials because the molecules are relatively small and straightforward, making it easier to understand the connections between molecular structures, optical properties, and transport properties in organic semiconductor materials [1].

The chemical activity of a molecule is shown by the highest occupied molecular orbital (HOMO) or singly occupied molecular orbital (SOMO) for the case of radicals, lowest unoccupied molecular orbital (LUMO), and their related energy gaps. A molecule's kinetic stability, chemical reactivity, optical polarizability, and chemical hardness-softness are all governed by the energy difference between LUMO and HOMO/SOMO [2]. Furthermore, in study on the Synthesis and Divergent Electronic Properties of Two Ring-Fused Derivatives of 9,10-Diphenylanthracene, the isomers revealed dissimilar photophysical and redox properties with 2 having a much smaller HOMO–LUMO gap than 1 [7]. The schematic of Molecular structure can be seen in Fig. 1. When considering the movement of electrons or holes in an organic molecular solid, one must keep in mind that ionic molecular states are involved. For instance, an electron must be removed to convert a neutral molecule into a radical cation. This defective electron can move from one molecule to the next [8].

Theoretical investigation of hole mobility in 9,10-diphenylanthracene by density functional calculations also revealed that using the coupling matrix calculated by the CTI method, they predicted a hole mobility of $2.15\text{cm}^2/(\text{Vs})$ for Diphenylanthracene (DPA), whereas the CTI method gave the values as 0.35 and $1.39\text{cm}^2/(\text{Vs})$ for naphthalene and anthracene, respectively [9].

Additionally, the energy differences between the lowest unoccupied molecular orbital (LUMO) and the highest occupied molecular orbital (HOMO) can be used to estimate the active mobility of polycyclic aromatic hydrocarbons (PAH). The organic molecule can easily give or accept an electron due to its tiny energy gap [10].

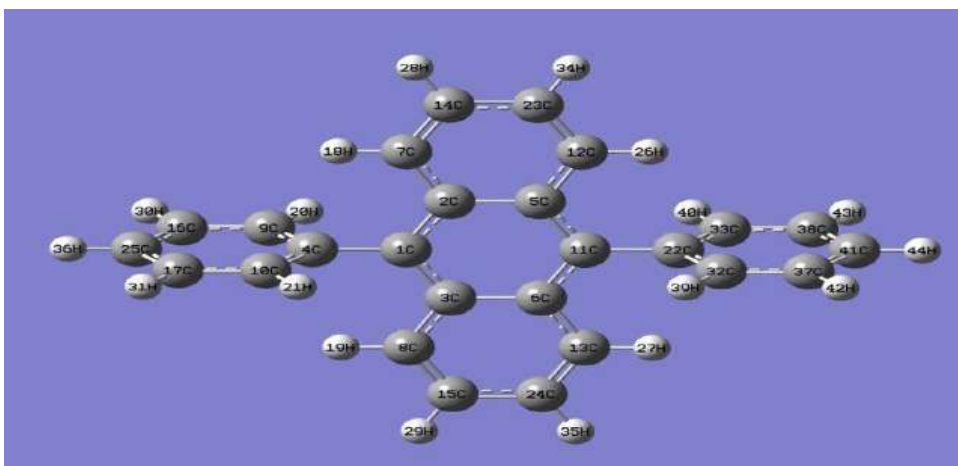


Figure 1. Molecular structure of 9,10-DPA and its derivative 2-bromo-9,10-DPA

In this study, to address some of the gaps in the literature, the electronic structure, properties and IR spectra of the isolated 9,10-DPA in neutral and at different charge states were computed using density functional theory embedded in Gaussian 09 software at two different basis sets b3lyp6-31+G(d) and b3lyp6- 311++ G(d,p).

2 Theoretical Background

Density Functional Theory (DFT)

Density functional theory (DFT) was first put on theoretical footing by Kohn and Hohenberg in the frame work of the two Hohenberg-Kohn theorems in 1964. While in 1965, Kohn and Sham (KS) reformulated in more familiar form and to the practical application of (DFT). [11].

Density functional theory (DFT) is a quantum mechanical method used in physics and chemistry to investigate and calculate the physical properties of atoms, molecules and solids. It is now consider as one of the most important tools for calculating the ground state properties of semiconductors, and to investigate the electronic structure of many electron systems [12]. The quantum mechanical wave function contains all the information about a given system, including the case of a simple 2-D square potential or even a hydrogen atom. One can solve the Schrödinger equation exactly in order to get the wave function of the system and the allowed energy states of the system can be determined. Unfortunately, it is difficult to solve the Schrödinger equation for N-body

system. Evidently, some approximations are involved to render the problem solvable. Kohn et al., (1996) defined Density Functional Theory (DFT) as a theory of electronic structure based on the electron density distribution $n(r)$, instead of many-electron wave function [13]:

However, the electron density $n(r)$ for many-electron system is defined as:

$$n(r) = N \int |\psi(r_1, r_2, r_3, \dots, r_N)|^2 dr_2 \dots dr_N \quad (2.1)$$

where N is the number of electrons, ψ is the many-electron wave function, and r represent the spatial coordinates of the electrons.

The total electron density is then expressed as the squared magnitudes of the Kohn-Sham orbitals.

$$\rho(r) = \sum_{i=1}^N |\psi_i(r)|^2 \quad (2.2)$$

where:

$\psi_i(r)$ = the Kohn-Sham orbitals

$\rho(r)$ = electron density

N = number of electrons in the system

Within DFT, the ground state energy can be determined using the density relation given above [14].

Ionization Potential (IP) And Electron Affinity (EA)

Beyond charge mobility, another crucial factor influencing the performance of organic materials in the context of organic devices is charge injection efficiency. It is an important aspect of organic materials used in various electronic and optoelectronic devices. It ensures that charges (electrons or holes) can effectively transition from the electrode into the organic material. Several parameters including electron affinity and ionization potential, significantly define the charge injection efficiency of organic semiconductors. These parameters play a vital role in facilitating the efficient injection of either electrons or holes into the vacant HOMO-LUMO levels [15].

The ionization potential (IP) represents the energy required to remove an electron from the highest occupied molecular orbital (HOMO) or singly occupied molecular orbital (SOMO) (for radicals), while electron affinity (EA) denotes the energy alteration that occurs when introducing an electron into the lowest unoccupied molecular orbital (LUMO). These properties are closely related to charge injection efficiency, as they define the ease with which charges can be injected into the HOMO-LUMO levels [15].

In the context of molecular orbital theory, there exists a direct relationship between the HOMO/SOMO energy and the ionization potential, as well as the LUMO energy and the electron affinity. This connection is formalized by Koopmans' theorem, which is utilized to estimate these fundamental properties ($IP = -EHOMO$ and $EA = -ELUMO$).

Koopmans' theorem establishes a direct relationship between HOMO energy and ionization potential (IP) and between LUMO energy and electron affinity (EA). This theorem provides a convenient way to estimate these important electronic properties from quantum mechanical calculations [15].

A molecule's capacity to either accept or release an electron hinges on its ionization potential (IP) and electron affinity (EA). When the electron affinity is low, it becomes more challenging to incorporate an additional electron into the molecule. Conversely, when the ionization potential (IP) is high, the process of removing an electron becomes more difficult [2].

Koopmans' equations can be used to calculate the ionization potential (IP) and electron affinities (EA) of the studied molecule [2]

$$IP = -EHOMO \quad (2.3)$$

$$EA = -ELUMO \quad (2.4)$$

where;

$EHOMO$ = energy of the HOMO

$ELUMO$ = energy of the LUMO

The HOMO-LUMO energy gap (Eg) can be obtained from the relation;

$$Eg = ELUMO - EHOMO \approx IP - EA \quad (2.5)$$

Global Chemical Reactivity Descriptors (GCRD)

Chemical potential, chemical hardness, softness, electronegativity, and electrophilicity index are parameters that aid in predicting and understanding trends in global chemical reactivity. Koopmans' equations can be used to calculate the ionization potential (IP) and electron affinities (EA) of the studied molecule [2];

$$IP = -EHOMO \quad (2.6)$$

$$EA = -ELUMO \quad (2.7)$$

where;

EHOMO = energy of the HOMO

ELUMO = energy of the LUMO

The HOMO-LUMO energy gap (*Eg*) can be obtained from the relation;

$$Eg = ELUMO - EHOMO \approx IP - EA \quad (2.8)$$

The global chemical reactivity descriptors (GCRDs) can be obtained as follows;

The chemical hardness (η) could be expressed in terms of IP and EA as;

$$\eta = (ELUMO - EHOMO)/2 \approx (IP - EA)/2 \quad (2.9)$$

Chemical softness is given by;

$$s = \frac{1}{\eta} \quad (2.10)$$

The chemical potential is given by;

$$\mu = -\left(\frac{IP+EA}{2}\right) \quad (2.11)$$

The electronegativity is given by;

$$X = \frac{IP+EA}{2} \quad (2.12)$$

Electrophilicity index (ω) - The electrophilicity index measures the amount of energy that is lost as a result of the maximum amount of electron flow between the donor and acceptor. It is expressed as [2];

$$\omega = \frac{\mu^2}{2\eta} \quad (2.13)$$

Computational Method

In this research, the Gaussian 09W package was used to study the electronic structure, properties and IR spectra of 9,10-DPA at different charge states. Optimization of the geometric structure of our target molecule was considered first, thereby allowing every parameter of the ground states to have total freedom to relax and each computation converged to an optimized geometry that corresponds to a true energy minimum. With the optimized geometry, single-point energy calculations of the molecules were performed to obtain parameters such as HOMO (highest occupied molecular orbital), SOMO (singly occupied molecular orbital), LUMO (lowest unoccupied molecular orbital) and total ground state energy were calculated using density functional theory (DFT) method with the three-parameter hybrid exchange functional of Becke and Lee-Yang-Parr correlation functional (B3LYP) [16] using the two basis sets {6-31+G (d) and 6-311++G (d, p)}. Other parameters like HOMO-LUMO energy gap, ionization potential, electron affinity as well as global chemical reactivity descriptors (such as chemical hardness, softness, electronegativity, chemical potential and electrophilicity index) and the vibrational frequencies of the target molecules were also calculated, while the IR spectra was computed from the vibrational frequencies using Gauss view package. The same procedure was also adopted for the computation of the ionic (anionic and cationic) molecules by changing the charge state from 0 to -1 and +1 respectively. All calculations

were carried out under the Gaussian 09 software program coding for Density Functional Theory (DFT).

3 Results and Discussions

Optimized Bond Length of 9,10- Diphenylanthracene

Tables 1 present data regarding bond lengths for 9,10-DPA, calculated based on DFT method using B3LYP level of theory with the 6-31+G(d) and 6-311++G(d,p) basis sets. Bond length represents the distance between two atoms covalently bonded in a molecule. The energy associated with molecules featuring shorter bond lengths is stronger compared to those with longer bond lengths [2].

The results shows that the calculated bond lengths of 9,10-DPA were found to be the least with the following values; (1.0849Å), (1.0834Å) and (1.0865Å) when using B3LYP/6-3+1G and (1.0823Å), (1.081Å) and (1.0837Å) while using B3LYP/6-311++G for neutral, cationic and anionic respectively at the following; R(C₇-H₁₈), R(C₈-H₁₉), R(C₁₂-H₂₆) and R(C₁₃-H₂₇). The bond lengths in R(C₁-C₄) and R(C₁₁-C₂₂) were found to be the highest with the following values; (1.4988Å), (1.484Å) and (1.4958Å) upon using B3LYP/6-3+1G and (1.4937Å), (1.483Å) and (1.4947Å) when B3LYP/6-311++G was used respectively. From these results, we can observed that the strongest bond was found in the cationic state which occurred at B3LYP/6-311++G level of theory for R(C₇-H₁₈), R(C₈-H₁₉), R(C₁₂-H₂₆) and R(C₁₃-H₂₇) with the value (1.081Å), while the weakest bond was found in the neutral state, occurred at B3LYP/6-31+G level of theory for R(C₁-C₄) and R(C₁₁-C₂₂) with the value of (1.4988Å). Both values were in agreement with the experimental values of (1.085Å) and (1.437Å) respectively for anthracene [17].

Table 1. Bond Length (Å) of 9,10-Diphenylanthracene

BOND LENGTHS (Å) OF 9,10-DIPHENYLANTHRACENE						
	B3LYP/6-31+G(d)			B3LYP/6-311++G(d,p)		
	Neutral	Cationic	Anionic	Neutral	Cationic	Anionic
R(C1-C2)	1.4125	1.4296	1.4259	1.4092	1.4264	1.4226
R(C1-C3)	1.4124	1.4296	1.426	1.4091	1.4264	1.4226
R(C1-C4)	1.4988	1.484	1.4958	1.4937	1.483	1.4947
R(C2-C5)	1.4479	1.4425	1.4526	1.4455	1.4398	1.4505
R(C2-C7)	1.4344	1.4191	1.4234	1.4321	1.4163	1.4209
R(C3-C6)	1.4479	1.4425	1.4526	1.4455	1.4398	1.4505
R(C3-C8)	1.4344	1.4191	1.4235	1.4321	1.4162	1.4209

R(C4-C9)	1.4037	1.4084	1.4063	1.4001	1.4045	1.4026
R(C4-C10)	1.4037	1.4084	1.4063	1.4001	1.4045	1.4027
R(C5-C11)	1.4125	1.4296	1.426	1.4092	1.4263	1.4226
R(C5-C12)	1.4344	1.4191	1.4234	1.4321	1.4162	1.4209
R(C6-C11)	1.4125	1.4296	1.4259	1.4092	1.4263	1.4226
R(C6-C13)	1.4344	1.4191	1.4235	1.4321	1.4162	1.4209
R(C7-C14)	1.3714	1.3886	1.3953	1.367	1.3848	1.3918
R(C7-H18)	1.0849	1.0834	1.0865	1.0823	1.081	1.0837
R(C8-C15)	1.3713	1.3886	1.3953	1.367	1.3848	1.3918
R(C8-H19)	1.0849	1.0834	1.0865	1.0823	1.081	1.0837
R(C9-H16)	1.3977	1.3951	1.3984	1.3941	1.3915	1.3948
R(C9-H20)	1.0875	1.0868	1.0877	1.0846	1.0841	1.0848
R(C10-C17)	1.3977	1.3951	1.3984	1.3941	1.3916	1.3947
R(C10-H21)	1.0875	1.0868	1.0877	1.0846	1.0841	1.0848
R(C11-C22)	1.4988	1.484	1.4958	1.4976	1.4831	1.4947
R(C12-C23)	1.3713	1.3886	1.3953	1.367	1.3848	1.3918
R(C12-H26)	1.0849	1.0834	1.0865	1.0823	1.081	1.0837
R(C13-C24)	1.3713	1.3886	1.3953	1.367	1.3848	1.3918
R(C13-H27)	1.0849	1.0834	1.0865	1.0823	1.081	1.0837
R(C14-C23)	1.4236	1.4041	1.4029	1.421	1.401	1.3994
R(C14-H28)	1.0871	1.0859	1.0892	1.0843	1.0834	1.0862
R(C15-C24)	1.4236	1.4041	1.403	1.421	1.401	1.3994
R(C15-H29)	1.0871	1.0859	1.0892	1.0843	1.0834	1.0862
R(C16-C25)	1.3978	1.3984	1.3986	1.3939	1.3946	1.3947
R(C16-H30)	1.0873	1.0863	1.0888	1.0845	1.0836	1.0859
R(C17-C25)	1.3978	1.3984	1.3986	1.3939	1.3946	1.3948
R(C17-H31)	1.0873	1.0863	1.0888	1.0845	1.0836	1.0859
R(C22-C32)	1.4037	1.4084	1.4063	1.4001	1.4045	1.4026
R(C22-C33)	1.4037	1.4084	1.4063	1.4001	1.4045	1.4026
R(C23-H34)	1.0871	1.0859	1.0892	1.0843	1.0834	1.0862
R(C24-H35)	1.0871	1.0859	1.0892	1.0843	1.0834	1.0862
R(C25-H36)	1.0871	1.0862	1.0885	1.0842	1.0835	1.0855
R(C32-C37)	1.3977	1.3951	1.3984	1.3941	1.3916	1.3948
R(C32-H39)	1.0875	1.0868	1.0877	1.0846	1.0841	1.0848
R(C33-C38)	1.3977	1.3951	1.3984	1.3941	1.3916	1.3948
R(C33-H40)	1.0875	1.0868	1.0877	1.0846	1.0841	1.0848
R(C37-C41)	1.3978	1.3985	1.3986	1.3939	1.3945	1.3948
R(C37-H42)	1.0873	1.0863	1.0888	1.0845	1.0836	1.0859
R(C38-C41)	1.3978	1.3984	1.3986	1.3939	1.3945	1.3948
R(C38-H43)	1.0873	1.0863	1.0888	1.0845	1.0836	1.0859
R(C41-H44)	1.0871	1.0862	1.0885	1.0842	1.0835	1.0855

Optimized Bond Angles of 9,10- Diphenylanthracene

Other structural properties that define molecular geometries of an organic material are; bond angles and torsional angles. A bond angle is the angle formed between three atoms across at least two bonds [15]. The optimized bond angles of 9,10-DPA at the DFT levels of theory within the basis sets were summarized and presented in Table 2. The calculated bond angles for 9,10-DPA at B3LYP/6-31+G and B3LPY/6-311++G were

found to be in good agreement with the experimental values, and it showed small deviations at some points of the basis sets.

Table 2. Bond Angle ($^{\circ}$) of 9,10-Diphenylanthracene

BOND ANGLE ($^{\circ}$) OF 9,10-DIPHENYLANTHRACENE						
	B3LYP/6-31+G(d)			B3LYP/6-31+1+G(d,p)		
	Neutral	Cationic	Anionic	Neutral	Cationic	Anionic
A(C2,C1,C3)	120.0465	119.3374	121.4131	120.0458	119.3671	121.4307
A(C2,C1,C4)	119.9787	120.3318	119.2918	119.9787	120.3135	119.2833
A(C3,C1,C4)	119.9749	120.3308	119.2951	119.9755	120.3194	119.286
A(C1,C2,C5)	119.9762	120.2885	119.2949	119.9766	120.2768	119.2858
A(C1,C2,C7)	121.7693	121.2662	122.672	121.7852	121.2637	122.6917
A(C5,C2,C7)	118.2584	118.4415	118.0333	118.2382	118.4554	118.0225
A(C1,C3,C6)	119.9773	120.2887	119.2925	119.9775	120.2742	119.2838
A(C1,C3,C8)	121.767	121.2658	122.6744	121.7832	121.2669	122.6937
A(C6,C3,C8)	118.2558	118.4417	118.0331	118.2393	118.4549	118.0225
A(C1,C4,C9)	120.7137	120.5091	121.2475	120.6927	120.4656	121.2179
A(C1,C4,C10)	120.7124	120.5082	121.244	120.6915	120.4674	121.2143
A(C9,C4,C10)	118.5739	118.9827	117.5085	118.6158	119.067	117.5677
A(C2,C5,C11)	119.9771	120.2885	119.2921	119.9774	120.2752	119.2833
A(C2,C5,C12)	118.2557	118.4413	118.0337	118.2393	118.4587	118.0232
A(C11,C5,C12)	121.7671	121.2664	122.6742	121.7834	121.2622	122.6935
A(C3,C6,C11)	119.9756	120.2884	119.2946	119.9769	120.2775	119.2857
A(C3,C6,C13)	118.2545	118.4411	118.0337	118.2382	118.4586	118.023
A(C11,C6,C13)	121.769	121.2666	122.6717	121.7849	121.26	122.6913
A(C2,C7,C14)	121.4787	121.3704	122.1477	121.4536	121.3089	122.1098
A(C2,C7,H18)	118.6362	119.2644	118.6772	118.6213	119.2239	118.6885
A(C14,C7,H18)	119.8851	119.3646	119.1751	119.9251	119.4669	119.2017
A(C3,C8,C15)	121.4783	121.3704	122.1481	121.4533	121.3099	122.1103
A(C3,C8,H19)	118.6357	119.2644	118.6774	118.6209	119.2249	118.6884
A(C15,C8,H19)	119.886	119.3647	119.1745	119.9258	119.4649	119.2013
A(C4,C9,C16)	120.7615	120.3788	121.4301	120.7234	120.3189	121.3811
A(C4,C9,H20)	119.2845	119.7398	118.5646	119.3163	119.8046	118.5797
A(C16,C9,H20)	119.954	119.8572	120.0053	119.9602	119.854	120.0382
A(C4,C10,C17)	120.7611	120.3788	121.4296	120.7231	120.3188	121.3805
A(C4,C10,H21)	119.2834	119.7398	118.5619	119.3151	119.8048	118.5769
A(C17,C10,H21)	119.9555	119.8573	120.0085	119.9618	119.8537	120.0426
A(C5,C11,C6)	120.0464	119.3377	121.413	120.0458	119.3696	121.4306
A(C5,C11,C22)	119.975	120.3308	119.2938	119.9756	120.3165	119.2847
A(C6,C11,C22)	119.9785	120.3314	119.2931	119.9786	120.3139	119.2847
A(C5,C12,C23)	121.4783	121.3704	122.1477	121.4532	121.3092	122.1099
A(C5,C12,H26)	118.636	119.2643	118.6783	118.6212	119.2233	118.6894
A(C23,C12,H26)	119.8857	119.3647	119.174	119.9256	119.4671	119.2007
A(C6,C13,C24)	121.4783	121.3704	122.1473	121.4533	121.3088	122.1094
A(C6,C13,H27)	118.6364	119.2643	118.6771	118.6215	119.2225	118.6883
A(C24,C13,H27)	119.8853	119.3647	119.1755	119.9252	119.4684	119.2023
A(C7,C14,C23)	120.2663	120.0873	119.8192	120.3077	120.1373	119.8676
A(C7,C14,H28)	119.9763	119.7506	119.7327	119.99	119.7731	119.7608
A(C23,C14,H28)	119.7574	120.1609	120.4482	119.7022	120.0885	120.3715
A(C8,C15,C24)	120.2663	120.0872	119.8183	120.3077	120.138	119.8667

A(C8,C15,H29)	119.9764	119.7506	119.7344	119.9901	119.7729	119.7627
A(C24,C15,H29)	119.7573	120.161	120.4473	119.7021	120.0881	120.3706
A(C9,C16,C25)	120.1591	120.1761	120.1762	120.1698	120.1831	120.1888
A(C9,C16,H30)	119.7052	119.6445	119.788	119.7364	119.6671	119.8132
A(C25,C16,H30)	120.1357	120.1793	120.0359	120.0938	120.1499	119.998
A(C10,C17,C25)	120.1594	120.1761	120.1766	120.1701	120.1833	120.1893
A(C10,C17,H31)	119.7055	119.6444	119.7911	119.7368	119.6665	119.8165
A(C25,C17,H31)	120.1351	120.1794	120.0323	120.0931	120.1503	119.9942
A(C11,C22,C32)	120.7132	120.5079	121.246	120.6923	120.4656	121.2164
A(C11,C22,C33)	120.7128	120.509	121.2457	120.6919	120.4645	121.2161
A(C32,C22,C33)	118.574	118.983	117.5082	118.6159	119.0698	117.5675
A(C12,C23,C14)	120.2665	120.0874	119.8185	120.3079	120.1371	119.8669

The bond angle in 9,10-DPA formed at B3LYP/6-31G level of theory for A(3,6,13) in neutral and cationic state and A(32,22,33) in anionic state with the values (118.2545⁰), (118.4411⁰) and (117.5082⁰) respectively as well as B3LYP/6-311++G level of theory for A(5,2,7) and A(3,6,13) in neutral, A(6,3,8) in cationic and A(32,22,33) in anionic state with the following values (118.2382⁰), (118.4547⁰) and (117.5675⁰) were the smallest and were in agreement with the other experimental values (112⁰-118.8⁰) for anthracene [17]. It was observed that some bond angles in table 2 were found to be more than 118.8⁰, these slight increments were attributed to ionizing and large steric hindrance as a result of substitution of one hydrogen atom with the functional molecule (phenyl group) at the central rings of anthracene structure [18].

Molecular Orbitals

The HOMO (Highest Occupied Molecular Orbital) energy is indicative of a molecule's ability to donate electrons, whereas the LUMO (Lowest Unoccupied Molecular Orbital) energy reflects its capacity to accept electrons. In molecular orbital theory, the HOMO and LUMO play crucial roles in understanding the reactivity of a molecule. The energy gap between the LUMO and HOMO, often referred to as the HOMO-LUMO energy gap, is a key determinant of a molecule's reactivity and conductivity, as a smaller gap suggests greater reactivity due to easier electron transfer [15].

The band gap is an essential property for characterizing the electrical structures of solids. Regard to this, a study has systematically examined how the band gap changes for anthracene at pressures ranging from 0 to 27GPa. They discovered that the band gap for

solid anthracene at ambient pressure is 2.2eV at the generalized gradient approximation (GGA) level, which is a little higher than the Local Density Approximations (LDA) value of 1.9eV [19].

Table 3 in our study provides insight into HOMO (Highest Occupied Molecular Orbital), SOMO (Singly Occupied Molecular Orbital), LUMO (Lowest Unoccupied Molecular Orbital) and HOMO/SOMO-LUMO gap (energy gap) values for both neutral and ionic forms of 9,10-DPA. These calculations were conducted using the two different basis sets (6-31+G(d) and 6-311++G(d,p)). It is well-established that compounds with smaller HOMO-LUMO energy gap values tend to exhibit higher reactivity and greater conductivity because it requires a small amount of energy for electron to transition from HOMO to the LUMO or to transition from the ground state to the excited state indicating its easiness in the charge injection making it a better choice for organic materials used in organic semiconductor applications such as organic light emitting diodes, organic photovoltaic (solar cell) or organic field-effect transistor. Conversely, a larger energy gap implies a greater kinetic stability but a lesser reactivity and conductivity [2].

The results clearly demonstrated that the anionic alpha molecular orbital of 9,10-DPA yielded a significantly smaller energy gap in comparison to the neutral and cationic counterparts, particularly with a band gap of about 1.3679eV, calculated using the basis set 6-311++G(d,p). Furthermore, it's evident that the neutral form of 9,10-DPA possesses the largest energy gap, measuring about 3.4540eV at 6-311++G(d,p) basis set. These observations suggest that neutral molecule is more stable and exhibit a greater aversion to donate electrons when compared to the ionic counterpart. Moreover, it's worth noting that the choice of basis set appears to have a relatively minor impact on the energy gap values compared to the influence of charging the molecules. These findings underscore the critical role of electron density and charge distribution in determining the conductivity, kinetic stability and reactivity of the molecule under investigation.

Table 3. The Frontier Orbital Energies for both Neutral and Ionic form of 9,10-Diphenylanthracene

NEUTRAL					
Molecule	Basis Set	MO	E _{HOMO} (eV)	E _{LUMO} (eV)	Energy Gap(eV)
9,10-DPA	6-31+G	Alpha	-5.3889	-1.9431	3.4458
	6-311++G	Alpha	-5.4556	-2.0016	3.4540
CATIONIC					
Molecule	Basis Set	MO	E _{SOMO} (eV)	E _{LUMO} (eV)	Energy Gap(eV)
9,10-DPA	6-31+G	Alpha	-9.2117	-6.1154	3.0963
		Beta	-10.0299	-7.8256	2.2043
	6-311++G	Alpha	-9.2895	-6.1786	3.1109
		Beta	-10.0971	-7.8980	2.1991
ANIONIC					
Molecule	Basis Set	MO	E _{SOMO} (eV)	E _{LUMO} (eV)	Energy Gap(eV)
9,10-DPA	6-31+G	Alpha	0.5165	2.2606	1.7441
		Beta	-1.2103	1.9248	3.1351
	6-311++G	Alpha	0.4620	1.8299	1.3679
		Beta	-1.2742	1.8282	3.1024

Ionization Potential (IP) and Electron Affinity (EA)

The ability of a molecule to accept or released an electron is determined by its ionization potential (IP) and the electron affinity (EA). The lower the electron affinity the less easy it is to add an electron and the higher the ionization potential (IP) the less easy it is to remove an electron [20]. The IPs and EAs of the neutral and ionic forms of the 9,10-DPA are presented in Table 4.

Table 4. The Ionization Potential (IP) and Electron Affinity of 9,10- Diphenylanthracene

Molecule	Basis Set	MO	Neutral		Ionic			
			IP (eV)	EA (eV)	Cationic		Anionic	
					IP (eV)	EA (eV)	IP (eV)	EA (eV)
9,10-DPA	6-31+G	Alpha	5.39	1.94	9.21	6.12	-0.52	-2.26
		Beta	-	-	10.03	7.83	1.21	-1.92
	6-311++G	Alpha	5.46	2.00	9.29	6.18	-0.46	-1.83
		Beta	-	-	10.10	7.90	1.27	-1.83

The analysis reveals some interesting findings regarding the ionization potential (IP) and electron affinity (EA) of the studied molecule, specifically in its cationic state. It was observed that the cationic beta molecular orbital (MO) displayed the highest ionization potential, measuring 10.10eV when calculated using 6-311++G(d,p) basis set. This signifies that a substantial amount of energy is required to remove an electron from this particular molecular state. On the other hand, the molecule with the greatest electron affinity was also identified as the cationic beta MO, with an EA value of 7.90eV when calculated with the same basis set. This suggested that this molecule has a strong tendency to accept an additional electron. Comparing these cationic molecules to their neutral and anionic counterparts, it becomes apparent that the cationic forms exhibit higher ionization potentials and electron affinities. This implies that cationic molecules are more inclined to act as electron acceptors than electron donors.

Furthermore, this study highlighted that the ionization potential and electron affinity of the study molecules are more influenced by charging the molecules than the choice of basis set. These findings highlight the importance of taking into account the molecular charge state when evaluating ionization potential and electron affinity, as these factors significantly influence the electronic properties of the molecules.

Global Quantities of 9,10-Diphenylanthracene

The global chemical reactivity descriptors such as chemical hardness (η), chemical softness (S), electronegativity (χ), chemical potential (μ), and electrophilicity index (ω) were calculated from HOMO/SOMO and LUMO energies which were obtained at the level of theory B3LYP using the two basis sets 6-31+G(d) and 6-311++G(d,p) as depicted in Table 5.

Table 5. Global Chemical Reactivity Descriptors (GCRD) of 9,10- Diphenylanthracene

Neutral			
Property	Basis Set	MO	GCRD Value
η (eV)	6-31+G	Alpha	1.72
	6-311++G	Alpha	1.73
S (eV)	6-31+G	Alpha	0.58
	6-311++G	Alpha	0.58
χ (eV)	6-31+G	Alpha	3.67
	6-311++G	Alpha	3.73

μ (eV)	6-31+G	Alpha	-3.67
	6-311++G	Alpha	-3.73
ω (eV)	6-31+G	Alpha	3.90
	6-311++G	Alpha	4.02
Cationic			
Property	Basis Set	MO	GCRD Value
η (eV)	6-31+G	Alpha	1.55
		Beta	1.10
	6-311++G	Alpha	1.56
		Beta	1.10
S (eV ⁻¹)	6-31+G	Alpha	0.65
		Beta	0.91
	6-311++G	Alpha	0.64
		Beta	0.91
χ (eV)	6-31+G	Alpha	7.66
		Beta	8.93
	6-311++G	Alpha	7.73
		Beta	9.00
μ (eV)	6-31+G	Alpha	-7.66
		Beta	-8.93
	6-311++G	Alpha	-7.73
		Beta	-9.00
ω (eV)	6-31+G	Alpha	18.93
		Beta	36.25
	6-311++G	Alpha	19.23
		Beta	36.81
Anionic			
Property	Basis Set	MO	GCRD Value
η (eV)	6-31+G	Alpha	0.87
		Beta	2.94
	6-311++G	Alpha	0.68
		Beta	1.55
S (eV)	6-31+G	Alpha	1.15
		Beta	0.34
	6-311++G	Alpha	1.46
		Beta	0.64
χ (eV)	6-31+G	Alpha	-1.39
		Beta	-0.26
	6-311++G	Alpha	-1.15
		Beta	-0.28
μ (eV)	6-31+G	Alpha	1.39
		Beta	0.26
	6-311++G	Alpha	1.15
		Beta	0.28
ω (eV)	6-31+G	Alpha	1.11
		Beta	0.01
	6-311++G	Alpha	0.96
		Beta	0.02

Chemical Hardness (η) and softness (S) concepts are valuable for characterizing the properties of molecules, and these calculations provide insights into the relative hardness

and softness of 9,10-DPA, within the context of the chosen basis sets and molecular orbitals. A hard molecule exhibits a substantial energy gap, while a soft molecule features a smaller energy gap [21]. Consequently, soft molecules tend to be more polarizable than hard ones. Theoretical calculations have revealed interesting insights. In particular, the molecule that possess the highest hardness value is the anionic beta molecular orbital ($\eta = 2.94$ eV) when analysing using the 6-31+G(d) basis set. This designation signifies that it is the hardest molecule in the context of this study. Conversely, its anionic alpha molecular orbital stands out for having the highest chemical softness ($S = 1.15$ eV) when calculated using the same basis set, 6-31+G(d). This observation highlights its distinction as the softest molecule within this study.

Electronegativity (χ) is a measure of a molecule's capacity to attract electrons. The values presented in table (4.5) clearly demonstrate that the cationic beta MO of 9,10-DPA exhibits the highest electronegativity value, approximately 9.00eV. This value surpasses that of all the other molecules as calculated using 6-311++G(d,p) basis set. This observation highlights the exceptional electron-attracting ability of the cationic beta MO of 9,10-DPA compared to the other molecules in the study [22]. Electronegativity is a fundamental concept in molecular reactivity, and the results provide valuable insights into the relative electron-attracting capabilities of these molecules.

The chemical potential (μ) serves as a measure of an electron's tendency to escape and can be correlated with molecular electronegativity. In this context, as μ becomes more negative, it indicates a higher resistance to electron loss but a greater ease in gaining electrons. The data presented in Table (4.5) demonstrates that the cationic beta molecular orbital of 9,10-DPA has a pronounced capacity to gain electrons, particularly evident when analysed using 6-311++G(d,p) basis set. This is supported by a chemical potential value of -9.00eV. Conversely, as revealed in Table (4.5) again, anionic alpha molecular orbital of 9,10-DPA, stands out as the least stable but most reactive and conductive among all the molecules under investigation. This conclusion is drawn from its notably high chemical potential value of 1.39eV, especially when employing the 6-31+G basis set.

In summary, the concept of chemical potential, as a measure of electron tendencies, provides valuable insights into the relative stabilities and reactivities of these molecules [22]. The data suggests that the cationic beta molecular orbital 9,10-DPA has a strong

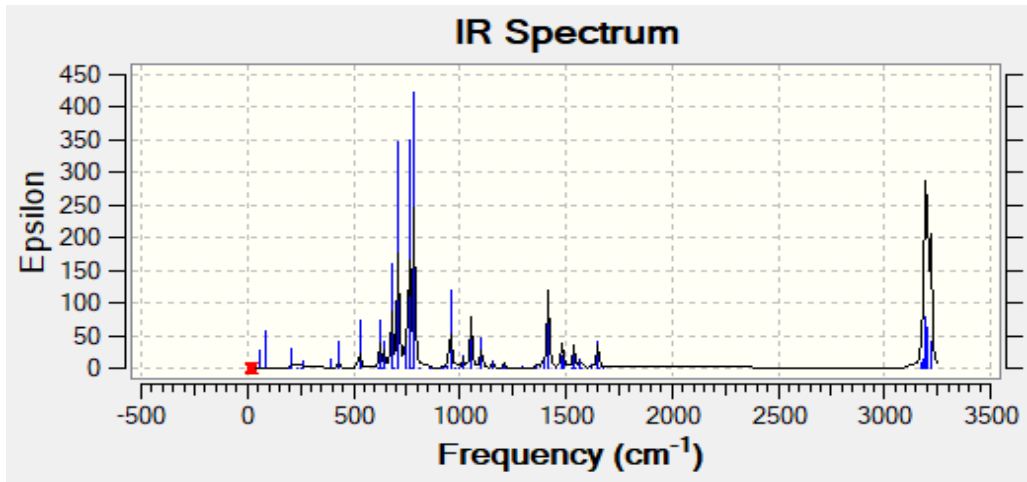
inclination to gain electrons, while the anionic alpha molecular orbital 9,10-DPA, exhibits higher reactivity due to its elevated chemical potential value.

Electrophilicity (ω) is a concept that provides insight into the energy of stabilization when a system becomes saturated with electrons from the external environment. This reactivity information helps determine a molecule's ability to donate charge. A molecule with a lower ω value is considered a strong nucleophile, indicating heightened reactivity in donating electrons, while higher ω values suggest the presence of a potent electrophile, capable of accepting electrons [22]. Our findings reveal interesting trends. Specifically, the anionic beta molecular orbital exhibits low ω values of approximately 0.01eV when analysed using the 6-31+G basis set. This observation characterizes it as a proficient nucleophile, highlighting its capacity to donate charge effectively. In contrast, the cationic beta molecular orbital exhibits a significantly higher ω value, approximately 36.81eV, as determined with the 6-311++G basis set. This elevated ω value characterizes it as a strong electrophile, indicating its ability to readily accept electrons.

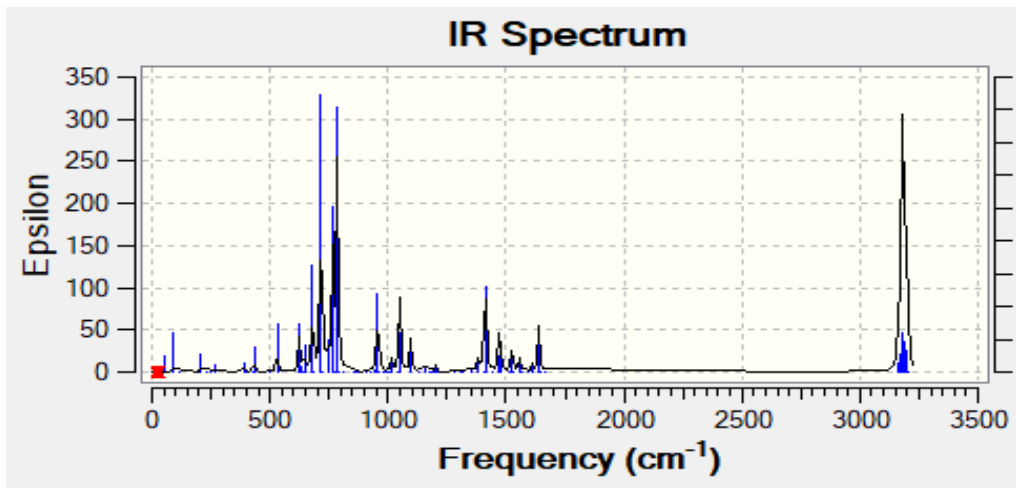
IR Spectra

Vibrational frequency analysis is a vital technique used to elucidate the vibrational characteristics of specific molecular structures within a compound. Molecular vibrations occur when atoms within a molecule engage in periodic motion while the molecule, as a whole, maintains translational and rotational motion. The frequency at which this periodic motion occurs is referred to as the vibrational frequency [15].

In the present study, vibrational frequencies were computed for 9,10-DPA, using Density Functional Theory (DFT) with the B3LYP exchange functional under 6-31+G(d) and 6-311++G(d,p) basis sets. The resulting infrared spectra were generated using Gauss View software, as illustrated in Figs. 2-4.

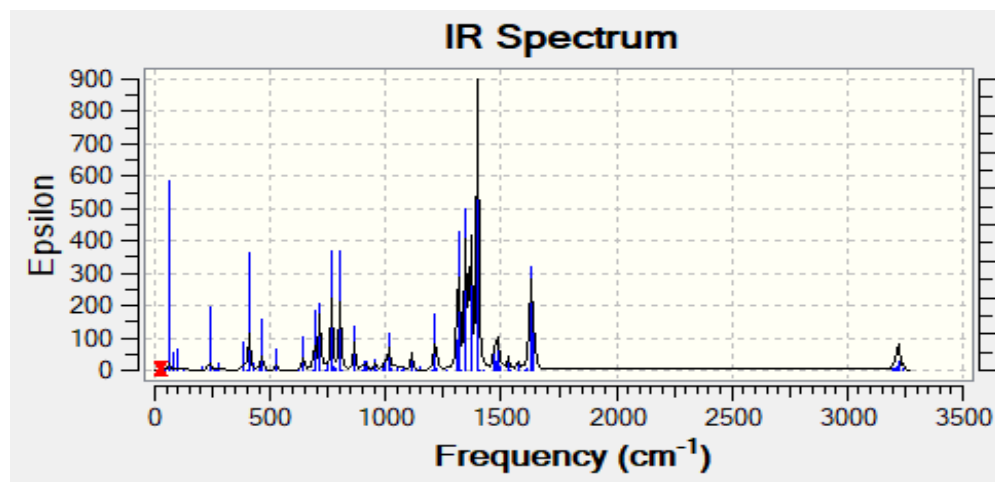


(a)

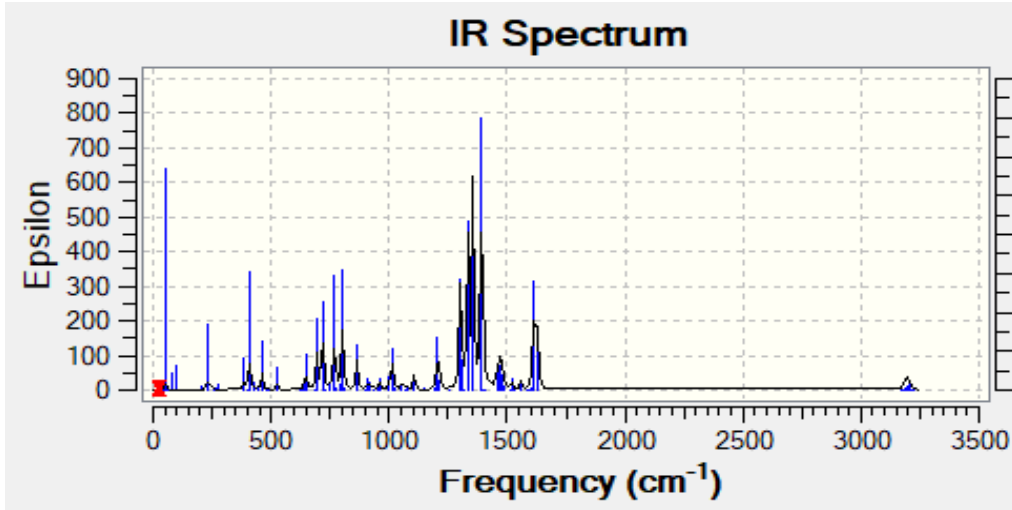


(b)

Figure 2. (a) Neutral 9,10-DPA(1), (b) Neutral 9,10-DPA(2)

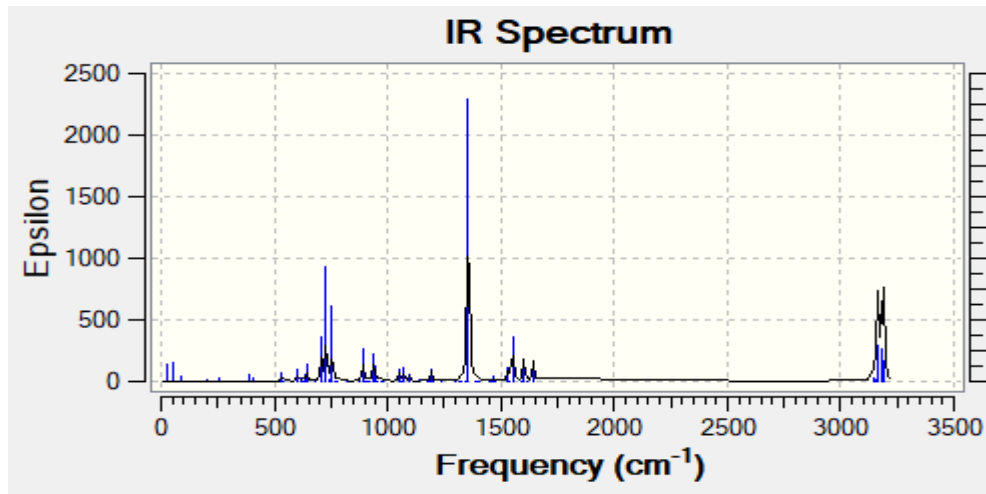


(a)

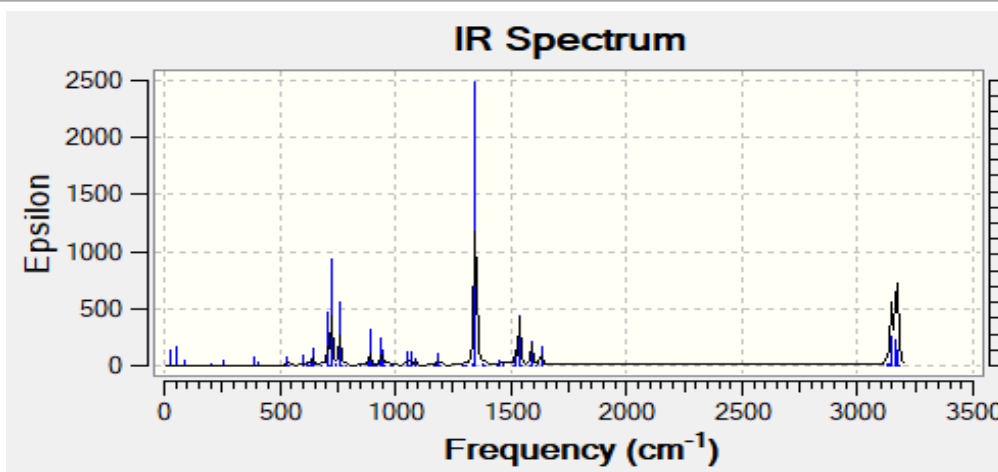


(b)

Figure 3. (a) Cationic 9,10-DPA(1), (b) Cationic 9,10-DPA(2)



(a)



(b)

Figure 4. (a) Anionic 9,10-DPA(1), (b) Anionic 9,10-DPA(2)

Figs. 2 (a)-(b) shows the IR spectrum of neutral 9,10-Diphenylanthracene under the two basis sets employed in this research, from the figures we observed the highest intense IR absorption (about $\epsilon = 425 \text{ Lmol}^{-1}\text{cm}^{-1}$) at a frequency around 785.545cm^{-1} in the first basis set and that of the second basis set is at frequency around 716.514cm^{-1} and has an absorption intensity (about $330 \text{ Lmol}^{-1}\text{cm}^{-1}$) which is less than that of the first basis set.

Figs. 3 (a)-(b) shows the IR spectrum of cationic 9,10-Diphenylanthracene under the two basis sets employed in this research, from the figures we observed the highest intense IR absorption (about $900 \text{ Lmol}^{-1}\text{cm}^{-1}$) at a frequency around 1398.26cm^{-1} in the first basis set and that of the second basis set is at frequency around 1393.14cm^{-1} and has an absorption intensity (about $790 \text{ Lmol}^{-1}\text{cm}^{-1}$) which is less than that of the first basis set.

Figs. 4 (a)-(b) shows the IR spectrum of cationic 9,10-Diphenylanthracene under the two basis sets employed in this research, from the figures we observed the highest intense IR absorption (about $2300 \text{ Lmol}^{-1}\text{cm}^{-1}$) at a frequency around 1356.54cm^{-1} in the first basis set and that of the second basis set is at frequency around 1346.96cm^{-1} and has an absorption intensity (about $2500 \text{ Lmol}^{-1}\text{cm}^{-1}$) which is greater than that of the first basis set.

Notably, the most intense vibrational frequency for 9,10-DPA was observed in its anionic form using 6-311++G(d,p) basis set at 1346.96cm^{-1} having the highest absorption

value (figure 4b). The above data indicates that the anionic 9,10-DPA has higher Infrared absorption compared to the remaining molecules. The symmetric stretching modes were observed in the spectral region below 3100 cm^{-1} , while the spectral region between 3100 and 3500 cm^{-1} featured the asymmetric stretching modes of vibration.

For these aromatic molecules, the in-plane vibrations were discerned in the frequency range of $1250\text{-}1750\text{ cm}^{-1}$, while the out-of-plane vibrations manifested below 1200 cm^{-1} for the ionic forms of 9,10-DPA. In the case of its neutral forms, the in-plane vibrations were observed in the frequency range between $500\text{-}900\text{ cm}^{-1}$, and the out-of-plane vibrations were evident between $900 - 1750\text{ cm}^{-1}$. In conclusion, the analysis suggests that anionic 9,10-DPA molecules possess the highest level of infrared (IR) absorption by exhibiting the highest peaks in the vibrational modes among other molecular state.

4 Conclusions

This study delved into the structural, electronic properties, and infrared absorption capabilities of 9,10-DPA, offering valuable insights into how molecular behaviour is influenced by charging. The analysis of bond lengths and angles emphasized that the following bond length $R(\text{C}_7\text{-H}_{18})$, $R(\text{C}_8\text{-H}_{19})$, $R(\text{C}_{12}\text{-H}_{26})$ and $R(\text{C}_{13}\text{-H}_{27})$ exhibits greater bond energy and strength in both neutral and ionic states because of having shorter bond length than the remaining regardless of the chosen basis set. The exploration of molecular orbitals and their energy gaps provided further insights into the electronic properties of the molecules under study. The smaller HOMO-LUMO energy gaps obtained in the ionic molecules (specifically the anionic alpha MO) indicates lower stability but higher reactivity and conductivity. This further indicates its greater tendency to donate electrons which makes it a better semiconductor among other molecular state. In the other hand, larger HOMO-LUMO energy gap values for neutral molecules implies a greater stability and a lower tendency to donate electrons compared to its ionic counterpart. In the case of global chemical reactivity descriptors (GCRDs), the hardest molecular orbital (MO) was found to be the anionic beta MO which occurred as the result of having the highest hardness value among all the MO, the MO with the highest reactivity was found to be anionic alpha MO because it exhibits higher chemical potential as well as higher softness

value. In the other, cationic beta MO was found to have the highest electron-attracting capability because of having the highest electronegativity value, lower and negative chemical potential (making it to have higher resistance to release electrons but greater ease in gaining electrons) and also considered to be strong electrophile because it possessed the highest electrophilicity index (it has the greater ability to accept electrons). The analysis of IR spectra suggests that anionic 9,10-DPA molecules possess the highest level of infrared (IR) absorption by exhibiting the highest peaks in the vibrational modes among other molecular state. In general, the results show a great novelty by contributing into a deeper understanding of the complex and delicate interaction or relationship between structure, stability, conductivity and reactivity in aromatic molecules. The findings emphasize the critical role of charge states in shaping these characteristics. These insights are crucial for advancing our understanding of molecular behaviour and for potential applications in various scientific and technological domains.

References

1. Ren, Z. (2010). *Molecular Vibration and Charge Transport in Crystalline Oligoacenes and Derivatives: Raman and DFT Combined Study*. Chapel Hill: University of North carolina.
2. Abubakar, A. A., Suleiman, A. B., & Gidado, A. S. (2021). Density Functional Theory Investigation of the Doping Effects of Bromine and Fluorine on the Electronic and Optical Properties of Neutral and Ionic Perylene. *Physical Science International Journal*, 1-13.
3. Hiszpanski, A. M., & Loo, Y. L. (2014). Directing the film structure of organic semiconductors via post-deposition processing for transistor and solar cell applications. *Energy Environ. Sci*, vol. 7, 592-608.
4. Sano, M., Pope, M., & Kallmann, H. (1965). Electroluminescence and Band Gap in Anthracene. *Journal of Chemical Physics*: Bibcode: 1965JChPh. 43.2920S. doi:10.1063/1.1697243, 2920-2921.

5. Arias, A. C., MacKenzie, J. D., McCulloch, I., Rivnay, J., & Salleo, A. (2010). Materials and Applications for Large Area Electronics: Solution-Based Approaches. In *Chemical Reviews* (pp. 3-24). American Chemical Society.
6. Martin-Palma, R. J., & Martinez-Duart, J. (2017). *Nanotechnology for Microelectronics and Photonics* (Second Edition). Elsevier Science.
7. Rajeswara, R. M., Hayden, T. B., & Dmitrii, F. P. (2015). Synthesis and Divergent Electronic Properties of Two Ring-Fused Derivatives of 9,10-Diphenylanthracene. *Organic letters: American Chemical Society*. DOI: 10.1021/acs.orglett.5b02009, A-D.
8. Bruetting, W. (2005). *Physics of Organic Semiconductors*, 1-14. <https://doi.org/10.1002/3527606637.ch>. Weinheim: WILEY-VCH Verlag GmbH and Co. KGaA.
9. Watanabe, S., Shimodo, Y., & Morihashi, K. (2011). Theoretical investigation of hole mobility in 9,10-diphenylanthracene by density functional calculations. *Theor. Chem. Acc.* Vol. 130:807–813. DOI 10.1007/s00214-011-1042-5, 807-813.
10. Yating, S., Yarui, S., Huiling, W., Hongsheng, Z., & Yufang, L. (2017). A theoretical Study on Electronic Properties of Two Ring-Fused Derivatives of 9, 10-Diphenylanthracene. *Royal Society of Chemistry: New Journal of Chemistry*: DOI: 10.1039/C7NJ02590D, 1-22.
11. Ndikilar, C. E., Gidado, A. S., Suleiman, A. B., & Maigari, A. (2022). Effects of Mono-Halogen-Substitution on the Electronic and Non-Linear Optical Properties of Poly (3-hexylthiophene-2, 5-diyl) for Solar Cell Applications: A DFT Approach. *Journal of Energy Research and Reviews*, 1-14.
12. Ajeel, F. N., Khudhair, A. M., & Mohammed, A. A. (2013). Density Functional Theory Investigation of the Physical Properties of Dicyano Pyridazine Molecules. *International Journal of Science and Research (IJSR)*, 4(1). ISSN (Online): 2319-7064, 2334-2339.
13. Abdulaziz, H., Gidado, A. S., Musa, A., & Lawal, A. (2019). Electronic Structure and Non-Linear Optical Properties of Neutral and Ionic Pyrene and Its Derivatives

-
- Based on Density Functional Theory. *Journal of Materials Science Research and Reviews*; Article no.JMSRR.45683, 1-13.
14. Gobre, V. V. (2016). Efficient modelling of linear electronic polarization in materials using atomic response functions. Berlin (Germany): Technische Universitaet.
 15. Musa, A., Gidado, A. S., Mohammed, L., Yunusa, K., & Suleiman, A. B. (2019). Molecular and Electronic Properties of Rubrene and Its Cyanide Derivative Using Density Functional Theory (DFT). Musa, A., Gidado, A.S., *IOSR Journal of Applied Physics (IOSR-JAP)*, 11(2), ., 10-18.
 16. Becke, A. D. (1992). Density-functional thermochemistry. III. The role of exact exchange. *The journal of chemical Physics*, 5648-5652.
 17. Ketkar, S. N., Kelley, M., Fink, M., & Ivey, R. C. (1981). An Electron Diffraction Study of the Structures of Anthraquinone and Anthracene. *Journal of Molecular Structure*, Elsevier Scientific Publishing Company, Amsterdam - printed in the Netherlands, 127-138.
 18. Sulaiman, N. M., Taura, L. S., Lawal, A., Gidado, A. S., & Musa, A. (2019). Solvent Effects on the Structural, Electronic, NonLinear Optical and Thermodynamic Properties of Perylene Based on Density Functional Theory. *Journal of Materials Science Research and Reviews*, 1-13.
 19. Ling-Ping, X., Guo-Hua, Z., Zhi, Z., & Xiao, J. (2015). Theoretical study on structural and electronic properties of solid anthracene under high pressure by density functional theory. *Molecular Physics. Molecular Physics (International Journal at the Interface between chemistry and physics)*, 1-7.
 20. Kumer, A., Ahmed, B., Sharif, M., & Al-mamun, A. (2017). A Theoretical Study of Aniline and Nitrobenzene by Computational Overview. *Asian Journal of Physical and Chemical Sciences* .<https://doi.org/10.9734/AJOPACS/2017/38092>, 1-12.
 21. Taura, L. S., Muhammad, R. N., Lawal, A., & Gidado, A. S. (2022). Electronic Structure and IR Spectra Analysis of Tetrathiafulvelene (TTF) Using RHF and DFT Quantum Mechanical Methods. *Journal of Energy Research and Reviews*. 10(4): 20-35; Article no.JENRR.84391, 20-35.

22. Muhammad, R. N., Mahraz, N. M., Gidado, A. S., & Musa, A. (2021). Theoretical Study of Solvent Effects on the Electronic and Thermodynamic Properties of Tetrathiafulvalene (TTF) Molecule Based on DFT. Asian Journal of Research and Reviews in Physics. Article no.AJR2P.77309, 42-54.

An Analysis of Principals' Digital Literacy Capabilities as Instructional Leaders in Indonesia

Jaja¹, Dwiniasih^{1*}, Jajo Firman Raharjo¹

¹*Faculty of Education and Sciences, Swadaya Gunung Jati University,
Pemuda Street No.1, West Java, 45131, Indonesia*

**Corresponding Author: dwiniasih@ugj.ac.id*

(Received 13-06-2024; Revised 24-07-2024; Accepted 29-07-2024)

Abstract

The role of principals as instructional leaders requires them to continuously improve their skills in designing and implementing 21st-century learning. This involves developing their digital literacy capabilities as part of technology integration. This research is a case study that aims to analyze the digital literacy capabilities of principals in Kuningan and Cirebon, Indonesia, as instructional leaders in designing and implementing 21st-century learning. The participants of this study were 20 elementary school headmasters. To collect the data, the authors used a teacher observation checklist, with the observer being the teacher in charge of the training. The results of this study showed that the headmasters, as supervisors and instructional leaders, had strong digital literacy capabilities. They were able to easily use technology, and the applications were clear and understandable to them. Furthermore, the participants found it easy to become skilled with the system, learn to operate it, and interact with it. They also showed high mental effort, required much care and attention, and found it easy to navigate and remember how to perform tasks with the system. Overall, this study highlights the importance of developing digital literacy capabilities among instructional leaders, particularly in the context of 21st-century learning. The study provides insights for educators and policymakers on how to support principals in improving their digital literacy capabilities to serve as effective instructional leaders in the digital age.

Keywords: Digital Literacy, instructional leaders, principals' capabilities

1 Introduction

Since 2015, the Indonesian government has included digital literacy as one of the six national literacies that need improvement in the National Literacy Campaign [1]. This inclusion is crucial due to the rapid and dynamic technological advancements affecting all sectors, necessitating digital literacy as an integral component of educational life [2-



4]. Therefore, acquiring new competencies and applications has become imperative to adapt to the ever-changing nature of ICT [5].

Digital literacy, also known as ICT competence or ICT literacy, entails the ability to address issues related to knowledge, information, and communication in a digital environment [6-8]. Similarly, ICT proficiency refers to higher-order learning processing capabilities that align with technological and application skills. These skills encompass the primary usage of software, as well as creative and innovative abilities, problem-solving, and critical thinking using the Internet and various devices [9-10].

Overall, the Indonesian government's focus on digital literacy as a crucial aspect of the National Literacy Campaign reflects the increasing importance of digital competencies in modern society. This underscores the need for individuals to develop and enhance their digital literacy skills to effectively navigate the digital landscape and take advantage of its many opportunities.

Therefore, it is necessary for principals to improve their self-quality by mastering digital literacy, as it is crucial for their survival in the twenty-first century [11]. Strengthening the role of literacy facilitators is one of the training programs available to principals. This training is designed to enhance their abilities in using and utilizing ICT to develop schools. Digital literacy encompasses more than just equipping oneself with high-tech capabilities to operate digital devices, menus, and tools, and searching for sources on the Internet. It comprises a range of knowledge, abilities, and attitudes required to enhance practical skills in a digital atmosphere [12], [13].

Thus, the education system must adjust its regulations by incorporating digital competence into the curricula and assessments [14-15]. By doing so, students will be better equipped to navigate the digital landscape and succeed in the ever-changing world of technology. Moreover, principals who have acquired digital literacy competencies will be better equipped to lead their schools effectively, integrating technology into their pedagogy and creating a more engaging and effective learning environment for their students.

One thing being inquired is the importance of technology in education and to what extent teachers' capabilities to integrate technology vary in learning activities [16-17]. Examining how teachers acknowledge and manage the acceptance of technology is

claimed to be one of the problems in education [18]. Meanwhile, other studies have investigated and found that both pre-service and in-service teachers can receive technology well [19]. However, certain aspects of major construction and the significance of external variables contrast with what individuals believe about the Technology Acceptance Model (TAM).

Based on the findings, it can be said that the acceptance of technology by teachers falls into a good category, which is analyzed using the Technology Acceptance Model (TAM). However, from the number of studies that have been conducted, it is found that analyses of the acceptance of technology focusing on principals' capabilities are still rare. Even though principals rarely teach in class, they have to be a model for their teachers as subordinates. This involves the capabilities to operate Microsoft Office, email, use online applications, or select appropriate media as the digital learning source.

Referring to the lack of research focused on principals' capabilities in implementing digital literacy to improve the quality of education, the authors aimed to analyze the principals' digital literacy capabilities. Through this study, the researchers aimed to ensure that the participants could easily use technology and that the applications were clear and understandable to them. Additionally, the study aimed to help participants become skilled with the system, allowing them to easily perform desired tasks, learn how to operate and interact with it. Another important goal of this study was to help participants handle high mental effort, requiring much care and attention, providing easy navigation, and reminding them how to operate functions within the system..

2 Material and Methods

This study was initiated due to recent issues that sparked the authors' interest in delving deeper into the case of principals' capabilities in using technology. Therefore, a case study was conducted, involving twenty principals of elementary schools. The principals were randomly selected from Cirebon and Kuningan in West Java, Indonesia. To investigate the capabilities of principals in implementing digital literacy, a teacher observation checklist was used for data collection.

The reliability and validity of the teacher observation checklist are crucial for ensuring accurate and meaningful data collection. The checklist was designed based on established theories, including the Theory of Reasoned Action (TRA), which has been validated in previous studies [12-13]. This theoretical foundation lends credibility to the instrument's content validity. However, it is essential to conduct further empirical validation to confirm its reliability and validity in this specific context.

To assess reliability, the consistency of the checklist across different observers and over time should be evaluated. In this study, the same observer (the training teacher) conducted all observations, which reduces inter-observer variability but may introduce observer bias. Future studies should consider using multiple observers and calculating inter-rater reliability coefficients to enhance the reliability of the findings. In terms of validity, the checklist's ability to accurately measure principals' digital literacy capabilities was supported by its alignment with key components of digital literacy, such as operating Microsoft Office applications, creating email accounts, and using digital media. The observation checklist included ten specific statements to guide the observer, which enhances its construct validity by covering various aspects of digital literacy implementation.

After conducting the observations, the researchers analyzed the data by calculating the percentages and explicitly describing the findings. This quantitative approach allows for a clear presentation of the results, but it also relies on the accuracy of the observer's initial judgments. Therefore, ensuring the reliability and validity of the observation checklist is fundamental to the integrity of the study's conclusions. Overall, while the teacher observation checklist used in this study has a solid theoretical foundation and covers relevant aspects of digital literacy, its reliability and validity could be further strengthened through empirical validation and measures to reduce observer bias.

3 Results and Discussions

This research involved several stages of implementation, starting with data collection by sharing an observation checklist with teacher training to guide the analysis of the principals' capabilities in implementing digital literacy. The digital literacy

implementation conducted by the principals included operating Microsoft Office, which involved Word files, Excel, and PowerPoint, creating an email account, saving files in Google Drive, and using digital media as a learning source from the internet browser.

The compiled observation checklist was adopted from several theories, including the Theory of Reasoned Action (TRA), which has been used in previous studies [12-13]. The indicators for the usage level focused on the perception of ease of use, where each indicator had a choice of Yes or No responses, as shown in Table 1.

Table 1. Teacher Observation Checklist for perspective ease of use

No.	Indicator	Condition	
		Yes	No
1.	Participants could easy to use		
2.	The applications are clear and understandable		
3.	Participants are easy to become skilful with system		
4.	Participants are easy to get it to do what they want it to		
5.	Participants are easy to learn to operate		
6.	Participants could interact with		
7.	Participants got a low mental effort		
8.	Participants do not demand much care and attention		
9.	Participants got navigation is easy		
10.	Participants are easy to remember how to perform tasks with system		

After distributing and collecting the questionnaire, the researchers entered the data into an Excel form for analysis. The analysis focused on the perception of ease of use, as indicated in Table 1. It was found that 70% of participants could easily operate Microsoft Office, create email accounts, save files in Google Drive, and use learning sources from internet browsers. After receiving explanations from the teacher training, 90% of participants claimed that the applications were clear and understandable. Additionally, 80% of participants became skilled with the system of each application. As they became more skilled, 95% of participants were able to accomplish their desired tasks, and 90% found it easy to learn how to operate after receiving explanations and practice from the teacher training as Perceived Usefulness and Perceived Ease of Use are important factors

that influence technology acceptance [19]. Moreover, 95% of participants were able to interact with each other through email accounts created during the training.

These findings suggest that principals possess robust digital literacy capabilities. However, several factors could influence these results. The immediate effects of the teacher training might have significantly impacted the participants' reported ease of use and proficiency, which may not reflect long-term capabilities. Participants' prior experiences with digital tools could have also influenced the results; those with more experience might have found it easier to become proficient, while those with less experience might have struggled more, even if the training temporarily boosted their skills.

Furthermore, despite these positive findings, 5% of participants exerted low mental effort in using the system, which was influenced by their age. These participants preferred to ask for assistance with operational necessities [20]. Age has been identified as a significant factor affecting technology use by teachers, as Iranian teachers with more experience tend to use technology less frequently [21]. In contrast, teachers from the millennial era have better understanding and ability to use technology, and they are more accepting of technological progress [22]. Furthermore, all participants demanded much care and attention from the system, as they all had their own computers. This highlighted the importance of providing adequate facilities to integrate education and technology to improve the quality of education. Appropriate technology policies and perceived institutional support have been found to influence technology use by teachers/principals [23]. However, teachers may not be able to apply technology in their teaching activities if their schools do not provide adequate facilities or if they lack experience in operating available technology [24].

After practicing with Microsoft Office, email, Google Drive, and internet browsers, 95% of the participants easily remembered how to use the systems. This was likely due to their prior experiences, as people tend to improve with practice. The success of integrating technology into language learning depends on various factors, including teachers' experience. Previous studies have shown that experience can positively influence technology use, but it can also hinder integration if teachers are not adequately trained on how to use technology for positive outcomes [23, 25].

Based on the above description, it can be concluded that elementary school principals in Cirebon and Kuningan, Indonesia are capable of effectively implementing digital literacy. They have demonstrated proficiency in operating various applications such as Microsoft Office (Word, Excel, and PowerPoint), creating email accounts, saving files in Google Drive, and using learning resources from internet browsers. These findings align with the results of the Technology Acceptance Model (TAM) analysis, which suggests that teachers (both pre- and in-service) generally accept technology well. However, the study also highlights the importance of certain intrinsic and extrinsic factors in technology acceptance, which contradicts some assumptions made about the TAM [26].

4 Conclusions

In conclusion, the findings of this study highlight the positive impact of technology integration on teaching strategies and the digital literacy capabilities of principals. However, challenges such as the age factor affecting mental effort in operating technology were identified. To address these challenges, it is recommended that educational institutions provide ongoing training and support for principals to enhance their digital literacy skills. Additionally, developing user-friendly interfaces and providing assistance through assistants can facilitate the effective use of technology in educational settings. Overall, preparing educators with adequate digital literacy skills is essential to ensure the successful integration of technology in education.

Future research should explore the long-term impact of these training programs and identify best practices for their implementation on a broader scale. By focusing on practical skills, providing ongoing support, considering age and experience, ensuring institutional support, incorporating feedback mechanisms, and addressing potential biases, digital literacy training programs can be improved to enhance the digital capabilities of principals, ultimately leading to better integration of technology in educational settings.

Acknowledgments

The authors would like to express their gratitude to all parties involved in the success of this research. The financial support and guidance from the Research Institute of Universitas Swadaya Gunung Jati were instrumental in the smooth progress and achievements of this project. We also extend our respect to the Rector of Universitas Swadaya Gunung Jati and the Dean of the Faculty of Education and Science UGJ for their opportunities and support. The contributions of all involved parties have provided a solid foundation for the completion of this research.

References

- [1] I. M. Adnyana, I. B. P. Arnyana, and I. G. Margunayasa, “Digital Phonics Literacy Media to Support the Initial Reading Skills of First-Grade Students in Multicultural Bilingual Schools,” *Jurnal Pendidikan Multikultural Indonesia*, vol. 6, no. 1, pp. 14–25, May 2023, doi: 10.23887/jpmu.v6i1.58838.
- [2] E. Sarva, G. Lāma, A. Oļesika, L. Daniela, and Z. Rubene, “Development of Education Field Student Digital Competences—Student and Stakeholders’ Perspective,” *Sustainability (Switzerland)*, vol. 15, no. 13, Jul. 2023, doi: 10.3390/su15139895.
- [3] S. Farias-Gaytan, I. Aguaded, and M. S. Ramirez-Montoya, “Transformation and digital literacy: Systematic literature mapping,” *Educ Inf Technol (Dordr)*, vol. 27, no. 2, pp. 1417–1437, Mar. 2022, doi: 10.1007/s10639-021-10624-x.
- [4] S. S. Khromov and N. A. Kameneva, “Отечественный и зарубежный опыт.”
- [5] S. O. Arshad, A. Graduate, B. School, and F. Noordin, “Career Adaptability and Intention To Leave Among Ict Professionals: An Exploratory Study,” 2013.
- [6] F. N. Hidayati, G. Giyoto, and L. Untari, “Management of digital literacy competence development in State Madrasah Aliyah Surakarta, Indonesia,” *INSANIA : Jurnal Pemikiran Alternatif Kependidikan*, vol. 28, no. 1, pp. 31–48, Jun. 2023, doi: 10.24090/insania.v28i1.7926.
- [7] Ukas *et al.*, “Digital Literacy on Information and Electronic Transactions in the Student Paradigm of SMAN 2 Koto Pariaman,” *Jurnal Pengabdian Masyarakat Bestari*, vol. 2, no. 5, pp. 419–428, May 2023, doi: 10.55927/jpmb.v2i5.4234.

-
- [8] P. Thapliyal, “Digital Literacy and Its Impact on the Inclination towards English Literature: An Analytical Study,” *Turkish Online Journal of Qualitative Inquiry*, 2023, doi: 10.52783/tojqi.v11i2.9993.
- [9] K. Aesaert and J. Van Braak, “Gender and socioeconomic related differences in performance based ICT competences,” *Comput Educ*, vol. 84, pp. 8–25, 2015, doi: 10.1016/j.compedu.2014.12.017.
- [10] M. T. da Rocha, A. G. V. Muñoz-Repiso, and E. Costa, “ICT Skills - Study concerning students from seventh to ninth grade in Viana do Castelo district,” *Journal of Information Systems Engineering and Management*, vol. 8, no. 2, 2023, doi: 10.55267/IADT.07.13229.
- [11] F. Zahrah and R. Dwiputra, “Digital Citizens: Efforts to Accelerate Digital Transformation,” *Jurnal Studi Kebijakan Publik*, vol. 2, no. 1, pp. 1–11, May 2023, doi: 10.21787/jskp.2.2023.1-11.
- [12] W. M. K. Wan Isa, M. Y. Mohd Nor, and J. L. Abdul Wahab, “Principal Change Facilitator Styles and the Effect on Teacher Technology Integration in School: A Literature Review,” *International Journal of Academic Research in Progressive Education and Development*, vol. 9, no. 3, Sep. 2020, doi: 10.6007/ijarped/v9-i3/7699.
- [13] D. Matsana, D. Negassa, Y. Seyoum, and A. Tekle, “Facilitators’ Engagement in Advocacy towards Inclusion of Adults with Disabilities in the Literacy Training Program in Gedeo Zone, Ethiopia,” *Educ Res Int*, vol. 2021, 2021, doi: 10.1155/2021/5353652.
- [14] F. Buitrago Flórez, R. Casallas, M. Hernández, A. Reyes, S. Restrepo, and G. Danies, “Changing a Generation’s Way of Thinking: Teaching Computational Thinking Through Programming,” *Rev Educ Res*, vol. 87, no. 4, pp. 834–860, Aug. 2017, doi: 10.3102/0034654317710096.
- [15] J. Mattar, C. C. Santos, and L. M. Cuque, “Analysis and Comparison of International Digital Competence Frameworks for Education,” *Educ Sci (Basel)*, vol. 12, no. 12, Dec. 2022, doi: 10.3390/educsci12120932.
- [16] L. L. Mariscal, M. R. Albarracin, F. D. Mobo, and A. L. Cutillas, “Pedagogical Competence Towards Technology-driven Instruction on Basic Education,” *International Journal of Multidisciplinary: Applied Business and Education Research*, vol. 4, no. 5, pp. 1567–1580, May 2023, doi: 10.11594/ijmaber.04.05.18.

-
- [17] F. Toma, A. Ardelean, C. Grădinaru, A. Nedelea, and D. C. Diaconu, “Effects of ICT Integration in Teaching Using Learning Activities,” *Sustainability (Switzerland)*, vol. 15, no. 8, Apr. 2023, doi: 10.3390/su15086885.
- [18] M. Á. García-Delgado, S. Rodríguez-Cano, V. Delgado-Benito, and M. Lozano-Álvarez, “Emerging Technologies and Their Link to Digital Competence in Teaching,” *Future Internet*, vol. 15, no. 4, Apr. 2023, doi: 10.3390/fi15040140.
- [19] S. Yutdhana and K. N. Kohler, “Technology Acceptance among English Pre-service Teachers: A Path Analysis Approach,” *English Language Teaching*, vol. 16, no. 6, p. 45, May 2023, doi: 10.5539/elt.v16n6p45.
- [20] A. Esfijani and B. E. Zamani, “Factors influencing teachers’ utilisation of ict: The role of in-service training courses and access,” *Research in Learning Technology*, vol. 28, pp. 1–16, 2020, doi: 10.25304/rlt.v28.2313.
- [21] J. K. Jacob, “teachers-perceptions-of-a-one-to-one-teacher-laptop-program-2iumkwznw2”.
- [22] R. Peng, R. A. Razak, and S. H. Halili, “Investigating the factors affecting ICT integration of in-service teachers in Henan Province, China: structural equation modeling,” *Humanit Soc Sci Commun*, vol. 10, no. 1, Dec. 2023, doi: 10.1057/s41599-023-01871-z.
- [23] C. K. Blackwell, A. R. Lauricella, and E. Wartella, “Factors influencing digital technology use in early childhood education,” *Comput Educ*, vol. 77, pp. 82–90, 2014, doi: 10.1016/j.compedu.2014.04.013.
- [24] A. M. Abunowara, “Using Technology in EFL/ESL Classroom,” 2014.
- [25] A. N. Çoklar and I. K. Yurdakul, “Technology Integration Experiences of Teachers,” *Discourse and Communication for Sustainable Education*, vol. 8, no. 1, pp. 19–31, Jun. 2017, doi: 10.1515/dcse-2017-0002.
- [26] R. Scherer, F. Siddiq, and J. Tondeur, “The technology acceptance model (TAM): A meta-analytic structural equation modeling approach to explaining teachers’ adoption of digital technology in education,” *Comput Educ*, vol. 128, pp. 13–35, Jan. 2019, doi: 10.1016/j.compedu.2018.09.009.

Laws of Gravitation and Motion in The Ancient Indian Texts

Jumisree Sarmah Pathak

*Department of Physics, Indian Institute of Teacher Education, Sector 15,
Gandhinagar 382016, Gujarat, India
Corresponding Author: jumishreep@iite.ac.in*

(Received 18-06-2024; Revised 29-07-2024; Accepted 30-07-2024)

Abstract

In this study, various verses from the Vedic Texts, which directly explains the fundamental laws of Gravitation and Motion in physical science are summarized. The correlation of each verse (mantra/ shloka) to the existing fundamental theory of Physical science shows the compatibility of Physical science with the Vedic Texts and we hope that the thorough analysis of all these ancient texts may open door to many probable insights to the undiscovered fundamental laws of basic science and its applications.

Keywords: Gravitation, Laws of Motion, Physical Science, Vaisheshika Sutra, Veda

1 Introduction

The theories of Physical Science have always been of utmost importance to humankind, as these laws have shaped the way human life has progressed over the years. The laws and theories of physical science have fundamentally influenced the advent of the technologies and the development of modern science [1].

Ancient Indian scriptures, such as the Vedas, Upanishads, and Puranas are known for their philosophical and spiritual insights, as well as observations about the natural world. In the Vedic Texts, everything in the universe is seen as interconnected and interdependent. Similarly, in Physical Sciences, the behavior and nature of the particles are interdependent, be it the particles of smaller dimension or the particles with larger dimensions. Another similarity between the two is their emphasis on the role of consciousness in shaping reality. In the texts pertaining to the Vedic period,



consciousness is believed to be the root of everything, including the creation of the universe. Similarly, in Physical Sciences, the act of observing a particle can change its behavior, suggesting that consciousness plays a role in shaping physical reality [2].

It is a significant observation on the part of the researcher is that the concepts underlying the theories of physical science are very much in agreement to the ideas expressed in the holy texts of ancient India, namely the Vedas, Upanishads, Puranas and other notable ancient Indian texts.

However, the fundamental concern that arises is that whether we can make any comparison between an exact science and spiritual ideas, which is the crux of Hindu philosophy. The authenticity of the translation of the verses of the ancient Indian Text that are written in the Sankrit language to the theories of Physical Science which are basically accepted in the English language worldwide is also a challenging task. The spiritual insights are often not completely expressible verbally, rather they pertain to some wonderful and amazing experiences of the inner self of a person. On the other hand, the theories of Physical Science are based on Experiments performed in the physical world. Often, mathematical equations are used to explain the outcomes of an experiment, which ultimately helps a scientist to formulate a theory. However, any scientific experiment is limited by different sources of error and there may arise the scope of an alternate explanation to the results of an experiment. In the words of Werner Heisenberg “every word or concept, clear as it may seem to be, has only a limited range of applicability.” While the intuitive element of a scientist comes handy for a researcher pursuing scientific research, the scientist prefers to follow the standard scientific method while navigating through his research. Similarly, the thoughts expressed in the verses of the ancient Indian texts are also governed by the quest for finding out the truth and to be able to give a rational explanation to the findings around us [3].

Not only the fundamental theories of Physical science, but also the key concepts behind the modern technologies developed by the scientists are already mentioned in Vedas, Puranas and Upanishads [4]. It is seen that these ancient texts contain many scientific truths, as explained by many scientists as well as spiritualists. However, even though the Vedic Texts contain so many scientific truths, the technology of Western world is proven to be more reachable to the masses as well as authenticated than that of

Eastern World. Most of the fundamental scientific discoveries are credited to the scientists of the Western countries. The underlying reason for this may be lack of awareness among the people to study the ancient texts carefully, analyze them, publish and authenticate the discoveries mentioned in the Vedic Texts. It is heartening to observe that over the last decade, more thorough studies of the Vedas and Upanishads are given importance to find answers to various unexplored and complex scenarios of the human life. Exploring the vast ancient Indian Texts can be extremely helpful in finding solutions to the complicated and unsolved situations of the world.

Keeping this objective in mind, in this paper, the correlation of the fundamental theories of motion and gravitation in Physical Science with reference to the mantras and shlokas of Vedic Texts are analyzed and presented.

2 Brief Outline of the Vedic Texts

Vedas and Upanishads

Vedic and Upanishadic thoughts are directed towards enquiry into the nature of truth. Not only that, the Vedas are also the discovery of truth, the laws of nature, the universe, and beings thus leading to ultimate truth (the enquiry into truth means the discrimination and determination of “real” and “unreal”). The Vedas are supposed to be “apauruseya granthi”, meaning not authored by man. These were revelations of the ultimate masters/sages while they were in deep meditation. The Vedas are believed to be the sacred scripture originated around 1500 to 500 BCE which originated through oral tradition passed down through generations as a Guru (Teacher)- Shishya (Student)- Parampara (Tradition). The word "Veda" comes from a Sanskrit word that with the meaning "knowledge". The Vedas are written in Classical Sanskrit language and are the oldest layer of Sanskrit literature. The four Vedas are Rigveda, Yajurveda, Samaveda, and Atharvaveda [5].

The Upanishads are the last component of the Vedas and are esoteric texts that emphasize philosophy and spiritualism. The word ‘Upanishad’ means "sit down carefully" which implies that the shishya should pay close attention to the Guru and memorize the verses. The Upanishads were written between 700 and 400 B.C.E in

Classical Sanskrit and convey religious teachings and ideas that are mostly based on philosophy [5].

The Vedas provide information about the origins of existence and one's reaction to it, while the Upanishads emphasize knowledge of the ultimate identity of all phenomena. The primary content in the Vedas are significant to the ritualistic details of worshipping the Gods/deities, while the Upanishads emphasize spiritualism and philosophy through the enchanting method of storytelling. The philosophical ideologies arising from the study of the Vedas and the Upanishads deal with going deeper into the understanding of reality, mind and the self. The study of these texts help an individual to hold a grasp of the way the universe functions based on observation and reasoning. Moreover, these studies help in the spiritual growth of an individual providing an excellent framework for moral comfort and intellectual courage [6].

Vaisheshika Sutra

The founder of the Vaisheshika school of Indian philosophy, Acharya Kanada, also known by the name Maharsi Kashyap, contributed a lot to the development of the earliest Indian Physics. During the 6th century B.C., he formulated the theory of atoms, which is considered to be the basis of the atomistic approach to Physics and Philosophy. The ideas put forwarded by Maharshi Kanada are collectively known as Vasisheshika Sutra or Aphorisms of Kanada. According to this great saint, the characteristics of all that can be conceptualized and hence named and defined in the world through comparison and contrast, is the science of Vaisheshika [7].

Maharshi Kanada was one of the earliest persons in the world to investigate the way atoms and molecules behave. He was the first saint who proposed that "Paramanu" (atoms) is an eternal particle of matter. Everything that is a part of the entire universe is consisting of "Paramanu" (atoms). He propounded that, when the matter is divided and subdivided till a stage is reached beyond which no division is possible, what remains is the "Pramanu" (atoms). According to him, this indivisible and indestructible "Paramanu" (atom) cannot be sensed through any human organ. However, the movement of the atoms is responsible for the effect of motion involving observables (matter), and Maharshi

Kanada offered a consistent framework for describing the motion involving physical entities in terms of certain laws [8].

Maharshi Kanada also gave the concept of biatomic molecules and triatomic molecules (“Dvyanuka” and “Tryanuka”) by stating that atoms of the same substance can be united with each other under certain conditions. He also gave the concept of chemical changes involving the atoms under certain factors such as heat, light or collisions.

The Vaisheshika sutra consists of 10 chapters with two sections each involving 370 sutras in total. The first chapter defines and discusses the three categories of substance, solid, liquid and gas, their attributes and their behaviours or actions. The second chapter describes the nine substances, while the third chapter deals with the self and the mind. The first part of the fourth chapter describes of the eternality of atoms and how sensory perception leads to acquisition of knowledge, while the second part of the fourth chapter deals with the composition of the physical bodies. The fifth chapter deals with actions involving the physical bodies, and the sixth chapter deals with the way of life that facilitates acquisition of knowledge. The seventh chapter explains the properties of atoms and further discusses the nature of ether, mind, space and time. The eighth and ninth chapters describe certain concepts psychology, like various types of cognition and negation, which contributes to the overall development of the personality. The tenth chapter discusses cause and effects of the actions of the physical entities under different conditions. Thus, the Vaisheshika Sutra encompasses a systematic exposition of principles and laws to describe the behaviour of the physical world [9].

Later many scholars came up with their own elaboration or explanation for the Vaisheshika Sutra. One of those scholars is Prashastada, who wrote two books namely ‘Padartha-dharma-sangraha’ (collection of [roperties of matter) and a commentary ‘Prasastaptada Bhasya’. In these texts, the properties of motion are discussed by Prashastada. ‘Prasastaptada Bhasya’ may also be considered as an independent compendium of the tenets of the Vaisheshika School of Philosophy [10].

3 Concepts of Gravitation in the Vedas

The natural phenomenon by which all things having a mass or energy are brought towards each other is known as gravity or gravitation. Gravity is the reason why the

universe exists. Gravitational force or gravitational interaction is one of the four fundamental force or interaction, and is the weakest of them all. That is why gravity has no significant influence at the level of subatomic particles, but it is the most significant interaction between objects at the macroscopic scale. Thus, gravity determines the motion of planets, stars, galaxies, and even light. The famous scientist Sir Isaac Newton is credited with the discovery of the fundamental law of Gravitation, which he explained in his ground-breaking book called *Philosophiæ Naturalis Principia Mathematica* (Mathematical Principles of Natural Philosophy). In this book, Newton described gravitation as a universal force, and claimed that "the forces which keep the planets in their orbits must be reciprocally proportional as the squares of their distances from the centers about which they revolve." [11]

In this section, we have correlated and summarize the laws of Gravitation, which are mentioned in the holy Vedas.

Table 1. Laws of Gravitation as mentioned in the holy Vedas.

Veda Mantra	Meaning
<p>1) Rig Veda 2.11.20</p> <p>अस्य सुवानस्य मन्दिनस्त्रितस्य न्यर्बुदं वावृधानो अस्तः । अवर्तयत्सूर्यो न चक्रं भिनद्धलमिन्द्रो अङ्गिरस्वान् ॥</p>	<p>“Indra had destroyed Arbud by attaining progress by the trita, who was pleased and squeezing the som. Just as the Sun moves the wheel of his chariot forward, Indra, with the help of the angiras, wielded his vajra and destroyed the force.”</p> <p>“The sun rotates like a wheel on its axis and the existence of the solar system is due to the Gravitational law of attraction and Gravitational force.” [12]</p>
<p>2) Rig Veda 10.149.1</p> <p>सविता युन्तैः पृथिवीमरम्णादस्कम्भुने सविता द्यामदंहत् ।</p>	<p>“The sun has bonded the Earth and other planets through attraction and moves them around itself as if a trainer moves newly</p>

<p>अश्वमिवाधुक्षुद्धुनिमन्तरिक्षमूर्ते संविता समुद्रम् ॥</p>	<p>बद्धं trained horses around itself holding their reins.” [12] “As a trainer moves the horse around him in circle by holding their reins, similarly Earth revolves around the Sun in an orbit, with the Sun at the centre. Similar to the rein of horse, there is a force of attraction between the Earth and the Sun, which is known as gravitational force, which allows Earth to revolve around it. The same sun is also the reason why humans enjoy the rain.”</p>
<p>3) Rigveda 10.22.14 अहस्ता यदपदी वर्धत क्षाः शचीभिर्वेद्यानाम् I शुष्णं परि प्रदक्षिणिद् विश्वायवे नि शिशन्थाः II</p>	<p>"This earth does not have hands and legs, still it can move ahead. It moves around the sun. All the objects on the Earth also move along with it." [12] “Earth revolves around the Sun.”</p>
<p>4) Rigveda 1.35.9 हिरण्यपाणिः सविता विचर्षणिरुभे द्यावापृथिवी अन्तरीयते । अपामीवां बाधते वेति सूर्यमभि कृष्णेन रजसा द्यामृणोति ॥</p>	<p>“The Savita (light energy), with its hands of gold Savitā travels between the heaven and earth, while connecting everything together, diminishes diseases, approaches the sun, and overspreads the sky with brilliant radiance.” [12] “Sun orbits in its orbit in the galaxy, holding earth and other heavenly bodies in such a manner that they do not collide with each other by the force of attraction.”</p>

<p>5) Rig Veda 8.12.28</p> <p>यदा ते हर्यता हरी वावृधाते दिवेदिवे । आदिते विश्वा भुवनानि येमिरे ॥</p>	<p>“When your beloved horses had augmented day by day, then all existent beings were subject unto you.” [12]</p> <p>“The glorious sun, by putting forth his powerful rays, which possess the properties of attraction, illumination and motion, keeps all the worlds in order through the force of his attraction.”</p>
<p>6) Rig Veda 8.12.30</p> <p>यदा सूर्यममुं दिवि शुक्रं ज्योतिरधारयः । आदिते विश्वा भुवनानि येमिरे ॥</p>	<p>“O God! You have created this Sun, which possess infinite power. You are uploading the Sun and the other spheres (planets) and you render them steadfast by your power of attraction.” [12]</p>
<p>7) Rig Veda 1.164.13</p> <p>पञ्चारे चक्रे परिवर्तमाने तस्मिन्ना तस्थुर्भुवनानि विश्वा । तस्य नाक्षस्तप्यते भूरिभारः सनादेव न शीर्यते सनाभिः ॥</p>	<p>“All beings abide in this five-spoked revolving wheel; the heavily-loaded axle is never heated; its eternal compact navel is never worn away.” [12]</p> <p>“Sun moves in its orbit which itself is moving. Earth and other bodies move around sun due to force of attraction, because sun is heavier than them.”</p>
<p>8) Rigveda 5.81.4</p> <p>उत यांसि सवित्स्त्रीणि रोचनोत सूर्यस्य रश्मिभिः समुच्यसि । उत रात्रीमुभयतः परीयस उत मित्रो भवसि देव धर्मभिः ॥</p>	<p>“Either you traverse, Savitā (light), the three regions, or combine with the rays of Sūrya (sun); or you pass between the night on either hand; or you, divine Savitā are Mitra, through your benevolent functions.” [12]</p> <p>“The gravitational effect of solar system makes the earth stable. The axle of the</p>

	Earth does not get rusted, the Earth continues to revolve on its axle.”
9) Atharvaveda 4.11.1 अ॒न॒ड्वान्दा॑धार पृथि॒वीमु॒त द्या॒मन॑ड्वान् दा॒धारो॑र्वन्तरि॒क्षम् । अ॒न॒ड्वान् दा॒धार प्र॑दिशः षडु॒वीर॑न॒ड्वान् विश्व॑भुवनमाविवेश ॥	“God (Sun) has held the Earth and other planets, the way a bull pulls a cart.” [13]
10) Yajurveda 33.43 आ कृ॒ष्णेन॑ रज॑सा॒ वर्त्त॑मानो निवेशय॑न्नमृ॒तं मर्त्यं॑ च । हि॒र॒ण्यये॑न सवि॒ता रथे॑ना दे॒वो या॑ति भु॒व॒नानि॑ पश्य॑न् ॥	“The sun moves in its own orbit in space taking along with itself the mortal bodies like earth through force of attraction.” [14]

4 Concepts of Gravitation in the Vedas

Sir Isaac Newton, who is credited with the three fundamental laws of motion involving all physical bodies, are the basis of understanding how a force acts on a physical object and how different bodies in motion interact among themselves. Newton’s first law states that “Every object will remain at rest or in uniform motion in a straight line unless compelled to change its state by the action of an external force.” This tendency to resist changes in termed as ‘inertia’. If all the external forces cancel each other out, then there is no net force acting on the object. If there is no net force acting on the object, then the object will maintain a constant velocity. Newton’s second law states that “The acceleration of an object depends on the mass of the object and the amount of force applied.” This law defines a force to be equal to change in momentum (mass times velocity) per change in time. Newton’s third law states that “For every action in nature there is an equal and opposite reaction.” Whenever one object exerts a force on a second

object, the second object exerts an equal and opposite force on the first. In other words, forces result from interactions [11].

Hence the idea of inertia, acceleration and force are of utmost importance for the understanding of any theory or experiment involving mechanics. The concept of acceleration is identified as the basic building blocks of scientific theories that are highly successful in explaining and predicting observable phenomena. The ability to apply this concept correctly is an essential prerequisite for any scientific work [15].

In this section, the researcher has summarised the laws of motion as mentioned in the Vaisheshika Sutra.

Table 2. Laws of Motion as mentioned in Vaisheshika Sutra.

1) Vaisheshika Sutra 1.1.11 कर्म कर्मसाध्यं न विद्यते॥ [10] [16]	“From motion, new motion is not known”.
2) Vaisheshika Sutra 1.2.1 कारणाभावात्कार्याभावः [10] [16]	“In the absence of cause, there is an absence of effect (motion).”
3) Vaisheshika Sutra 5.2.7 संयोगाभावे गुरुत्वात् पतनम् [10] [16]	“In the absence of conjunction, gravity causes objects to fall.”
4) Vaisheshika Sutra 1.2.7 सदिति यतोद्रव्यगुणकर्मसु सा सत्ता ॥ [10] [16]	“Existence is self-defined. Thus, substance, attribute, and motion are potential (sattā)”.
5) Vaisheshika Sutra 5.2.8 नोदनविशेषाभावान्नोर्ध्वं न तिर्यग्गमनम् [10] [16]	“In the absence of a force, there is no upward motion, sideward motion or motion in general.”
6) Vaisheshika Sutra 5.2.17 नोदनादाद्यमिषोः कर्म तत्कर्मकारिताच्च संस्कारादुत्तरं तथोत्तरमुत्तरञ्च	“The initial pressure on the bow leads to the arrow’s motion; from that motion can have momentum, from

[10] [16]	which is the motion that follows and the next and so on.”
7) Vaisheshika Sutra 1.2.14 कार्यविरोधि कर्म [10] [16]	“Action (kārya) is opposed by reaction (karman).”
8) Praśastapāda Bhāṣya, (a commentary on Vaisheshika Sutra) वेगः निमित्तविशेषात् कर्मणो जायते [10] [16] [17]	“The change of motion is due to applied force.”
9) Praśastapāda Bhāṣya, (a commentary on Vaisheshika Sutra) वेग निमित्तापेक्षात् कर्मणो जायते नियत्दिक् क्रिया प्रबंध हेतु [10] [16] [17]	“The change of motion is proportional to the motive force impressed and is made in the direction of the right line in which the force is impressed.”
10) Praśastapāda Bhāṣya, (a commentary on Vaisheshika Sutra) वेगः संयोगविशेषाविरोधी [10] [16] [17]	“To every action there is always an equal and opposite reaction.”

5 Conclusions

Vedas are often mentioned as Anadi and Sanatana, which means Vedas are eternal and has no beginning and end. Further, it is a fact that Vedas were revealed to the world at the very ancient period of time, by the great Rishis of our Nation. Hence, these Rishis are often called as Mantra Drushta, i.e. who has seen the Vedic Mantra and not as Mantra Karta i.e. the creator of Veda Mantra. This is because Veda Mantra is in subtle form and these Rishis realised and experienced them through their penance and for the benefit of mankind, they revealed them to the world. Thus, even at the remotest antiquity itself, our Rishis clearly explained the cosmology and the process of creation of our Universe in a

better and complete manner. Hence, these Rishis can be called as Rishi Scientists. Thus, all these narrations clearly prove the greatness of our Nation and our ancestor's admirable and adorable high knowledge and wisdom. An analysis and thorough study of all these ancient texts can surely open door to many insights to the yet undiscovered fundamental laws of physical science and its applications.

References

- [1] F. Capra, *The Tao of Physics: An Exploration of the Parallels Between Modern Physics and Eastern Mysticism*. Shambala Publication, Inc., Boston, Massachusetts, 1975.
- [2] J. D. Barrow, *The World within the World*, Oxford University Press, Oxford, 1990.
- [3] R.P. Brennan, *Heisenberg Probably Slept Here, The Lives, Times, and Ideas of the Great Physicists of the 20th Century*, John Wiley and Sons, Inc, 1996.
- [4] S.R. Verma, "Physics: An Integral Part of Vedic Wisdom", *Veda Vidya*, Vol 24, pp 184-188, 2014.
- [5] N. D. Sharma, "On the Concept of Space-Time and Consciousness: Some Western and Indic Thoughts", *Journal of Consciousness Exploration & Research*, Vol 9, No 4, pp 328-349, 2018.
- [6] WJEC A Level: Religious Studies "Nature and Significance of the Upanishads," https://resource.download.wjec.co.uk/vtc/2018-19/18-19_2-16/WJEC%20Unit%203E%20Hinduism%20Theme%201A.pdf [accessed on 10th June, 2024]
- [7] D. Chakravarty, *Vaisesika Sutra of Kanada*, D. K. Printworld (P) Ltd., New Delhi, 2003.
- [8] S. Kak, *Indian Physics: Outline of Early History*; arXiv: physics/0310001, 2003
- [9] S. Kak, *Kaṇāda, Great Physicist and Sage of Antiquity*, 2018 <https://subhashkak.medium.com/ka%E1%B9%87%C4%81da-the-great-physicist-and-sage-of-antiquity-5a2abd79b6f>, [accessed on June 10th, 2024]
- [10] V. P. Dwivedi (Ed), *The Prasastapada Bhasya with commentary, Nyayakandali of Shridhara*, Sri Satguru Publications, India, 1985.

- [11] B. Cohen. A Guide to Newton's "*Principia. The Principia: mathematical principles of natural philosophy*" By Newton, Isaac. Translated by I. Bernard Cohen. University of California Press, 1999 (1687)
- [12] <https://www.wisdomlib.org/hinduism/book/rig-veda-english-translation> (accessed on June 10th, 2024)
- [13] G. Sharma, *Atharva Veda*, Sanskrit Sahitya Prakashan, New Delhi, 2015.
- [14] <https://xn--j2b3a4c.com/yajurveda/33/43> [accessed on June 10th, 2024]
- [15] T. Sarkim, "Misconceptions about Acceleration among Prospective Physics Teacher: The Importance of Discussion of Acceleration as a Vector Quantity", *International Journal of Applied Sciences and Smart Technologies*, Vol 6, Issue 1, pp 41-52, 2024.
- [16] <https://subhashkak.medium.com/ka%E1%B9%87%C4%81da-the-great-physicist-and-sage-of-antiquity-5a2abd79b6f1> (accessed on June 10th, 2024)
- [17] www.puranavedas.com/vedic-physics (accessed on June 10th, 2024)

This page intentionally left blank

Red Wine Classification Using SVM and RBF Kernel

Kevin Silvanus Hutabarat ^{1*}, Rosalia Arum Kumalasanti¹

¹*Department of Informatics, Faculty of Science and Technology, Sanata
Dharma University, Yogyakarta, Indonesia*

Corresponding Author: kevinilvanus@gmail.com

(Received 27-10-2023; Revised 27-06-2024; Accepted 01-08-2024)

Abstract

Today's cultural diversity has influenced lifestyle, especially at the time of certain events. Food and drink are important in the event. Quality food is a key ingredient in a person's eating. Red wine is one of the most popular beverages in the West because of its cold climate but today Red wine has become a popular drink not only among Western countries. The love of red wine should also be balanced with his knowledge of the quality of the beverage because it has various variations. The duration of fermentation and the materials used will give different quality products. Nowadays technology is present to provide solutions to these problems by using the SVM algorithm on Machine Learning. The approach is carried out by performing several experiments to obtain optimal evaluation results. The study has achieved accuracy of 90.93%, precision of 72.5% and recall of 61.70%.

Keywords: SVM, machine learning, accuracy, precision, recall

1 Introduction

The recent cultural diversity has influenced people's lifestyles, especially in celebrating certain events. The event usually has a companion dish which is the main attraction in enlivening the event. Often classy dishes and drinks become a specific value at the event. One drink that is often served at certain events is "anggur merah" or red wine. Red Wine is an alcoholic drink made from red grapes which undergoes a fermentation process. The fermentation process here is the process of dipping the grape skins and seeds into the squeezed fruit juice and letting it sit for some time [1]. Red Wine is a drink that is commonly consumed in western countries, because the climate conditions are very cold so this drink is quite popular there.



In fact, Red Wine is already quite popular apart from in western countries, but not all Red Wine fans know the quality of this drink. The length of time during the fermentation process will provide different variations in alcohol levels and this will affect the quality of each Red Wine. Until now, Red Wine has various variants and this drink still has many fans. The number of variants, the various quality produced. Red Wine Producers can of course easily determine the quality of the Red Wine to be produced, but consumers must also know that choosing a Red Wine variant based on quality will also be a very important thing to know before buying.

In determining the quality of Red Wine, the current technology is here to provide convenience in determining quality. It's well known that producing wine is an age-old craft that necessitates in depth understanding of the circumstances and ingredients that a wine may contain. Since wine consumption has increased across the board throughout the epidemic, wineries should look into less expensive ways to improve wine quality [2].

One method that is quite popular today is Machine Learning. Machine Learning is a sub-field of artificial intelligence which is still frequently used today. Machine Learning enables software applications to be more accurate in predicting outcomes without being explicitly programmed. One of the Machine Learning algorithms that is often used for classification is SVM. SVM (Support Vector Machine) is one of the Machine Learning algorithms used for classification and regression. The primary objective of SVM in classification tasks is to find the best line or hyperplane that can separate two different data classes as best as possible. The SVM was used by a team of researchers to identify the quality of red wine with an accuracy of 87.5% [1]. Other research has also been done by comparing the Naïve Bayes algorithm with the SVM in classifying wine. These studies yield significant results with fairly good accuracy [3].

The SVM on this study will be used to classify the quality of red wine by setting the correct parameters. It is hoped that SVM can provide optimal accuracy results in classifying red wine by quality, so that red wine lovers can use it in balancing quality before deciding to buy.

SVM is an algorithm to help classify data. Classification is a process involving the creation of models that can be used to predict a class or category of an object based on a set of attributes or features given. The aim is to generalize patterns from training data that

are known as class labels on new data that does not have labels [4] In the process of classification, there are several concepts that need to be understood:

Data Training: Data sets used to train classification models. Each example in this data set has an attribute or feature that is associated with a known class label.

Testing: Once the classification model is built, the next step is to test the model using test data that has never been used before. Test data to measure model performance in predicting classes of unknown objects. The evaluation results of accuracy, precision, and recall are used to evaluate the performance of the classification model.

2 Material and Methods

Red Wine Data Set

Based on experiments, it is noticed that the majority of the chemical components used in the manufacture of wine are the same for different wines, and that the influence or concentration of each grade of chemical composition varies depending on the kind of wine. The objective of this case study was to forecast a wine's quality based on feature sets that were provided as inputs and output rating scale ranging from 0 to 10. With regard to red wine, the quality is measured on a scale with values of [3,4,5,6,7,8]. The quality gets better as the scale value increases (3 = lowest and 8 = highest) [2]

Preprocessing

Preprocessing is a set of steps that must be taken before applying data analysis methods or building models. The goal is to prepare the data in accordance with the requirements of the algorithm to be used, as well as maximize the quality of the analysis to be performed [5].

Kernel Function

The kernel on SVM is one of the key concepts that enables SVM to deal with nonlinear problems effectively. The kernel functions on the SVM perform the transformation of data from the original feature space to the higher feature space. There are several common types of kernels that are often used in SVM, such as [4]:

- **Linear Kernel:** is the simplest kernel and only performs linear mapping of data into the same feature space.
- **Polynomial Kernel:** This kernel carries data into a higher feature space using a polynomic function.
- **Radial Base Function (RBF) Kernel:** This kernel is very commonly used to mapp data into an unlimited feature space using the Gauss function. Gamma parameters need to be set to control how sharply the function of the kernel decreases.
- **Sigmoid Kernel:** This kernel also performs nonlinear transformations and is used in some special cases.
- **Custom Kernels:** In addition to the above-mentioned kernels, there are also specific custom kernels to customize classification/regression tasks.

Support Vector Machine

SVM is a powerful and well-known classification method that operates on the principles of optimization theory and utilizes kernel function. When there are fewer training samples available and the image is represented in more spectral bands, SVM has been shown to be more effective classification tool [6] [7]. SVM is a technique for making predictions, both in the case of regression and classification. The SVM technique is used to obtain an optimal hyperplane to separate observations that have different target variable values [8]. Hyperplane visualization can be seen in Fig. 1 where there are two classes separated by hyperplane lines. The best separator between the two classes can be found by measuring the margin and looking for the maximum point. Margin is the distance between the hyperplane and the closest pattern of each class. The nearest pattern is called a support vector.

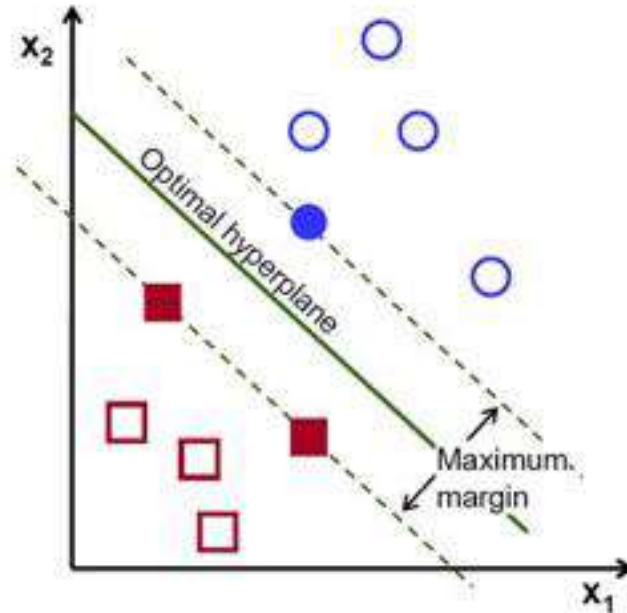


Figure 1. Visualization of discrimination [4].

Hyperplane can be searched using the following equation:

$$W \cdot X_i + b = 0 \tag{1}$$

Where:

W: Weight of vector

X_i: Value of attribute

B: Bias

In this equation there are two classes: positive class and negative class. There are patterns that are members of these two classes. Positive and negative classes can be obtained from the following equations:

$$W \cdot X_i + b \geq +1 \text{ if } y_i = +1 \tag{2}$$

$$W \cdot X_i + b \leq -1, \text{ if } y_i = -1 \tag{3}$$

In obtaining the best hyperplane is by maximizing the margin or distance between two sets of objects of each class.

Confusion Matrix

The confusion matrix is very useful for analyzing the quality of the classifier in recognizing the tuples of existing classes. In the evaluation process of classification there are four possibilities that occur from the classification process. The result of binary classification on a dataset can be represented in Table 1 below.

Table 1. Binary classification on a dataset.

Prediction	Actual		
	Class	Positive	Negative
	Positive	True Positive	False Negative
Negative	False Positive	True Negative	

There are several common formulas used to calculate the performance of classification, namely:

$$Accuracy = \frac{TP+TN}{TP+FP+TN+FN} \tag{4}$$

$$Precision = \frac{True\ Positive}{True\ Positive+False\ Positive} \tag{5}$$

$$Recall = \frac{True\ Positive}{True\ Positive+False\ Negative} \tag{6}$$

This study goes through several stages and is the steps that will be taken to obtain optimal results. The results can be seen in Fig. 2 below.

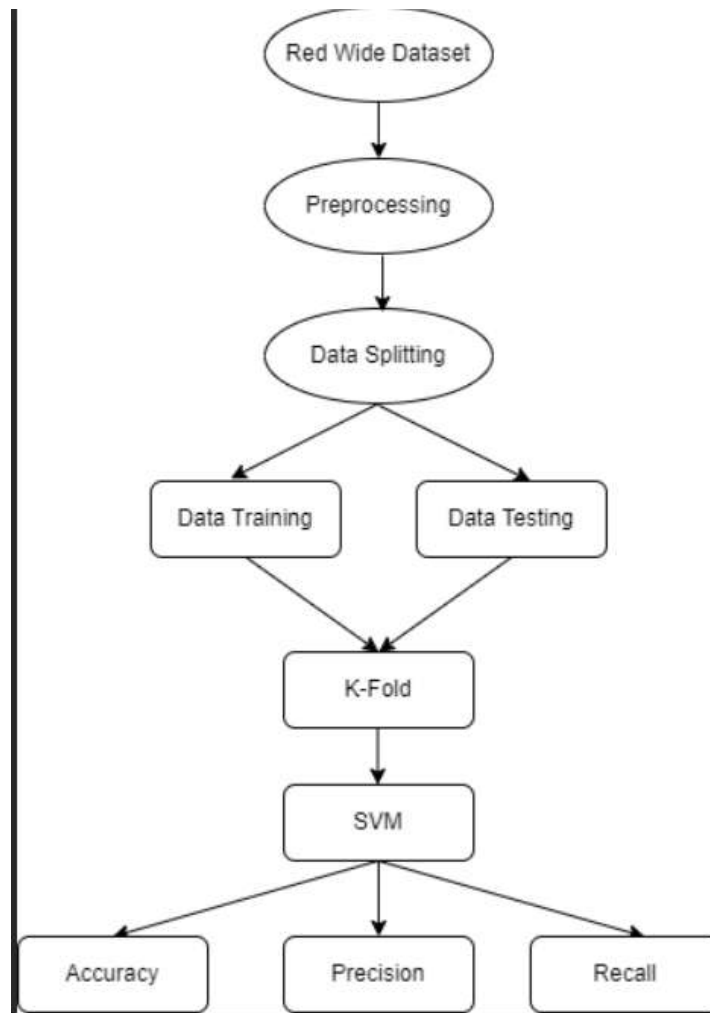


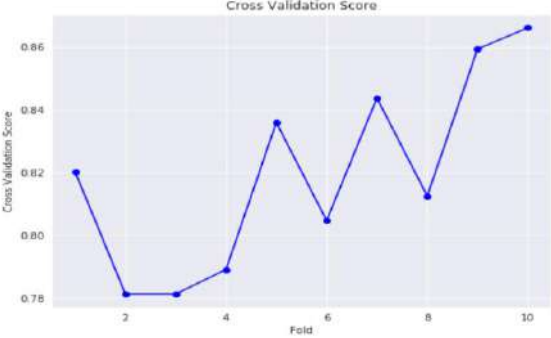
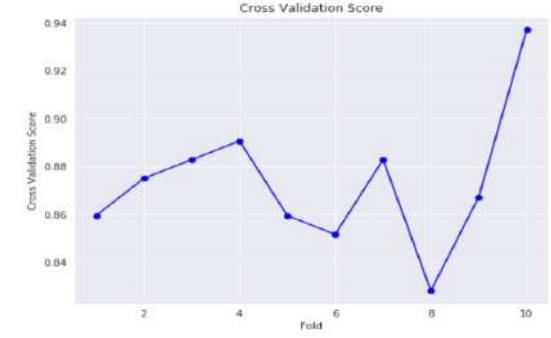
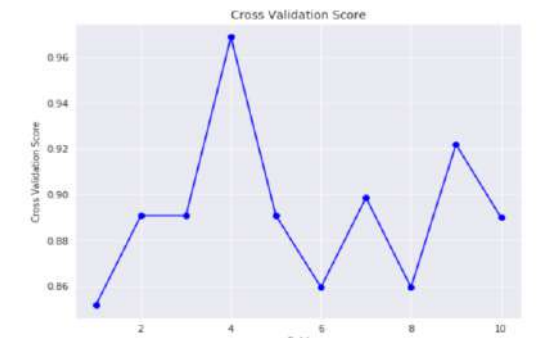
Figure 2. Flow of Research

3 Results and Discussions

The study used a data set of Red Wine with 12 attributes namely solid acid, volatile acid, citric acid, residual sugar, chloride, free sulfur, total sulfur dioxide, density, pH, sulfate, alcohol and quality. The quality limit for red wines that have good quality is with the label 2-6, while the bad quality is 7-8 on the label.

SVM offers several kernels to use, so in this study it is necessary to compare several nuclei to get optimal results. The sigmoid, polynomial and RBF kernels have been made and can be seen in Table 2 below.

Table 2. SVM’s Kernel

<p style="text-align: center;">Kernel Sigmoid</p>  <table border="1" data-bbox="347 376 900 712"> <caption>Kernel Sigmoid Cross Validation Score Data</caption> <thead> <tr> <th>Fold</th> <th>Cross Validation Score</th> </tr> </thead> <tbody> <tr><td>1</td><td>0.82</td></tr> <tr><td>2</td><td>0.78</td></tr> <tr><td>3</td><td>0.78</td></tr> <tr><td>4</td><td>0.79</td></tr> <tr><td>5</td><td>0.835</td></tr> <tr><td>6</td><td>0.805</td></tr> <tr><td>7</td><td>0.845</td></tr> <tr><td>8</td><td>0.815</td></tr> <tr><td>10</td><td>0.86</td></tr> </tbody> </table>	Fold	Cross Validation Score	1	0.82	2	0.78	3	0.78	4	0.79	5	0.835	6	0.805	7	0.845	8	0.815	10	0.86	<p>Accuracy: 85.3 Precision: 50.0 Recall :59.57</p>		
Fold	Cross Validation Score																						
1	0.82																						
2	0.78																						
3	0.78																						
4	0.79																						
5	0.835																						
6	0.805																						
7	0.845																						
8	0.815																						
10	0.86																						
<p style="text-align: center;">Kernel Polynomial</p>  <table border="1" data-bbox="347 795 900 1131"> <caption>Kernel Polynomial Cross Validation Score Data</caption> <thead> <tr> <th>Fold</th> <th>Cross Validation Score</th> </tr> </thead> <tbody> <tr><td>1</td><td>0.86</td></tr> <tr><td>2</td><td>0.875</td></tr> <tr><td>3</td><td>0.885</td></tr> <tr><td>4</td><td>0.89</td></tr> <tr><td>5</td><td>0.86</td></tr> <tr><td>6</td><td>0.85</td></tr> <tr><td>7</td><td>0.885</td></tr> <tr><td>8</td><td>0.83</td></tr> <tr><td>10</td><td>0.935</td></tr> </tbody> </table>	Fold	Cross Validation Score	1	0.86	2	0.875	3	0.885	4	0.89	5	0.86	6	0.85	7	0.885	8	0.83	10	0.935	<p>Accuracy : 90.93 Precision : 72.5 Recall :61.7</p>		
Fold	Cross Validation Score																						
1	0.86																						
2	0.875																						
3	0.885																						
4	0.89																						
5	0.86																						
6	0.85																						
7	0.885																						
8	0.83																						
10	0.935																						
<p style="text-align: center;">Kernel RBF</p>  <table border="1" data-bbox="347 1214 900 1550"> <caption>Kernel RBF Cross Validation Score Data</caption> <thead> <tr> <th>Fold</th> <th>Cross Validation Score</th> </tr> </thead> <tbody> <tr><td>1</td><td>0.85</td></tr> <tr><td>2</td><td>0.89</td></tr> <tr><td>3</td><td>0.89</td></tr> <tr><td>4</td><td>0.965</td></tr> <tr><td>5</td><td>0.89</td></tr> <tr><td>6</td><td>0.86</td></tr> <tr><td>7</td><td>0.895</td></tr> <tr><td>8</td><td>0.86</td></tr> <tr><td>9</td><td>0.92</td></tr> <tr><td>10</td><td>0.89</td></tr> </tbody> </table>	Fold	Cross Validation Score	1	0.85	2	0.89	3	0.89	4	0.965	5	0.89	6	0.86	7	0.895	8	0.86	9	0.92	10	0.89	<p>Accuracy :90.93 Precision : 72.5 Recall : 61.70</p>
Fold	Cross Validation Score																						
1	0.85																						
2	0.89																						
3	0.89																						
4	0.965																						
5	0.89																						
6	0.86																						
7	0.895																						
8	0.86																						
9	0.92																						
10	0.89																						

This research also carries out several approaches by processing cost parameters to obtain optimal results. The cost experiment can be seen in Fig. 3 below.

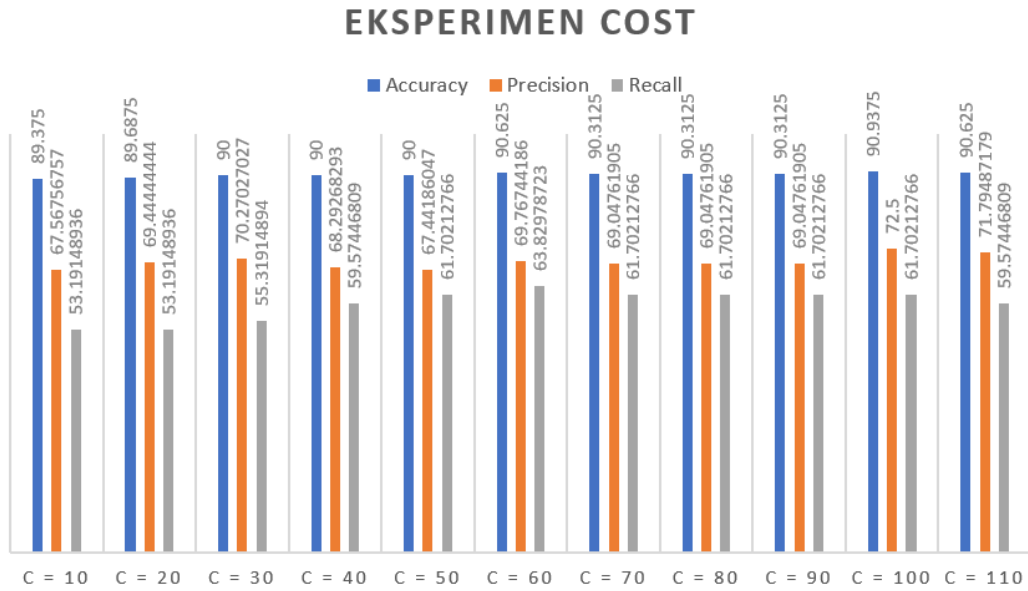


Figure 3. Experimental cost graph

After performing the fitting classifier then the next step is to determine the most optimal K-Fold Cross Validation by performing several K values experiments. K-fold cross validation is a model validation technique commonly used in machine learning. Experiments to obtain the best K value have been carried out ranging from K=1 to K=11 and in can K=10 the most optimal. The experiment can be seen in Fig. 4 below.

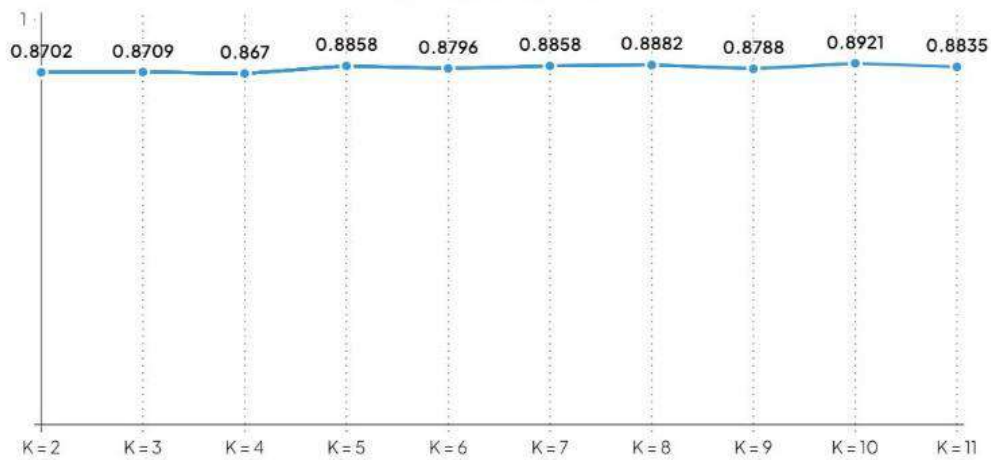


Figure 4. K-fold experiment

4 Conclusions

This research has been carried out using the SVM approach and some parameters in it. The most important parameters are cost, tolerance, gamma and degree. The Radial Basic Function (RBF) kernel gets the most optimal outcomes compared to other kernels. The evaluation results showed that optimum accuracy was achieved at 90.93%, precision at 72.5% and recall at 61.70%.

Acknowledgements

The work is supported by the Faculty of Science Technology, University Sanata Dharma.

References

- [1] M. R. Kushalatha, P. Rachana, P. Sameep and S. B. Shreesha, "Machine Learning Approach for Attribute Identification and Quality Prediction of Red Wine," *An International Open Access*, vol. 9, no. 4, pp. 4906-4910, 2021.
- [2] A. C. Benjamin, "Wine Quality Classification Using Machine Learning Algorithms," *International Journal of Computer Applications Technology and Research*, vol. 11, no. 6, pp. 241-246, 2022.
- [3] M. Aslam, "Wine Quality Prediction By using Machine Learning Algorithms," *Global Scientific*, vol. 10, no. 12, pp. 631-649, 2022.
- [4] G. Bonaccorso, *Machine Learning Algorithms*, Brimingham: Packt, 2018.
- [5] C. M. Andreas and S. Guide, *Machine Learning With Python*, USA: O'reilly, 2018.
- [6] B. N. Ramya, S. Adithi and R. Kruthika, "Study on Red Wine Quality Detection Using Machine Learning," *International Journal of Research Publication and Reviews*, vol. 4, no. 12, pp. 1579-1587, 2023.
- [7] A. G. Bhavya, "Wine Quality Prediction Using Different Machine Learning Techniques," *International Journal of Science Engineering and Technology*, vol. 8, no. 4, pp. 1-6, 2020.
- [8] D. Haroon, *Python Machine Learning Case Studies*, Karachi, Pakistan: Apress, 2017.

Recent Developments in The Influencing Variables of Hydrodistillation for Enhancing Essential Oil Yields in Indonesia: A Brief Review

Awaly Ilham Dewantoro^{1,2}, Alvita Rahma Alifia², Tanti Handini², Latifah Zainul Qolbi², Dita Amelia Ihsani²,
Desy Nurliasari^{2*}

¹ *Postgraduated Students in Technology of Agro-Industry, Faculty of Agro-Industrial Technology, Universitas Padjadjaran, Jatinangor, Indonesia*

² *Department of Agricultural Industrial Technology, Faculty of Agro-Industrial Technology, Universitas Padjadjaran, Jatinangor, Indonesia*

**Corresponding Author: desy.nurliasari@unpad.ac.id*

(Received 17-07-2024; Revised 04-08-2024; Accepted 06-08-2024)

Abstract

Hydrodistillation is widely known as the simplest essential oils (EOs) isolation technique and is widely used by small-scale producers, such as in Indonesia. The main characteristic of hydrodistillation is the plant-source material of EOs soaked in water, followed by boiling and diffusion. Various problems arise from the use of hydrodistillation, including the possibility of overheating, degradation of EOs because of the long heating time, difficulty in controlling the heat, and a slow process. The aim of this study was to review the recent developments in hydrodistillation technology that have been developed in Indonesia to improve the quality and yield of EOs. Bibliometric analysis through the Methodi Ordinatio was used to compile a systematic review of prior studies in the recent decade regarding the application of hydrodistillation in Indonesia. The results showed that five plant-source commodities were extensively isolated consisting of citrus, lemongrass, cinnamon, nutmeg, and ginger. Furthermore, this study investigated the variables that influence the hydrodistillation process for EOs isolation. The variables were often evaluated according to the results are distillation time, pretreatment of raw materials, feed-to-solvent ratio, particle size, growth place, and plant developmental stage. A future perspective was considered and outlined to be carried out further novel study and development strategies.

Keywords: Bibliometric analysis, Hydrodistillation, Plant commodities, Process variables, Pretreatment.



1 Introduction

Essential oils (EOs) are one of the leading agro-industrial commodities with increasing demand each year. This is reinforced by the fact that worldwide EOs production has increased from 150 thousand tons to 370 thousand tons in the period of 2007-2020 [1]. Indonesia is the third largest EOs producer after China and India [2]. Despite its considerable market share, the quality of Indonesian EOs remains mediocre because of simple isolation and purification technology. This drives the evaluation of EOs isolation technologies, particularly in developing simple technologies that are suitable for developing countries, such as Indonesia. One simple technology that is widely applied in developing countries is hydrodistillation, which has been widely applied globally by micro- and small-scale producers [3].

Hydrodistillation, similar to common distillation, proceeds by evaporating the EOs content of the plant cells, which is then cooled (condensed) to separate it from water [4]. The main characteristic of employing hydrodistillation, compared to other techniques, is that the source of the material is soaked in water, followed by boiling and diffusion of the material [5,6]. This technology is concerned with isolating EOs from highly soluble materials in water, and is susceptible to damage by heat. However, hydrodistillation has several problems, including the possibility of overheating, degradation of essential oils because of the long heating and distillation time, difficulty in controlling the heat, and a slow process [7]. This phenomenon requires further investigation to resolve problems and enhance the hydrodistillation performance and the quality of EOs.

This study was carried out with the aim of reviewing the recent developments in hydrodistillation technology that have been developed in Indonesia to improve the quality of the obtained EOs. This is due to the simplicity with which hydrodistillation installations may be established by small-scale producers, such as Indonesian farmers. In addition, the yields still have strong notes that motivated the authors to investigate recent developments in hydrodistillation in Indonesia, despite the fact that the quality of EOs still has to be improved. Thus, the results of this study can serve as a reference for designing and developing further novel studies related to hydrodistillation of EOs.

2 Material and Methods

Data Collection

Methodi Ordinatio was used to collect data from numerous papers in the Google Scholar database, followed Pagani et al. [8] procedures with slight modifications. Data were collected on June 30, 2024, with search queries such as "**hidrodistilasi**" OR "**distilasi air**" OR "**penyulingan air**" OR "**penyulingan rebus**" AND "**minyak atsiri**" in Bahasa Indonesia terms, and 50 documents were collected. Data filtering is then performed on these documents to obtain high-quality documents by checking the accreditation and indexation of the journal in the Sinta and Garuda databases. Table 1 outlines the data collection procedures for the systematic review, which resulted in 42 documents for further analysis. An investigation was then carried out on the national indexation, year of publication, and keyword co-occurrences (related to the types of EOs commodities and variables that influence the hydrodistillation process).

2.2 Bibliometric Analysis

Bibliometric analysis was performed on the final portfolio (42 documents) by creating a visual map network using VOSviewer v1.6.20 [9, 10], following the analysis conditions as:

- Map based on bibliographic data;
- Type of analysis: co-occurrences;
- Unit of analysis: keywords;
- Minimum number of occurrences: 4;
- Number of terms selected: total number of itmes;
- Show: all items.

The resulting visual map network was then used as a reference for conducting a brief systematic review in this study, and it performed focused and minimized the bias of discussion.

Table 1. Main steps to perform the systematic review through Methodi Ordinatio

Steps		Description	
Database search	I	Initial Portfolio	
		Database	Google Scholar
		Keywords	129
		Number of documents	50
Filtering procedures	II	Filtering based on Sinta and/or Garuda	
	III	Screening title and keywords	
	IV	Reading abstracts	
	V	Reading full texts	
	Final Portfolio		
	Number of documents	42	
Content analysis	VI	Year of publication	
		Indexation of documents	
		Keywords	

3 Results and Discussions

Visual Map Network

Fig. 1a shows an increase in the interest in hydrodistillation studies of EOs from 2021 to 2023 after experiencing fluctuations in the previous seven years. In terms of the number of related publications in 2024, four documents were discovered, with the number expected to increase owing to a positive trend of interest among Indonesian researchers. Further investigation was conducted to filter the data to obtain documents that had been indexed nationally (Sinta and Garuda) based on the latest journal indexation status. This was done to obtain high-quality data at the national level for a comprehensive review. Based on Fig. 1b, journals accredited by Sinta 4 and indexed by Garuda are researchers' favorites for publishing their studies in numerous documents after indexation screening (final portfolio). It is envisaged that these findings will increase the motivation among

researchers and the number of studies published, particularly in journals with national indexation and international reputation.

Fig. 2 depicts the visual map network of the final portfolio obtained by applying Methodi Ordinatio. The development of hydrodistillation technology can be illustrated through this map, such as the results studies after 2021, which focus on evaluating the duration of distillation time and the effect of pretreatment on the EOs yield [11, 12]. Citrus is a commodity that has recently been developed as a source of EOs through

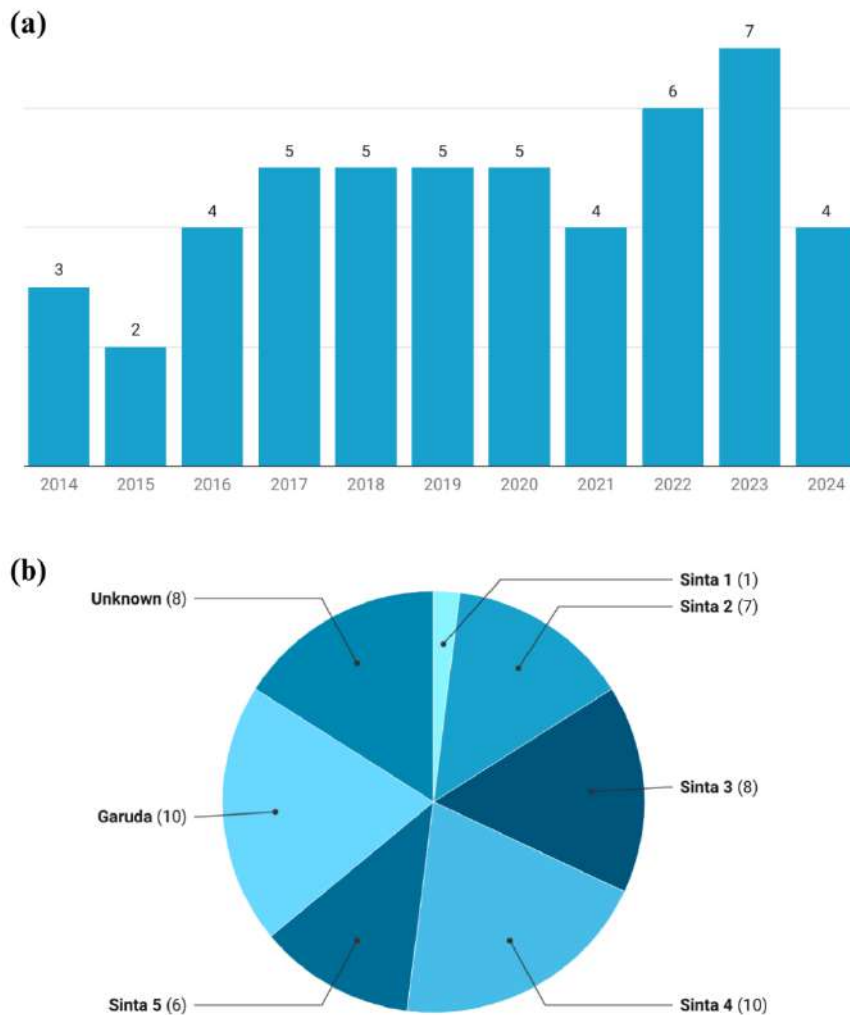


Figure 1. Distribution of the number of published documents: (a) based on publication years until June 30, 2024; and (b) national indexation.

hydrodistillation. Furthermore, the visual map network could be further studied in the future, based on the latest numerous results that have been evaluated. Some of these include the evaluation of the material's moisture content, particle size, microwave and/or ultrasound pretreatment, and the influence of plant development stages as promising novel topics to be investigated in the future.

A more in-depth investigation was carried out on EOs plant-source commodities based on keyword co-occurrences. Fig. 3 summarizes the findings for five EOs plant-source commodities that have been widely developed through hydrodistillation in the recent decade. As discussed in the previous section, citrus is the most often isolated commodity for its EOs content, both from the fruit peel and leaves [13-15]. In addition, lemongrass is another commodity that is often isolated, similar to citrus, with seven co-occurrences. Three other commodities have been developed in the recent decade to isolate their EOs content through hydrodistillation, namely cinnamon [16-18], nutmeg [19, 20], and ginger [21, 22].

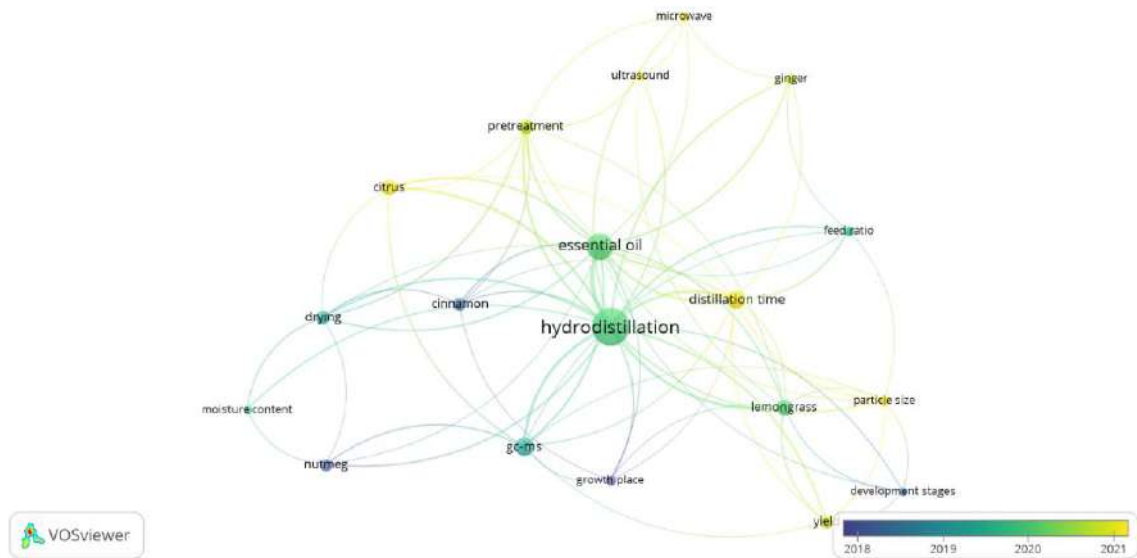


Figure 2. Visual map network of hydrodistillation development for EOs isolation in Indonesia (2014 to 2024).



Figure 3. Most developed Eos plant-source commodities in Indonesia based on bibliometric analysis results.

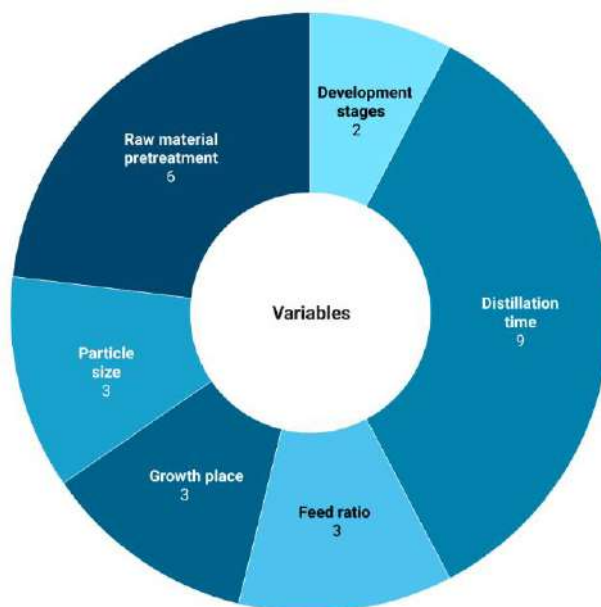


Figure 4. Most evaluated hydrodistillation variables for EOs isolation in Indonesia.

This study then evaluated the variables that influenced the hydrodistillation process based on the results of the bibliometric analysis. The results are shown in Fig. 4, with distillation time being the most frequently evaluated variable because it had nine co-occurrences. Pretreatment of raw materials is an interesting variable to evaluate in more

depth because it can increase EOs yield and can be a promising novel study. Other commonly evaluated variables include feed ratio and particle size. The upstream variables that appear, such as growth place and plant development stages, show promising potential for further development, as well as referring to their position in the visual map network.

Distillation Time

Distillation time has become a crucial variable and has been most frequently evaluated in the recent decade in relation to EOs isolation through hydrodistillation. This is because the distillation process runs for a prolonged time, which can cause EOs degradation that is isolated from the plant source, which reduces the yield and quality [23, 24]. In addition, it is difficult to control the temperature, which can cause overheating and the formation of char in a still reactor that occurs if the process runs for a prolonged time [7]. Thus, a comprehensive investigation was performed on this variable to obtain recent developments in employing hydrodistillation according to collected data on Table 2.

Citrus and lemongrass are the most widely used plant-source commodities in the hydrodistillation isolation process, based on bibliometric analysis results. Leaves are an organ of citrus plants that are often used as a source of limonene, and hydrodistillation for 3 h can produce 0.65–0.80% of EOs [25]. A prolonged time to 7 h of hydrodistillation could not increase the yield of citrus leaf EOs because it only produced 0.72% [14]. Meanwhile, hydrodistillation of citrus leaves for 1-3 hours resulted in the highest yield at a distillation time of 2 h, that is, 1.48% of citrus leaves EOs [26]. In addition, interesting findings were observed in the hydrodistillation of lemongrass distilled for 1-5 hours. Hydrodistillation of untreated lemongrass resulted in the highest yield after distillation process for 4.5 hours [27]. The distillation time was proven to be shorter than 1 h by evaluating other variables, such as the size reduction and drying of the plant-source materials [12].

Table 2. Recent studies on the effects of hydrodistillation time to essential oils isolation.

Materials	Time	Other Operational Variables and Results	Ref.
Citrus leaves	1–2 h	<ul style="list-style-type: none"> • Feed-to-solvent ratio that used was 1:10. • Hydrodistillation for 2 h resulted in the highest yield and decreased the results obtained after a 3 h. 	[26]
Lemongrass	3–5 h	<ul style="list-style-type: none"> • Performed different two-level temperatures (120°C and 130°C). • Time and temperature influenced to the results. • The highest yield obtained after 5 h. • Better quality of EOs achieved by employing hydrodistillation at 130°C for 4.5 h. 	[27]
Lemongrass	30–90 min	<ul style="list-style-type: none"> • Lemongrass harvested at 3 months old then size reduced and wind-dried. • Ultrasound pretreatment employed to dried lemongrass for further EOs isolation. • Distillation time between 60 min and 90 min provided similar results (in 1:20 and 90% amplitudes). 	[12]
Cinnamon leaves	3–7 h	<ul style="list-style-type: none"> • Several pretreatment performed, such as the use of fresh and dried leaves in whole and in reduced sizes. • The fresh and whole size cinnamon leaves provided high EOs yield. • Optimum distillation time at 5 h, because of no significant influence to the results after 6 h. • Cinnamaldehyde content was 13.60–25.57% 	[28]
Red ginger	2–6 h	<ul style="list-style-type: none"> • Red ginger powder has 10.72% moisture content and size of 60 mesh. • The feed-to-solvent ratio employed as 1:12. • The longest distillation time provide the highest yields as 1.65%, but the optimum results was achieved after 4 h. • No significant influence between the results of 4 h (1.55%) and 5 h (1.57%). 	[29]
Red ginger	2–6 h	<ul style="list-style-type: none"> • Others operational variables emplyed consist of 24 mesh of size, different feed-to-solvent ratio (1:8, 1:10, and 1:12), and hydrodistillation run at 80°C of temperature. • There was no significant influence from distillation time, feed-to-solvent ration, and the interaction. • The optimum variables achieved by 6 h hidrodistillation and 1:12 feed-to-ratio that provide 0.14% of yield. 	[30]

An increase in the EO yield through hydrodistillation can also be achieved by prolonging the distillation time, for example, in red ginger. Evaluation was successfully performed by hydrodistillation for 2–6 h with the highest yield of 1.65% at 6 h [29]. The results of these studies showed that there was no significant difference between distillation times of 4 and 5 h, but when distillation was extended to 6 h, the yield of red ginger EOs increased. Similar findings were obtained from a hydrodistillation optimization study of red ginger, which obtained the highest yield after 6 h of distillation [30]. However, the distillation time in these studies did not have a significant effect, and the quality of the EOs obtained was not better than that in previous studies. This phenomenon shows that implementing a short distillation time is more considered, especially if combined with engineering other process variables such as size reduction and drying of the material which is a pretreatment for the plant-source material.

Pretreatment of Raw Materials

Process variables regarding the pretreatment of EOs plant sources should be evaluated more comprehensively in this study. This is because pretreatment has the second highest number of keyword co-occurrences after distillation time (Fig. 4). Various studies have shown that the pretreatment of plant-source materials can increase the yield and quality of EOs. As seen on Fig. 5, several pretreatment techniques have been developed in the recent decade, starting from the simplest technology, namely drying (related to plant material moisture content), to modern technologies such as microwaves and ultrasonics.

Drying is the simplest pretreatment technology and is directly related to the moisture content of the material, which can inhibit the EOs isolation process. Investigation of EOs yields from plant-source materials in several previous studies proved that material moisture content has an effect. Investigation of EOs yields from plant-source materials in several previous studies proved that material moisture content has an effect. Nutmeg flesh was dried until the initial moisture content decreased by 25% and had the highest yield compared to undried flesh [31]. Similar results were obtained after drying sintok bark until the moisture content reached 15%, which could increase the yield of EOs compared with undried bark [32]. A different finding occurred when the plant source was

leaves because the moisture content in fresh leaves could catalyze the process of isolating EOs [33]. Further evaluations were performed on cinnamon leaves that were subjected to different treatments (without drying, withering, and wind drying), which showed that the yield of fresh leaves was higher than that of the wind dry and withering results [28]. This is in accordance with the results of studies on the different effects of drying cinnamon leaves (ripening, wind drying, and sun drying), which did not show any influence on EO yield [34]. These findings demonstrated the need for appropriate drying strategies, particularly for different plant organs.

Recent trends have led to the use of modern technologies to increase the yield of isolated EOs using hydrodistillation techniques. Some of these studies have successfully used microwave and ultrasonic technologies. Isolation of zingiberene from ginger showed the highest content after microwave pretreatment at 100 Watt for 2 min [35]. Isolation of zingiberene from ginger showed the highest content after microwave pretreatment at 100

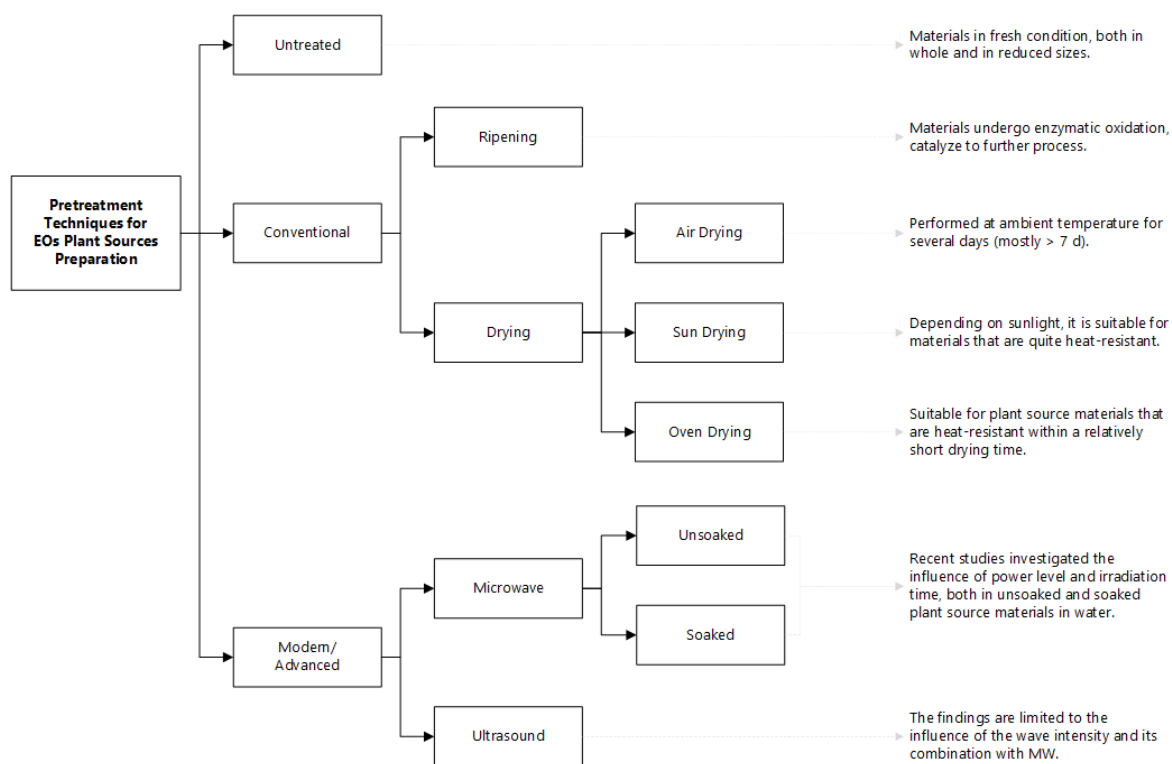


Figure 5. Most applicable pretreatment technologies in hydrodistillation for EOs isolation in Indonesia.

Watt for 2 min. These studies found a zingiberene content of 24.7%, which is close to that of commercial ginger EOs (24.8%). The innovative strategies for microwave pretreatment were then conducted by prolonging the soaking duration, as was done for agarwood. Soaking was performed to increase the yield and bioactive content of the product for 1-4 weeks which shows an increase in the last week of soaking [36]. However, the authors consider this additional treatment to be ineffective because it increases the duration of EOs isolation, driving the modern pretreatment combination of microwaves and ultrasonics. This combination has been proven to increase the yield, such as black cumin EOs, which have the highest yield through a combination of microwave and ultrasonic pretreatment, rather than applying each technology separately [37].

Various findings in recent decades have shown the effects of pretreatment on the produced EOs. The difference in plant organs as source material is one of the factors determining the appropriate pretreatment technique to be applied. In addition, the use of modern technology is a recent trend that has advantages in terms of duration compared to drying, such as withering, wind drying, and sun drying. Further investigation is required to apply modern pretreatment, particularly in terms of combining technologies that can increase the yield of EOs. An interesting topic that can be further developed in the future and is promising as a novel study is combining simple and modern pretreatment in a short treatment time.

Feed-to-Solvent Ratio and Particle Size

The feed-to-solvent ratio is a key variable in the isolation of EOs through hydrodistillation. This is related to the volume of solvent used, if the ratio is large (in w/v) it indicates that a large amount of solvent was used. Various studies have evaluated the effect of feed-to-solvent ratio, such as ginger. Under the same hydrodistillation conditions ($T = 100^{\circ}\text{C}$ for 6 h), a ratio of 1:2 gave a higher yield than that obtained using a ratio of 1:5 [22, 35]. Different findings occurred in red ginger because investigations into different ratios (1:8, 1:10, and 1:12 with a particle size of 24 mesh) had no effect on the yield of as 0.06–0.23% [30]. However, other findings have shown that hydro-distillation of red ginger at a ratio of 1:12 produced a yield of up to 1.65% after distillation for 6 h with a different particle size of 60 mesh [29]. These results show that, apart from the feed-

to-solvent ratio, there are other variables that can influence EOs isolation yields, such as the particle size of the plant material.

Further investigation into the combined interaction of feed-to-solvent ratio with particle size has been performed for black pepper EOs. Optimization studies were performed on the variables of feed-to-solvent ratio (7/100, 12/100, and 17/100), size (10-20, 20-30, and 30-40 mesh), and distillation time (60, 135, and 210 min), which yielded an optimum EOs of 5.81% [11]. Based on these results, the feed-to-solvent ratio did not have a significant influence on the yield, meanwhile the particle size and distillation time had a significant influence. This led to further evaluation of the differences in particle size and/or plant materials used for isolating EOs via hydrodistillation. As previously discussed, the difference in the size of red ginger between 24 mesh and 60 mesh showed different results, with increased yield at smaller particle sizes [29, 30]. Other evaluation studies have been performed on lemongrass (whole size, 5 cm, 10 cm, and 15 cm), which had the highest yield at the smallest size of 5 cm [18]. These various findings led to further studies through optimization design, because these two variables, the feed-to-solvent ratio and particle size, have an influence that has an uncertain trend (because it can increase and/or decrease). Moreover, hydrodistillation requires soaking the plant source material and preventing agglomeration, which can inhibit the EOs isolation process.

3.5 Growth Places and Plant Developmental Stages

The growth and development environment of EOs plant sources is one of the variables that influences the results of hydrodistillation. Growth environment variables, or growth places, have three keyword co-occurrences in the development of EOs hydrodistillation studies. Several studies have shown a significant effect, such as the isolation of EOs from lemongrass, cinnamon, and basil. Isolation of EOs from lemongrass cultivated in the highlands resulted in higher yields than those cultivated in the lowlands [38]. Similar results were obtained from the hydrodistillation of basil leaves, which had a higher yield in plants cultivated in highlands [39]. In contrast, different findings show that cinnamon EOs that grow in lower areas, such as Purwokerto, have a higher yield than those from the Tawangmangu area, which is in the highlands [40]. Furthermore, these studies have investigated the differences in plant organs (leaves, twigs, and bark), and generally, the yield of EOs from the Cinnamons' Purwokerto area remains higher. These

findings demonstrate the need for further investigation of the differences in growth location due to differences in environmental factors.

One of the variables that influences the results of the hydrodistillation of EOs is the developmental stage of the plant source materials. This is shown by the lack of studies on this variable because there have been only two keyword co-occurrences over the last decade. The findings that the authors discovered regarding studies evaluating this variable are still limited to lemongrass EOs. The yield of lemongrass EOs was known to be higher when this plant was harvested at six months, and there was a decrease when the lemongrass was nine months old [16]. This is similar to the results of hydrodistillation of 6 month old lemongrass under fresh conditions, which can produce approximately 1.35–2.09% of EOs [18]. Moreover, the EOs content of 3 month old lemongrass is known to remain high because it had a yield of 1.62%, but there was additional pretreatment through ultrasonic technology [12]. These findings can provide insights for further investigation into the influence of the developmental stages of EOs plant sources, especially for conducting studies on plant sources other than lemongrass. In addition, because of the lack of research on this topic, it can become a novel development study regarding hydrodistillation, particularly in Indonesia.

Future Perspective

Novel strategies for developing hydrodistillation technology to isolate EOs can be found in recent studies. Various influence variables have been briefly summarized and reviewed, showing promising potential for future development studies. Optimization studies are considered an appropriate strategy for investigating variables related to the hydrodistillation process, such as distillation time, feed-to-solvent ratio, and particle size [11, 12, 30]. To control the conditions of the optimized variables, instrumentation devices that can be controlled, such as microcontrollers, can be used to increase the yield of EOs [41]. In addition, optimization can be carried out on the pretreatment of plant source materials to catalyze the EOs isolation process. Some of them could investigate differences in pretreatment techniques and parameters or conduct experiments to combine the commonly applied pretreatment techniques [36, 37]. There are interesting and promising variables to be further investigated in the future because the biodiversity in

Indonesia that can be cultivated in various locations is related to the differences in growth places. This variable can be combined with plant developmental stages because the authors discovered that there was a peak in the yield of lemongrass EOs, and related published studies are still lacking [16]. The potency of novel studies has been described and is considered promising for future development to improve the performance of hydrodistillation technology for isolating EOs from various plant sources.

4 Conclusions

The trend of increasing interest in the development of hydrodistillation technology in Indonesia has been demonstrated by an increasing number of documents published in nationally indexed journals. Over the past decade, there have been five commonly used EOs plant source commodities, including citrus, lemongrass, cinnamon, nutmeg, and ginger. This finding provides novel strategies for developing other commodities isolated through hydrodistillation. To improve the performance and isolation results, this study investigated various variables that influence the process, especially those related to the yield. Distillation time, plant source material pretreatment, feed-to-solvent ratio, particle size, growth place, and plant developmental stages are variables that have often been evaluated in the recent decade. These variables have been successfully summarized and reviewed briefly and comprehensively to demonstrate their potential for performing novel studies that can be developed in the future. Several of these include conducting optimization studies, evaluating and combining pretreatment techniques, and investigating variables from upstream sectors (such as places of growth and plant developmental stages).

References

- [1] C. Barbieri and P. Borsotto, "Essential oils: Market and legislation," in *Potential of Essential Oils*, H. El-Shemy, Ed., IntechOpen, 2018. doi: 10.5772/intechopen.77725.
- [2] S. Khan, A. Sahar, T. Tariq, A. Sameen, and F. Tariq, "Essential oils in plants Plant

-
- physiology, the chemical composition of the oil, and natural variation of the oils (chemotaxonomy and environmental effects, etc.),” in *Essential Oils: Extraction, Characterization and Applications*, G. A. Nayik and M. J. Ansari, Eds., Academic Press Inc., 2023. doi: 10.1016/B978-0-323-91740-7.00016-5.
- [3] M. A. Hanif, S. Nisar, G. S. Khan, Z. Mushtaq, and M. Zubair, “Essential oils,” in *Essential Oils Research: Trends in Biosynthesis, Analytics, Industrial Applications and Biotechnological Production*, S. Malik, Ed., Springer Nature Switzerland AG, 2019, pp. 3–17. doi: 10.1007/978-3-030-16546-8_1.
- [4] S. Kholiya, A. Chauhan, K. Dipender, K. Venkatesha, R. K. Upadhyay, and R. C. Padalia, “Essential oils, application, and different extraction methods,” in *Essential Oils: Sources, Production and Applications*, R. C. Padalia, D. K. Verma, C. Arora, and P. K. Mahish, Eds., Walter de Gruyter GmbH, 2023, pp. 25–45. doi: 10.1515/9783110791600-002.
- [5] I. Hasbay and C. M. Galanakis, “Recovery technologies and encapsulation techniques,” in *Polyphenols: Properties, Recovery, and Applications*, C. Galanakis, Ed., Elsevier Inc., 2018, pp. 233–264. doi: 10.1016/B978-0-12-813572-3.00007-5.
- [6] A. Oreopoulo, D. Tsimogiannis, and V. Oreopoulou, “Extraction of polyphenols from aromatic and medicinal plants: An overview of the methods and the effect of extraction parameters,” in *Polyphenols in Plants (Second Edition)*, R. R. Waston, Ed., Academic Press, 2019, pp. 243–259. doi: 10.1016/B978-0-12-813768-0.00025-6.
- [7] S. S. Handa, S. P. S. Khanuja, G. Longo, and D. D. Rakesh, *Extraction technologies for medicinal and aromatic plants*. Trieste, Italy: ICS-UNIDO, 2008.
- [8] R. N. Pagani, J. L. Kovaleski, and L. M. Resende, “Methodi Ordinatio: a proposed methodology to select and rank relevant scientific papers encompassing the impact factor, number of citation, and year of publication,” *Scientometrics*, vol. 105, no. 3, pp. 2109–2135, 2015, doi: 10.1007/s11192-015-1744-x.
- [9] A. Arias, S. González-Rodríguez, M. Vetroni Barros, R. Salvador, A. C. de Francisco, C. Moro Piekarski, and M. T. Moreira, “Recent developments in bio-based adhesives from renewable natural resources,” *J. Clean. Prod.*, vol. 314, no.
-

- September 2021, 2021, doi: 10.1016/j.jclepro.2021.127892.
- [10] A. Hariry, E. Mardawati, and N. Masruchin, “Nanocellulose research trends from pineapple plant waste in Indonesia: Bibliometric analysis using VosViewer,” *AJARCADE (Asian J. Appl. Res. Community Dev. Empower.*, vol. 7, no. 2, pp. 1–7, 2023, doi: 10.29165/ajarcde.v7i2.247.
- [11] S. Shintawati, A. Analianasari, and Z. Zukryandry, “Pemodelan kondisi optimum ekstraksi dan identifikasi senyawa penyusun minyak atsiri lada hitam,” *J. Agro Ind. Perkeb.*, vol. 9, no. 2, pp. 99–108, 2021, doi: 10.25181/jaip.v9i2.2132.
- [12] D. Sukandar, A. Sulaswatty, and I. Hamidi, “Profil senyawa kimia minyak atsiri sereh wangi (*Cymbopogon nardus* L.) hasil hidrodistilasi dengan optimasi perlakuan awal sonikasi,” *ALCHEMY J. Penelit. Kim.*, vol. 18, no. 2, p. 221, 2022, doi: 10.20961/alchemy.18.2.60007.221-233.
- [13] Q. R. Fakhira, S. Nurjanah, and S. Rosalinda, “Karakteristik dan komposisi minyak atsiri kulit jeruk nipis pada berbagai lama waktu penyulingan menggunakan metode hidrodistilasi,” *Teknotan J. Ind. Teknol. Pertan.*, vol. 17, no. 3, pp. 217–226, 2023, doi: 10.24198/jt.vol17n3.8.
- [14] D. R. Febrianti and N. Ariani, “Uji potensi minyak atsiri daun jeruk purut (*Citrus hystrix* D.C) sebagai antioksidan dan antibakteri,” *J. Insa. Farm. Indones.*, vol. 3, no. 1, pp. 66–74, 2020, doi: 10.36387/jifi.v3i1.458.
- [15] A. S. Ulandari, D. M. Ningrum, and D. A. S. Permana, “Identifikasi kandungan senyawa minyak jeruk nipis (*Citrus aurantifolia*) dan minyak nilam (*Pogostemon cablin* B.) sebagai anti repellent dengan metode GC-MS,” *J. Etnofarmasi*, vol. 1, no. 2, pp. 1–9, 2022.
- [16] R. Prabandari, “Perbandingan randemen minyak atsiri sereh (*Cymbopogon citratus*) yang umur panennya 6 bulan dan 9 bulan dengan metode destilasi air,” *Viva Med. J. Kesehatan, Kebidanan dan Keperawatan*, vol. 11, no. 1, pp. 66–71, 2017, doi: 10.35960/vm.v10i3.430.
- [17] D. Pratimasari, A. D. S. Saputri, A. Ariyanti, and S. Shania, “Perbandingan karakteristik minyak atsiri palmarosa (*Cymbopogon martinii*) hasil destilasi uap air dan destilasi air,” *Benzena Pharm. Sci. J.*, vol. 2, no. 2, pp. 1–11, 2023, doi: <http://dx.doi.org/10.31941/benzena.v2i02.3770>.

- [18] S. Shintawati, O. Rina, and D. Ermaya, "Sifat antimikroba dan pengaruh perlakuan bahan baku terhadap rendemen minyak sereh wangi," *J. Sylva Lestari*, vol. 8, no. 3, pp. 411–419, 2020, doi: 10.23960/jsl38411-419.
- [19] H. M. Ansory, P. K. P. Putri, N. 'Aini Hidayah, and A. Nilawati, "Analisis senyawa minyak atsiri fuli pala secara GC-MS dan uji aktivitas antibakteri terhadap *Escherichia coli* dan *Staphylococcus aureus*," *Maj. Farm.*, vol. 13, no. 2, pp. 56–64, 2018, doi: 10.22146/farmaseutik.v13i2.40915.
- [20] S. G. Sipahelut, "Perbandingan komponen aktif minyak atsiri dari daging buah pala kering cabinet dryer melalui metode distilasi air dan air-uap," *Agritekno J. Teknol. Pertan.*, vol. 8, no. 1, pp. 8–13, 2019, doi: 10.30598/jagritekno.2019.8.1.8.
- [21] T. Barki, N. Kristiningrum, E. Puspitasari, and F. A. Fajrin, "Penetapan kadar fenol total dan pengujian aktivitas antioksidan minyak jahe gajah (*Zingiber officinale* var. *officinale*)," *J. Pustaka Kesehat.*, vol. 5, no. 3, pp. 432–436, 2017, doi: <https://doi.org/10.19184/pk.v5i3.5897>.
- [22] E. D. Daryono and G. F. Hutasoit, "Ekstraksi minyak atsiri jahe (*Zingiber officinale*) dengan proses Distilasi: Pengaruh jenis jahe dan metode distilasi," *Eksergi J. Ilm. Tek. Kim.*, vol. 21, no. 2, pp. 55–59, 2024, doi: <https://doi.org/10.31315/e.v21i2.11625>.
- [23] F. Chemat and C. Boutekedjiret, "Extraction // Steam Distillation," in *Reference Collection in Chemistry, Molecular Sciences and Chemical Engineering*, Elsevier, 2015. doi: 10.1016/B978-0-12-409547-2.11557-4.
- [24] P. Kapadia, A. S. Newell, J. Cunningham, M. R. Roberts, and J. G. Hardy, "Extraction of high-value chemicals from plants for technical and medical applications," *Int. J. Mol. Sci.*, vol. 23, no. 18, p. 10334, 2022, doi: 10.3390/ijms231810334.
- [25] D. Febrina, "Pengaruh perbedaan perlakuan pendahuluan terhadap rendemen minyak atsiri daun jeruk purut (*Citrus hystrix* DC)," *Viva Med. J. Kesehatan, Kebidanan dan Keperawatan*, vol. 11, no. 02, pp. 104–110, 2019, doi: 10.35960/vm.v11i02.471.
- [26] S. R. Ekasari, "Pengaruh metode pengambilan minyak atsiri dari daun jeruk purut (*Citrus hystrix*) terhadap kandungan geraniol dan sitronelal," *Inov. Tek. Kim.*, vol.

- 5, no. 1, pp. 5–11, 2020, doi: <http://dx.doi.org/10.31942/inteka.v5i1.3394>.
- [27] J. Adiandasari, W. Wusnah, and A. Azhari, “Pengaruh suhu dan waktu terhadap proses penyulingan minyak sereh wangi (*Cimbopogon nardus* L.),” *Chem. Eng. J. Storage*, vol. 1, no. 1, pp. 22–28, 2021, doi: 10.29103/cejs.v1i1.1493.
- [28] R. Irwanto, A. Kasim, and S. D. Ismanto, “Penentuan kadar minyak atsiri daun kayu manis (*Cinnamomum burmannii*, Blume) dengan perlakuan pendahuluan pada daun,” *J. Teknol. Pengolah. Pertan.*, vol. 4, no. 1, pp. 1–11, 2022, doi: 10.35308/jtpp.v4i1.5661.
- [29] A. F. Iskandar, S. Nurjanah, S. Rosalinda, and F. Nuranjani, “Penyulingan minyak atsiri jahe merah (*Zingiber officinale* var. *Rubrum*) menggunakan metode hidrodistilasi dengan variasi waktu penyulingan,” *Teknotan J. Ind. Teknol. Pertan.*, vol. 17, no. 1, pp. 53–60, 2023, doi: 10.24198/jt.vol17n1.7.
- [30] A. Ramadhanti, S. Nurjanah, A. Widyasanti, and N. Ainina, “Pemodelan kondisi hidrodistilasi minyak atsiri jahe merah (*Zingiber officinale* var. *Roscoe*) dengan menggunakan Response Surface Methodology,” *Agrointek J. Teknol. Ind. Pertan.*, vol. 18, no. 2, pp. 429–439, 2024, doi: 10.21107/agrointek.v18i2.18904.
- [31] L. Sari, D. Lesmana, and T. Taharuddin, “Ekstraksi minyak atsiri dari daging buah pala (Tinjauan pengaruh metode destilasi dan kadar air bahan),” in *Seminar Nasional Sains dan Teknologi 2018*, 2018, pp. 1–6.
- [32] N. Nuwa, R. Jemi, and H. Joni, “Isolasi dan uji anti jamur minyak atsiri kulit kayu sintok (*Cinnamomum sintoc* BL) pada beberapa jamur perusak kayu,” *Agrienvi J. Ilmu Pertan.*, vol. 12, no. 2, pp. 32–36, 2020.
- [33] D. B. G. Utomo and M. Mujiburohman, “Pengaruh kondisi daun dan waktu penyulingan terhadap rendemen minyak kayu putih,” Universitas Muhammadiyah Surakarta, 2018.
- [34] K. S. Nugraheni, L. U. Khansanah, R. Utami, and B. K. Anandhito, “The effect of pretreatment and variation method of distillation on quality of cinnamon leaf oil,” *J. Teknol. Has. Pertan.*, vol. IX, no. 2, pp. 51–64, 2016, doi: <https://doi.org/10.20961/jthp.v9i2.17466>.
- [35] B. D. Argo and F. A. Amaliyah, “Pengaruh gelombang mikro terhadap kualitas hasil minyak atsiri jahe (*Zingiber officinale*) dengan hidrodistilasi,” *agriTECH*,

- vol. 40, no. 4, pp. 332–339, 2020, doi: 10.22146/agritech.40651.
- [36] D. Defiza, A. Az Zahra, S. Supandi, and H. Aldrat, “Pengaruh pretreatment microwave terhadap rendemen dan profil kimiawi minyak gaharu *Aquilaria Sp.*,” *J. Farm. Higea*, vol. 15, no. 2, pp. 114–123, 2023, doi: 10.52689/higea.v15i2.555.
- [37] E. R. W. Hapsari, A. F. P. Putra, and A. H. Sofani, “Optimasi proses pemisahan minyak jintan hitam dengan kualifikasi food grade menggunakan metode hydrodistillation melalui variasi treatment pra-ekstraksi,” *Akta Kim. Indones.*, vol. 7, no. 2, pp. 133–148, 2022, doi: 10.12962/j25493736.v7i2.14686.
- [38] M. Dacosta, S. K. Sudirga, and I. K. Muksin, “Perbandingan kandungan minyak atsiri tanaman sereh wangi (*Cymbopogon nardus L. Rendle*) yang ditanam di lokasi berbeda,” *Simbiosis*, vol. 5, no. 1, pp. 25–31, 2017, doi: 10.24843/jsimbiosis.2017.v05.i01.p06.
- [39] S. Nur, J. A. Baitanu, and S. A. Gani, “Pengaruh tempat tumbuh dan lama penyulingan secara hidrodestilasi terhadap rendemen dan profil kandungan kimia minyak atsiri daun kemangi (*Ocimum canum Sims L.*),” *J. Fitofarmaka Indones.*, vol. 6, no. 2, pp. 363–367, 2019, doi: 10.33096/jffi.v6i2.507.
- [40] M. Budiarti, W. Jokopriambodo, and A. Isnawati, “Karakterisasi minyak atsiri dari simplisia basah ranting dan daun sebagai alternatif substitusi kulit batang *Cinnamomum burmannii Blume*,” *J. Kefarmasian Indones.*, vol. 8, no. 2, pp. 125–136, 2018, doi: 10.22435/jki.v8i2.323.
- [41] E. Parikesit, W. Kusbandono, and F. R. Sambada, “Microcontroller Based Simple Water Flow Rate Control System to Increase the Efficiency of Solar Energy Water Distillation,” *Int. J. Appl. Sci. Smart Technol.*, vol. 01, no. 02, pp. 129–146, 2019, doi: 10.24071/ijasst.v1i2.1923.

Automated Detection of Spine Deformities: Advancing Orthopedic Care with Convolutional Neural Networks

Deepesh Pratap¹, Saran Sinha¹, A. Charan Kumari^{1*},
K. Srinivas¹

¹*Department of Electrical Engineering, Faculty of Engineering, Dayalbagh
Educational Institute, Dayalbagh, Agra, India*

**Corresponding Author: charankumari@dei.ac.in*

(Received 24-07-2024; Revised 04-08-2024; Accepted 06-08-2024)

Abstract

This paper proposes Spine-CNN, a deep learning model for the detection of spinal deformities that can assist orthopedic doctors as a reliable tool for diagnosis. This technology promises to dramatically simplify the diagnostic process, freeing valuable time, and resources for healthcare professionals. To achieve this objective, a dataset of spine deformity X-ray images was curated from the PhysioNet database. The Spine-CNN was specially designed for detecting the spine deformity by incorporating features to leverage its ability to extract intricate features from radiographic images and by fine tuning the hyperparameters to properly train the model. Model performance was evaluated using standard metrics. Results from the Spine-CNN demonstrated promising performance in detecting spinal deformities. The model achieved an accuracy of 74%, with precision, recall, and F1-score values of 77%, 70%, and 73% respectively. Specifically, this research work introduces a Spine-CNN that underscore the potential of deep learning techniques to revolutionize diagnostic practices in orthopedic medicine, leading to improved treatment outcomes and patient care.

Keywords: Computer-aided detection, Convolutional neural network, Image classification, Spine Deformation, X-ray imaging

1 Introduction

Malformations of the spine, for instance, scoliosis or kyphosis, are physical impairments that affect the patient's health situation and his or her quality of life. Spinal deformities inevitably lead to discomfort, if left untreated, to life-threatening complications. Just counting injuries to the spinal cord, between 250,000 and 500,000



people are affected per year worldwide. The lethality of injuries to the spine is two to five times higher than it is without injuries, in low and middle-income countries even higher. The orthopedist must recognize these deformities early and make a precise diagnosis to initiate effective medical treatment.

The evaluation of spine deformity in conventional form leans mainly on straightforward measurements and radiographic analysis. Long-term methods present few obstacles in the direction of precision and performance. Straight measurements are partly subject to careless fallacy, and radiographic inspection requests particular resources and skills. Additionally, they tend to be more time-intensive than these approaches potentially slow up correct diagnosis and effective administration.

Over the last few years, deep learning has made major strides, particularly with Convolutional Neural Networks (CNNs). This technology has shown great promise in taking up medical image analysis. CNNs are artificial neural networks that are particularly well suited to pulling out characteristics from complex visual data. This talent makes them good candidates to look for structural irregularities in medical images, like those used in diagnosing spinal deformities.

The aim of this research is to improve the accuracy and swiftness of spine deformity detection by leveraging the capabilities of CNNs. Employing a dataset made up of medical imaging, the Spine-CNN trained in this research offers the possibility of establishing a resilient system. Although this is accurate, various other crucial determinants are necessary when deciding on the course of treatment. A patient's global health, current condition, and the extent to which the curvature has altered their breathing are all significant facets. Additionally, it is important to recommend and develop additional methods that aid in diagnosing scoliosis abnormalities with a high level of accuracy.

Several works have represented strategies that rely on various geometric models centered on depicting spinal curvature. These models lead to a detailed and exact depiction of spinal shape and flexure, benefitting diagnosis and treatment of spinal deformity. By fusing these geometric models with the power of CNNs, this work enabled a holistic and convincing framework for spine deformity detection and treatment.

The primary contributions of this research paper are as follows:

1. Implementation of Spine-CNN, a deep learning model to effectively categorize spinal deformities from image datasets, presenting a novel approach to addressing a critical medical challenge
2. A meticulously curated dataset is used that encompasses diverse images representing various spinal disorders, facilitating robust model training to tackle real-world complexities and enhance performance in handling clinical scenarios.
3. Enhancement of model performance through rigorous hyperparameter optimization, ensuring optimal training and fine-tuning of Spine-CNN for accurate spine deformity classification.
4. A comprehensive evaluation of the model's effectiveness by employing sensitivity, specificity, and precision calculations, providing insights into its ability to precisely classify spinal irregularities.
5. To leverage the capabilities of CNNs to speed up accurately diagnosing spine deformities, with a vision to develop a computerized diagnostic system equipped with extensive medical image data, thereby empowering CNNs to achieve advanced diagnostic capabilities.

The following is the arrangement of the upcoming sections of the paper: A concise synopsis of the literature study is given in Section 2. The employed methodology is explained in Section 3. Section 4 highlights the obtained results together with its analysis. The conclusions from the study's findings and the direction of future research are summarized in Section 5.

2 Literature Review

This section presents a brief overview of spine deformity detection strategies in a concise way, covering both conventional image processing methods and the most recent developments in deep learning. The objective is to present a comprehensive analysis of the current literature, highlighting the advantages and disadvantages of different strategies to provide insightful background information for the selected methodology.

Zhang L. et al. [1] performed human X-ray image spine model positioning based on an R-CNN. They concentrated on the placement, detection, and segmentation of

human radiograph spine models using Mask R-CNN, as well as object detection and image segmentation. They achieved good accuracy by concentrating on radiographic spine model location while considering application instructions. Lin. H. [2] implemented a multilayer feed-forward, back-propagation (MLFF/BP) artificial neural network (ANN) to identify the classification patterns of the scoliosis spinal deformity using X-ray images. He achieved fairly good accuracy. Lee et al. [3] created a CNN model to diagnose CSM using only one lateral cervical spine radiograph, with an acceptable diagnostic accuracy. However, the study was limited by the small number of subjects with MR images. Kim et al. [4] proposed a technique for analyzing a moire image of a human back in a 2-D way to automate the primary screening of spinal deformity detection based on neural network. Saravi et al. [5] concluded that AI-based decision-making tools in spine surgery utilize multimodal data to predict outcomes and detect disease patterns, requiring collaboration between healthcare providers and industries to implement good machine learning principles. Leveraging techniques like Federated Learning and continuous updates with new data are essential for safe integration into clinical practice. Mezghani N. et al. [6] studied Computer applications employing fuzzy clustering, support vector classifiers, artificial neural networks (ANN), and surface topography algorithms aid in managing Adolescent Idiopathic Scoliosis (AIS) by regrouping similar spine geometries, predicting Cobb angles accurately, and enhancing classification reliability. Salehi et al. [7] applied the deep convolutional neural networks (CNNs) in computer-aided diagnosis of three types of disc herniation disease based on lumbar axial MR Images. Pinheiro et al. [8] proposed and validated a novel computerized methodology for detecting elliptical patterns from X-ray images to evaluate the extent of the underlying scoliotic deformity. Hieu T. Nguyen et al. [9] aimed at developing and evaluating a deep learning-based framework, named VinDr-SpineXR, for the classification and localization of abnormalities from spine X-rays. B. L. Qasthari et al. [10] used a pre-trained model VGG19 to categorize histological images of lung and colon cancer into five labels to aid medical professionals' categorization job.

The literature review revealed several potential designs for identifying spinal deformities, with an emphasis on the CNN model. While some research has produced promising results in the recognition and categorization of spinal deformities, other studies

encountered challenges with achieving greater accuracy. Pretrained models and transfer learning techniques have shown potential for improving performance across multiple tasks.

3 Methodology

This section presents the description of the dataset, Spine-CNN architecture, the model parameters, and performance evaluation metrics.

Dataset

This research work uses PhysioNet dataset contributed by Pham *et al.* [11] supported with comma-separated values (CSV) labels for the spinal X-ray DICOM images with a total of 10466 images. It has 13 types of abnormalities and contains basic demographic information. The dataset was divided into training, testing and validation sets of images, with 8389 images in the training dataset and 2077 in validation and testing.

All collected images are organized into two separate folders based on their respective classes: "Deform" and "Normal". This structuring facilitates the efficient handling and processing of data during model development. The dataset is split into three subsets: training, testing, and validation sets - 80% of the data is allocated for training and 20% of the data is reserved for testing and validation.

Model Architecture of Spine-CNN

The model summary of the Spine-CNN architecture is shown in Table 1.

Table 1. Architecture of Spine-CNN

Layer (type)	Output Shape	Param
conv2d (Conv2D)	(None, 222, 222, 16)	160
batch_normalization (BatchNormalization)	(None, 222, 222, 16)	64
activation (Activation)	(None, 222, 222, 16)	0
max_pooling2d (MaxPooling2d)	(None, 111, 111, 16)	0
conv2d_1 (Conv2D)	(None, 109, 109, 32)	4640

batch_normalization_1 (BatchNormalization)	(None, 109, 109, 32)	128
activation_1 (Activation)	(None, 109, 109, 32)	0
max_pooling2d_1 (MaxPooling2D)	(None, 54, 54, 32)	0
conv2d_2 (Conv2D)	(None, 52, 52, 32)	9248
batch_normalization_2 (BatchNormalization)	(None, 52, 52, 32)	128
activation_2 (Activation)	(None, 52, 52, 32)	0
dropout (Dropout)	(None, 52, 52, 32)	0
max_pooling2d_2 (MaxPooling2D)	(None, 26, 26, 32)	0
conv2d_3 (Conv2D)	(None, 24, 24, 64)	18496
batch_normalization_3 (BatchNormalization)	(None, 24, 24, 64)	256
activation_3 (Activation)	(None, 24, 24, 64)	0
dropout_1 (Dropout)	(None, 24, 24, 64)	0
max_pooling2d_3 (MaxPooling2D)	(None, 12, 12, 64)	0
flatten (Flatten)	(None, 9216)	0
dense (Dense)	(None, 256)	2359552
batch_normalization_4 (BatchNormalization)	(None, 256)	1024
activation_4 (Activation)	(None, 256)	0
dropout_2 (Dropout)	(None, 256)	0
dense_1 (Dense)	(None, 1)	257
Total params: 2393953 (9.13 MB)		
Trainable params: 2393153 (9.13 MB)		
Non-trainable params: 800 (3.12 KB)		

It consists of the following layers.

A. Convolutional Layers (Conv2D):

Four convolutional layers are employed to extract hierarchical features from input images. These layers use 3x3 filters with varying depths (16, 32, 32, 64) to capture different levels of abstraction.

B. Batch Normalization Layers:

The training process is stabilized and accelerated by interleaving convolutional layers with batch normalization layers. They normalize activations, improving gradient flow and mitigating the vanishing gradient problem.

C. Activation Layers (Activation):

ReLU activation functions introduce non-linearity, enabling the model to learn complex patterns in the data. They follow each convolutional layer to introduce non-linear transformations.

D. Max Pooling Layers (MaxPooling2D):

Max pooling layers downsample feature maps, reducing computational complexity and prevent overfitting. 2x2 pooling windows are used to retain the most salient features.

E. Dropout Layer:

A total of three dropout layers are utilized. The Convolution layer consists of two dropouts at a probability of 0.2, while the dense layer is equipped with a single dropout at a probability of 0.3.

F. Flatten Layer (Flatten):

The flatten layer comes after the last max pooling layer. It transforms the 2D feature maps into a 1D vector, so that they can be fed into the fully connected layers.

G. Fully Connected Layers:

The model contains two dense layers for classification, with the initial dense layer possessing 256 neurons that can capture high-level features and the last layer consisting of only a single neuron aimed at tasks focused on binary classification, thereby outputting classes. The model is made up of 2,393,953 parameters.

The process flow of the spine deformation detection of Spine-CNN is presented in Fig. 1, where process starts with the input X-ray image, which is preprocessed by resizing to 224x224 pixels and rescaling pixel values for normalization. This preprocessed image is passed through the Spine-CNN Model explained above which uses a sigmoid activation function to output a probability score, which is thresholded to classify the image as either "Deform" (indicating a spinal deformity) or "Normal" (indicating no deformity).

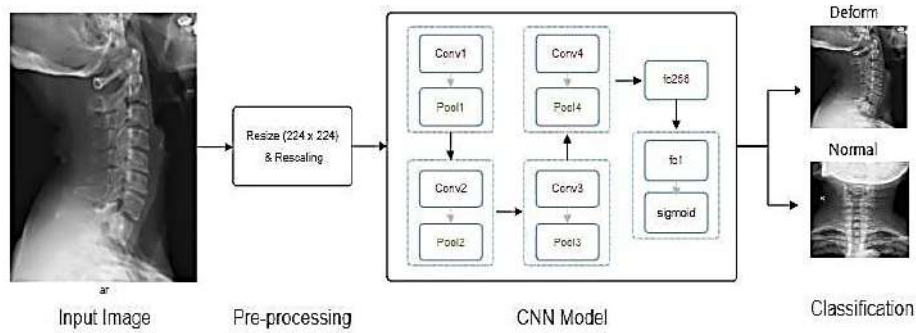


Figure 1. Flow diagram for Spine deformity detection

3.3 Model parameters

The following parameters are used in the Spine-CNN model:

- Epochs: 50
- Batch Size: 64
- Loss Function: Binary Cross-Entropy
- Optimizer: Adam
- Learning rate = 0.001

Learning rate scheduler: ReduceLROnPlateau (monitor='val_loss')

Evaluation metrics

While evaluating a Convolutional Neural Network (CNN) model for image classification, several metrics are used to assess its performance. A brief description of these metrics is presented below:

1. Accuracy:

Accuracy is defined as the proportion of accurately identified instances to all instances as shown in equation 1.

$$Accuracy = \frac{\text{Number of Correct Predictions}}{\text{Total Number of Predictions}} \quad (1)$$

2. Precision:

The precision metric, as described in equation 2, quantifies the percentage of true positive predictions among all the positive predictions generated by the model. It shows that the model can prevent false positives.

$$Precision = \frac{True\ Positives}{True\ Positives + False\ Positives} \quad (2)$$

3. Recall (Sensitivity):

The percentage of true positive predictions among all actual positive data instances is known as recall. It illustrates how the model may prevent false negatives by capturing all positive cases as depicted in equation 3.

$$Recall = \frac{True\ Positives}{True\ Positives + False\ Negatives} \quad (3)$$

4. F1-Score:

The F1-score, as described in equation 4, is the harmonic mean between recall and precision. It offers an equitable assessment of a model's effectiveness, particularly in cases where the dataset exhibits class imbalances.

$$F1 - Score = 2 \times \frac{Precision \times Recall}{Precision + Recall} \quad (4)$$

5. Confusion Matrix:

A tabular overview of the model's predictions compared to the actual class labels is given by a confusion matrix. It allows for a more in-depth analysis of the model's performance, showing the counts of true negatives, true positives, false negatives, and false positives.

6. Receiver Operating Characteristic Curve (ROC) and Area Under the Curve (AUC):

ROC curves illustrate how threshold values alter the trade-off between the true positive rate (sensitivity) and the false positive rate (1-specificity). The model's overall

performance is represented by a single scalar value, or AUC, which summarizes the ROC curve.

4 Results

This section reports the results obtained by Spine-CNN. Table 2 presents the results of the model after 50 epochs of training.

Accuracy: The accuracy shows overall accuracy of the model's predictions. The model achieves an accuracy of 74%, suggesting that it correctly identifies spinal deformities approximately three-fourths of the time. Although accuracy is a valuable metric, it should be read in conjunction with other metrics to provide a complete picture of the model's performance.

Precision: The percentage of true positive predictions among all positive predictions the model made is referred to as precision. The model's precision is 77%, meaning that 77% of the time, it accurately predicts a spine deformity. In medical applications, a low percentage of false positives is indicative of high precision and helps prevent misdiagnosis.

Recall: The percentage of true positive predictions among all actual positive cases in the dataset is determined by recall, which can also be referred to as sensitivity. Here, the model achieves a recall of 70%, implying that it identifies 70% of all actual spine

Table 2. Performance of Spine-CNN

Metric	Value
Accuracy	74%
Precision	77%
Recall	70%
F1-Score	73%
ROC AUC	81%

deformities. A high recall indicates that the model effectively captures most instances of spinal deformities, reducing the chances of false negatives.

F1-Score: The harmonic mean of precision and recall results in the F1-score, which provides a balance between the two measures. It is especially helpful in cases where there is an imbalance in classes. The F1-score in this instance is 73%, suggesting that recall and precision are fairly balanced.

ROC AUC: The Receiver Operating Characteristic Area Under Curve (ROC AUC) evaluates the model's ability to differentiate between classes that are negative and positive at different thresholds. The model's 81% AUC indicates that it can distinguish between positive and negative occurrences with reasonable accuracy.

Fig. 2 shows the obtained ROC curve, where the x-axis represents the False Positive Rate (FPR), while the y-axis represents the True Positive Rate (TPR). The curve plots TPR against FPR at various threshold settings, illustrating the trade-off between sensitivity (true positive rate) and specificity (false positive rate).

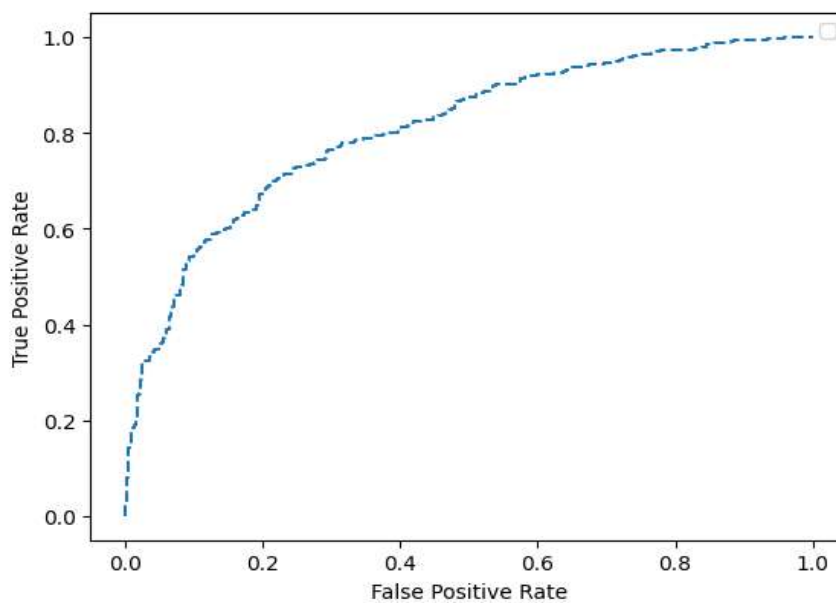


Figure 2. ROC Curve

Overall, the results demonstrate promising performance of Spine-CNN for spinal deformity detection. The precision and recall values indicate a balanced performance in correctly identifying deformities while minimizing false positives and false negatives. Although analysis of the model's predictions is shown with a confusion matrix in Fig. 3

True Positives (TP): A total of 374 instances of spine deformities were accurately predicted by the model. (Positive class)

False Positives (FP): 114 instances were incorrectly classified by the model as spine abnormalities when they weren't. (Negative class)

True Negatives (TN): For 400 instances, the model accurately predicted that there were no spine deformities. (Negative class)

False Negatives (FN): 159 instances were wrongly predicted by the model to not have spinal abnormalities when in fact they had. (Positive class).

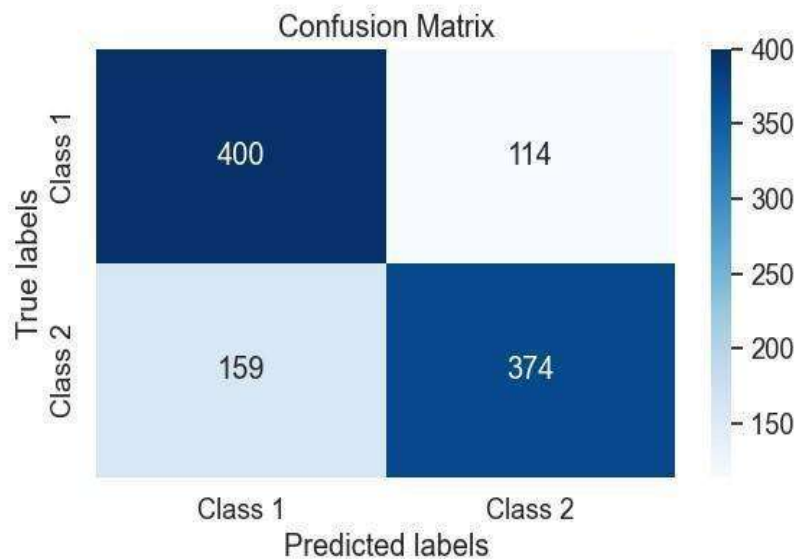


Figure 3. Confusion Matrix obtained by Spine-CNN

5 Conclusions and Future work

To conclude, this research introduces a method for deep learning utilizing Convolutional Neural Networks (CNNs) to detect spinal abnormalities using Spine-CNN. This study designed and implemented a CNN model to detect and differentiate kinds of spine deformities substantially. This work succeeded in presenting that through intensive experimentation and fine-tuning a CNN of substantial size which could achieve an accuracy of 74%. In terms of recall, precision, and F1 score, the Spine-CNN achieved impressive results, with 70%, 77%, and 73%, respectively. The study emphasizes the potential of deep learning technology, specifically Convolutional Neural Networks (CNNs), to change orthopedic medicine. With deep learning, the CNN model fuels a powerful engine for automatically detecting intricate details from radiographic imaging, which could make the diagnosis process smarter, thereby improving subsequent care and perhaps saving time and resources for all clinicians.

Future research endeavors aimed at enhancing the diagnostic capabilities of Spine-CNN could investigate the potential integration of 3D imaging data obtained from modalities such as MRI or CT scans, offering a more comprehensive understanding of spinal structures. Furthermore, the incorporation of multi-modal data, such as integrating X-ray images with a patient's medical history or other clinical information, holds significant potential for a thorough evaluation, thereby improving diagnostic outcomes.

To ensure Spine-CNN's predictions are reliable in clinical settings, it can be integrated with explainable AI (XAI) techniques that allow clinicians to interpret the model's decisions. By providing insights into which features of the X-ray images the model focuses on, XAI will enable doctors to understand the rationale behind each prediction. This transparency will certainly gain clinician confidence, as it allows for cross-verification with medical knowledge and enhances the model's utility in real-world clinical settings to ensure its practical applicability.

Acknowledgements

The authors are extremely grateful to the Revered Prof. P.S. Satsangi, Chairman, Advisory Committee on Education, Dayalbagh for continued guidance and support.

References

- [1]. L. Zhang, J. Zhang, and S. Gao, "Region-based convolutional neural network-based spine model positioning of X-ray images," *BioMed Research International*, vol. 2022, Art. no. 7512445, 2022. [Online]. Available: <https://doi.org/10.1155/2022/7512445>.
- [2]. Lin, "Identification of spinal deformity classification with total curvature analysis and artificial neural network," *IEEE Transactions on Biomedical Engineering*, vol. 55, no. 1, pp. 376-382, 2008. [Online]. Available: <https://doi.org/10.1109/TBME.2007.894831>.
- [3]. G. W. Lee, H. Shin, and M. C. Chang, "Deep learning algorithm to evaluate cervical spondylotic myelopathy using lateral cervical spine radiograph," *BMC Neurology*, vol. 22, no. 1, Art. no. 147, 2022. [Online]. Available: <https://doi.org/10.1186/s12883-022-02670-w>.
- [4]. H. Kim, S. Ishikawa, M. Khalid, Y. Otsuka, H. Shimizu, Y. Nakada, T. Shinomiya, and M. A. Viergever, "Automatic spinal deformity detection based on neural network," in *Medical Image Computing and Computer-Assisted Intervention - MICCAI 2003*, R. E. Ellis and T. M. Peters, Eds., *Lecture Notes in Computer Science*, vol. 2878. Berlin, Heidelberg: Springer, 2003, pp. 1014-1016. [Online]. Available: https://doi.org/10.1007/978-3-540-39899-8_98.
- [5]. B. Saravi, F. Hassel, S. Ülkümen, A. Zink, V. Shavlokhova, S. Couillard-Despres, M. Boeker, P. Obid, and G. M. Lang, "Artificial intelligence-driven prediction modeling and decision making in spine surgery using hybrid machine learning models," *Journal of Personalized Medicine*, vol. 12, no. 4, Art. no. 509, 2022. [Online]. Available: <https://doi.org/10.3390/jpm12040509>.
- [6]. N. Mezghani, P. Phan, H. Labelle, C. Aubin, and J. Guise, "Computer-aided Lenke classification of scoliotic spines," *International Journal of Computer and*

- Information Engineering, vol. 3, no. 5, pp. 1351-1354, 2009. World Academy of Science, Engineering and Technology, Open Science Index 29.
- [7]. E. Salehi, S. Khanbare, H. Yousefi, H. Sharpasand, and O. S. Sheyjani, "Deep convolutional neural networks for automated diagnosis of disc herniation on axial MRI," in Proc. 2019 Scientific Meeting on Electrical-Electronics & Biomedical Engineering and Computer Science (EBBT), Istanbul, Turkey, 2019, pp. 1-6. doi: 10.1109/EBBT.2019.8741895.
- [8]. A. P. Pinheiro, J. C. Coelho, A. C. P. Veiga, and T. Vrtovec, "A computerized method for evaluating scoliotic deformities using elliptical pattern recognition in X-ray spine images," *Computer Methods and Programs in Biomedicine*, vol. 161, pp. 85–92, 2018. doi: 10.1016/j.cmpb.2018.04.015.
- [9]. H. T. Nguyen, H. H. Pham, N. T. Nguyen, H. Q. Nguyen, T. Q. Huynh, M. Dao, and V. Vu, "VinDr-SpineXR: A deep learning framework for spinal lesions detection and classification from radiographs," in Proc. International Conference on Medical Image Computing and Computer-Assisted Intervention (MICCAI), 2021.
- [10]. B. L. Qasthari, E. Susanti, and M. Sholeh, "Classification of lung and colon cancer histopathological images using convolutional neural network (CNN) method on pre-trained models," *International Journal of Applied Sciences and Smart Technologies*, vol. 5, no. 1, pp. 133-142. [Online]. Available: <https://doi.org/10.24071/ijasst.v5i1.6325>.
- [11]. H. H. Pham, H. Nguyen Trung, and H. Q. Nguyen, "VinDr-SpineXR: A large annotated medical image dataset for spinal lesions detection and classification from radiographs (version 1.0.0)," *PhysioNet*, 2021. doi: 10.13026/q45h-5h59.

This page intentionally left blank

Essay Answer Detection System Uses Cosine Similarity and Similarity Scoring in Sentences

Diah Hidayatul Ula¹, Siti Yuliyanti^{1*}

¹*Informatics Department, Faculty of Engineering,
Universitas Siliwangi, Indonesia.*

**Corresponding Author: sityuliyanti@unsil.ac.id*

(Received 12-07-2024; Revised 06-08-2024; Accepted 08-08-2024)

Abstract

Essay exams are often an option to evaluate a person's understanding and interpretation of the material they have studied, rather than simply testing knowledge or understanding through essay exams that still rely on manual methods. The disadvantage of manual assessment is that it is prone to errors due to variations between examiners in providing assessments, coupled with the number of questions that must be assessed which is sometimes quite large, so it takes significant time. So this research carried out the development of an application with an automatic answer correction model with cosine similarity to measure how similar or how far two vectors are in multidimensional space. The result, system's potential in educational contexts was demonstrated by testing it on essay responses. To improve accuracy and usability, future developments could use sophisticated text scoring algorithms and provide more features. This study highlights the importance of automated grading systems for optimizing essay scoring in educational settings while maintaining scalability and reliability.

Keywords: essay exams, automated grading, essay checker, cosine similarity

1 Introduction

Exams with essay questions are frequently used to gauge a student's comprehension and interpretation of the content they have studied. This is a result of teachers' desire to probe more into students' comprehension as opposed to only using multiple-choice exams to assess students' knowledge [1]. Nevertheless, in spite of these benefits, essay exams are still assessed manually. The disadvantage of manual grading is that it is labor-intensive and error-prone due to grade discrepancies among examiners. In addition,



grading a large number of questions might take a considerable amount of time. This is why an application that can automatically correct student answers is an urgent need, expected to help teachers in conducting essay exam grading more quickly and efficiently [2]

This study employed the cosine similarity method in conjunction with a prototype model as a system development approach. A mathematical method called the cosine similarity method can be used to calculate the degree of similarity between two vectors in multidimensional space. Cosine similarity is a tool used to compare how close student answers are to the right key answers while editing essay test responses [3].

In previous research [1], entitled 'Application of Automatic Essay Answer Assessment Using Web-Based Synonym Recognition and Cosine Similarity Methods', an automatic essay answer assessment system was developed using cosine similarity, synonym recognition and filtering methods. Test results show that these systems have a high error rate due to low similarity between student answers and answer keys, typing errors, and missing words in the filtering process. Although it can help in the process of automatically correcting student answers, improvements such as increasing the level of text similarity, creating more dynamic applications, and increasing accuracy testing are needed to improve the performance of automated essay answer grading systems [4]. Research[2], [3], has proven that the use of cosine similarity can produce an accuracy of 89.5%, but there are several types of questions that are different because there are unique words and the answer key does not contain the keywords that are searched for with the correct answer.

Another study [4], et al. entitled "Application of Automatic Essay Exam Grading Using the Cosine Similarity Method" discusses the development of an automatic essay grading system using the Latent Semantic Analysis, Cosine Similarity, and Rabin Karp methods. The research highlights different approaches to automatic essay scoring, focusing on the application of the cosine similarity method to the scoring of essay exams in English. The discussion includes text processing techniques such as stop word removal and stemming, term frequency calculation, word weighting, and similarity calculation using cosine similarity. The results show that the system is effective in overcoming subjectivity in essay grading. The paper also discusses the conversion of similarity scores

into exam scores, the development of an essay auto-grading application, and presents the conclusions and implications of the research [5]. Automated essay scoring is a task implementation of machine learning in NLP, by building money modeling implemented to automate the value of answers to essay questions[5], [6].

Using this method, the system can automatically evaluate students' answers and assign a score based on how close their answers are to the correct answer. This allows teachers to correct essay answers quickly and efficiently without the need for time-consuming manual grading [7], [8]. This cosine similarity method helps overcome essay grading challenges such as examiner inconsistency and a large number of questions. This research applies the model to an answer checking system with advantages such as being able to assess answers quickly and objectively [9], where the assessment model consists of three types, namely multiple choice, true false and essay (description). Descriptive answers are an appropriate method for assessing the results of learning activities, because descriptive answers will involve students' ability to remember and express the ideas they have [10], [11]. The problem of assessment is the description of subjectivity, the assessment between one lecturer and another lecturer may be different or objectivity from different points of view, so it is possible that the lecturer makes mistakes in assessment such as the same student's answer but has a different value.

2 Material and Methods

The stages of this research include collecting datasets, text preprocessing, weighting trams, mapping answers using sosine similarity and scoring, then visualizing test scores which are illustrated in Fig. 1.

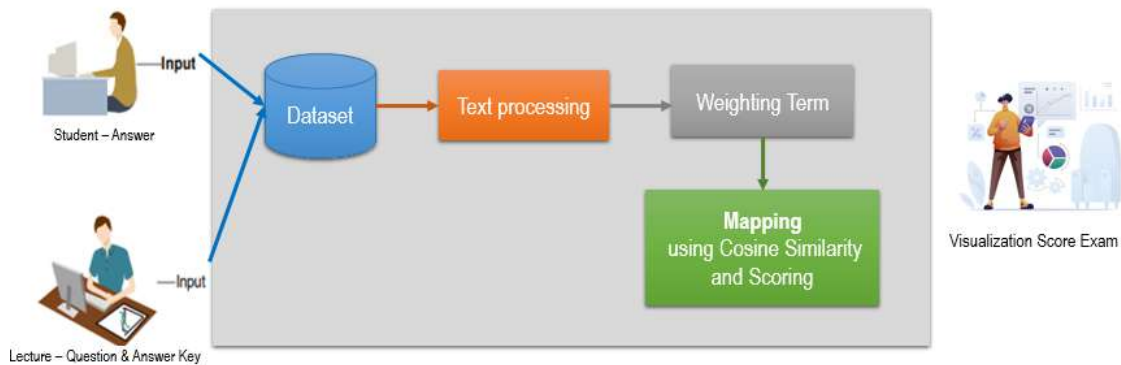


Figure 1. Framework Research

Dataset Collect

Dataset collect using essay assessments and answer key from student. Essay assessments can also be considered assessment tests because they consist of organized questions with answers that provide clarification or additional information. Teachers are still the ones who decide how best to assess their students' talents, usually through essay exams. Because each student's answer is considered objective [12], the assessment process is not actually simple [13] [14], [15]. The essay test is a method or tool that is considered to be highly successful in determining students' academic success as well as their ability to think critically [6].

Text Preprocessing

Text that is to be used as a data source for the next stage can be prepared using text preprocessing [7]. At this point, a number of complex types of actions are possible. They are complicated in nature. The following are the steps that can be performed in text preprocessing:

a. Case Folding

To make it easier to identify sentences at this point in the process, a text document is converted to lowercase.

b. Tokenization Process

The creation of tokens processing tokens that are present in a collection of data is known as tokenization [5]. In a sentence, symbols based on tabulation, spaces, enter, commas (,), and periods (.) are used to separate each word.

c. Stop-word Removal

At this point, the stop-word is removed as part of the filtering process. Here, a "stop-word" is a term that frequently occurs but has no real significance[4], [16]. The solution is to create a library of stop-words that can be eliminated, like "which, from, in, until, to, and with," which is a mix of the most common word and the stop list [8].

d. Stemming

At this point, affixes—prefixes and suffixes—are eliminated from each document in order to look for commonly used fundamental words. This procedure basically makes use of a database known as the basic-word list [9]. Stemming is a preprocessing part of an information retrieval system which aims to change words in a document into basic words with a certain set of rule [3].

Term Weight

The process of assigning a weight to words in a document according to how often they occur is known as term weighting [17]. This plan can combine Term Weight TF-IDF, which is something that should be taken into account based on a number of papers. In this case, Term Weight - an indicator - must be assigned to each term [10].

a. Terms Frequency

Based on how often a term occurs in a document, a weight is applied [18]. The more occurrences there are, the higher the weight and the higher the match rate (high TF).

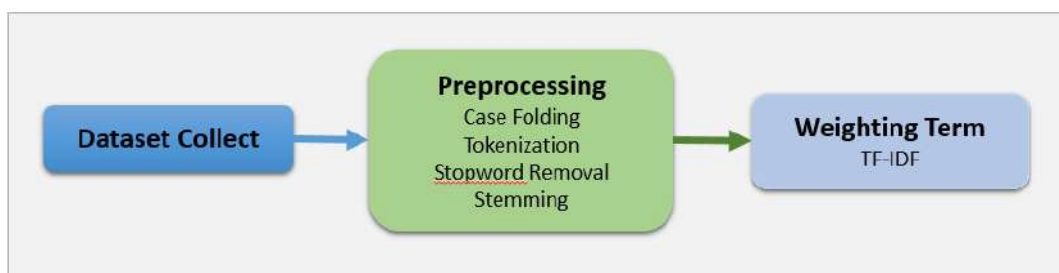


Figure 2. Text Processing

b. Inverse Document Frequency

An estimate derived from the distribution of a word over a set of documents [5], [19]. The IDF shows the relationship between the availability of a word across all documents. The IDF value increases as the number of documents containing the word decreases.

c. TF-IDF

This approach combines two different types of notions for calculating the weight: the inverse frequency of documents containing a word and the frequency of a word occurring in a particular document of the term [17], [19]. The frequency of occurrence of a word in a given document indicates the importance of the word. Importance of the word in the text. The number of documents containing a word indicates how common it is. For the association between a word and a document to have a high weight value, the word must appear frequently in the document and the total frequency of all documents in the document collection that contain low-frequency terms must be high [11]. The formula 1 that can be used for TF-IDF.

Similarity calculation using cosine similarity

In this step, the similarity between the students' essay answers and the instructor's key answers is calculated using the following formula 2 and 3.

$$\text{Similarity} = \cos (\Theta) = \frac{A \cdot B}{|A||B|} \quad (1)$$

At this stage, only two responses are analyzed, so the degree of similarity between the two responses is the output, which is then translated into student scores [6], [20].

Conversion of Similarity Score to Essay Exam Score

The similarity scores generated earlier are converted into answer scores for the of the student's essay exam [5], [16]. These values are based on the human judgment version of the value range, which is a reference from Fuat's research in 2010 following in Table 1.

Table 1. Range of Score

Rentang Nilai “Essai Checker”	
Similarity	Grade
90-100	A
80-89	B
70-79	C
60-69	D
<59	E

3 Results and Discussions

The Fig. 3 shows a web-based tool called "Essay Checker". Its purpose is to facilitate the grading of student essays using the cosine similarity approach. Users of the system, such as instructors or professors, can upload two Excel files: “Excel Kunci Jawaban” and “Excel Jawaban Siswa”, which contain the solution keys to the students' answers.

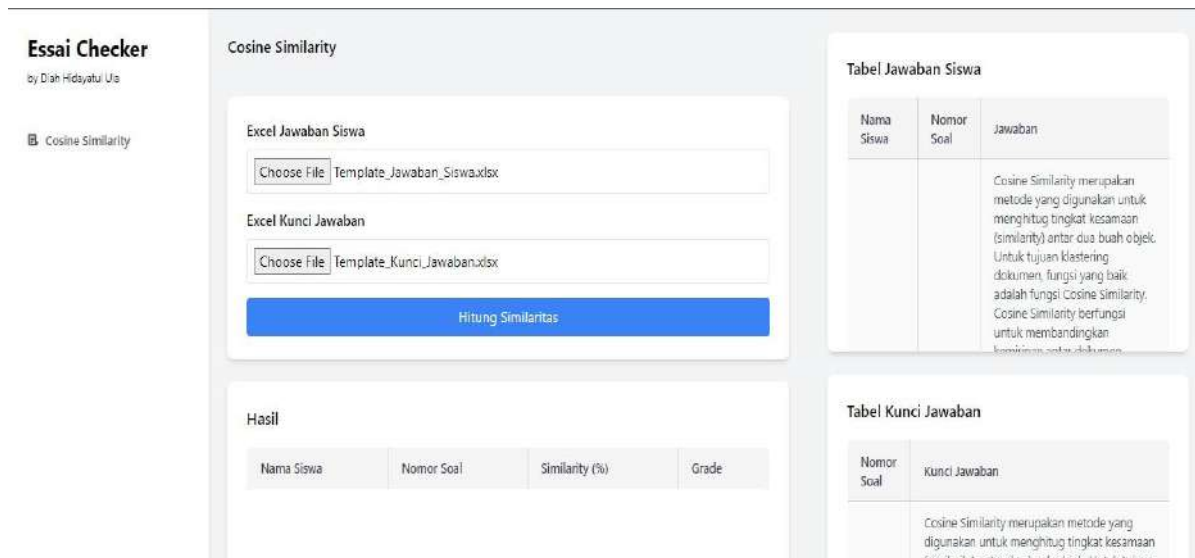


Figure 3. Website “Essai Checker”

The Fig. 4 shows two Excel files to be uploaded into the “Essai Checker” system. The first file, "Template_Jawaban_Siswa", contains the essay answers of several students. This file has three columns: "NAMA_SISWA" which contains the student's name, "NO_SOAL" which contains the question number, and "JAWABAN" which contains the student's answer text for each question. For example, there is a student named "DIAH" who provided answers to question number 1 on cosine similarity, as well as a student named "JISOO" who provided answers to several other questions.

The second file, "Template_Kunci_Jawaban", contains the correct answer key for each question. This file has two columns: "NO_SOAL", which contains the question number, and "JAWABAN", which contains the text of the answer that is considered correct for each question. For example, the answer to question number 1 is a description of cosine similarity and how it works, while the answer to question number 2 is an explanation of the definition of a system.

These two files are uploaded into the “Essai Checker” system to calculate the percentage of similarity between the student's answers and the answer key using the cosine similarity method. The system will process the data from both files and produce a result table showing the degree of similarity and grade for each student answer based on its compatibility with the provided answer key.

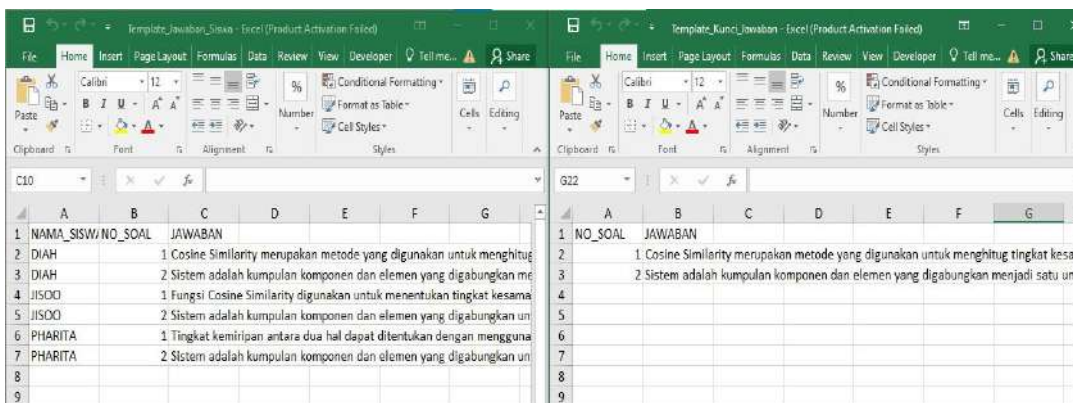


Figure 4. File Uploaded

Hasil			
Nama Siswa	Nomor Soal	Similarity (%)	Grade
DIAH	1	85.67%	A
	2	100.00%	
JISOO	1	94.12%	A
	2	91.29%	
PHARITA	1	78.27%	B
	2	91.29%	

Figure 5. Results for the calculation

After both files are uploaded, the user can press the "Hitung Similaritas" button to start the process of calculating the similarity between the student's answer and the answer key.

The results of this calculation are then displayed in several tables as shown in Fig. 5. "Jawaban Siswa table" displays information about the student's name, the question number and the answer given. "Kunci Jawaban" table displays the question number and the correct answer according to the answer key. In addition, the "Hasil" table displays the percentage of similarity between student answers and answer keys in the form of numbers. In addition, this system also provides a grade based on the degree of similarity.

4 Conclusions

In this research, the authors successfully implemented the cosine similarity method on a web-based automatic assessment system of essay answers based on climate matching. Overall, the "Essay Checker" system proved its potential as an effective tool in the essay assessment process in an educational environment. Further development could include integration with more advanced text scoring algorithms and the addition of new features to improve the accuracy and functionality of the system.underway.

Acknowledgements

We extend our deepest gratitude to the professor in charge of the Natural Language Processing course for their guidance and support throughout this research. We also thank all parties who have contributed to this research.

References

- [1] A. Salim, K. Rijal, and B. Hendrik, “Studi Literatur Sistem Penilaian Esai Otomatis Pada E-Learning Dengan Algoritma Winnowing,” *J. Sist. Inf. dan Ilmu Komput.*, vol. 1, no. 3, pp. 163–172, 2023, [Online]. Available: <https://doi.org/10.59581/jusiik-widyakarya.v1i3.1227>
- [2] A. C. Herlingga, I. P. E. Prisma, D. R. Prehanto, and D. A. Dermawan, “Algoritma Stemming Nazief & Adriani dengan Metode Cosine Similarity untuk Chatbot Telegram Terintegrasi dengan E-layanan,” *J. Informatics Comput. Sci.*, vol. 2, no. 01, pp. 19–26, 2020, doi: 10.26740/jinacs.v2n01.p19-26.
- [3] R. R. Et.al, “The Similarity of Essay Examination Results using Preprocessing Text Mining with Cosine Similarity and Nazief-Adriani Algorithms,” *Turkish J. Comput. Math. Educ.*, vol. 12, no. 3, pp. 1415–1422, 2021, doi: 10.17762/turcomat.v12i3.938.
- [4] R. I. Pratama, Munir, and R. Megasari, “Detector Similarity Answers Between Students on Essay Digital Exam System,” *Proc. 7th Math. Sci. Comput. Sci. Educ. Int. Semin. MSCEIS 2019*, 2020, doi: 10.4108/eai.12-10-2019.2296348.
- [5] T. Wahyuningsih *et al.*, “Text Mining an Automatic Short Answer Grading (ASAG), Comparison of Three Methods of Cosine Similarity, Jaccard Similarity and Dice’s Coefficient,” *J. Teknol. Inf. dan Ilmu Komput.*, vol. 1, no. 2, pp. 343–348, 2021, doi: 10.17762/turcomat.v12i3.938.
- [6] W. A. S. S L B Ginting, Y R Ginting, Sutomo, “Aplikasi Deteksi Kemiripan Kata Menggunakan Algoritma Rabin-Karp,” *J. Teknol. dan Inf.*, vol. 12, no. 2, pp. 162–175, 2022, doi: 10.34010/jati.v12i2.

-
- [7] R. Vinayakumar, M. Alazab, K. P. Soman, P. Poornachandran, A. Al-Nemrat, and S. Venkatraman, “Deep Learning Approach for Intelligent Intrusion Detection System,” *IEEE Access*, vol. 7, pp. 41525–41550, 2019, doi: 10.1109/ACCESS.2019.2895334.
- [8] F. Al-Turjman, H. Zahmatkesh, and L. Mostarda, “Quantifying uncertainty in internet of medical things and big-data services using intelligence and deep learning,” *IEEE Access*, vol. 7, pp. 115749–115759, 2019, doi: 10.1109/ACCESS.2019.2931637.
- [9] J. R. Saura, B. R. Herraiez, and A. Reyes-Menendez, “Comparing a traditional approach for financial brand communication analysis with a big data analytics technique,” *IEEE Access*, vol. 7, pp. 37100–37108, 2019, doi: 10.1109/ACCESS.2019.2905301.
- [10] D. Nallaperuma *et al.*, “Online Incremental Machine Learning Platform for Big Data-Driven Smart Traffic Management,” *IEEE Trans. Intell. Transp. Syst.*, vol. 20, no. 12, pp. 4679–4690, 2019, doi: 10.1109/TITS.2019.2924883.
- [11] M. M. Fawzy, A. S. Elsharkawy, Y. A. Khalifa, and A. A. hassan, “Contractor selection by using multi-criteria decision-making for Egyptian road maintenance,” *Int. J. Syst. Assur. Eng. Manag.*, 2024, doi: 10.1007/s13198-024-02249-3.
- [12] S. Yuliyanti and Rizky, “Implementasi Algoritma Rabin Karp Untuk Mendeteksi Kemiripan Dokumen Stmik Bandung,” *J. Bangkit Indones.*, vol. 10, no. 02, p. 1, 2020, doi: 10.52771/bangkitindonesia.v10i02.124.
- [13] S. Legianto, “Implementasi Text Mining Untuk Mendeteksi Hate Speech Pada Twitter,” p. 60, 2019.
- [14] R. A. Raharjo, I. M. G. Sunarya, and D. G. H. Divayana, “Perbandingan Metode Naïve Bayes Classifier Dan Support Vector Machine Pada Kasus Analisis Sentimen Terhadap Data Vaksin Covid-19 Di Twitter,” *Elkom J. Elektron. dan Komput.*, vol. 15, no. 2, pp. 456–464, 2022, doi: 10.51903/elkom.v15i2.918.
- [15] F. Muhammad, N. M. Maghfur, and A. Voutama, “Sentiment Analysis Dataset on COVID-19 Variant News,” *Sci. J. Inromation Syst. Informatics*, vol. 4, no. 1, pp. 382–391, 2022.

- [16] L. R. Setiawan and D. Nasien, “Cosine Similarity for Essay Answer Detection,” *J. Appl. Bus. Technol.*, vol. 1, no. 1, pp. 36–40, 2020, doi: 10.35145/jabt.v1i1.21.
- [17] F. Setio Pribadi, U. Hasanah, and D. Nur Sa, “Automatic Short Answer Scoring (ASAS) Using String-based Similarity and Query Expansion,” pp. 678–684.
- [18] B. L. Qasthari, E. Susanti, and M. Sholeh, “Classification Of Lung and Colon Cancer Histopathological Images Using Convolutional Neural Network (CNN) Method An A Pre-Trained Models,” *Int. J. Appl. Sci. Smart Technol.*, vol. 5, no. 1, pp. 133–142, 2023, doi: 10.24071/ijasst.v5i1.6325.
- [19] E. L. Amalia, A. J. Jumadi, I. A. Mashudi, and D. W. Wibowo, “Analisis Metode Cosine Similarity Pada Aplikasi Ujian Online Otomatis (Studi Kasus JTI POLINEMA),” *J. Teknol. Inf. dan Ilmu Komput.*, vol. 8, no. 2, pp. 343–348, 2021, doi: 10.25126/jtiik.2021824356.
- [20] N. Vendyansyah and Y. A. Pranoto, “Perancangan dan Pembuatan Aplikasi untuk Mendeteksi Kemiripan Jawaban Menggunakan Cosine Similarity,” *J. Tek. (Jurnal Fak. Tek. Univ. Islam Lamongan)*, vol. 13, no. 1, pp. 23–28, 2021.

Comparative Analysis of Three Solid Waste Management Systems Towards Full Automation

A.D. Omiyale ¹, L.F. Ogunwolu ^{1*}, O.O. Ajibola ¹

¹ *Department of Systems Engineering, Faculty of Engineering
University of Lagos, Akoka, Yaba, Lagos, Nigeria*

**Corresponding Author: fogunwolu@unilag.edu.ng*

(Received 12-07-2024; Revised 07-08-2024; Accepted 08-08-2024)

Abstract

This study uses a four-week simulation to evaluate traditional, semi-automatic, and autonomous waste management systems, employing Principal Component Analysis (PCA), Discrete Event Simulation (DES), and an ANOVA test. PCA was used to visualise and understand the variations in waste collection volumes between the three systems, with the first two principal components accounting for 100% of the variance (PC1: 56.3%, PC2: 43.7%). Each system was classified into distinct clusters: traditional in the lower-left quadrant, semi-automatic in the upper-left and lower-right quadrants, and autonomous in the upper-right quadrant, with ANOVA indicating significant variations. DES simulated everyday waste collection for 120 days. The traditional system collected an average of 50 kg/day with a 10-kilogramme variance, the semi-automatic 48 kg/day with an 8 kg variability, and the autonomous 45 kg/day with a 5 kg variability. The total waste collected was 6012.34 kg (traditional), 5824.29 kg (semi-automatic), and 5482.67 kg (autonomous). Fuel consumption, cost savings, and environmental impacts were analyzed. The autonomous system showed the lowest fuel consumption and highest cost savings, significantly reducing carbon emissions compared to others. The results from PCA and DES, supported by ANOVA, indicate that while the traditional system is most efficient in waste collection, the autonomous system offers consistent performance and significant environmental benefits. This comprehensive analysis provides valuable insights for optimizing waste management strategies and balancing efficiency, cost, and environmental impact.

Keywords: Solid waste management, Autonomous systems, urbanization, environmental impact, and Sustainability.

1 Introduction

Effective solid waste management is crucial for both environmental sustainability and public health [1]. The introduction of technology has resulted in a significant shift toward automation in waste management systems, enhancing efficiency and efficacy.



Advances in technology such as Cloud computing, deep learning algorithms, blockchain, and the Internet of Things (IoT) are some of the technologies being proposed as approaches to automating waste classification, sorting, and recycling in urban and smart cities [2]. These technological advancements have the potential to improve waste management by improving recycling and lowering environmental impact. The use of machine learning techniques, such as Support Vector Machines (SVM), offers a fresh approach to assessing public opinion towards waste management challenges. This strategy allows for the examination of large data sets to yield relevant insights [3].

Smart Waste Management (SWM) has evolved as an alternative to the inefficiencies and environmental repercussions of traditional waste management practices. SWM uses data-driven solutions to increase operational efficiency while reducing environmental impact [4]. Traditional waste management systems frequently involve waste pickup delays, additional travel, and a reliance on manual labour [5]. The move to SWM is critical because it can address these difficulties by delivering real-time data and optimising waste-collecting systems [6].

The introduction of Autonomous Waste Management Systems (AWMS) represents a paradigm shift in waste management, incorporating advanced automation and artificial intelligence technology such as self-driving pickup trucks and real-time environmental sensors [7]. While smart waste management offers numerous advantages, limitations such as considerable research investments and the societal concern about job displacement must be addressed. Effective data privacy protection is essential in fostering trust among citizens and encouraging their active participation in smart city ecosystems [8]. To create a more sustainable, secure, and clean future, a delicate balance of technological innovation, ethical considerations, and economic feasibility is required. This balance is critical for addressing several aspects of waste management and sustainability [9].

Waste management systems can be improved by integrating modern technologies and ethical concepts. Autonomous Waste Management Systems (AWMS) represent a substantial leap in automation and artificial intelligence technologies. There are various challenges to implementing autonomous waste management systems in cities. Technical concerns include assuring sensor functionality in a variety of weather situations, negotiating complicated urban infrastructures, and preventing system failures.

Additionally, public approval and regulatory frameworks are important issues. Economic issues such as initial investment cost and continuous maintenance provide major obstacles to widespread adoption [10].

Traditional Methods in Different Shades of Means for Disposal, Routing, and General Management.

Due to the growing volume of solid waste generated by human activities as a result of population explosion and rural-urban drift, effective waste management systems are critical. While new technologies emerge, traditional waste management approaches remain critical in the global setting [11]. This study provides a full examination of different waste management systems and their standard procedures, focusing on their use in routing, disposal, and general administration.

Composting, trenching, and incineration are just a few examples of traditional waste disposal processes utilized by various societies throughout history. Composting is the spontaneous decomposition of organic waste into nutrients that benefit the soil [12], [13]. In agricultural settings, trenching is a common practice for burying biodegradable waste to facilitate decomposition. In various societies, incineration of waste has been a typical approach for reducing waste volume, even though it is not always environmentally friendly.

Landfilling remains a popular waste disposal strategy due to its simplicity and economic effectiveness [14]. However, issues with landfill capacity, environmental degradation (such as leachate contamination of groundwater and landfill gas emissions), and resource depletion pose substantial obstacles [14]. In developing nations, uncontrolled waste disposal practices, known as "open dumping," pose health and environmental dangers such as disease transmission, leachate contamination, and air pollution [15]. To alleviate landfill strain, waste can be burned at high temperatures to minimize volume while also producing energy [16]. Nonetheless, incineration can cause concerns like emissions-related air pollution and the formation of bottom ash, which must be disposed of in a landfill [17].

Routing and General Management in Traditional Waste Management System

Traditional waste management practices include two basic routing strategies:

Fixed Routes: Traditional waste collection method often follow established routes with predetermined pickup places and schedules [18]. While this system is noted for its simplicity and predictability, it can be inefficient due to factors such as unpredictable waste generation patterns and excessive travel distances. To overcome these difficulties, researchers are investigating novel techniques for optimizing waste-collecting routes and transportation.

Manual route planning: Manual waste disposal route planning, although based on experience and historical data, may result in suboptimal collection due to its time-consuming and subjective nature. In contrast, modern waste management solutions are rooted in sustainability principles, aiming to harmonize with local ecosystems while minimizing environmental impacts. By exploring these contemporary tools, communities can gain insights into resource conservation and sustainable living practices [18].

Semi-automatic Systems in Different Shades and Means for disposal, routing, and general management.

Semi-automatic waste management systems offer a promising alternative to existing manual systems, focusing on disposal alternatives, routing optimization, and overall management strategies to counteract environmental contamination and resource depletion caused by increased waste generation [19].

Sustainable waste management options, like recycling, composting, and waste-to-energy programs, are becoming increasingly popular as semi-automatic waste management solutions due to their environmental benefits [20]. Adopting semi-automatic waste management systems aligns with sustainable practices, enabling organizations to handle waste efficiently throughout its entire lifecycle, from generation to disposal. Innovations in separation and sorting technologies are critical to semi-automatic waste management systems because they enable the recovery of valuable materials from waste streams, reduce landfill utilisation, and improve recycling efforts.

A conceptual and simulated semi-automatic urban waste management system based on Customer Reliability Indices and Global Systems for Mobile Communication (GSM)

technology is presented in [19]. To plan the routes for waste collection vehicles, the system depends on waste generators reporting waste levels via GSM handsets. Customer reporting and reliability indices are computed in a pay-as-you-generate system to penalize false reporting which ultimately affect billing. Simulation results indicate that the system can improve waste collection efficiency and reliability in addressing Municipal Solid Waste Management challenges, with advantages over traditional fixed routing systems in terms of reduced travel distance, collection time, and costs.

Routing and General Management in Semi-Automatic Waste Management System

Optimizing waste collection routes is vital for minimizing operational costs and environmental effects. Semi-automatic systems utilise the following technologies:

Real-time Bin Fill Level Data: Sensors embedded in waste bins give real-time fill level data, allowing routing algorithms to optimize collection schedules by guiding vehicles to bins that require emptying. This strategy saves unnecessary travel while improving operational efficiency [21]. Predictive analytics uses machine learning algorithms to analyse past data, allowing for the forecasting of future waste generation trends. This approach enables proactive route planning, which improves efficiency and optimises resource allocation.

The integration of technology is critical for improving waste management techniques. smart bins with communication capabilities can monitor fill levels in real time and detect potential difficulties, allowing for more proactive waste management. These containers can remind homeowners to properly dispose of rubbish and separate recyclables, encouraging better waste management practices [21]. Furthermore, techniques such as gamification and educational materials are used to involve customers in waste reduction campaigns. Mobile applications linked to waste management systems use gamification and educational features to encourage active engagement in waste reduction and proper waste segregation [22].

Autonomous Systems Implementation in Different Shades of Means for Disposal, Routing, and General Management.

The integration of autonomous waste management systems marks a significant step forward in waste management practices. These systems use artificial intelligence, robots, and sensor-based monitoring to enhance waste collection, sorting, and disposal processes [23]. Organizations that use autonomous systems can increase the accuracy and efficiency of their waste management processes. Recent advances in autonomous waste management systems have demonstrated the application of deep learning algorithms to optimize waste classification, monitoring, and collection activities, to lower costs and improve overall waste management operations. The incorporation of automated sentiment analysis into waste management systems helps improve decision-making. Understanding public opinion helps policymakers build more targeted and effective waste management plans [3].

Challenges of Implementing Autonomous Waste Management Systems

The successful implementation of autonomous waste management systems in metropolitan areas necessitates overcoming myriads of technological, regulatory, economic, social, and environmental challenges.

The technical challenges in implementing advanced waste management systems (AWMS) in urban ecosystems include ensuring system stability, accuracy, and interoperability with existing infrastructure, and ensuring data integration and infrastructural compatibility [24].

Regulatory and legal challenges as highlighted in [25] affect the deployment of AWMS, necessitating clear accountability frameworks, compliance with laws, and navigating complex regulatory landscapes for successful implementation.

Furthermore, economic constraints, such as high initial costs and long-term financial challenges, hinder the adoption of AWMS, necessitating the development of robust cost-benefit evaluations and innovative financing options [26].

Addressing social and ethical issues, ensuring fair access to AWMS services, and addressing employment displacement, privacy, and safety are crucial for public approval and trust [25].

AWMS's sustainable waste management practices require careful consideration of environmental and lifespan concerns, thorough environmental impact studies, effective planning, and collaboration with human workers [27]. Data privacy and security are crucial for general data protection regulation compliance, ensuring protection against data breaches and unauthorised access, preventing system breakdowns, and protecting sensitive information. Addressing technical, regulatory, economic, social, environmental, and ethical concerns is crucial for ensuring the successful deployment of AWMS in urban areas [24].

2 Material and Methods

This paper presents the design of an autonomous waste management system (AWMS) system. The AWMS design consists of three essential sub-systems: the Administrative Center (AC), the Autonomous Car Base (ACB), and the Smart Waste Bins (SWB), each of which plays a unique role in the waste management process. The SWB sub-system, a critical component of the AWMS, consists of Arduino microcontrollers, compactors, solar panels/batteries, DC motors, a variety of sensors (such as level, odor, and human proximity detectors), and an Intelligent Reporting Unit.

The SWB sub-system utilizes ultrasonic sensors to continuously monitor waste levels in the bin and activates the compactor periodically to compress waste. An electronic nose sensor, a metal oxide semiconductor (MOS) evaluates the biodegradability and odour of waste materials. To facilitate efficient data collection and reporting, the Intelligent Reporting Unit (IRU) in the SWB sub-system provides a platform for reporting and monitoring. The IRU communicates with the microcontroller via the GSM/GPRS module to gather information on fill levels, odour strength, and AWMS locations. Waste capacity in the SWB sub-system is measured through four calibration levels, with each level corresponding to a specific percentage of fill capacity. Additionally, waste materials' odour intensity is categorized for biodegradability assessment. Real-time data collection and interpretation are enabled through ThingSpeak, supporting effective waste evacuation procedures based on predefined thresholds.

The autonomous movement and operation of the waste by AWMS is facilitated by the ACB sub-system, which includes navigation devices, obstacle avoidance units,

perception modules, decision-making units, and actuation modules. The Intelligent Management Unit (IMU) located within the Administrative Centre is responsible for tasks such as data analysis, vehicle routing, billing, and network coordination. Effective communication between these subsystems is crucial for the smooth operation of the AWMS.

3 Results and Discussions

A four-month simulation was conducted in a residential estate with 180 houses and approximately 2,000 occupants to assess the efficacy of three different waste management systems. The estate also consists of schools and offices. The results are shown in Table 1 below.

Table 1 shows how much waste each waste management system collects monthly. The traditional, semi-automatic, and autonomous methods collected 60,957 kg, 57,179 kg, and 51,774 kg, respectively. Table 2 indicates considerable differences in waste collection volume between the three waste management systems (traditional, semi-automatic, and autonomous) using a test of ANOVA. The F-statistic of 22.888 ($p < 0.05$) shows significant variability in waste collection volume across systems. The critical F-value of 5.143 validates the statistical significance of the results.

Table 1. Volume of Waste Collected by Waste Management Systems (kg)

	(Traditional)	(Semi-automatic)	(Autonomous)
1	14304	13927	12706
2	15437	14240	13122
3	16547	15427	12597
4	14669	13585	13349
Total	60957	57179	51774

Table 2. ANOVA Analysis of Volume of Waste Collected

Anova: Single Factor

SUMMARY

<i>Groups</i>	<i>Count</i>	<i>Sum</i>	<i>Average</i>	<i>Variance</i>
14304	3	46653	15551	891468

13927	3	42252	14084	195493
10706	3	33768	11256	787143

ANOVA

Source of Variation	SS	Df	MS	F	P-value	F crit
Between Groups	28596698	2	14298349	22.8883	0.001556	5.143253
Within Groups	3748208	6	624701.3			
Total	32344906	8				

Challenges of Implementing Autonomous Waste Management Systems

PCA was used to visualise and comprehend the differences in waste collection quantities across the three systems as shown in Fig. 1. The first two principal components were preserved, accounting for 100% of the variance in the data (PC1: 56.3%, PC2: 43.7%).

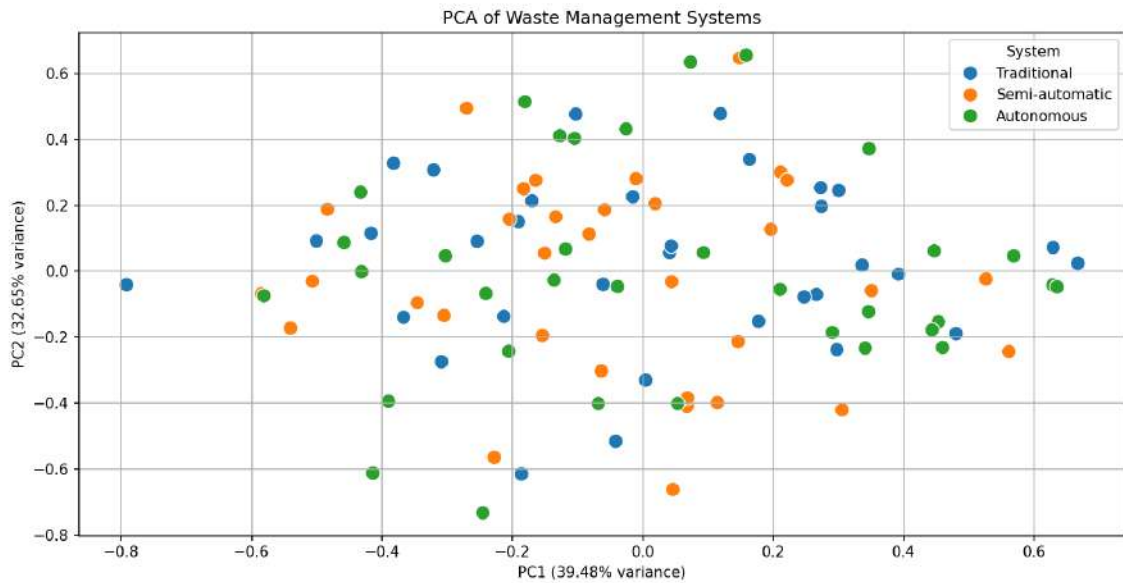


Figure 1. PCA of Waste Management Systems

- **Component Loadings:** The variables' loadings on the principal components were substantial, indicating that they correlated strongly.
- **Principal Component Scores:** A scatter plot of the principal component scores (Figure 1) revealed unique clusters corresponding to each waste management system.
 - Traditional: Lower-left quadrant.
 - Semi-automatic: Upper-left and lower-right quadrants.
 - Autonomous: Upper-right quadrant.

These clusters show distinct separations across the three systems, supporting the results obtained with the test of ANOVA significantly.

Discrete Event Simulation (DES) Analysis

A Discrete Event Simulation (DES) was also run to further investigate the variability among the systems. This method depicts system operation as discrete events, capturing the dynamic behaviour of traditional, semi-automatic, and autonomous waste management systems in the test residential estate. Using SimPy, we replicated the daily waste collection operation for each system :

- **Traditional System:** This has an average daily collection rate of 50 kg, with a 10-kilogramme fluctuation.
- **Semi-automatic System:** This collects an average of 48 kilogramme each day, with an 8 kg variability.
- **Autonomous System:** This collects 45 kilogrammes every day on average, with a variability of 5kg.

The simulation ran for 120 days, tracking the total volume of waste collected by each system as presented in Table 3 below. The DES results reveal that the traditional system gathered the most waste, followed by the semi-automatic and autonomous systems. These results are consistent with the results obtained through ANOVA, and PCA, providing additional support for the Traditional system's efficiency. The autonomous system performed more consistently while gathering less waste. These results are illustrated in a bar chart (Fig. 2).

Table 3. Total waste collected by each waste management system

System	Total Waste Collected (kg)
Traditional	6012.34
Semi-automatic	5824.29
Autonomous	5482.67

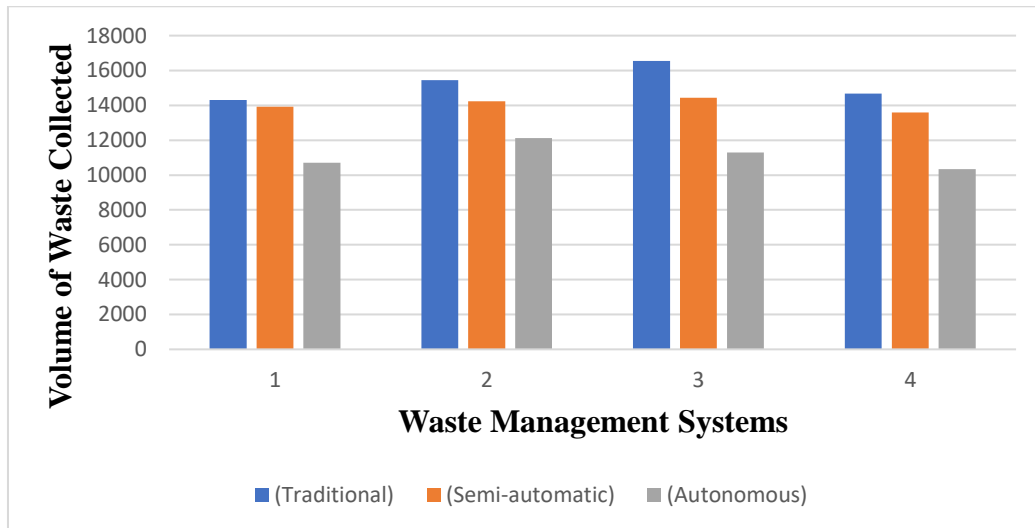


Figure 2. Total Waste Collected by Each System (120 days)

Comparing waste collection efficiency across the three systems, traditional, semi-automatic, and autonomous. It was discovered that the traditional system collected the highest volume of waste, but faced challenges in managing overflowing bins, posing health risks. The semi-automatic system, which uses a GSM mechanism through the user to notify collection authorities when bins are nearing full capacity, prevents overflow to a great extent and maintains cleanliness. The autonomous system, which operates without human intervention, effectively prevented the problem of overflowing bins while preserving environmental aesthetics and preventing potential health risks. The study emphasizes the importance of integrating technological advancements in waste management systems to enhance operational efficiency, mitigate environmental risks,

while also promoting public health. The advantages of semi-automatic and autonomous systems over traditional methods emphasize the potential of automation to revolutionize waste collection processes for a cleaner, healthier, and more sustainable environment.

Fuel Consumption and Waste Overflow Management

This section compares traditional, semi-automatic, and autonomous waste management systems based on fuel usage and waste overflow management to assess their environmental impact. Fuel consumption plays a crucial role in the environmental impact of waste management systems. Table 4 shows the fuel consumption of each of the systems during the test period.. The average fuel usage rates are shown below:

- **Traditional System:** 15 litres/day
- **Semi-automatic System:** 10 litres/day
- **Autonomous System:** 5 litres/day

Fig. 3 above depicts an examination of fuel consumption by the three waste management methods. Significant differences in fuel efficiency and environmental impact were discovered. Traditional systems consumed 676.10 litres of fuel due to inadequate waste collection procedures. Semi-automatic systems raised fuel consumption to 797.54 litres as a result of fuzzy human perceptions of waste bin level and notifications to the collecting authority. Autonomous systems with full automation reduced fuel consumption by 67% making it the most environmentally friendly option.

Table 4. Fuel Consumption Over Four Months.

System	Fuel Consumption (litres)	Reduction from Traditional System
Traditional	1800	0%
Semi-automatic	1200	33%
Autonomous	600	67%

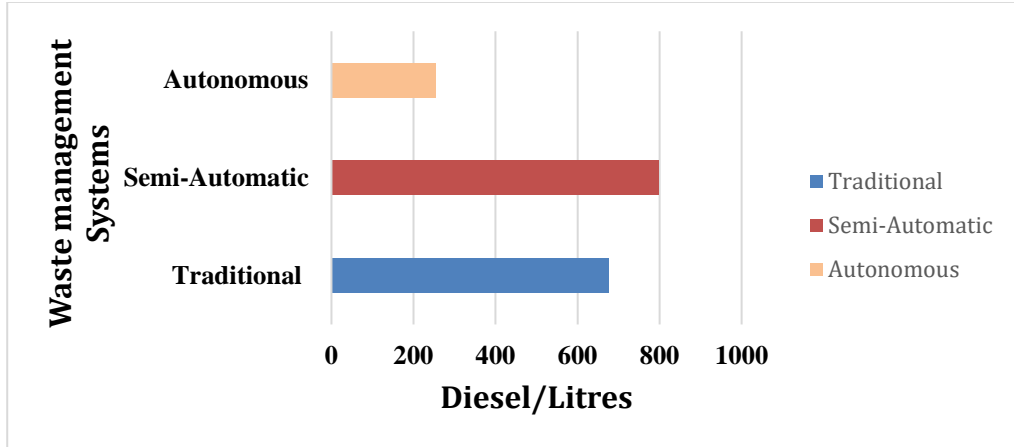


Figure 2. Graph of Fuel Consumption

Waste Overflow Management

Table 5 shows the capacity of each system to manage waste overflow. Waste management is influenced by how frequently and efficiently waste is collected. The three systems - traditional, semi-automatic, and autonomous - were evaluated for performance and effectiveness. Traditional systems experienced frequent overflows of waste due to infrequent waste collection, resulting in inefficient waste management. Semi-automatic systems improved moderately, but there were still occasional overflows caused by collection scheduling mistakes. Autonomous systems demonstrated the most effective strategy, effectively minimising overflow events through continuous monitoring and adaptive scheduling. These solutions not only increased waste collection efficiency, but also highlighted the transformative power of automation in waste management.

The autonomous system outperforms the traditional system by 75%, while semi-automatic methods show a 50% improvement against the traditional method in handling waste overflow incidents. This demonstrates the efficiency and efficacy of the autonomous system in waste management through continuous monitoring and adaptive scheduling.

Table 5. Waste Overflow Incidents

System	Overflow Incidents	Relative Performance
Traditional	High	1 (baseline)

Semi-automatic	Moderate	2 (50% improvement)
Autonomous	Low	3 (75% improvement)

Environmental Benefits

There are various environmental advantages to autonomous waste management:

Reduced Fuel Consumption: Autonomous systems consume 67% less fuel compared to the traditional due to well-planned routes and effective waste management thereby reducing emissions into the environment.

Minimized Waste Overflow: Autonomous systems monitor waste levels and adjust collection schedules, thus reducing overflow events and maintaining a cleaner environment, and reducing public health risks.

Improved Efficiency: Real-time data optimization of routes and collection schedules reduces fuel consumption and time waste, and overall reduction environmental impact.

4 Conclusions

The study evaluating three waste management systems in a residential area showed that traditional systems collected the most waste but led to overflowing bins and unsanitary conditions. The semi-automatic system, which alerted authorities when bins were nearing capacity, improved aesthetics but consumed more fuel. The autonomous system, with its automation and advanced technology, achieved the lowest waste volume but effectively managed overflowing bins and eliminated the problem of pungent odours in waste. These findings suggest that semi-automatic and autonomous systems offer significant advantages in waste management, such as improving operational efficiency, mitigating environmental risks, promoting public health, and lowering fuel consumption. The study supports the integration of technology and automation in waste management for a cleaner, more efficient, and sustainable future.

References

- [1]. R. Abubakar et al., "Environmental Sustainability Impacts of Solid Waste Management Practices in the Global South," *Int. J. Environ. Res. Public Health*, vol. 19, no. 19, p. 12717, 2022. [Online]. Available: <https://doi.org/10.3390/ijerph191912717>
- [2]. R. W. Ahmad, K. Salah, R. Jayaraman, I. Yaqoob, and M. Omar, "Blockchain for Waste Management in Smart Cities: A Survey," *IEEE Access*, vol. 9, pp. 131520–131541, 2021. [Online]. Available: <https://doi.org/10.1109/access.2021.3113380>
- [3]. R. A. Nugroho, U. S. Dharma, S. H. Wijono, K. Pinaryanto, R. Gunawan, and F. Sinungharjo, "Sentiment analysis on tweets about waste problem in Yogyakarta using SVM," *Int. J. Appl. Sci. Smart Technol.*, vol. 6, pp. 183-196, 2024, doi: 10.24071/ijasst.v6i1.7415.
- [4]. S. Vishnu, S. Ramson, S. Senith, T. Anagnostopoulos, A. Abu-Mahfouz, X. Fan, and A. Kirubaraj, "IoT-enabled solid waste management in smart cities," *Smart Cities*, vol. 4, no. 3, pp.1004-1017, 2021. doi: 10.3390/smartcities4030053.
- [5] A. Abdullahi, "Development of a smart waste management system with automatic bin lid control for smart city environment," *EAI Endorsed Transactions on Smart Cities*, vol. 7, no. 3, 2024. doi: 10.4108/eetsc.4385
- [5]. A. Shah, S. Fauzi, R. Gining, T. Razak, M. Jamaluddin, and R. Maskat, "A review of IoT-based smart waste level monitoring system for smart cities," *Indonesian Journal of Electrical Engineering and Computer Science*, vol. 21, no. 1, p. 450, 2021. doi: 10.11591/ijeecs.v21.i1.pp450-456.
- [6]. S. Khan, B. Ali, A. A. K. Alharbi, S. Alotaibi, and M. Alkhatami, "Efficient IoT-assisted waste collection for urban smart cities," *Sensors*, vol. 24, no. 10, p. 3167, 2024. [Online]. Available: <https://doi.org/10.3390/s24103167>
- [7]. S. Manik, M. Berawi, Gunawan, & M. Sari, "Smart waste management system for smart & sustainable city of indonesia's new state capital: a literature review", *E3S Web of Conferences*, vol. 517, p. 05021, 2024. <https://doi.org/10.1051/e3sconf/202451705021>

-
- [8]. K. Paritosh, S. Kushwaha, M. Yadav, N. Pareek, A. Chawade, & V. Vivekanand, "Food waste to energy: an overview of sustainable approaches for food waste management and nutrient recycling", *Biomed Research International*, vol. 2017, p. 1-19, 2017. <https://doi.org/10.1155/2017/2370927>
- [9]. Cicceri, "An intelligent hierarchical cyber-physical system for beach waste management: the bioblu case study", *Ieee Access*, vol. 11, p. 134421-134445, 2023. <https://doi.org/10.1109/access.2023.3317689>
- [10]. S. E. Vergara and G. Tchobanoglous, "Municipal Solid Waste and the Environment: A Global Perspective," *Annual Review of Environment and Resources*, vol. 37, no. 1, pp. 277–309, 2012. [Online]. Available: <https://doi.org/10.1146/annurev-environ-050511-122532>
- [11]. K. R. Atalia, D. M. Buha, K. A. Bhavsar, and N. K. Shah, "A review on composting of municipal solid waste," *J. Environ. Sci., Toxicol. Food Technol.*, vol. 9, no. 5, pp. 20-29, 2015. [Online]. Available: <https://doi.org/10.9790/2402-09512029>
- [12]. M. Ayilara, O. Olanrewaju, O. Babalola, and O. Odeyemi, "Waste Management through Composting: Challenges and Potentials," *Sustainability*, vol. 12, no. 11, p. 4456, 2020. [Online]. Available: <https://doi.org/10.3390/su12114456>
- [13]. R. Weber, A. Watson, M. Forter, and F. Oliaei, "Review Article: Persistent organic pollutants and landfills - a review of past experiences and future challenges," *Waste Management & Research*, vol. 29, no. 1, pp. 107–121, 2011. [Online]. Available: <https://doi.org/10.1177/0734242x10390730>
- [14]. L. Luo, G. Kaur, and J. W. C. Wong, "A mini-review on the metabolic pathways of food waste two-phase anaerobic digestion system," *Waste Management & Research*, vol. 37, no. 4, pp. 333–346, 2019. [Online]. Available: <https://doi.org/10.1177/0734242x18819954>
- [15]. G. Wang, L. Qin, G. Li, and L. Chen, "Landfill site selection using spatial information technologies and AHP: A case study in Beijing, China," *Journal of Environmental Management*, vol. 90, no. 8, pp. 2414–2421, 2009. [Online]. Available: <https://doi.org/10.1016/j.jenvman.2008.12.008>

-
- [16]. M. Vaverková and D. Adamcová, "Long-Term Temperature Monitoring of a Municipal Solid Waste Landfill," *Polish Journal of Environmental Studies*, vol. 24, pp. 1373–1378, 2015. [Online]. Available: <https://doi.org/10.15244/pjoes/29940>
- [17]. S. Das and B. Kr. Bhattacharyya, "Optimization of municipal solid waste collection and transportation routes," *Waste Manage.*, vol. 43, pp. 9–18, 2015. [Online]. Available: <https://doi.org/10.1016/j.wasman.2015.06.033>
- [18]. L. Ogunwolu, A. D. Omiyale, and O. O. E. Ajibola, "Conceptual and Simulated Semi-Automatic Urban Waste Management System Using Global Systems for Mobile Communication and Customer Reliability Indices," *J. Appl. Sci. Environ. Manage.*, vol. 23, no. 7, pp. 1371-1376, 2019. [Online]. Available: <https://doi.org/10.4314/jasem.v23i7.28>
- [19]. A. Vico, M. Pérez-Murcia, M. Bustamante, E. Agulló, F. Marhuenda-Egea, J. Sáez et al., "Valorization of date palm (*Phoenix dactylifera* L.) pruning biomass by co-composting with urban and agri-food sludge", *Journal of Environmental Management*, vol. 226, p. 408-415, 2018. <https://doi.org/10.1016/j.jenvman.2018.08.035>
- [20]. M. Mohan, R. M. K. Chetty, V. Sriram, M. Azeem, P. Vishal, and G. Pranav, "IoT enabled smart waste bin with real-time monitoring for efficient waste management in metropolitan cities," *IJASC*, vol. 1, no. 3, pp. 13–19, 2019. [Online]. Available: <https://doi.org/10.22662/ijasc.2019.1.3.013>.
- [21]. M. A. Hannan, Md. Abdulla Al Mamun, A. Hussain, H. Basri, and R. A. Begum, "A review on technologies and their usage in solid waste monitoring and management systems: Issues and challenges," *Waste Manage.*, vol. 43, pp. 509–523, 2015. [Online]. Available: <https://doi.org/10.1016/j.wasman.2015.05.033>
- [22]. R. Sarc, A. Curtis, L. Kandlbauer, K. Khodier, K. E. Lorber, and R. Pomberger, "Digitalisation and intelligent robotics in value chain of circular economy oriented waste management – A review," *Waste Management*, vol. 95, pp. 476–492, 2019. [Online]. Available: <https://doi.org/10.1016/j.wasman.2019.06.035>
- [23]. S. Liu and J. Gaudiot, "Rise of the autonomous machines", *Computer*, vol. 55, no. 1, p. 64-73, 2022. <https://doi.org/10.1109/mc.2021.3093428>

- [24]. N. Azam, L. Michala, S. Ansari, & N. Truong, "Data privacy threat modelling for autonomous systems: a survey from the gdpr's perspective", *IEEE Transactions on Big Data*, vol. 9, no. 2, p. 388-414, 2023. <https://doi.org/10.1109/tbdata.2022.3227336>
- [25]. D. Mmereki, "Current status of waste management in botswana: a mini-review", *Waste Management & Research: The Journal for a Sustainable Circular Economy*, vol. 36, no. 7, p. 555-576, 2018. <https://doi.org/10.1177/0734242x18772097>
- [26]. O. Osibanjo and I. Nnorom, "The challenge of electronic waste (e-waste) management in developing countries", *Waste Management & Research: The Journal for a Sustainable Circular Economy*, vol. 25, no. 6, p. 489-501, 2007. <https://doi.org/10.1177/0734242x07082028>

The Effect of Gamma Irradiation as A Food Preservation Technology on The Shelf Life and Quality of Fresh-cut Watermelon

Rieka Arkaninto Adeska^{1, *}, Nur Octaviany¹, Renaldy Bernardo Saragih³, Retno Andrianti¹, Ridho¹, Harum Azizah Darojati¹, Dhita Ariyanti¹

¹ Study Program of Nuclear Chemical Engineering, Polytechnic Institute of Nuclear Technology Indonesia, Special Region of Yogyakarta, Indonesia

*Corresponding Author: riekaarkanintoadeska@gmail.com

(Received 22-07-2024; Revised 08-08-2024; Accepted 19-08-2024)

Abstract

Several methods for preserving food, particularly fresh fruit, aim to extend shelf life without compromising nutritional value. Food preservation technology utilizing irradiation techniques ensures food safety and stability by eliminating microbes and microorganisms while preserving nutrients. This study investigates the food preservation process using gamma irradiation, analyzes the physical changes in irradiated food over time, and examines the effects of varying gamma irradiation doses on the weight loss and shelf life of fresh-cut watermelon. The research method involves gamma irradiation at doses of 1, 1.5, 2, 2.5, and 3 kGy. Findings indicate that gamma irradiation at these doses affects the weight loss of fresh-cut watermelon. The highest weight loss, approximately 87.36%, was observed at a dose of 3 kGy, indicating significant cellular and membrane damage. Furthermore, high-dose irradiation leads to nutrient degradation and accelerates water loss, resulting in physical changes in fresh-cut watermelon, such as increased softness, wateriness, and odor.

Keywords: Food irradiation, Food preservation, Watermelon.

1 Introduction

Red watermelon (*Citrullus lanatus*) is a fruit rich in water content (up to 90%) and is commonly served as fresh-cut pieces. Fresh-cut watermelon is more susceptible to damage and spoilage compared to whole watermelon. Naturally, fruits undergo a ripening process due to ethylene oxide over time, leading to food spoilage. This ripening process



is accelerated by bacteria and microorganisms present around the fruit, as well as by temperature and oxygen[1]. Additionally, damage to the fruit results in quality degradation due to ongoing metabolic processes and physical and biological treatments[2]. The cells of the watermelon can be damaged during the cutting process[3].

The spoilage of fresh-cut watermelon can be slowed down by storing it at a cool temperature around 4°C and using plastic wrapping to suppress microbial growth and prevent contamination[3]–[5]. Additionally, UV irradiation can also delay the spoilage process of fresh-cut watermelon[6], [7]. Nevertheless, ensuring food safety and stability through the elimination of microbes remains crucial, and various methods are continuously being researched. One such method is food irradiation. This technique aims to eliminate spoilage-causing microbes and microorganisms by damaging their cell membranes, enzymes, or DNA, thereby extending the shelf life and maintaining the nutritional quality of the food[4].

Compared to UV irradiation, gamma irradiation, using sources such as cobalt-60 or Cs-137, is now emphasized for food preservation. Cobalt-60 is commonly used in food irradiation[8]. The radiation dose in food irradiation is adjusted based on its effectiveness, with preservation doses ranging from 1 kGy to 10 kGy[9], [10].

The irradiation process is often referred to as “cold pasteurization” because it can kill bacteria without using heat[11]. During the irradiation preservation process, no heating occurs, thus preserving the freshness and physical state of the food. Spoilage agents such as bacteria and insects are eliminated from the food and its packaging, preventing recontamination. This method is particularly beneficial in maintaining hygiene in areas where food is handled or processed, such as in tropical conditions[12], [13].

In the radiation preservation process, most of the radiation passes through the food without being absorbed. A small fraction of the radiation targets spoilage microorganisms and bacteria. These organisms are destroyed by electrons breaking the bonds in their DNA, leading to DNA damage, which disables their ability to grow and reproduce[14]. DNA Bond Disruption is shown in Fig. 1.

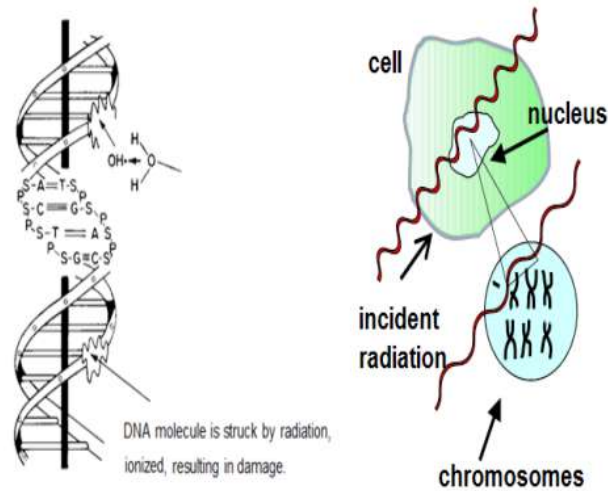


Figure 1. DNA Bond Disruption

(Source: Health Physics Society, The Effect of Radiation on Living Things)

Fruit ripeness can be measured by weight loss. During ripening, physical and chemical changes occur in the fruit, including alterations in texture, color, and weight loss. Weight loss in fruit can be influenced by varying doses of gamma radiation[15]. Gamma irradiation slows down the respiration process. As respiration progresses, O_2 intake decreases while CO_2 output increases. Respiration converts sugars into carbon dioxide and water[16].

During respiration, complex compounds within the cells are broken down into simpler molecules such as carbohydrates and volatile water (free water). This continuous respiration process leads to increasing weight loss over time. Weight loss also results from water loss through evaporation (free water) and carbon loss due to respiration during storage[17], [18]. Weight loss is calculated using the following equation:

$$\% \text{ weight loss} = \frac{W_0 - W_t}{W_0} \times 100\% \quad (1)$$

where W_0 = mass of the watermelon sample before irradiation (grams); W_t = mass of the watermelon sample after irradiation (grams).

This study investigates the food preservation process using gamma irradiation facilities, analyzes physical changes in irradiated food over time, and examines the effects of varying gamma irradiation doses on weight loss and shelf life of fresh-cut watermelon.

2 Material and Methods

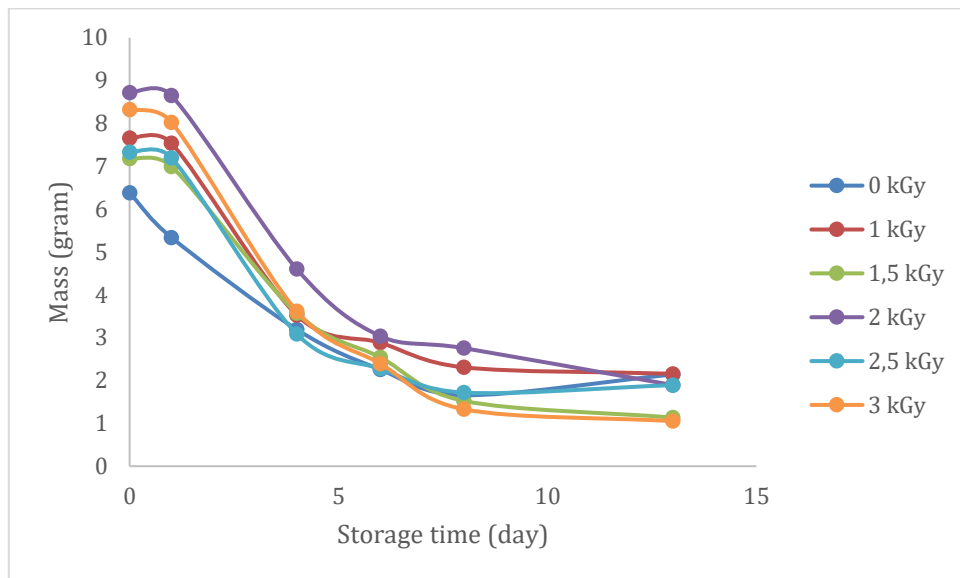
This study used local red watermelon samples cut into 2 cm x 2 cm x 2 cm cubes, categorized into six groups based on the gamma irradiation doses received. The fresh-cut watermelon was packaged with clip-on plastic bags labeled with mass and sample identity. Irradiation was performed using a Co-60 source with a dose rate of 2493 Gy/hour on March 6, 2024, at the Gamma Irradiator Type I, Observognis Yogyakarta. The irradiation doses applied were 0 kGy (control), 1 kGy, 1.5 kGy, 2 kGy, 2.5 kGy, and 3 kGy. After irradiation, samples were stored at room temperature in sealed plastic bags. Physical changes and weight loss of the watermelon were monitored and compared with the control.

3 Results and Discussions

Gamma radiation technology aims to eliminate spoilage microbes and microorganisms through DNA damage. Preservation of fresh-cut watermelon with radiation is designed for energy efficiency and ease of control. Gamma rays provide effective penetration without altering the temperature of the watermelon, thus preserving its nutrients and vitamins. Radiation technology requires dose optimization to be effective for its purpose. Incorrect doses can result in undesired cellular damage. In this preservation study, doses ranging from 1 kGy to 3 kGy were used, as shown in Table 1.

Table 1. Mass of fresh-cut watermelon and percent weight loss

Radiation Dose (kGy)	Mass of Fresh-cut Watermelon and % Weight Loss (%WL)										
	D-0	D-1	%WL D-1	D-4	%WL D-4	D-6	%WL D-6	D-8	%WL D-8	D-13	%WL D-13
0	6,80	6,78	0,41	6,59	3,15	6,27	7,81	6,06	10,92	5,97	12,29
1	8,09	8,09	0,00	7,81	3,48	7,56	6,59	7,12	12,00	6,31	22,00
1,5	7,64	7,65	-0,03	7,40	3,15	7,06	7,60	3,11	59,33	2,58	66,21
2	9,18	9,18	0,02	9,08	1,07	7,99	13,00	7,29	20,54	7,17	21,94
2,5	7,78	7,78	-0,06	7,66	1,49	7,40	4,85	7,13	8,30	6,97	10,30
3	8,77	8,76	0,02	8,63	1,55	8,31	5,18	2,38	72,82	2,33	73,44

**Figure 2.** Depicts the correlation between storage time and mass loss in fresh-cut watermelon

Fresh-cut watermelon exhibited a trend of decreasing mass over time following gamma irradiation, as depicted in Fig. 2. Initially, the mass remained relatively stable or decreased slowly. However, over time, the mass loss became more significant. For example, at an irradiation dose of 2 kGy, the watermelon mass on day 8 was 2.756 grams, decreasing to 1.894 grams by day 13. This indicates a significant weight reduction over that period. This loss is attributed to the continuous respiration process, leading to increased mass reduction over time. Additionally, mass reduction is due to water loss from evaporation (free water) and carbon loss from respiration during storage. Monitoring

watermelon mass changes helps evaluate the quality of the food after gamma irradiation, aiding in determining food safety and shelf life.

In cases of watermelon slices irradiated at different doses, higher irradiation doses resulted in higher weight loss percentages, as shown in Fig. 3. This is due to radiolysis effects caused by radiation exposure, which can alter the molecular structure of the food, including cellular and nutritional damage, affecting weight loss. High doses not only damage microbial DNA but also the structure of the watermelon itself. Additionally, the cutting process damages the cell walls of the watermelon, leading to accelerated ripening.

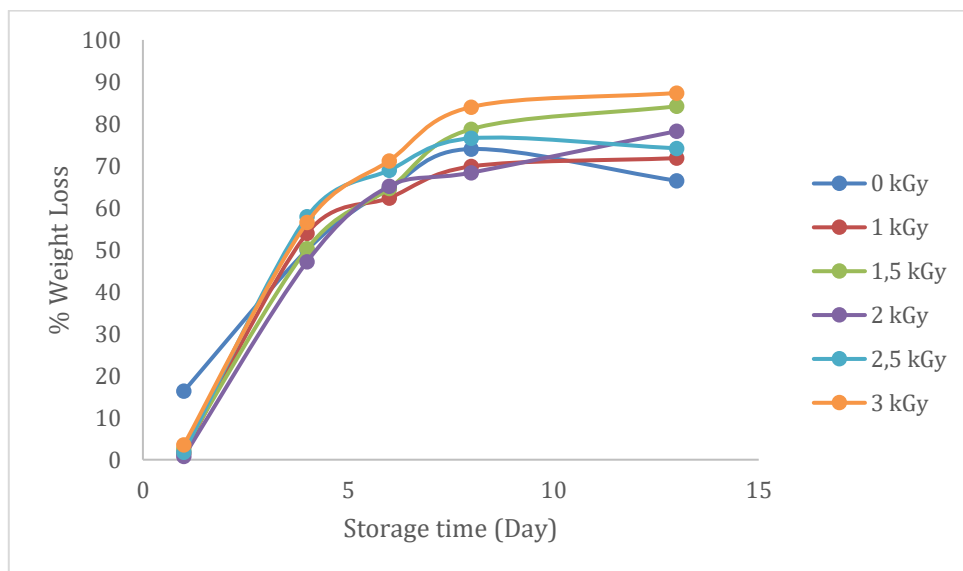


Figure 3. Depicts the correlation between storage time and percentage weight loss

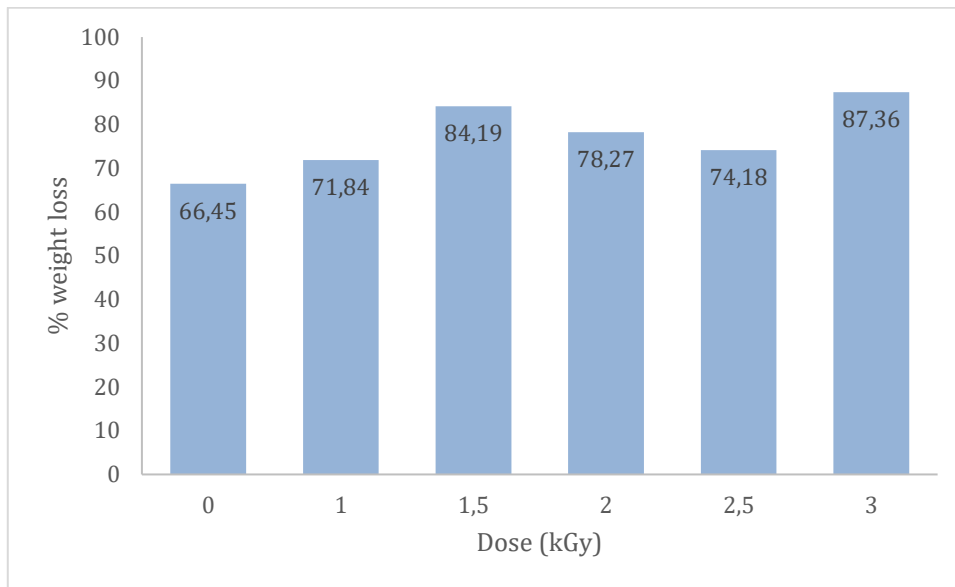


Figure 4. Illustrates the relationship between radiation dose and average weight loss

Fig. 4 illustrates the impact of irradiation dose on watermelon mass changes over time. Higher irradiation doses tend to cause faster mass loss compared to lower doses. Lower doses result in slower mass loss, suggesting they may be sufficient to inhibit microorganism growth without causing significant structural damage to the watermelon. At 0 kGy, the average weight loss was the lowest (66.45%), indicating that without radiation, the watermelon structure remained relatively intact but was more susceptible to microorganism growth. Conversely, at 3 kGy, the highest weight loss percentage (87.36%) was observed, indicating significant cellular damage and water loss. The average weight loss increased with higher radiation doses, consistent with the theory that higher doses cause more damage to cell walls and membranes, leading to greater water and nutrient loss.

Changes in watermelon mass depicted in the graphs provide insight into the effectiveness of specific irradiation doses in slowing food degradation. In addition to irradiation dose, storage time also influences the mass change of food post-irradiation. Longer storage time increases the likelihood of weight loss in the food. The data show that the percentage of weight loss in watermelon tends to increase over time after irradiation.



Figure 5. Fresh-cut watermelon on day 1 (left) and fresh-cut watermelon on day 13 (right)

Increased irradiation doses result in worsening physical and chemical changes in fresh-cut watermelon. The watermelon becomes soft, watery, and odorous due to damage to cell walls and nutrient degradation, as seen in Fig. 5. These changes lead to increased mass loss, reflected in high weight loss percentages after irradiation. Gamma irradiation induces radiolysis, where gamma rays interact with the water molecules in the fresh-cut watermelon at excessively high doses. Radiolysis generates free radicals that damage cell structures and organic molecules. This damage includes nutrient degradation, cell wall and membrane damage, and accelerated water loss. These negative effects arise from excessively high doses, necessitating optimal doses to target only microbes and microorganisms. Based on this study, the optimal dose for preserving fresh-cut watermelon is at lower doses around 1 kGy or lower.

4 Conclusions

Based on the data presented in this study on the preservation of fresh-cut watermelon using gamma irradiation, the following conclusions can be drawn:

1. Gamma irradiation can be utilized as a food preservation method to extend shelf life and maintain food quality when applied at optimal doses.

2. The dose of gamma radiation significantly affects the weight loss of food products. Higher doses result in an increased percentage of weight loss in watermelon.

Prolonged storage time after irradiation leads to greater mass loss. The graph depicting the relationship between storage time and mass of watermelon illustrates a consistent trend of mass reduction over time, which can be utilized as a monitoring tool for product quality.

Acknowledgements

The author expresses profound gratitude to the Polytechnic Institute of Nuclear Technology Indonesia also The National Research and Innovation Agency (BRIN) for their invaluable support in providing facilities and raw materials.

References

- [1] S. Koswara, "Teknologi Pengawetan Bahan Segar," *Eb. Pangan*, no. c, pp. 1–31, 2009.
- [2] F. G. Winarno and A. Moehammad, *Fisiologis Lepas Panen*. Jakarta: Sasta Hudaya, 1981.
- [3] D. A. Kirana, W. H. Delin Fitriana, M. I. Susanto, A. Otter Sorbo, and P. M. Adhi, "Pengaruh Variasi Wadah dan Suhu Terhadap Pembusukan Buah Semangka Potong (*Citrullus Lanatus*)," *J. Teknol. Pangan dan Has. Pertan.*, vol. 17, no. 1, pp. 23–28, 2022.
- [4] B. H. Lado and A. E. Yousef, "Alternative food-preservation technologies: Efficacy and mechanisms," *Microbes Infect.*, vol. 4, no. 4, pp. 433–440, 2002, doi: 10.1016/S1286-4579(02)01557-5.
- [5] Y. Hu *et al.*, "Systematic Study of the Sensory Quality, Metabolomics, and Microbial Community of Fresh-Cut Watermelon Provides New Clues for Its Quality Control and Preservation," *Foods*, vol. 11, no. 21, 2022, doi: 10.3390/foods11213423.
- [6] F. Artés-Hernández, P. A. Robles, P. A. Gómez, A. Tomás-Callejas, F. Artés, and G. B. Martínez-Hernández, "Quality Changes of Fresh-Cut Watermelon During

- Storage as Affected by Cut Intensity and UV-C Pre-treatment,” *Food Bioprocess Technol.*, vol. 14, no. 3, pp. 505–517, 2021, doi: 10.1007/s11947-021-02587-1.
- [7] F. Artés-Hernández, P. A. Robles, P. A. Gómez, A. Tomás-Callejas, and F. Artés, “Low UV-C illumination for keeping overall quality of fresh-cut watermelon,” *Postharvest Biol. Technol.*, vol. 55, no. 2, pp. 114–120, 2010, doi: 10.1016/j.postharvbio.2009.09.002.
- [8] R. D. zaria Mshelia, N. I. Dibal, and S. M. Chiroma, “Food irradiation: an effective but under-utilized technique for food preservations,” *J. Food Sci. Technol.*, vol. 60, no. 10, pp. 2517–2525, 2023, doi: 10.1007/s13197-022-05564-4.
- [9] Sukaryono, “Kajian Jenis-Jenis Dosimeter Pada Fasilitas Iradiator,” vol. 17, no. November, pp. 101–105, 2015.
- [10] B. Smith, A. Ortega, S. Shayanfar, and S. D. Pillai, “Preserving quality of fresh cut watermelon cubes for vending distribution by low-dose electron beam processing,” *Food Control*, vol. 72, pp. 367–371, 2017, doi: 10.1016/j.foodcont.2016.02.017.
- [11] O. J. Ajibola, “An overview of irradiation as a food preservation technique,” *Nov. Res. Microbiol. J.*, vol. 4, no. 3, pp. 779–789, 2020, doi: 10.21608/nrmj.2020.95321.
- [12] H. M. Gottschalk, “Food preservation by irradiation.,” *Food Nutr. (Roma)*, vol. 4, no. 3–4, pp. 30–32, 1978, doi: 10.1002/9781119237860.ch32.
- [13] S. Ganguly, K. Mukhopadhyay, and S. Biswas, “Preservation of food items by irradiation process,” *Int. J. Chem. Biochem. Sci.*, vol. 1, no. January, pp. 11–13, 2012, [Online]. Available: www.iscientific.org/Journal.html
- [14] M. K. Akinloye, G. A. Isola, S. K. Olasunkanmi, and D. A. Okunade, “Irradiation as a Food Preservation Method in Nigeria: Prospects and Problems,” *Int. J. Res. Appl. Sci. Eng. Technol.*, vol. 3, no. 11, pp. 85–96, 2015.
- [15] M. Akrom and E. Hidayanto, “Kajian Pengaruh Radiasi Sinar Gamma Terhadap Study Effect of Gamma Radiation on Weight,” *J. Pendidik. Fis. Indones. (Indonesian J. Phys. Educ.)*, vol. 10, no. 1, pp. 86–91, 2014, doi: 10.15294/jpfi.v10i1.3055.
- [16] K. A., “Basis for effect of controlled and modified atmosphere on fruit and vegetables,” *J. Food Technol.*, vol. 90, no. 5, pp. 99–104, 1989.

- [17] E. Syaefullah, “Optimasi Keadaan Penyimpanan Buah Pepaya Sebelum Pemeraman dengan Algoritma Genetika,” 2008.
- [18] W. RBH, L. TH, G. D, G. WBM, and H. EG, *An Introduction to the Physiology and Handling of Fruit and Vegetables*, 3rd ed. New York, 1989.

This page intentionally left blank

Evaluation of Tartrazine Solution as a Potential Gamma Dosimeter Material

Farhansyah Yunandani Arumbifa^{1*}, Deni Kurniawan¹,
Desalsa Anggoro Diani¹, Dika Bhakti Praja¹,
Fauziah Ulfah Ajri¹, Ariyani Kusuma Dewi¹, Dhita Ariyanti¹

¹*Indonesian Polytechnic of Nuclear Technology*

*Corresponding Author: farhansyah.yunandani@polteknuklir.ac.id

(Received 24-07-2024; Revised 08-08-2024; Accepted 19-08-2024)

Abstract

Radiation dosimetry plays a crucial role in various fields, including medical, industrial, and environmental applications. Accurate and reliable dosimeters are essential for measuring and controlling radiation exposure. This study aims to evaluate the stability of the food dye tartrazine as a potential gamma radiation dosimeter. The need for accessible and cost-effective dosimetric materials motivates the exploration of tartrazine's capabilities in this regard. This research investigates the response of tartrazine solutions under varying gamma radiation doses (0 to 3.118 kGy) using UV-Vis spectrophotometry to measure absorbance at a wavelength of 424 nm. The results demonstrate a significant decrease in absorbance with increasing radiation doses, indicating decolorization due to oxidative reactions triggered by hydroxyl radicals (OH⁻) generated during irradiation. Tartrazine, which imparts a yellow color through its diazenedyl (-N=N-) bonds, undergoes bond cleavage upon gamma radiation exposure, resulting in a permanent color change. Further analysis reveals that tartrazine-based dosimeters exhibit optimal stability for less than four weeks. Therefore, tartrazine solution can serve as an effective gamma radiation dosimeter for short-term applications. This study provides a foundation for developing new dosimetric materials, emphasizing the importance of ongoing research to enhance radiation safety and measurement accuracy.

Keywords: Dosimeter, Gamma Irradiation, Radiation, Stability, Tartrazine.

1 Introduction

Radiation dose measurement is conducted using dosimeters. Essentially, any material that undergoes changes due to irradiation can be used as a dosimeter, provided these changes can be measured with available instruments, are stable, have good



reproducibility, are easy to manufacture, and are easy to use [1]. Based on their quality and relative usage, dosimeters can be categorized into four main classes [2], [3]:

1. Primary Standard Dosimeter

These dosimeters are used by national standard laboratories to calibrate radiation fields. This category includes calorimeter dosimeters and ionization chamber dosimeters.

2. Reference Standard Dosimeter

These dosimeters are used to calibrate radiation fields and for routine dosimetry. Since not all laboratories or irradiation facilities have primary standard dosimeters, reference standard dosimeters can be used for calibrating radiation fields.

3. Routine Dosimeter

These dosimeters are used for routine measurement of absorbed radiation doses. Common examples include red/clear Perspex (PMMA) dosimeters, cellulose triacetate (CTA) dosimeters, radiochromic film dosimeters (FW-Technology), and alanine dosimeters.

4. Transfer Standard Dosimeter

These dosimeters are mainly selected from reference standard dosimeters or routine dosimeters that can be exchanged between different laboratories. This is important for the accreditation of irradiation facilities, allowing national laboratories to verify the validity of specific radiation processes carried out by an irradiation facility.

Gamma radiation is energy emitted by an element as it releases excess energy to achieve stability. It originates from the nuclei of radioactive atoms, which are typically beta emitters, though many also emit alpha particles. When these nuclei emit beta or alpha radiation, their energy decreases. However, if the nucleus still has excess energy beyond the lowest energy required to emit beta or alpha radiation, this excess energy is emitted as gamma radiation. Gamma radiation can also come from excited atomic nuclei, which can be achieved by bombarding the nucleus with neutrons. The excited nucleus returns to its original state by emitting gamma radiation [4]

Gamma radiation is not affected by magnetic fields, indicating it is uncharged. Additionally, gamma radiation has no mass, giving it greater range and penetration power compared to alpha and beta radiation. Gamma radiation falls under the category of

electromagnetic radiation. There are three possible interactions of gamma rays with matter: the photoelectric effect, Compton scattering, and pair production. These interactions produce charged particles (electrons or positrons) with energy. These electrons or positrons ionize the atoms they pass through, meaning electromagnetic waves can ionize matter indirectly [5].

When ionizing radiation, such as an electron beam, interacts with water, it produces electronically excited species and ionized molecules. This leads to the formation of reactive species (e_{aq}^- , OH^* , H^* , and HO_2^* or O_2^*) and molecular products (H_2 and H_2O_2). These species are primary products of water radiolysis that react with dissolved substances and decompose them. These primary products tend to react with the functional groups of organic molecules rather than the entire molecule [6].

Exposure is the ability of X-rays or gamma rays to cause ionization in air within a specific volume. The unit of measurement is the Roentgen. One Roentgen is the radiation intensity of X-rays or gamma rays that can produce 1.61×10^{15} ion pairs per kilogram of air. However, the Roentgen unit does not fully describe the extent of radiation exposure received by a medium [4].

Dosimetry is the activity of measuring radiation dose based on the ionization caused by radiation in specific materials. To measure the energy of radiation absorbed by a material, it is necessary to determine a quantity that does not depend on the type of radiation, its energy, or the properties of the absorbing material, but only on the amount of radiation energy per unit mass of the material [7]. Radiation dosimetry is a method for measuring the amount of radiation energy, whether in the form of electromagnetic waves or charged particle currents emitted by a radiation source at a specific point and absorbed by irradiated material. Materials that undergo changes due to irradiation can be used as dosimeters if the changes can be measured by instruments, are stable, have good reproducibility, and are easy to manufacture and use. Based on their quality and function, dosimeters are categorized into four main classes: primary standard dosimeters, reference standard dosimeters, routine dosimeters, and transfer standard dosimeters [1].

Radiochromic dosimeters are a type of dosimeter that utilize color change (chromatic change) in special polymers as a response to exposure to ionizing radiation. Gamma radiation is energy emitted by an element to release excess energy and achieve

stability. When gamma radiation is used, dyes can decompose into organic compounds with lower molecular weights, such as organic acids[8]. The primary material used is a polymer containing chromogenic compounds, which undergo photochemical reactions and permanently change color when exposed to radiation such as X-rays, gamma rays, or electron beams. This color change occurs due to modifications in the chemical structure of the polymer caused by the radiation.

Radiochromic dosimeters allow for direct observation based on the color change that occurs. These dosimeters are among the types of radiation dose monitoring systems that are easier and more practical to manufacture and use. Dosimetry observation is conducted directly by observing the color change that occurs. The color change reaction is caused by the interaction between ionizing radiation and the material used as the radiochromic agent. The characteristic color change of the radiochromic material is used as the basis for monitoring radiation dose, as the change in absorption spectra is proportional to the absorbed dose [9]. Radiochromic dosimeters are available in various forms such as liquids, gels, and thin labels. In the process of making liquid radiochromic dosimeters, solvents, dyes, and additives are required in the correct formulation. The type of solvent depends on the characteristics of the dye to be used, which can be obtained from synthetic or natural sources. Radiochromic dosimeters are widely employed for monitoring low to medium dose ranges, such as in food irradiation. Its use as a dosimeter for food irradiation necessitates the selection of radiochromic dosimeter materials that are safe for health. One potential material for use as a radiochromic dosimeter is food coloring, which is inherently safe for human consumption.

Tartrazine is a synthetic lemon yellow azo dye used as a food coloring. The yellow color of tartrazine is produced by the azo group that connects two benzene rings within its molecule. This azo group contains a nitrogen double bond (N=N) capable of absorbing specific wavelengths of visible light. Tartrazine absorbs light at a wavelength of approximately 427 nm, which lies within the blue region of the visible spectrum. Its structure is shown in the Fig. 1 below:

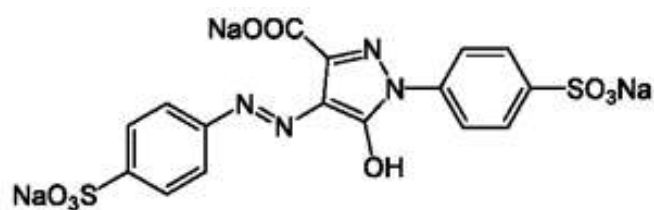


Figure 1 Chemical Structure of Tartrazine

Tartrazine is an orange-yellow powder that is easily soluble in water, producing a golden-yellow solution. Its solubility in 95% alcohol is limited, but it dissolves easily in glycerol and glycol. Tartrazine is resistant to light, acetic acid, HCl, and 10% NaOH. However, 30% NaOH will turn the color reddish. It fades easily in the presence of oxidizers; FeSO₄ makes the dye solution cloudy, although aluminum (Al) does not affect it. The presence of copper (Cu) will change the yellow color to reddish[10]. Tartrazine was selected for this study due to its widespread use as a food dye, ensuring its safety and accessibility. Moreover, its distinct chemical structure, which allows for noticeable color changes under gamma irradiation, makes it a suitable candidate for dosimetry.

2 Material and Methods

In this study, we used distilled water (aquadest) and food coloring (Koepoe Light Yellow). The instruments included a 10 ml volumetric pipette, a measuring cylinder, a beaker, a stirrer, vial bottles, and cuvettes.

The sample solution was prepared by adding one drop of food coloring to 150 ml of aquadest. This solution was then divided into six different vial bottles, ensuring that each vial contained a sufficient volume for analysis in a UV-Visible spectrophotometer. Each vial was irradiated for different durations (0, 15, 30, 45, 60, and 75 minutes), and the vials were labeled accordingly. The gamma radiation dose rate was recorded during the experiment, and the estimated gamma radiation dose absorbed by the solution was calculated using the formula: radiation dose = dose rate × irradiation time. The irradiator used in this research is the Servo Ignis irradiator at KSE Ahmad Baequni from a Co-60 radioactive source (gamma ray source) with a dose rate of 2,494 kGy/h

The absorbance of each irradiated vial was measured using a Shimadzu UV Mini-1240 UV-Visible spectrophotometer within the wavelength range of 300-650 nm, with aquadest used as the blank. The maximum absorbance observed for each vial was recorded. The data were then used to plot a curve of wavelength (nm) against absorbance for the different radiation doses (six variations). Additionally, a curve of gamma radiation dose versus the change in maximum absorbance ($\Delta A = A_i - A_0$) was plotted, where A_i represents the maximum absorbance at a specific radiation dose and A_0 represents the maximum absorbance of the non-irradiated solution.

The stability of the tartrazine solution as a radiochromic dosimeter was evaluated by measuring the solution's absorbance every week over a 4-week period. The decrease in absorbance was recorded weekly to assess whether the solution remained stable during this time. The difference in absorbance (ΔA) was calculated as the difference between the absorbance at dose 0 and other doses each week. The average %Error of each absorbance measurement in weeks 2, 3, and 4 was then compared to the first week.

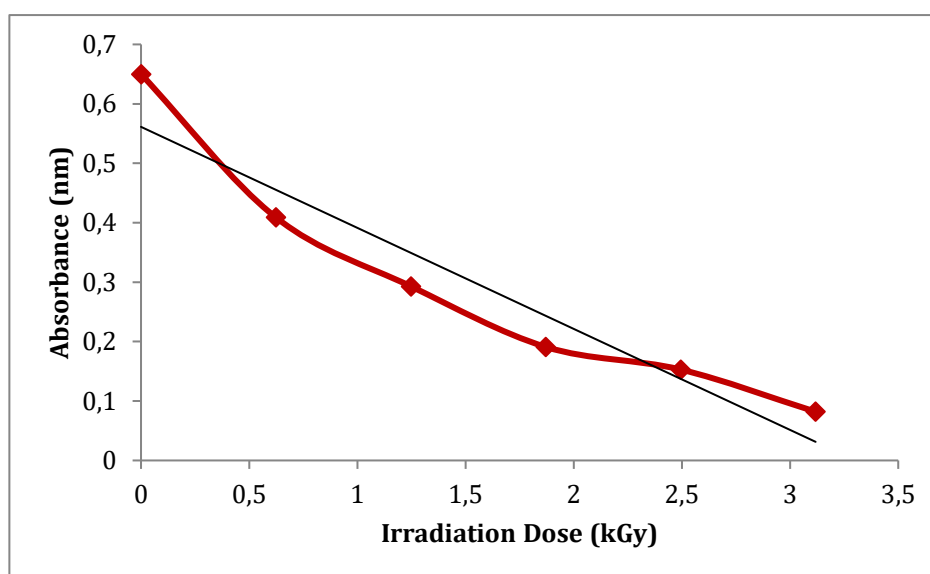
3 Results and Discussions

1. UV-Vis Absorbance Analysis

The irradiated sample solution was analyzed using a UV-Vis spectrophotometer at a maximum wavelength (λ) of 424 nm. This maximum wavelength was determined by analyzing the highest absorbance of the non-irradiated tartrazine solution. Typically, the absorption spectrum of tartrazine shows two main peaks: one in the near-UV range at 250-260 nm and another in the visible range at 420-430 nm. The peak at 250-260 nm is characteristic of individual aromatic rings, while the peak at 420-430 nm is responsible for the yellow color of the dye, caused by $\pi-\pi^*$ transitions of the N=N, C=N, and C=O groups [11]. Table 1 shows the absorbance and ΔA of the six sample solutions at a wavelength of 424 nm.

Table 1 UV-Vis Analysis in The First Week

Time (minutes)	Dose (kGy)	Absorbance (nm)	ΔA
0	0	0,650	0
15	0,62	0,409	0,241
30	1,25	0,293	0,357
45	1,87	0,191	0,459
60	2,49	0,153	0,497
75	3,12	0,082	0,568

**Figure 2** Dose Radiation Effect on Tartrazine Solution Absorbance

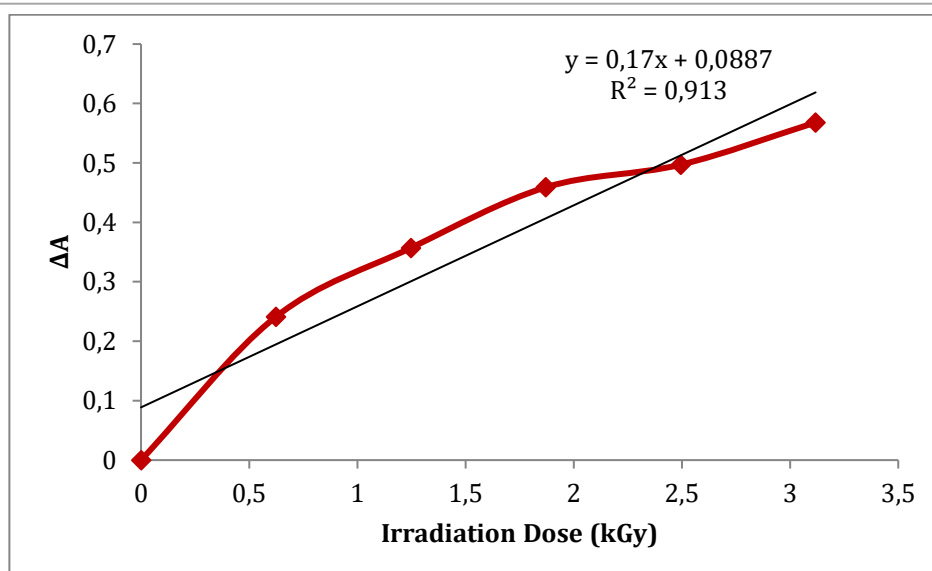


Figure 3 Dose Radiation Effect on Difference in Absorbance

From the research results, it was found that there was a decrease in the absorbance of the tartrazine solution with the increase in gamma radiation dose, as shown Fig. 2. This decrease is interpreted as the result of the degradation of tartrazine molecules into products that absorb less at the wavelength (λ) of 424 nm. The reduction in absorbance indicates that tartrazine undergoes molecular structure degradation due to radiation exposure. This change is consistent with the theory that gamma radiation causes the breaking of azo/diazenedyl ($-N=N-$) bonds in tartrazine molecules, resulting in compounds with lower absorbance [11], [12].



Figure 4 Change in Color of Tartrazine Solution after Irradiation with Dose (from left to right) 0; 0.62 ; 1.24 ; 1.87 ; 2.49 ; 3.11 kGy

The color degradation in tartrazine compounds due to gamma irradiation is caused by the breaking of bonds in the tartrazine molecules. Tartrazine produces a yellow color because of the azo/diazenedyl ($-N=N-$) bonds that form two aromatic rings in the compound. The $OH\cdot$ radicals generated by the hydrolysis during gamma irradiation cause oxidative decolorization by reacting with the diazenedyl bonds. This reaction ultimately fades the color of the sample solution and reduces the absorbance at the wavelength of 424 nm. Furthermore, the degradation products of tartrazine typically do not have the same conjugated structure, so they do not absorb light at the same wavelength, resulting in a paler or colorless solution, as shown in Fig. 3. The longer and higher the irradiation dose, the more $OH\cdot$ radicals are produced, leading to an increased oxidative decolorization reaction in the solution.

The graph of absorbance decrease against radiation dose shows a nearly linear relationship. In Fig. 2, it can be seen that the absorbance decrease is quite linear in the dose range of 0 - 2 kGy, while data instability occurs at doses above 2 kGy. This indicates that a radiocromic dosimeter using tartrazine solution can be effectively used for radiation doses up to 2 kGy. For higher doses, adjustments in composition, irradiation conditions, and methods, or the replacement of the dosimeter material with a more stable compound at high doses, are required.

2. Stability and Potential Use Of Tartrazine as a Dosimeter

The stability study of the tartrazine solution was conducted by measuring the solution's absorbance weekly over a four-week period. This measurement aimed to determine whether the tartrazine solution remained stable in preserving optical changes due to gamma radiation exposure over a longer duration at room temperature.

The results, presented in Table 2 and Fig. 5, indicate that the absorbance difference (ΔA) between the 0 dose and other doses from week to week is relatively consistent. The average percentage error (%Error) obtained from comparing the absorbance of weeks 2, 3, and 4 with week 1 is 2.16%. This low %Error value demonstrates that the tartrazine solution maintains good stability over four weeks at room temperature.

The good stability of tartrazine indicates that tartrazine-based dosimeters can be used for radiation dose measurements that require storage time before analysis. This extends its potential application in situations where immediate measurement is not always feasible. With an average %Error of 2.16%, the tartrazine solution demonstrates that changes in absorbance remain within acceptable limits for dosimeter applications. This shows that tartrazine-based dosimeters are stable not only in the short term but also in the medium to long term.

The results of this study demonstrate that tartrazine, a widely available and safe food dye, exhibits promising potential as a gamma radiation dosimeter, particularly for low to medium doses. The linear decrease in absorbance up to 2 kGy indicates that tartrazine can effectively measure radiation doses within this range. Furthermore, the stability study showed that the tartrazine solution maintained its dosimetric properties over a four-week period, with an average percentage error of only 2.16%. This suggests that tartrazine-based dosimeters can be stored and used reliably over time, extending their practical applicability.

The significance of this research lies in the potential for tartrazine to be used in various fields requiring radiation dose measurement, such as food irradiation, medical applications, and environmental monitoring. Given its cost-effectiveness, ease of use, and safety profile, tartrazine could provide a practical alternative to more expensive or complex dosimetric materials currently in use.

Future research should explore the response of tartrazine at low to medium doses with a more narrowly defined dose range under longer storage conditions, allowing for the precise determination of the optimal dose range, capabilities and limitations. Additionally, investigating other azo dyes with similar chemical structures may lead to the development of a broader range of dosimetric materials suitable for different applications.

Table 2 Measurement of The Difference in Absorbance Each Week and The Average % Error Obtained

Dose (kGy)	ΔA 1 st Week	ΔA 2 nd Week	ΔA 3 rd Week	ΔA 4 th Week
0	0	0	0	0
0,62	0,241	0,235	0,247	0,2389
1,25	0,357	0,356	0,369	0,3807
1,87	0,459	0,452	0,454	0,4633
2,49	0,497	0,518	0,522	0,5002
3,12	0,568	0,561	0,566	0,5606
Average %Error				2,16%

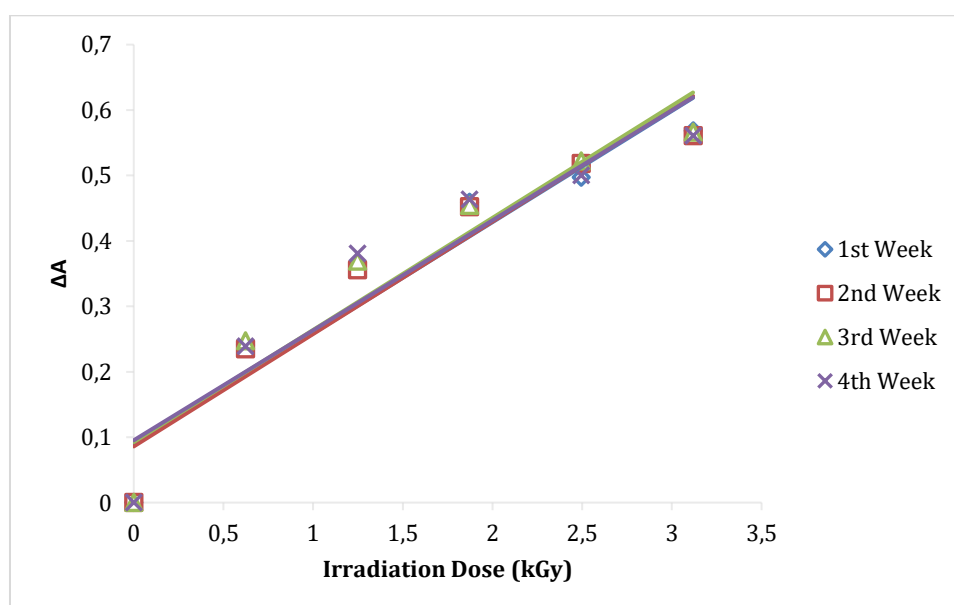


Figure 5 Absorbance Difference Stability of The Irradiated Tartrazine Solution

4 Conclusions

Based on the data obtained in this study, the following conclusions can be drawn:

1. Colorants exposed to radiation such as X-rays, gamma rays, or electron beams undergo photochemical reactions resulting in permanent color changes. These alterations occur due to radiation-induced modifications of the chemical structure within the polymer.
2. The color degradation of tartrazine compounds due to gamma irradiation is likely caused by bond cleavage. Tartrazine produces a yellow color due to the diazenedyl (-N=N-) bond forming two aromatic rings in the compound. OH- · radicals generated by gamma irradiation-induced hydrolysis cause oxidative decolorization by reacting with the diazenedyl bond. This reaction ultimately fades the color of the sample solution. The duration and magnitude of the irradiation dose are directly proportional to the OH- · radicals produced, thus increasing the oxidative decolorization reaction in the solution.

The dye (tartrazine) used as a dosimeter material in this experiment, containing tartrazine compound, demonstrates usage stability for less than four weeks. The tartrazine solution demonstrated good stability as a radiochromic dosimeter for applications at low to medium radiation doses. The time stability shown by tartrazine in this study reinforces its potential for use in dosimeter applications that require storage and analysis over a certain period. Further research may be needed to explore the response of tartrazine at higher radiation doses and under longer storage conditions.

Acknowledgements

The author extends sincere appreciation to the Polytechnic Institute of Nuclear Technology Indonesia and the National Research and Innovation Agency (BRIN) for their essential support in supplying facilities and raw materials.

References

- [1] Sukaryono, *Kajian Jenis Jenis Dosimeter Pada Fasilitas Iradiator*. Yogyakarta: Pusat Sains dan Teknologi Akselerator – BATAN, 2015.
- [2] T. Surindro, *Dosimetri Iradiator*. Jakarta: Pelatihan Petugas Iradiator Gamma, Pusdiklat Batan, 2015.
- [3] R. Saptaji, *Teori Dosimetri Akselerator*. Yogyakarta: Pelatihan Pekerja Akselerator, Pusat Pendidikan dan Pelatihan- Badan Tenaga Nuklir Nasional, 2009.
- [4] W. A. Wardhana, *Teknologi Nuklir, Proteksi Radiasi dan Aplikasinya*. Yogyakarta: Batan. Penerbit Andi, 2007.
- [5] A. Nurmanjaya, S. Putra, and K. Megasari, “Degradasi Zat Warna Lithol Dalam Medium Air Dengan Radiasi Gamma,” *J. Inov. Tek. Kim.*, vol. 3, no. 1, 2018, doi: 10.31942/inteka.v3i1.2121.
- [6] M. C. Prihatiningsih and K. Megasari, *Buku Ajar Kimia Radiasi dan Percobaan-Percobaannya*. 2009. doi: 10.25105/jetri.v20i2.16144.
- [7] Sukaryono, Suhartono, and A. E. Andjioe, “Penentuan Dosis Radiasi Menggunakan Dosimeter Fricke,” *Pus. Sains dan Teknol. Akselerator, BATAN*, pp. 73–78, 2016.
- [8] P. Sugita, E. K. Winarno, and L. Anriani, “Pengaruh Iradiasi Gamma Terhadap Degradasi Zat Warna Direct Orange 34 Dalam Air,” *J. Teknol. Lingkung. BPPT*, vol. 1, no. 2, 2000, doi: 10.29122/jtl.v1i2.170.
- [9] I. N. Handayani, C. Imawan, D. Handoko, S. Soekirno, and S. A. Pawiro, “Detektor Radiasi Sinar Gamma menggunakan Cairan Radiokromik dari Ekstrak Bunga Hibiscuss Sabdariffa L. (Rosela),” Universitas Indonesia, 2019. [Online]. Available: <https://lib.ui.ac.id/detail?id=20489599&lokasi=lokal>
- [10] L. O. Sumarlin, “Identifikasi Pewarna Sintetis Pada Produk Pangan Yang Beredar di Jakarta dan Ciputat,” *J. Kim. Val.*, vol. 1, no. 6, pp. 274–283, 2010, doi: 10.15408/jkv.v1i6.239.
- [11] M. Gobara and A. Baraka, “Tartrazine Solution as Dosimeter for Gamma Radiation Measurement,” *Int. Lett. Chem. Phys. Astron.*, vol. 33, pp. 106–117,

2014.

- [12] Á. D. Gálvez-Serna, I. F. Macías-Quiroga, G. I. Giraldo-Gómez, M. T. Dávila-Arias, and N. R. Sanabria-González, “Catalytic oxidation of tartrazine in aqueous solution using a pillared clay with aluminum and iron,” *Bull. Chem. React. Eng. Catal.*, vol. 16, no. 1, pp. 76–87, 2021, doi: 10.9767/BCREC.16.1.9978.76-87.

Prediction of Life Expectancy in Indonesia by Implementing Website-Based Lagrange Polynomial Interpolation

Syamsul Maarip¹, Aam Hermansyah², Sopi Nuryani Hadraeni¹,
Salman Miqdad¹, Ardhan Dimas Nuryadin¹, Siti Yuliyanti^{1*}

¹*Department of Informatics, Faculty of Engineering, Siliwangi University,
Tasikmalaya, West Java, Indonesia*

**Corresponding Author: sityuliyanti@unsil.ac.id*

(Received 15-07-2024; Revised 14-08-2024; Accepted 19-08-2024)

Abstract

Life Expectancy (AHH) is a measurement of the average human lifespan accepted and used to assess the quality of health and welfare of a country's population. Accepted to develop a prediction system that can be easily accessed by the general public via a web platform. The method used to predict is the Lagrange polynomial interpolation method. The Lagrange polynomial interpolation method was chosen because it can model irregular numerical data with a fairly high level of accuracy. The data used to predict AHH comes from the Indonesian Central Statistics Agency (BPS). Known data on life expectancy in Indonesia for men from 2020 to 2023 shows 69.59, 69.67, 69.93 and 70.17. Predictions for 2024, 2025 and 2026 respectively show 70.19, 69.79, 68.77 with a Root Mean Squared Error result of 0.085875 or around 8.58% of the total data tested. The results of implementing the Lagrange polynomial interpolation method into an application in the form of this website show that this method is able to provide accurate predictions for life expectancy in Indonesia and can make it easier to use.

Keywords: Interpolasi, Polinom Langrange, Life Expectancy, prediction, lifespan

1 Introduction

Life Expectancy (AHH) is an important indicator used to assess the quality of health and welfare of a country's population. However, understanding and predicting life expectancy trends remains a challenge [1], especially in the context of public policy planning and data-based decision making [2] Developments in the social, economic and technological fields play an important role in determining a country's Life Expectancy



(AHH). According to Sihaloho, life expectancy is a measurement of the expected average human lifespan.

According to data from the World Health Organization (WHO) in 2024, Indonesia is ranked 115th in the world AHH list with an average age of 71.3 years, which is still below the global average of 73.3 years [3]. However, compared with Population Reference Bureau (PPB) data in 2022, Indonesia's AHH experienced a significant increase from 46.45 years in 1960 to 68.25 years in 2022. However, this figure is still relatively low when compared to countries in Southeast Asia.

Along with technological developments, data analysis for AHH predictions can be carried out more accurately and efficiently using various mathematical and computational methods. One method that can be used is Lagrange polynomial interpolation. This method is an interpolation technique that is suitable for estimating unknown values in a data range based on known values. Lagrange polynomial interpolation is an effective mathematical method for making predictions based on existing data.

The Lagrange polynomial interpolation method has several advantages, including its ability to produce accurate results with a limited amount of data and simplicity in implementation. However, this method also has limitations, especially when applied to large datasets or to highly volatile data [2], where the resulting polynomials may become too complex or less accurate [7].

To overcome this challenge, an application was created that uses the Lagrange Polynomial Interpolation method to predict AHH in Indonesia. One system that can be used is a website-based system [9]. The development of a website-based system for implementing the Lagrange polynomial interpolation method in predicting life expectancy offers several advantages [10-12]. The interactive and easily accessible website allows users from various groups, including policy makers, academics, and the general public, to make practical use of this prediction tool. In addition, integration with dynamic databases and user-friendly interfaces can increase the effectiveness of using this method on a wider scale [14].

To overcome this challenge, a website-based application is needed that uses the Lagrange polynomial interpolation method to predict AHH in Indonesia [15]. Website-based system development offers several advantages, including easy and interactive

access for users from various circles, as well as integration with dynamic databases and a user-friendly interface. With this system, it is hoped that it can help in providing more accurate and up-to-date information regarding AHH, thus supporting better decision making in various sectors.

2 Material and Methods

There are two methods used to implement Lagrange Polynomial Interpolation to Predict Life Expectancy in Indonesia Based on Province and Gender. The first method is the literature study method and the second method is the Lagrange polynomial interpolation method.

Literature Study Method

The library study method, also known as library research, is a data collection technique used to understand and study theories from various literature related to the research [16]. This method is used to look for references related to the research to be carried out and becomes a benchmark in carrying out the research stages [17]. This method is also used in collecting test data related to research.

Lagrange Polynomial Interpolation Method

Lagrange polynomial interpolation comes from a numerical analysis of interpolation. Interpolation is the process of finding and calculating the value of a function whose graph passes through a certain set of points [7]. Because it uses functions in polynomial form, Lagrange interpolation is a polynomial interpolation that is very well known in numerical methods [8]. Lagrange interpolation is used to obtain a polynomial function (x) of a certain degree that passes through a number of data points [18]. For example, look for a polynomial function of degree one or order 1 that will pass through two points [19], namely (x_2, y_2) and (x_1, y_1) , then it can be [21] written with the linear equation in equations 1 and 2.

$$y_0 = a_0 + a_1x_0 \quad (1)$$

$$y_1 = a_0 + a_1x_1 \quad (2)$$

Equations (1) and (2) are then eliminated and produce equation 3

$$a_1 = \frac{y_1 - y_0}{x_1 - x_0} \tag{3}$$

The result of equation (1) is then substituted

$$\begin{aligned} y_0 &= a_0 + a_1 x_0 \\ y_0 - a_1 x_0 &= a_0 \\ a_0 &= y_0 - \left(\frac{y_1 - y_0}{x_1 - x_0}\right) \cdot x_0 \end{aligned} \tag{4}$$

Then substitute equations (3) and (4) into linear functions

$$\begin{aligned} f(x) &= a_0 + a_1 x \\ &= \left(y_0 - \left(\frac{y_1 - y_0}{x_1 - x_0}\right) \cdot x_0\right) + \left(\frac{y_1 - y_0}{x_1 - x_0}\right) \cdot x \\ &= y_0 + \left(\frac{y_1 - y_0}{x_1 - x_0}\right) \cdot (x - x_0) \\ &= \frac{y_0(x_1 - x_0) + (y_1 - y_0)(x - x_0)}{x_1 - x_0} \\ &= \frac{y_0 x_1 - y_0 x_0 + y_1 x - y_1 x_0 - y_0 x + y_0 x_0}{x_1 - x_0} \\ &= \frac{(x_1 - x) \cdot y_0 + (x - x_0) \cdot y_1}{x_1 - x_0} \\ &= \frac{(x_1 - x)}{(x_1 - x_0)} \cdot y_0 + \frac{(x - x_0)}{(x_1 - x_0)} \cdot y_1 \\ &= \frac{(x - x_0)}{(x_0 - x_1)} \cdot y_0 + \frac{(x - x_1)}{(x_1 - x_0)} \cdot y_1 \\ &= L_0(x)y_0 + L_1(x)y_1 \end{aligned}$$

So equation 5 is a Lagrange polynomial of degree 1.

$$P_1(x) = \sum_{i=0}^1 L_i(x)y_i \tag{5}$$

And for equation 6 the degree is more than 1.

$$L_i(x) = \prod_{\substack{j=0 \\ j \neq i}}^x \frac{(x - x_j)}{(x_i - x_j)} = \frac{(x - x_0)(x - x_1) \dots (x - x_{i-1})(x - x_{i+1}) \dots (x - x_n)}{(x_i - x_0)(x_i - x_1) \dots (x_i - x_{i-1})(x_i - x_{i+1}) \dots (x_i - x_n)} \tag{6}$$

Equations 5 and 6 are implemented in calculations using Excel [22]. If the prediction calculation results have a small mean error, then the Lagrange polynomial interpolation calculation will be implemented in the Java Script programming language to display in the form of an application in the form of a website.

3 Results and Discussions

Data collection

Data collection for the Life Expectancy Rate test was obtained from the Indonesian Central Statistics Agency (BPS), where three data were taken, namely based on gender, birth and national parameters. The data obtained will be categorized into four categories, namely:

- a. Data on Indonesian Life Expectancy Rates for Male 2020-2023
- b. Data on Indonesian Life Expectancy Rates for Female Gender 2020-2023
- c. Data on Indonesian Life Expectancy at Birth, Male, 2020-2023
- d. Data on Indonesian Life Expectancy at Birth, Female Gender, 2019-2023

Tabel 1 shows the highest value in 2023 of 70.17 and is likely to increase in the following year considering the development of media and the level of health awareness based on male gender, and of 74.18 on female gender in Tabel 2. Similarly, gender for birth prediction also has the highest level in 2023 for both males and females as shown in Tables 3 and 4.

Table 1. Data on Indonesian Life Expectancy Rates for Male

Year	Data on Life Expectancy for Men
2020	69.59
2021	69.67
2022	69.93
2023	70.17

Table 2. Data on Indonesian Life Expectancy Rates for Female

Year	Data on Life Expectancy for Woman
2020	73.46
2021	73.55
2022	73.86
2023	74.18

Table 3. Data on Life Expectancy for Birth Male genital

Year	Data on Life Expectancy for Birth Male genital
2020	71.25
2021	71.30
2022	71.46
2023	71.61

Table 4. Data on Life Expectancy on Life Expectancy for Birth Male genital

Year	Data on Life Expectancy for Birth Male genital
2020	75.60
2021	75.72
2022	76.05
2023	76.37

Data Processing

Based on the data that has been obtained, the data is then calculated using the Lagrange polynomial interpolation method to predict Life Expectancy in Indonesia from 2024 to 2026. To predict 2024, the Lagrange polynomial interpolation calculation uses Lagrange interpolation 4 or order 4. Table 5 is the result. AHH predictions in Indonesia in 2024 for males.

It can be seen that the AHH prediction for 2024 for male gender in Indonesia is at the age of 70.19 years. The results were obtained from the addition of Lagrange interpolation of orders 1 to 4 from the available data. To find the AHH prediction for 2025, the 2024 prediction results will be used as calculation data. And to find the AHH prediction for 2025, the 2024 and 2025 prediction data will also be used as calculation data.

Table 5. AHH Prediction Results in Indonesia in 2024 for Male Gender

i	Year	x	f(xi)	L1	L2	L3	L4
0	2020	1	69.59				
1	2021	2	69.67				
2	2022	3	69.93	-69.59	278.68	-419.58	280.68
3	2023	4	70.17				
4	2024	5	70.19				

Table 6. Result prediction AHH Indonesia in 2025 for male gender

i	year	x	f(xi)	L1	L2	L3	L4	L5
0	2020	1	69.59					
1	2021	2	69.67					
2	2022	3	69.93	69.59	-348.35	699.3	-701.7	350.95
3	2023	4	70.17					
4	2024	5	70.19					
5	2025	6	69.79					

Based on Table 6, the prediction of AHH in Indonesia for male gender in 2025 shows AHH is 69.79 years old. And to find out the prediction of AHH in 2026, the prediction data obtained in 2025 will be used. Lagrange interpolation used in the calculation uses order 6.

By using Lagrange polynomial interpolation of order 4 to 6, you can find out the predicted life expectancy for men in Indonesia in 2024 to 2025 with respective prediction results of 70.19 for 2024, 69.79 for 2025 and 68.77 for 2026. These calculations apply to other test data and the following are the prediction results for other test data. AHH Prediction Results in Indonesia for Female Gender are shown in Fig. 1 and Male in Fig. 2. Fig. 3 shows AHH Prediction Results in Indonesia for Birth Female Genital.

Table 7. Result prediction AHH Indonesia in 2026 for male gender

i	year	x	f(xi)	L1	L2	L3	L4	L5	L6
0	2020	1	69.59						
1	2021	2	69.67						
2	2022	3	69.93						
3	2023	4	70.17	-69.59	418.02	-1048.95	1403.4	-1052.85	418.74
4	2024	5	70.19						
5	2025	6	69.79						
6	2026	7	68.77						

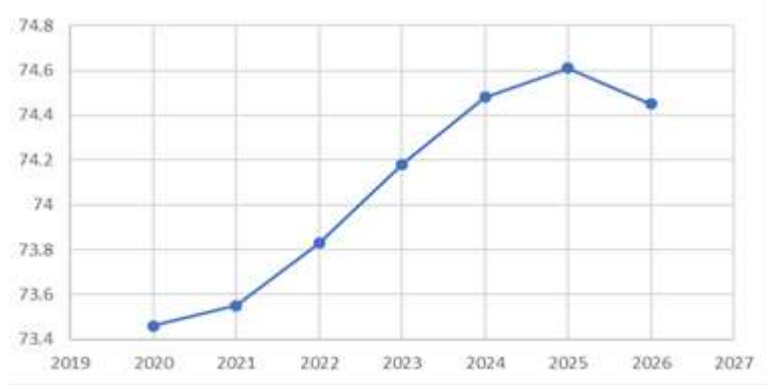


Figure 1. AHH Prediction Results in Indonesia for Female Gender

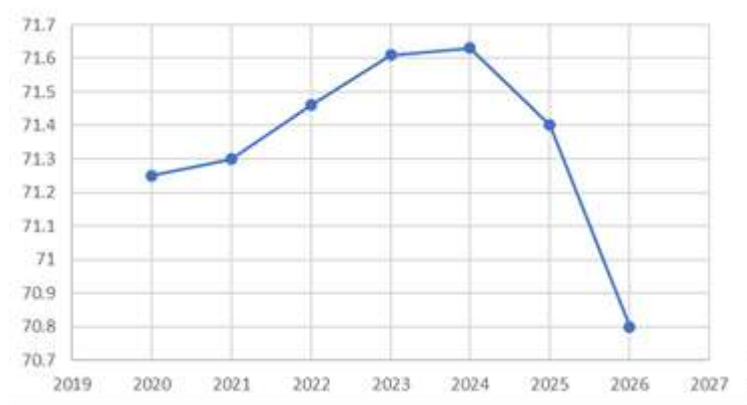


Figure 2. AHH Prediction Results in Indonesia for Male Gender

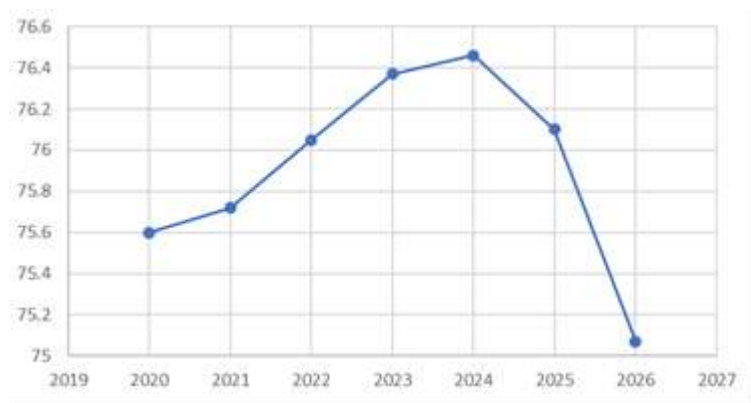


Figure 3. AHH Prediction Results in Indonesia for Birth Female Genital

Root Mean Squared Error Testing

Based on the calculation results of the predicted life expectancy in Indonesia for 2024-2026, an error test was carried out using the Root Mean Squared Error (RMSE) method. Where the RMSE value is used to measure the average size of the error to find out whether the calculation method used is working well or not. In RMSE testing, actual data and predicted data are needed so that it is based on the data obtained and [7] predictions that have been made. RMSE testing can only be carried out until 2023. For the following year, we must first wait for actual data on Indonesia's life expectancy, which uses Equation 7.

$$RMSE = \sqrt{\frac{\Sigma(Aktual-Prediksi)^2}{n}} \quad (7)$$

The results of the RMSE test for predicting life expectancy in Indonesia using the Lagrange polynomial interpolation method are shown in Table 8. Based on Table 8, it can be concluded that the RMSE value for predicting life expectancy in Indonesia using the Lagrange polynomial interpolation method based on four categories from 2019-2023 falls within the provisions of the RMSE test results, namely Moderate with an average RMSE of 0.085875 or around 8.58%.

Implementation

After carrying out calculations and testing errors using the RSME method, the next step is to implement the process that has been carried out into an application in the form of a website. Home and preview interfaces can be seen in Figs. 4 and 5, respectively.

Table 8. RMSE Test Results for Life Expectancy in Indonesia

AHH	RSME	RSME Mean
Data 1	0,124	
Data 2	0,082	0,085875
Data 3	0,045	
Data 4	0,0925	



Figure 4. Home interface

Preview

Provinsi	2020	2021	2022	2023
ACEH	74.75	74.77	74.99	75.18
SUMATERA UTARA	75.09	75.23	75.63	76.01
SUMATERA BARAT	75.78	75.91	76.3	76.65
RIAU	76	76.08	76.39	76.71
JAMBI	75.55	75.61	75.93	76.24
SUMATERA SELATAN	75.63	75.74	76.13	76.52
BENGKULU	74.65	74.71	74.97	75.25
LAMPUNG	76	76.09	76.39	76.69

Figure 5. Preview Interface

In the Home section, there is a Navbar that says "Numerical Analysis", and there is a footer that has 2 buttons "home" and "About". Next, there is an area for uploading the CSV file that you want to calculate, as well as a guide on how to use the application for users.

In the preview section, before the user performs calculations, there is a preview table sourced from the .csv file uploaded by the user. Users can perform calculations with the "Calculate" button, and there are options for the number of interpolations desired by the user.

In the calculation results section, there is a graph and table of results that will appear from the CSV file that has been calculated by the website. This website is able to calculate

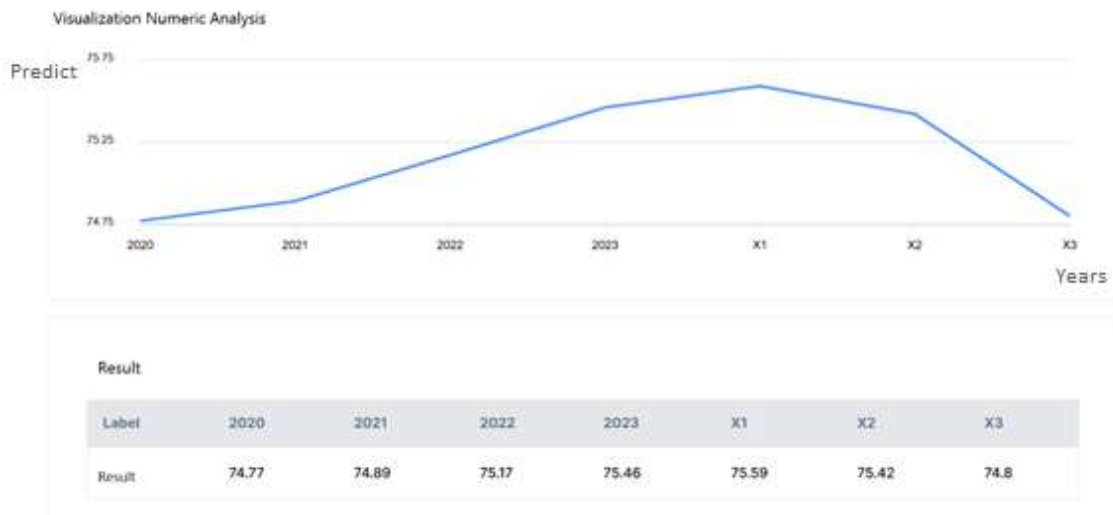


Figure 6. Display graphs visualization of calculation results

predictions for more than 3 years in the future according to the number of predictions selected in the number of interpolation options. Display graphs visualization of calculation results are shown in Fig. 6.

4 Conclusions

It can be concluded that life expectancy in various provinces in Indonesia has increased consistently from 2019 to 2024. Although there are variations between provinces, data that frequently appears shows a significant increase in population life expectancy, reflecting improvements in overall health and quality of life. Based on the calculation results, it shows that women tend to have a higher life expectancy than men in each province, and this gender difference is relatively stable from year to year. The average prediction of AHH based on gender in Indonesia shows an increase and decrease. This increase and decrease occurs in every data used and also in every calculation tool used.

It can be concluded that in terms of the calculation tool used, the Lagrange polynomial interpolation method can be implemented to predict life expectancy in Indonesia because it has a Root Mean Squared Error with a value of 0.085875 or around

8.58%, which means it is included in the moderate category, which means the prediction results are included in the category which can be good [8]. And implementing Lagrange polynomial interpolation on an application in the form of a website can make it easier to carry out calculations automatically.

Acknowledgements

The author thanks the Indonesian Central Statistics Agency (BPS) for providing various data on Life Expectancy Rates in Indonesia which we can use as material for testing the use of the Lagrange Polynomial Interpolation method in predicting Life Expectancy Rates in Indonesia.

References

- [1] E. D. Sihaloho, "Pengaruh Belanja Kesehatan Terhadap Angka Harapan Hidup Kabupaten Kota Di Jawa Barat," *Ekspansi: Jurnal Ekonomi, Keuangan, Perbankan dan Akuntansi*, vol. 11, no. 1, p. 117, May 2019, doi: 10.35313/ekspansi.v11i1.1308.
- [2] World Health Organization, *Framework and standards for country health information systems*. 2008. [Online]. Available: <http://www.healthmetricsnetwork.org>
- [3] A. S. Rahma and R. I. Fajar, "Daftar Negara dengan Penduduk Paling Panjang Umur Menurut Data WHO, Indonesia Posisi Berapa?," *Geriatrici*. Accessed: Jun. 20, 2024. [Online]. Available: <https://www.geriatrici.id/artikel/2043/daftar-negara-dengan-penduduk-paling-panjang-umur-menurut-data-who-indonesia-posisi-berapa>
- [4] Jennifer. Niederst Robbins, *Learning Web design : a beginner's guide to HTML, CSS, JavaScript, and web graphics*. 2012.
- [5] M. Nina Adlini, A. Hanifa Dinda, S. Yulinda, O. Chotimah, and S. Julia Merliyana, "Metode Penelitian Kualitatif Studi Pustaka," 2022.
- [6] W. Rahmadani and S. C. Sihombing, "Analisis Penyebaran Virus Covid-19 di Provinsi Sumatera Selatan Menggunakan Metode Interpolasi Lagrange," *Jurnal Penelitian Fisika dan Terapannya (JUPITER)*, vol. 2, no. 1, p. 12, Jul. 2020, doi: 10.31851/jupiter.v2i1.5314.

- [7] T. Safitri, N. Dwidayati, and K. Kunci, "Perbandingan Peramalan Menggunakan Metode Exponential Smoothing Holt-Winters dan Arima," *Unnes Journal of Mathematics*, vol. 6, no. 1, pp. 48–58, 2017, [Online]. Available: <http://journal.unnes.ac.id/sju/index.php/ujm>
- [8] V. Hariadi, A. Saikhu, N. Zakiya, A. Y. Wijaya, and F. Baskoro, "Multivariate Time Series Forecasting Using Recurrent Neural Networks for Meteorological Data," *Conference SENATIK STT Adisutjipto Yogyakarta*, vol. 5, Nov. 2019, doi: 10.28989/senatik.v5i0.365.
- [9] S. Yuliyanti and Saripudin, "Implementasi Algoritma FG-Growth untuk Sistem Rekomendasi Penjualan Produk," *JUMANJI*, vol. 5, no. 1, pp. 41-51, 2021.
- [10] Y. D. Lestari, "Penerapan Data Mining Menggunakan Algoritma Fp-Tree Dan Fp-Growth Pada Data Transaksi Penjualan Obat," *Seminar Nasional Teknologi Informasi dan Komunikasi (SNASTIKOM)*, pp. 60-65, 2015.
- [11] A. X. A. Sim, "Pengenalan Desain dan Analisis Algoritma," 01 July 2013. [Online]. Available: <http://dev.bertzzie.com/knowledge/analisis-algoritma/PengenalanDesaindanAnalisisAlgoritma.html#algoritma-yang-baik>.
- [12] H. Aprillia, H. Yang and C. Huang, "Statistical load forecasting using optimal quantile regression random forest and risk assessment index," *IEEE Transactions on Smart Grid*, vol. 12, no. 2, pp. 1467-1480, 2020.
- [13] P. G. Arepalli and K. J. N. *, "Water contamination analysis in IoT enabled aquaculture using deep learning based AODEGRU," *Elsevier : Ecological Informatics*, vol. 2024, no. 12, pp. 1-16, 2024.
- [14] F. A. Pangruruk and S. P. Barus, "Comparison of Prediction of the Number of People Exposed to Covid 19 Using the Lagrange Interpolation Method with the Newton Gregory Maju Polynomial Interpolation Method," *Formosa Journal of Applied Sciences (FJAS)*, pp. 1405-1426, 2023.
- [15] D. Feng, Q. Han, L. Xu, F. Sohel, S. G. Hassan and S. L. a, "An ensemble method for predicting dissolved oxygen level in aquaculture environment," *Ecological Informatics*, vol. 80, no. 1, pp. 1-15, 2024.

- [16] H. A. A. a. V. M. Dewi, "Factors Affecting Life Expectancy in East Java: Predictions with A Bayesian Model Averaging Approach," *Jurnal Perencanaan The Indonesian Journal of Development Planning*, vol. V, no. 2, pp. 283-295, 2021.
- [17] Z. Ahmed and H. Le, "Linking Information Communication Technology, trade globalization index, and CO2 emissions: evidence from advanced panel techniques," *Environmental Science and Pollution Research*, vol. 28, no. 7, pp. 8770-8781, 2021.
- [18] A. Kurniadi, Kusriani and M. F. Sadikin, "Implementasi Convolutional Neural Network Untuk Klasifikasi Varietas Pada Citra Daun Sawi Menggunakan Keras," : *Journal of Computer and Information Technology* , vol. 4, no. 1, pp. 25-33, 2020.
- [19] Maulana, "Black Box Testing Adalah : Pengertian dan Contohnya," /TBox by Course-Net Indonesia, 20 Maret 2023. [Online]. Available: <https://itbox.id/blog/black-box-testing-adalah/>. [Accessed 4 Juli 2023].
- [20] E. Prakasa, B. Sugiarto, A. P. S. Utama and S. Yuliyanti, "Development of Real-time Handwashing Assessment using Video Analysis," in *IC3INA 2021: The 2021 International Conference on Computer, Control, Informatics and Its Applications*, New York, 2021.
- [21] H. Santoso, *Rekayasa Perangkat Lunak*, Medan: UINSU Medan, 2019.
- [22] D. T. Larose, *Discovering Knowledge in Data: An Introduction to Data Mining*, John Willey & Sons, Inc., 2014.

Quantitative Analysis of Magnetohydrodynamic Sustained Convective Flow via Vertical Plate

D. R. Kirubaharan¹, A. D Subhashini¹, NVN. Babu², G. Murali^{2*}

¹*Department of Mathematics, PRIST University, Thanjavur, India.*

²*Department of Mathematics, Geethanjali College of Engineering and technology, Cheeryal, India.*

*Corresponding author Email address: muraligundagani@gmail.com

(Received 15-07-2024; Revised 08-08-2024; Accepted 12-08-2024)

Abstract

In this paper, the effects of heat and mass transfer on MHD flow in an incompressible, heated fluid that has been accelerated to a steady free stream are investigated. It examines mass movement in a magnetic field as well as heat absorption qualities. In the model, non-linear governing equations and the Laplace transform method are applied. The relationship between temperature, concentration, and velocity and flow parameters is illustrated by studies utilizing parametric data.

Keywords: Magnetohydrodynamics, Laplace Transform method, Free Convection, vertical Plate

1 Introduction

The growth of an electrically directed fluid in a magnetic field is studied by MHD, a fluid element. It can be used in many different ways, including sun-facing cookers, concentrators that use sunlight, and self-explanatory solar-powered gatherers. These appliances can be used for a variety of tasks, including expanding waste water disappearing rates, cooking, broiling, and refining. Laplace transform is an essential technique in domains such as quantum material science, basic design, electrical and electronic building, fluid physics, and basic design because it converts differential situations into elementary mathematical structures. Research progress has made it possible to recreate Laplace transformable circumstances.



The effects of thermo-dispersion, warm age/assimilation, and depicted movement were investigated by H.T. Kataria and Patel [1] on a second-grade fluid hazardous-free convective MHD stream that is artificially responsive and transmits an infinite vertical plate. The repercussions of unstable MHD free convection flow via a vertical permeable moving plate with radiation for heat and mass transport were studied by M.C. Krishna Reddy et al. [2]. The effects of an unstable hydromagnetic free convective flow across an infinite vertical plate submerged in a porous environment with heat absorption were examined by Murali et al. [3] in order to determine the mass and heat transfer consequences. Deepa Gadipally, et al. [4] used the finite difference method to analyze the effects of Soret and Dufour on unsteady MHD flow across a semi-infinite vertical porous plate, while Murali et al. [5] examined their influence on unstable hydromagnetic free convective fluid flow. For a system that solves problems using MHD, Murali et al. [6]–[7] offered a finite element solution. N.V.N. Babu et al. [8] conducted an analysis of the Casson fluid performance on natural convective dissipative Couette flow via an infinite vertically inclined plate. A numerical analysis of the convective MHD Jeffrey Fluid Flow resulting from vertical plate movements was carried out by Murali et al. [9]. Muthucumaraswamy and Geetha [10] talk about impacts of explanatory movement on an isothermal vertical plate with consistent mass transition.

Velocity, mass and temperature analysis of gravity-driven convection nanofluid flow past an oscillating vertical plate was studied by [11]–[12]. A few writers have examined the consequences of heat and mass transfer, and their analyses have greatly influenced our comprehension of the nature of the work that has been documented [13]–[21].

Heat absorption and temperature variations were taken into account when analyzing the MHD heat and mass transfer flow via vertical plate using the Laplace transform method. The method effectively understood coupled non-straight halfway differential conditions and deduced the local Nusselt number, neighboring Sherwood number, and adjacent skin-friction coefficients.

2 Material and Methods

An incompressible fluid's unstable MHD flow was examined using an infinite vertical plate that was uniformly heated, with variable mass diffusion, and exponential acceleration. At first, there is a concentration level at each site, and the fluid and plate are at the same temperature and motionless.

Fig. 1 depicts both the physical illustration and the coordinate arrangement. This inquiry assumes fluid physical attributes are stable, with a transverse magnetic field applied to the plate. The induced magnetic field is smaller due to low conductive quality. Viscous dissipation and Joule heating are ignored.

Boussinesq's approximation states that the following set of equations controls the unsteady flow:

Momentum Equation:

$$\left[\frac{\partial u'}{\partial t'} \right] = g \left[\frac{\partial^2 u'}{\partial y'^2} \right] - \left[\frac{\sigma B_o^2}{\rho} \right] u' + [g\beta(T' - T'_\infty)] + [g\beta^*(C' - C'_\infty)] \tag{1}$$

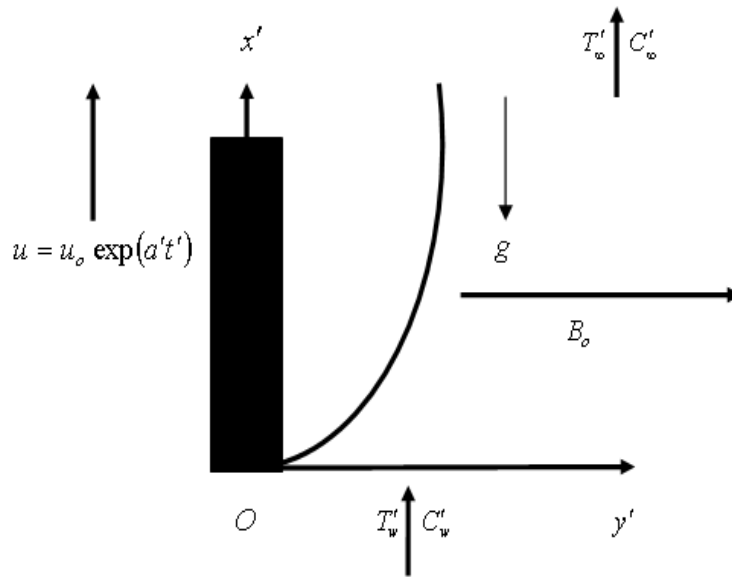


Figure 1. Physical formation and coordinate system

Energy Equation:

$$C_p \left[\frac{\partial T'}{\partial t'} \right] = \kappa \left[\frac{\partial^2 T'}{\partial y'^2} \right] + [Q_o(T'_\infty - T')] \quad (2)$$

Species Diffusion Equation:

$$\left[\frac{\partial C'}{\partial t'} \right] = D \left[\frac{\partial^2 C'}{\partial y'^2} \right] - D[K_r'(C' - C'_\infty)] \quad (3)$$

The corresponding initial and boundary conditions are

$$\left. \begin{aligned} t' \leq 0: & \quad u' = 0, T' = T'_\infty, C' = C'_\infty \text{ for all } y' \\ t' > 0: & \quad \left\{ \begin{aligned} u' = u_0 \exp(a't'), T' = T'_\infty + (T'_w - T'_\infty) At', C' = C'_\infty + (C'_w - C'_\infty) At' \text{ at } y' = 0 \\ u' = 0, T' \rightarrow T'_\infty, C' \rightarrow C'_\infty \text{ as } y' \rightarrow \infty \end{aligned} \right\} \end{aligned} \right\} \quad (4)$$

On introducing the following non-dimensional quantities into the Eqs. (1), (2) and

(3)

$$\left. \begin{aligned} u = \frac{u'}{u_0}, t = \frac{t' u_0^2}{g}, y = \frac{y' u_0}{g}, \theta = \frac{T' - T'_\infty}{T'_w - T'_\infty}, \phi = \frac{C' - C'_\infty}{C'_w - C'_\infty}, M = \frac{\sigma B_0^2 g}{\rho u_0^2}, Gr = \frac{g \beta g (T'_w - T'_\infty)}{u_0^3}, \\ Gc = \frac{g \beta^* g (C'_w - C'_\infty)}{u_0^3}, Pr = \frac{g C_p}{\kappa}, Sc = \frac{g}{D}, S = \frac{Q_0 g^2}{\kappa u_0^2}, a = \frac{a' g}{u_0^2}, \lambda = \frac{g K_r'}{u_0^2}, Re_x = \frac{u_0 x}{g}, A = \frac{u_0^2}{g} \end{aligned} \right\} \quad (5)$$

Changed governing equations as follows:

Momentum Equation:

$$\frac{\partial u}{\partial t} = Gr\theta + Gc\phi + \frac{\partial^2 u}{\partial y^2} - Mu \quad (6)$$

Energy Equation:

$$\frac{\partial \theta}{\partial t} = \frac{1}{Pr} \frac{\partial^2 \theta}{\partial y^2} - \frac{S}{Pr} \theta \quad (7)$$

Concentration Equation:

$$\frac{\partial \phi}{\partial t} = \frac{1}{Sc} \frac{\partial^2 \phi}{\partial y^2} - \frac{\lambda}{Sc} \phi \quad (8)$$

Boundary conditions for the flow are as follows:

$$\left. \begin{array}{l} t \leq 0: u = 0, \theta = 0, \phi = 0 \text{ for all } y \\ t > 0: \left\{ \begin{array}{l} u = \exp(at), \theta = t, \phi = t \text{ at } y = 0 \\ u = 0, \theta \rightarrow 0, \phi \rightarrow 0 \text{ as } y \rightarrow \infty \end{array} \right\} \end{array} \right\} \quad (9)$$

The following are important parameters like Skin-friction, Nusselt number and Sherwood number

$$Cf = -\left(\frac{\tau'_w}{\rho u_o \mathcal{G}}\right) = -\left(\frac{\partial u}{\partial y}\right)_{y=0} \quad (10)$$

$$Nu = -x \frac{\left(\frac{\partial T'}{\partial y'}\right)_{y'=0}}{T'_w - T'_\infty} \Rightarrow Nu Re_x^{-1} = -\left(\frac{\partial \theta}{\partial y}\right)_{y=0} \quad (11)$$

$$Sh = -x \frac{\left(\frac{\partial C'}{\partial y'}\right)_{y'=0}}{C'_w - C'_\infty} \Rightarrow Sh Re_x^{-1} = -\left(\frac{\partial \phi}{\partial y}\right)_{y=0} \quad (12)$$

3 Results and Discussions

The following equations were modeled for an unsteady MHD convective problem and solved using the laplace transform approach.

$$\theta(y,t) = \left(\frac{t}{2} + \frac{y \text{Pr}}{4\sqrt{S}}\right) \exp(y\sqrt{S}) \operatorname{erfc}\left(\frac{y\sqrt{\text{Pr}}}{2\sqrt{t}} + \sqrt{\frac{St}{\text{Pr}}}\right) + \left(\frac{t}{2} - \frac{y \text{Pr}}{4\sqrt{S}}\right) \exp(-y\sqrt{S}) \operatorname{erfc}\left(\frac{y\sqrt{\text{Pr}}}{2\sqrt{t}} - \sqrt{\frac{St}{\text{Pr}}}\right) \tag{13}$$

$$\phi(y,t) = \left(\frac{t}{2} + \frac{y}{4}\sqrt{\frac{Sc}{\mu}}\right) \exp(y\sqrt{\mu Sc}) \operatorname{erfc}\left(\frac{y\sqrt{Sc}}{2\sqrt{t}} + \sqrt{\mu t}\right) + \left(\frac{t}{2} - \frac{y}{4}\sqrt{\frac{Sc}{\mu}}\right) \exp(-y\sqrt{\mu Sc}) \operatorname{erfc}\left(\frac{y\sqrt{Sc}}{2\sqrt{t}} - \sqrt{\mu t}\right) \tag{14}$$

$$u(y,t) = \frac{e^{\alpha}}{2} \left[e^{\sqrt{M+a}y} \operatorname{erfc}\left(\frac{y}{2\sqrt{t}} + \sqrt{(M+a)t}\right) + e^{-\sqrt{M+a}y} \operatorname{erfc}\left(\frac{y}{2\sqrt{t}} - \sqrt{(M+a)t}\right) \right] \\ - \frac{\alpha}{2} \left[\frac{e^{\alpha}}{b^2} \left\{ e^{\sqrt{M+b}y} \operatorname{erfc}\left(\frac{y}{2\sqrt{t}} + \sqrt{(M+b)t}\right) + e^{-\sqrt{M+b}y} \operatorname{erfc}\left(\frac{y}{2\sqrt{t}} - \sqrt{(M+b)t}\right) + \exp\left(y\sqrt{\text{Pr}\left(\frac{S}{\text{Pr}} + b\right)}\right) \right\} \right. \\ \left. + \operatorname{erfc}\left(\frac{y}{2}\sqrt{\frac{\text{Pr}}{t}} + \sqrt{\left(\frac{S}{\text{Pr}} + b\right)t}\right) - \exp\left(-y\sqrt{\text{Pr}\left(\frac{S}{\text{Pr}} + b\right)}\right) \operatorname{erfc}\left(\frac{y}{2}\sqrt{\frac{\text{Pr}}{t}} - \sqrt{\left(\frac{S}{\text{Pr}} + b\right)t}\right) \right] + \\ + \frac{1}{b} \left(t + \frac{1}{b} + \frac{y}{2\sqrt{M}} \right) \exp(y\sqrt{M}) \operatorname{erfc}\left(\frac{y}{2\sqrt{t}} + \sqrt{Mt}\right) - \frac{1}{b} \left(t + \frac{1}{b} - \frac{y}{2\sqrt{M}} \right) \exp(-y\sqrt{M}) \operatorname{erfc}\left(\frac{y}{2\sqrt{t}} - \sqrt{Mt}\right) \\ + \frac{1}{b} \left(t + \frac{1}{b} + \frac{y \text{Pr}}{2\sqrt{S}} \right) \exp(y\sqrt{S}) \operatorname{erfc}\left(\frac{y}{2}\sqrt{\frac{\text{Pr}}{t}} + \sqrt{\frac{St}{\text{Pr}}}\right) + \frac{1}{b} \left(t + \frac{1}{b} - \frac{y \text{Pr}}{2\sqrt{S}} \right) \exp(-y\sqrt{S}) \operatorname{erfc}\left(\frac{y}{2}\sqrt{\frac{\text{Pr}}{t}} - \sqrt{\frac{St}{\text{Pr}}}\right)$$

Using (10) and (15), Skin-friction coefficient is of the following form

$$C_f = e^{\alpha} \left[\sqrt{(M+a)} \left(1 - \operatorname{erfc}\left(\sqrt{(M+a)t}\right) \right) + \frac{1}{\sqrt{\pi t}} \exp\left(-\sqrt{(M+a)t}\right) \right] + \\ \alpha \left[\frac{\exp(bt)}{b^2} \left\{ \sqrt{(M+b)} \left(\operatorname{erfc}\left(\sqrt{(M+b)t}\right) - 1 \right) - \frac{1}{\sqrt{\pi t}} \exp\left(-\sqrt{(M+b)t}\right) \right. \right. \\ \left. \left. - \sqrt{\text{Pr}\left(\frac{S}{\text{Pr}} + b\right)} \left(\operatorname{erfc}\left(\sqrt{\left(\frac{S}{\text{Pr}} + b\right)t}\right) - 1 \right) + \sqrt{\frac{\text{Pr}}{\pi t}} \exp\left(-\sqrt{\left(\frac{S}{\text{Pr}} + b\right)t}\right) \right\} + \right. \\ \left. - \frac{1}{2b} \left(\frac{\text{Pr}}{\sqrt{S}} \right) \left(1 - \operatorname{erfc}\left(\sqrt{\frac{St}{\text{Pr}}}\right) \right) - \frac{1}{b} \left(t + \frac{1}{b} \right) \left\{ \sqrt{S} \left(1 - \operatorname{erfc}\left(\sqrt{\frac{St}{\text{Pr}}}\right) \right) + \left(\sqrt{\frac{\text{Pr}}{\pi t}} \right) \exp\left(-\sqrt{\frac{St}{\text{Pr}}}\right) \right\} \right] \\ - \psi \left[\frac{\exp(dt)}{d^2} \left\{ \sqrt{(M+d)} \left(\operatorname{erfc}\left(\sqrt{(M+d)t}\right) - 1 \right) - \frac{1}{\sqrt{\pi t}} \left(\exp\left(-\sqrt{(M+d)t}\right) - \sqrt{Sc(\mu+d)} \left(\operatorname{erfc}\left(\sqrt{(\mu+d)t}\right) - 1 \right) \right) \right. \right. \\ \left. \left. + \left(\sqrt{\frac{Sc}{\pi t}} \right) \exp\left(-\sqrt{(\mu+d)t}\right) \right\} \right. \\ \left. + \frac{1}{2b\sqrt{M}} \left(1 - \operatorname{erfc}\left(\sqrt{Mt}\right) \right) + \frac{1}{d} \left(t + \frac{1}{d} \right) \left\{ \sqrt{M} \left(1 - \operatorname{erfc}\left(\sqrt{Mt}\right) \right) + \frac{1}{\sqrt{\pi t}} \left(\exp\left(-\sqrt{Mt}\right) \right) \right\} - \frac{1}{2d} \sqrt{\frac{Sc}{\mu}} \left(1 - \operatorname{erfc}\left(\sqrt{\mu t}\right) \right) \right. \\ \left. - \frac{1}{d} \left(t + \frac{1}{d} \right) \left\{ \sqrt{\mu Sc} \left(1 - \operatorname{erfc}\left(\sqrt{\mu t}\right) \right) + \sqrt{\frac{Sc}{\pi t}} \left(\exp\left(-\sqrt{\mu t}\right) \right) \right\} \right] \tag{16}$$

4 Conclusions

It can be concluded that life expectancy in various provinces in Indonesia has increased consistently from 2019 to 2024. Although there are variations between provinces, data that frequently appears shows a significant increase in population life expectancy, reflecting improvements in overall health and quality of life. Based on the calculation results, it shows that women tend to have a higher life expectancy than men in each province, and this gender difference is relatively stable from year to year. The average prediction of AHH based on gender in Indonesia shows an increase and decrease. This increase and decrease occur in every data used and also in every calculation tool used.

It can be concluded that in terms of the calculation tool used, the Lagrange polynomial interpolation method can be implemented to predict life expectancy in Indonesia because it has a Root Mean Squared Error with a value of 0.085875 or around 8.58%, which means it is included in the moderate category, which means the prediction results are included in the category which can be good [8]. And implementing Lagrange polynomial interpolation on an application in the form of a website can make it easier to carry out calculations automatically.

Acknowledgements

The author thanks the Indonesian Central Statistics Agency (BPS) for providing various data on Life Expectancy Rates in Indonesia which we can use as material for testing the use of the Lagrange Polynomial Interpolation method in predicting Life Expectancy Rates in Indonesia.

References

- [1] E. D. Sihaloho, "Pengaruh Belanja Kesehatan Terhadap Angka Harapan Hidup Kabupaten Kota Di Jawa Barat," *Ekspansi: Jurnal Ekonomi, Keuangan, Perbankan dan Akuntansi*, vol. 11, no. 1, p. 117, May 2019, doi: 10.35313/ekspansi.v11i1.1308.
- [2] World Health Organization, *Framework and standards for country health information systems*. 2008. [Online]. Available: <http://www.healthmetricsnetwork.org>

- [3] A. S. Rahma and R. I. Fajar, "Daftar Negara dengan Penduduk Paling Panjang Umur Menurut Data WHO, Indonesia Posisi Berapa?," *Geriatrici*. Accessed: Jun. 20, 2024. [Online]. Available: <https://www.geriatrici.id/artikel/2043/daftar-negara-dengan-penduduk-paling-panjang-umur-menurut-data-who-indonesia-posisi-berapa>
- [4] Jennifer. Niederst Robbins, *Learning Web design : a beginner's guide to HTML, CSS, JavaScript, and web graphics*. 2012.
- [5] M. Nina Adlini, A. Hanifa Dinda, S. Yulinda, O. Chotimah, and S. Julia Merliyana, "Metode Penelitian Kualitatif Studi Pustaka," 2022.
- [6] W. Rahmadani and S. C. Sihombing, "Analisis Penyebaran Virus Covid-19 di Provinsi Sumatera Selatan Menggunakan Metode Interpolasi Lagrange," *Jurnal Penelitian Fisika dan Terapannya (JUPITER)*, vol. 2, no. 1, p. 12, Jul. 2020, doi: 10.31851/jupiter.v2i1.5314.
- [7] T. Safitri, N. Dwidayati, and K. Kunci, "Perbandingan Peramalan Menggunakan Metode Exponential Smoothing Holt-Winters dan Arima," *Unnes Journal of Mathematics*, vol. 6, no. 1, pp. 48–58, 2017, [Online]. Available: <http://journal.unnes.ac.id/sju/index.php/ujm>
- [8] V. Hariadi, A. Saikhu, N. Zakiya, A. Y. Wijaya, and F. Baskoro, "Multivariate Time Series Forecasting Using Recurrent Neural Networks for Meteorological Data," *Conference SENATIK STT Adisutjipto Yogyakarta*, vol. 5, Nov. 2019, doi: 10.28989/senatik.v5i0.365.
- [9] S. Yuliyanti and Saripudin, "Implementasi Algoritma FG-Growth untuk Sistem Rekomendasi Penjualan Produk," *JUMANJI*, vol. 5, no. 1, pp. 41-51, 2021.
- [10] Y. D. Lestari, "Penerapan Data Mining Menggunakan Algoritma Fp-Tree Dan Fp-Growth Pada Data Transaksi Penjualan Obat," *Seminar Nasional Teknologi Informasi dan Komunikasi (SNASTIKOM)*, pp. 60-65, 2015.
- [11] A. X. A. Sim, "Pengenalan Desain dan Analisis Algoritma," 01 July 2013. [Online]. Available: <http://dev.bertzzie.com/knowledge/analisis-algoritma/PengenalanDesaindanAnalisisAlgoritma.html#algoritma-yang-baik>.

-
- [12] H. Aprillia, H. Yang and C. Huang, "Statistical load forecasting using optimal quantile regression random forest and risk assessment index," *IEEE Transactions on Smart Grid*, vol. 12, no. 2, pp. 1467-1480, 2020.
- [13] P. G. Arepalli and K. J. N. *, "Water contamination analysis in IoT enabled aquaculture using deep learning based AODEGRU," *Elsevier : Ecological Informatics*, vol. 2024, no. 12, pp. 1-16, 2024.
- [14] F. A. Pangruruk and S. P. Barus, "Comparison of Prediction of the Number of People Exposed to Covid 19 Using the Lagrange Interpolation Method with the Newton Gregory Maju Polynomial Interpolation Method," *Formosa Journal of Applied Sciences (FJAS)*, pp. 1405-1426, 2023.
- [15] D. Feng, Q. Han, L. Xu, F. Sohel, S. G. Hassan and S. L. a, "An ensembled method for predicting dissolved oxygen level in aquaculture environment," *Ecological Informatics*, vol. 80, no. 1, pp. 1-15, 2024.
- [16] H. A. A. a. V. M. Dewi, "Factors Affecting Life Expectancy in East Java: Predictions with A Bayesian Model Averaging Approach," *Jurnal Perencanaan The Indonesian Journal of Development Planning*, vol. V, no. 2, pp. 283-295, 2021.
- [17] Z. Ahmed and H. Le, "Linking Information Communication Technology, trade globalization index, and CO2 emissions: evidence from advanced panel techniques," *Environmental Science and Pollution Research*, vol. 28, no. 7, pp. 8770-8781, 2021.
- [18] A. Kurniadi, Kusriani and M. F. Sadikin, "Implementasi Convolutional Neural Network Untuk Klasifikasi Varietas Pada Citra Daun Sawi Menggunakan Keras," : *Journal of Computer and Information Technology* , vol. 4, no. 1, pp. 25-33, 2020.
- [19] Maulana, "Black Box Testing Adalah : Pengertian dan Contohnya," /TBox by Course-Net Indonesia, 20 Maret 2023. [Online]. Available: <https://itbox.id/blog/black-box-testing-adalah/>. [Accessed 4 Juli 2023].
- [20] E. Prakasa, B. Sugiarto, A. P. S. Utama and S. Yuliyanti, "Development of Real-time Handwashing Assessment using Video Analysis," in *IC3INA 2021: The 2021 International Conference on Computer, Control, Informatics and Its Applications*, New York, 2021.

- [21] H. Santoso, *Rekayasa Perangkat Lunak*, Medan: UINSU Medan, 2019.
- [22] D. T. Larose, *Discovering Knowledge in Data: An Introduction to Data Mining*, John Willey & Sons, Inc., 2014.

Evaluating The Performance of DWT-DCT Feature Extraction in Guitar Chord Recognition

Linggo Sumarno

*Department of Electrical Engineering, Faculty of Science and Technology,
Sanata Dharma University, Yogyakarta, Indonesia
lingsum@usd.ac.id*

(Received 07-10-2024; Revised 25-10-2024; Accepted 26-10-2024)

Abstract

This study presents advancements in audio signal processing techniques, specifically in enhancing the efficiency of guitar chord recognition. It is a continuation of the previous studies, which also aim at minimizing the feature extraction length with the intended performance. This study adopted two signal processing techniques that are common: Discrete Wavelet Transform (DWT) and Discrete Cosine Transform (DCT) for use in the feature extraction method. By conducting a systematic evaluation of two key parameters: frame blocking length and wavelet filter selection, a significant achievement could be achieved. The recognition system managed to obtain chord recognition with an accuracy of up to 91.43%, by using a feature extraction length of only three, which brought about smaller representation than the previous studies. The outcome of this study will help improve the data processing, which can be applied in real time, in this case in Field Programmable Gate Array (FPGA)-based chord recognition systems.

Keywords: chord recognition, Discrete Wavelet Transform, Discrete Cosine Transform, feature extraction

1 Introduction

The extraction of relevant information from the data is one of the crucial and critical processes in tasks like chord recognition. It is the transformation of raw information, usually a lot and difficult to work with, into a small number of useful features. These features encapsulate relevant information contained in the data and are useful in subsequent processes like classification and clustering. The feature extraction approaches



can be roughly separated into two types: spectral representation-based and non spectral representation-based.

The spectral representation-based feature extraction approach tries to represent the harmonic content of the musical data. One of the popular methods is the so-called Pitch Class Profile (PCP) [1], where it has the feature extraction length of 12, which represents the distribution of power across the pitches in a chord. Several improvements [2-4] have been developed to enhance the performance of this PCP further. However, the feature extraction length for these improvements is also 12.

On the other side, the non spectral representation-based approach tries to represent the spectral shape of the musical data. Thus, two examples of feature extraction methods based on this approach are Mel Frequency Cepstral Coefficients (MFCC) [5-6] and Discrete Sine Transform (DST-Wavelet) [7]. Recently, some studies on chord recognition in MFCC [6] and DST-Wavelet [7] showed effective recognition with a length of four in feature extraction. By using these feature extraction methods, the chord recognition system was able to achieve up to 92.14% and 92.86%, respectively.

Developments in the above chord recognition methods still leave scope for further optimization. Reducing the feature extraction length may further enhance data processing efficiency and make applications like chord recognition viable on FPGA systems [8-9]. This FPGA system will provide an added advantage of creating Application-Specific Integrated Circuits (ASICs) for electronic devices that can be customized and enabled for low power and performance.

This study introduces adopting DCT-DWT for feature extraction in a chord recognition, in order to further reduce the feature extraction length. This study particularly investigates the impact of evaluating two parameters—frame blocking length and wavelet filter selection—on attaining fewer than four feature extraction lengths while keeping the intended recognition accuracy.

2 Methodology

2.1 Recognition System Development

Fig. 1 depicts the chord recognition system built for this study, including a full block diagram of the system. It is necessary to point out that this system was implemented using Python software. The following subsections give an in-depth description of each block represented in Fig. 1.

Input and output. The input are isolated guitar chord recordings in WAV format. These recordings consist of seven major chords (C, D, E, F, G, A, B) and are sourced from a publicly available GitHub repository (<https://github.com/lingsum/Chord-DST-DWT>). The output indicates the corresponding chord text (C, D, E, F, G, A, or B) for each input signal.

Normalization. Normalization modifies the incoming signal data such that its peak value falls within a predetermined range, usually from 1 to -1. This modification must be made because the maximum loudness of recorded chord signals might vary greatly depending on recording conditions and how the musical equipment is used.

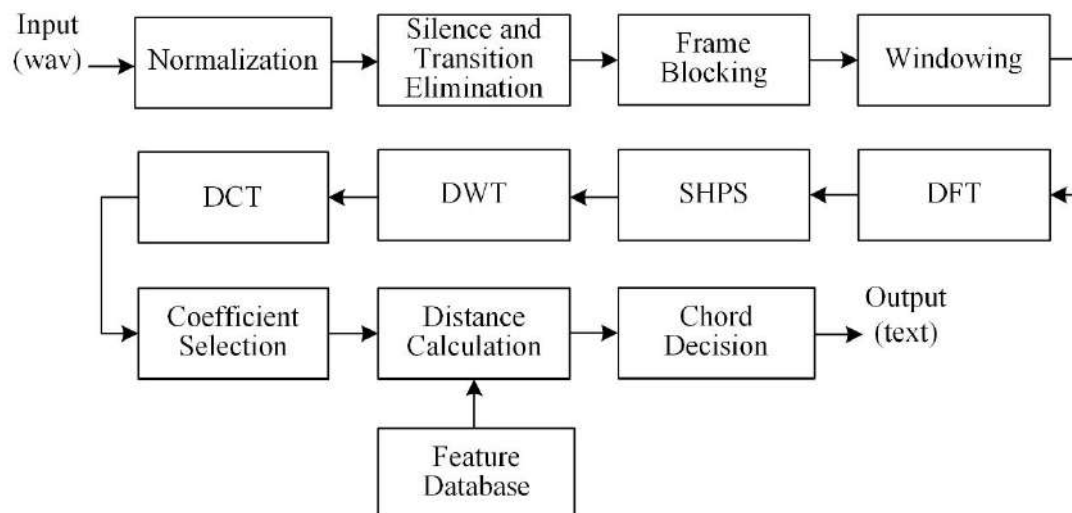


Figure 1. The developed recognition system.

Silence and transition elimination. Silence and transition elimination eliminates unnecessary portions from the signal data array. These eliminations are detailed in more depth below.

1. **Silence elimination:** A threshold of $|0.5|$ was set, identified through visual examination, in order to distinguish between silence and audible segments. Data points with absolute values below this threshold are eliminated during the left-to-right scan. The scanning stops once a data point with an absolute value meeting or exceeding the threshold is found.
2. **Transition elimination:** The initial time of 200 milliseconds of the signal was set, identified through visual examination, in order to distinguish between transition and steady state segments. By using this initial time, the initial 200 milliseconds of the signal are eliminated.

Frame blocking. Frame blocking entails segmenting a small array of signal data [10]. This segmentation is normally carried out on the left side of the signal data. The length of this small array, also known as the frame blocking length, has a major influence on the signal's resolution resulting from the Discrete Fourier Transform (DFT) step. Either too low or too high signal resolution could have a negative impact on feature extraction discriminating capabilities, resulting in decreased identification accuracy. This study explored frame blocking lengths of 128, 256, 512, 1024, and 2048.

Windowing. Windowing diminishes the impact of a signal data array's left and right edges. If these edges are not diminished, the signal data may exhibit spectral leakage resulting from the DFT step. This leakage introduces unimportant frequencies that do not relate the chord's actual frequencies. Windowing is used to help diminish spectral leakage. This study made use of the Hamming window, a popular window in signal processing [11].

DFT. The Discrete Fourier Transform (DFT) converts a finite array of signal data into a finite array of complex values in the frequency domain. This study made use of the magnitude of the signal data's complex values. Since, the magnitude sequence is symmetric, so only the left side of the data array will be used. As a note, this study used

Fast Fourier Transform (FFT) instead of DFT. This is because FFT computation is more efficient than DFT.

SHPS. The Simplified Harmonic Product Spectrum (SHPS) is useful for reducing harmonic distortion and noise in the frequency domain. SHPS could reduce the influence of non-harmonic noise by accentuating the fundamental frequency and its harmonics while decreasing non-harmonic components. Sumarno [12] offered this technique, which is a lite version of the Harmonic Product Spectrum (HPS) introduced by Noll [13].

DWT. The Discrete Wavelet Transform (DWT) transforms a signal into a number of scales and frequency bands. Fig. 2 shows the type of DWT employed in this study. The symbols L_0 and L_1 represent low-pass (LPF) and high-pass (HPF) filters, respectively, generated from the chosen wavelet filter. The $\downarrow 2$ notation indicates a down sampling factor of 2. The notation a_3 denotes the input to the DWT, while $a_0, d_0, \dots, d_{n-2},$ and d_{n-1} represent the resulting DWT coefficients at different scales and frequency bands. To maintain the signal length, periodization was applied during filtering. This study evaluated Haar, Daubechies (2-6), and Symlet (2-7) wavelet filters.

DCT. The Discrete Cosine Transform (DCT) compacts the signal's energy into a relatively small set of coefficients, a phenomenon known as energy compaction. This means that the lower-frequency components in the transformed data hold most of the important information about the signal. As a result, the DCT is especially effective for

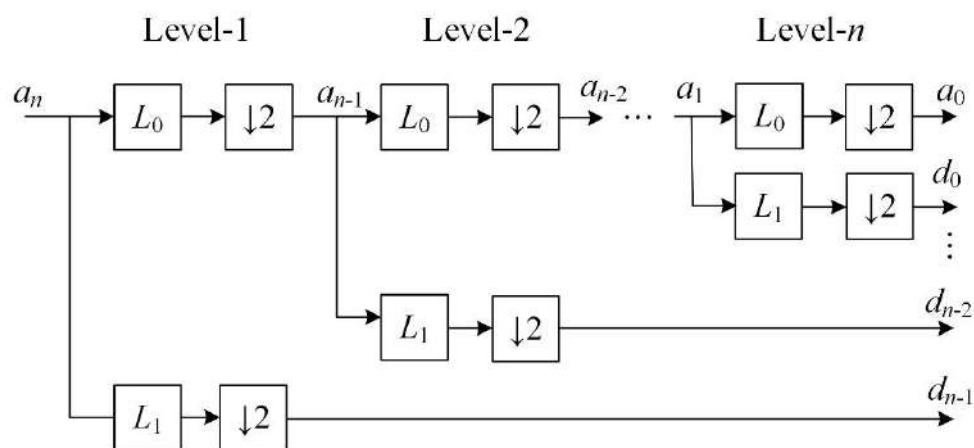


Figure 2. The type of DWT used in this study.

feature extraction, as these lower-frequency components typically carry the most discriminative information.

Coefficient Selection. Coefficient selection entails picking a subset of DCT coefficients to represent the feature extraction of the input signal. The selection process is conducted as follows.

1. Let the result of the previous DCT step be $C = \{c_0, c_1, \dots, c_{N-1}\}$ where N is the length of C .
2. Determine the number of coefficients to be selected, n , where $n \leq N - 1$.
3. The result of the coefficient selection is $S = \{c_1, c_2, \dots, c_n\}$

This study evaluated the number of coefficients to be selected (the feature extraction length) 1, 2, ..., and 6.

Distance Calculation and Feature Database. Distance calculation and feature database relate to a classification method that uses template matching techniques [14-16]. The feature database contains a collection of reference feature extraction of the chords used. Distance calculation in this study used the cosine distance function, which is derived from cosine similarity. This similarity is frequently used to calculate similarity scores [17-18]. The distance calculation produces seven distance values, which indicate the comparison between the feature extraction of the input signal data and the seven feature extraction references in the feature database.

Chord decision. Chord decision entails determining the chord that corresponds to the given input signal. The smallest distance value is chosen among the seven calculated distances. The chord corresponding to this smallest distance is then assigned as the output chord.

2.2 Training and Testing

The training procedure entailed creating a thorough feature database. Firstly, features were extracted from ten training samples for each chord using the Coefficient Selection step's output in Fig. 1. Secondly, the average of these features (from ten training samples) was then calculated. Finally, these average results (from each chord) were used as feature extraction references. The final feature database had seven feature extraction

references, one for each chord. For testing purposes, other 140 samples were utilized, with 20 samples for each chord.

3 Results and Analysis

3.1 Testing Results

Tables 1 and 2 show the study's testing findings. They were acquired by systematically evaluating two parameters: frame blocking length and wavelet filter selection. Details on the variations of these two parameters can be seen in the Methodology section above.

Table 1. Testing results using Symlet 6 wavelet filter.
Results shown: Recognition accuracy (%).

Frame blocking size	Feature set size					
	1	2	3	4	5	6
128	14.29	26.43	37.86	57.86	62.14	82.86
256	25.71	66.43	82.14	90.00	90.71	94.29
512	28.57	39.29	91.43	95.00	94.29	95.00
1024	27.14	79.29	81.43	82.86	87.14	87.14
2048	21.43	67.86	74.29	80.00	84.29	84.29

Table 2. Testing results using a frame blocking size 512.
Results shown: Recognition accuracy (%).

Wavelet filter	Feature set size					
	1	2	3	4	5	6
Haar	28.57	41.43	74.29	75.00	66.43	75.00
Daubechies 2	25.71	62.86	82.86	87.86	87.14	91.43
Daubechies 3	28.57	79.29	82.86	90.00	88.57	88.57
Daubechies 4	28.57	75.71	85.71	80.00	83.57	90.00
Daubechies 5	25.71	63.57	80.00	81.43	82.14	82.14
Daubechies 6	16.43	41.43	72.86	78.57	80.00	80.00

Symlet 2	25.71	62.86	82.86	87.86	87.14	91.43
Symlet 3	28.57	79.29	82.86	90.00	88.57	88.57
Symlet 4	28.57	40.00	91.43	90.71	94.29	95.71
Symlet 5	28.57	48.57	72.14	80.71	71.43	79.29
Symlet 6	28.57	39.29	91.43	95.00	94.29	95.00
Symlet 7	28.57	77.14	74.29	85.71	84.29	85.71

3.2 Discussions

Table 1 shows that recognition accuracy suffers from either too short or too long frame blocking lengths. A too-short frame blocking length cannot capture enough detail in the signal data from the DFT step, leading to a too-low resolution of the signal. On the contrary, a too-long frame blocking length captures too much detail, leading to a too-high resolution of the signal. Both too low or too high a resolution of the signal has a negative impact on the discrimination level of feature extraction, thereby reducing recognition accuracy.

Table 2 shows that choosing the proper wavelet filter can increase recognition accuracy. This improvement is due to the wavelet filter's ability to properly separate low-frequency and high-frequency components through its LPF and HPF in a multi-resolution domain. This proper separation enhances the discrimination level of feature extraction, leading to increased recognition accuracy.

Tables 1 and 2 show that generally, increasing the feature extraction length from 1 to 6 improves recognition accuracy. This suggests that up to a length of 6, the extracted features still capture the essential features. These essential features help in capturing the most important and discriminative characteristics from the input data, aiding in class separation [19]. In this study, increasing the number of essential features from 1 to 6 enhances the discrimination level of feature extraction, thereby increasing recognition accuracy.

Table 3 compares the performance between the introduced feature extraction method with the other previous methods. Table 3 shows the feature extraction method in this study is the most efficient for accuracy greater than 90%. With a feature extraction

Table 3. Performance comparison between the introduced feature extraction method with the other previous methods.

Feature Extraction Methods	Feature Extraction Length	Recognition Accuracy (%)	Chord Test Set Size
Improved PCP [2]	12	95.83	192
CRP Enhanced PCP [3]	12	99.96	4608
MFCC [5]	6	91.43	140
MFCC with Kaiser windowing [6]	4	92.14	140
DST-Wavelet [7]	4	92.86	140
DWT-DCT (this study)	3	91.43	140

Note: The table shows the shortest feature extraction length required to achieve more than 90% recognition accuracy

length of three, the recognition system is able to achieve a recognition accuracy of up to 91.43%.

Notes on FPGA Implementation

There are two notes on FPGA implementation related to this study. These notes are described as follow.

1. This study uses three kinds of transformation, namely DFT, DWT, and DCT. For FPGA implementation, in order to reduce the processing time, we can use some examples of efficient architectures [20-22] for these kinds of transformations.
2. The improved data processing in this study can be applied in real-time FPGA based system by utilizing hardware-software co-design, which exploit native parallelism of the FPGA hardware [23].

4 Conclusions and Future Studies

This study explored, in detail, the recognition accuracy of a novel feature extraction method that adopted DWT-DCT. The novel method was able to achieve a recognition accuracy of 91.43% with this particular feature extraction length of only three. Such

accuracy was achieved by using a frame blocking length of 512 and also by using the Symlet 4 and 6 wavelet filters. With this adoption of DWT-DCT in the feature extraction method, it is further ensured that the relevant and discriminative features of the guitar chords are well captured, leading to better recognition performances.

This study still leaves room for improvement in terms of accuracy and efficiency. Therefore, in future studies, the focus should be directed to exploring different methods for feature extraction. In this case, the methods are expected to provide recognition accuracy that exceeds 91.43%, and the length of feature extraction is three or less.

Acknowledgements

The Institute for Research and Community Services at Sanata Dharma University has supported this study.

References

- [1] T. Fujishima, "Realtime chord recognition of musical sound: a system using Common Lisp Music", *Proceeding of the International Computer Music Conference (ICMC)*, Beijing, pp. 464–467, 1999.
- [2] K. Ma, "Automatic Chord Recognition", Department of Computer Sciences, University of Wisconsin-Madison, May 2016. [Online]. Available : <http://pages.cs.wisc.edu/~kma/projects.html>. [Accessed Jul. 22, 2024].
- [3] P. Rajparkur, B. Girardeau, and T. Migimatsu, "A Supervised Approach to Musical Chord Recognition", *Stanford Undergraduate Research Journal*, Vol. 15, pp. 36-40, 2015.
- [4] E. Demirel, B. Bozkurt, and X. Serra, "Automatic chord-scale recognition using harmonic pitch class profiles", *Proc. Sound Music Comput. Conf.*, pp. 72–79, 2019.
- [5] L. Sumarno, "Chord Recognition using FFT Based Segment Averaging and Subsampling Feature Extraction," *Proceeding of 8th International Conference on Information and Communication Technology (ICoICT 2020)*, pp. 465–469. 2020.

-
- [6] L. Sumarno, “Guitar chord recognition using MFCC based feature extraction with Kaiser windowing”, *Proceeding of Transdisciplinary Symposium on Engineering and Technology (TSET 2022)*, Published 2024.
- [7] L. Sumarno, “The performance of DST-Wavelet feature extraction for guitar chord recognition”, *Proceeding of The 1st International Conference on Applied Sciences and Smart Technologies (InCASST 2023)*, Published 2024.
- [8] K. Vaca, M. M. Jefferies, and X. Yang, “An Open Audio Processing Platform with Zync FPGA”, *Proceeding of 22nd IEEE Int. Symp. Meas. Control Robot. Robot. Benefit Humanit. ISMCR 2019*, pp. D1-2-1–D1-2-6, 2019.
- [9] K. Vaca, A. Gajjar, and X. Yang, “Real-Time Automatic Music Transcription (AMT) with Zync FPGA”, *Proceeding of IEEE Comput. Soc. Annu. Symp. VLSI, ISVLSI, Vol. 2019-July (2019)*, pp. 378–384, 2019.
- [10] O.K. Hamid, “Frame Blocking and Windowing Speech Signal”, *J. Information, Commun. Intell. Syst.*, Vol. 4, No. 5, pp. 87–94, 2018.
- [11] H. Rakshit, and M. A. Ullah, “A comparative work on window functions for designing efficient FIR filter”, *Proceeding of 2014 9th Int. Forum Strateg. Technol. (IFOST 2014)*, pp. 91–96, 2014.
- [12] L. Sumarno, “Chord recognition using segment averaging feature extraction with simplified harmonic product spectrum and logarithmic scaling”, *Int. J. Electr. Eng. Informatics*, Vol. 10, No. 4, pp. 753–764, 2018.
- [13] A.M. Noll, “Pitch Determination of Human Speech by the Harmonic Product Spectrum, the Harmonic Sum Spectrum and a Maximum Likelihood Estimate”, *Proceeding of the Symposium on Computer Processing in Communications, Vol. 19, Polytechnic Press, Brooklyn, New York*, pp. 779-797, 1970.
- [14] I. Izonin, R. Tkachenko, N. Shakhovska, B. Ilchyshyn, and K.K. Singh, “A Two-Step Data Normalization Approach for Improving Classification Accuracy in the Medical Diagnosis Domain”, *Mathematics*, Vol. 10, No. 11, 2022
- [15] A.K. Jain, R.P.W. Duin, and J. Mao, “Statistical pattern recognition: A review”, *IEEE Trans. Pattern Anal. Mach. Intell.* Vol. 22, No. 1, pp. 4–37, 2000.

-
- [16] A. Massari, R.W. Clayton, and M. Kohler, "Damage detection by template matching of scattered waves", *Bull. Seismol. Soc. Am.* Vol. 108, No. 5, pp. 2556–2564, 2018.
- [17] H.U. Zhi-Qiang, Z. Jia-Qi, W. Xin, L.I.U. Zi-Wei, and L.I.U. Yong, "Improved algorithm of DTW in speech recognition", in *Proceeding of IOP Conf. Ser. Mater. Sci. Eng.*, Vol. 563, No. 5, 2019.
- [18] S. Sohangir, and D. Wang, "Improved sqrt-cosine similarity measurement", *J. Big Data*, Vol 4, No 1, 2017.
- [19] H.R. Shahdoosti, and F. Mirzapour, "Spectral–spatial feature extraction using orthogonal linear discriminant analysis for classification of hyperspectral data", *Eur. J. Remote Sens.*, Vol. 50, No. 1, 2017.
- [20] Y. Zhao, H. Lv, J. Li, and L. Zhu, "High performance and resource efficient FFT processor based on CORDIC algorithm", *EURASIP J. Adv. Signal Process*, Vol. 23, 2022.
- [21] M.A.M. Basiri, and P. Bharadwaja, "Efficient FPGA Implementations of Lifting based DWT using Partial Reconfiguration," *2023 36th International Conference on VLSI Design and 2023 22nd International Conference on Embedded Systems (VLSID)*, Hyderabad, India, pp. 319-324, 2023.
- [22] C.A. Kumar, G.R. Poornima, R. Aruna, B.P.P. Kumar, S. Harish, & D.A.L. Vaishnavi, "Implementation of an Efficient and Reconfigurable Architecture for DCT on FPGA", *International Journal of Intelligent Systems and Applications in Engineering*, Vol. 12, No. 10s, pp. 597–604, 2024.
- [23] I. Bravo-Munoz, J.L. Lazaro-Galilea, and A. Gardel-Vicente, "FPGA and SoC Devices Applied to New Trends in Image/Video and Signal Processing Fields", *Electronics*, Vol. 6, No. 25, 2017.

The Study of 3D Simulation on Heat Transfer Enhancement on Fin Tube Heat Exchanger Using Delta Wing and Winglet Vortex Generators

Stefan mardikus^{1,*}, Claudia Agata Putri¹ Michael Seen¹, Rines¹,
Y.B. Lukiyanto¹, Doddy Purwadianto¹, Heryoga Winarbawa¹,
Gilang Argya Dyaksa¹, Wibowo Kusbandono¹

¹*Faculty of Science and Technology, Sanata Dharma University,
Yogyakarta, 55598, Indonesia*

**Corresponding Author: stefan@usd.ac.id*

(Received 21-11-2024; Revised 28-11-2024; Accepted 29-11-2024)

Abstract

The vortex generator is one of the methods to improve heat transfer augmentation on flow characteristics in the air side of the fin and tube heat exchanger. There are some models of vortex generators to produce longitudinal vortices when the airflow passes the surface of the vortex generator. In the previous studies, the longitudinal vortices were able to reduce the wake region phenomenon behind the tube heat exchanger. This research aims to investigate the thermal performance of heat transfer on the collaboration between two models of vortex generators namely delta wing and winglet vortex generators on plate fin and tube heat exchanger. The simulation used four models (1) without the vortex generator (2) with the delta wing vortex generators (3) with delta winglet (4) with the combination of delta wing and winglet. The study was generated with computational fluid dynamics. The boundary conditions were set in the inlet as velocity and the outlet as pressure outlet. The airflow of velocity is represented by Reynolds numbers in the range of 4000 - 8000 with an interval of 500. The wall temperature of the tube is given at 400 Kelvin and the temperature of the airflow is given at 300 Kelvin. The epsilon model was used in the turbulence model of the simulation. The result explained that the thermal performance of heat transfer on delta winglets improved the airflow to induce longitudinal vortices and then reduced the wake region to improve the heat transfer coefficient more than other vortex generator models.

Keywords: Heat Transfer, Vortex Generator, Heat Exchanger



1 Introduction

Heat Exchanger is a device that can be used to transfer energy by heat between two or more types of fluid which has a different temperature [1]. Based on the construction a heat exchanger, has four types such as tubular, plate type, extended surface, and regenerator heat exchanger. Fin and tube heat exchangers are a heat exchanger of most common and can be applied in air conditioning, heating, cooling systems, refrigerators, radiators, and also the industry of petroleum and natural gas [2]. This type has a higher heat transfer coefficient and high-pressure capacity, thus; it is better than other types of heat exchangers. On the other side, the fin and tube heat exchanger have also an obstacle to the heat transfer process in the air side because there is a wake region behind the tube heat exchanger. The wake region occurred because the momentum of the fluid stream weakened and it was difficult to cause a heat transfer [3]. The wake region can reduce the pressure drop of the stream in the heat exchanger [4]. One of the solutions to reduce the wake region is with use of vortex generators. A vortex generator is an extended surface that can produce longitudinal vortices and reduce wake regions [5]. There are some types of vortex generators such as delta wing, rectangular wing, delta winglet, and rectangular winglet [3]. Liu et al. [6] have studied using a delta winglet vortex generator with the improvement of configuration to enhance heat transfer. It showed that the wake region dramatically reduces behind the tube and it was caused by the turbulent intensity around 27.8% to 67.5% based on using the without vortex generator. Garelli et al. [7] studied the effect of delta-wing vortex generators on radiators using a numerical study. They found that the overall heat transfer increased by 12% on a single delta wing between two plates in the heat exchanger. The investigation of vortex generators for delta wing and winglet types also has been studied by Hoards. Fiebig [8]. The result showed that the extended surface for the delta winglet type is superior to the delta wings in the overall heat transfer coefficient. The experiment about curved delta winglets on the effect of geometry was investigated to determine the thermal-hydraulic performance of fin and tube heat exchangers. Song et al. [9] tried to change winglet sizes, fin pitches, and tube pitches in 15 items on fin and tube configuration. The measurement of smaller and closer vortex

generators to the tube produced better thermal-hydraulic performance enhancement in the low Reynold numbers but larger vortex generators were more suitable for the high Reynold numbers. Around 15 mm x 20 mm with an angle of attack of 30° on delta winglet vortex generators has been studied by Kharge and Ghuge [10] on tube-in-tube heat exchangers, the results showed that the heat transfer performance augmented than other types of vortex generators. In the previous studies, there is no yet found study about the comparison of wing and winglet vortex generators in fin and tube heat exchangers. This study aims to investigate heat transfer performance on three model vortex generators such as types plain, wing, winglet, and a combination of wing and winglet vortex generators.

2 Model Description and Methods

In this study, the type of fin and tube heat exchanger is analyzed using computational fluid dynamics. The illustration of the fin and tube is shown in Fig. 1. There are six tubes in one line fin as in Fig. 2. The Diameter of the tube is 19 mm and the distance between one tube and another tube is 60 mm. The domain of this simulation is created in Fig. 3, with the length of the fin of 500 mm and a width of 165 mm. In Fig. 4, Four models of vortex generator (VGs) are applied such as (1) Model fin and tube heat exchanger without, (2) with wing VGs, (3) with winglet VGs, (4) a combination between wing and winglet VGs. This simulation used the variation of Reynold Numbers starting from 4000 until 8000 with intervals of 500. In the inlet domain, the fluid of air was chosen as the working fluid which has a temperature of 273 K, the heat generation in this study is established as the temperature on the wall of the tube which was 400 K. The turbulence model of this study used the k-epsilon model and the material of the tube was copper. For the boundary condition, the inlet was defined by velocity inlet, the outlet was defined by pressure outlet and the symmetry was established on four sides on right, left, top, and bottom. The solution method of this simulation used a scheme of SIMPLE with pressure as second order, momentum, and energy as second-order upwind.

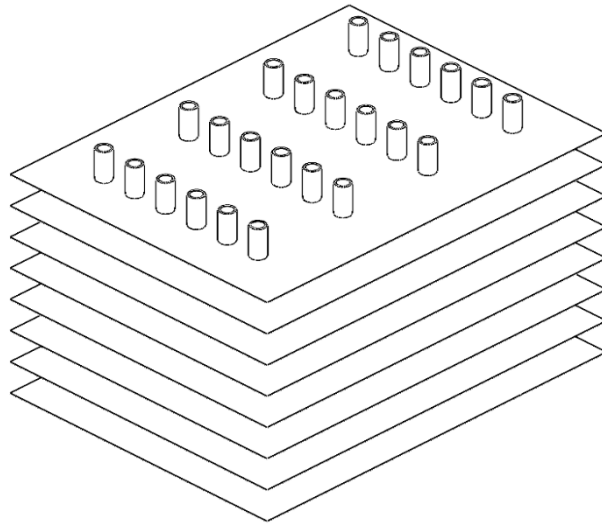


Figure 1. The Illustration of fin and tube heat exchanger without vortex generators.

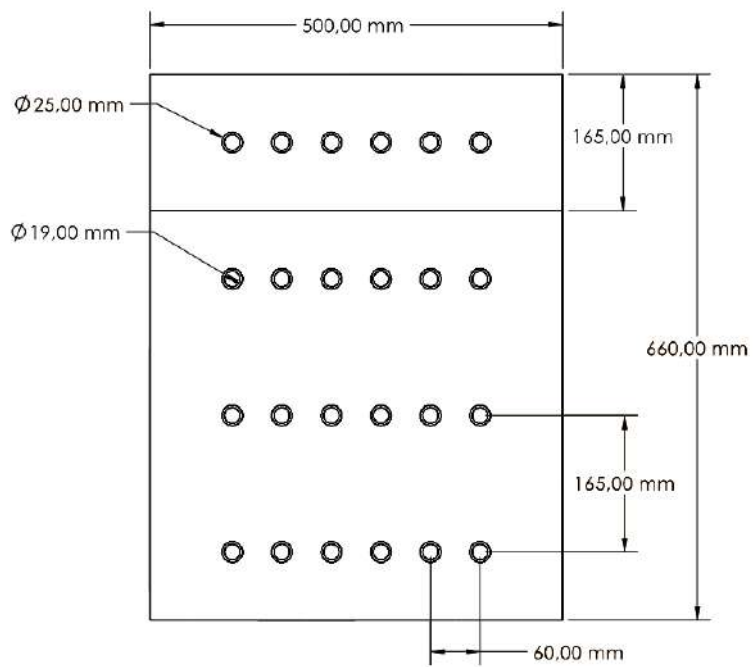


Figure 2. The Geometry Schematic of fin and tube heat exchanger.

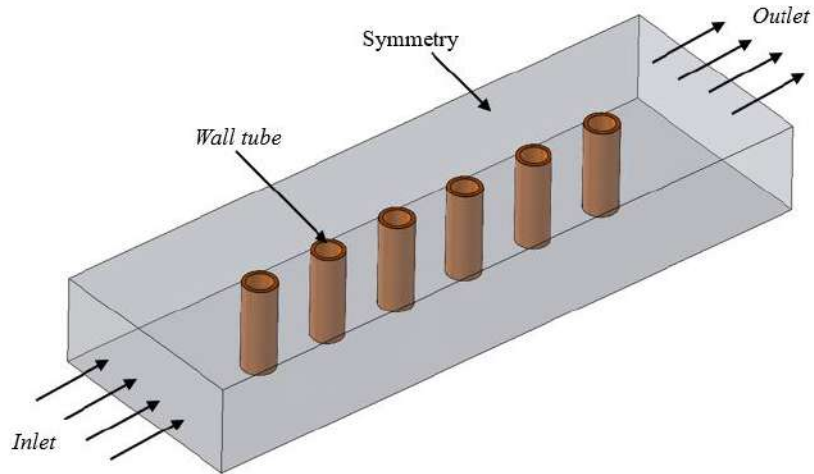


Figure 3. The computational domains for this study on fin and tube heat exchangers.

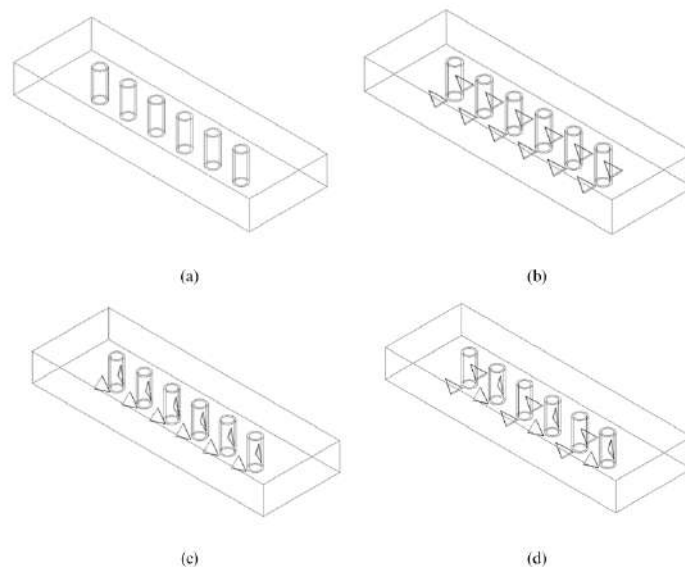


Figure 4. schematic of simulation domain of fin and tube heat exchanger for some models, (a) without VG, (b) Delta wing, (c) Delta Winglet, (d) Combination VG of Wing and Winglet.

3 Results and Discussions

This study uses the Nusselt number to represent heat transfer performance. Fig. 5 shows the simulation results, indicating an increase in the Nusselt number with each rise in the Reynolds number. The increase in Reynolds number enhances the Nusselt number depending on the case variation. [4]. This increase occurs due to the presence of a vortex generator, which can create longitudinal vortices that disrupt the main flow, reduce the wake region, and improve heat transfer. [4]. Fig. 5 demonstrates that the use of a vortex generator can enhance heat transfer performance.

The variation of the Reynolds number from 4000 to 8000, with intervals of 500, produced an average Nusselt number increase of 6.042% - 6.744% for the delta wing vortex generator, 8.450% - 12.075% for the delta winglet vortex generator, and 6.621% - 8.170% for the combination of delta wing and winglet vortex generators compared to the baseline. The overall average increase in Nusselt number for Reynolds numbers from 4000 to 8000, at 500 intervals compared to the baseline, was 6.249% for the delta wing vortex generator, 10.042% for the delta winglet vortex generator, and 6.594% for the combined delta wing and winglet vortex generator. The delta winglet vortex generator achieved higher Nusselt number values compared to both the delta wing vortex generator and the combined delta wing and winglet vortex generator. Therefore, it can be concluded that the delta winglet vortex generator enhances heat transfer more effectively, as it creates strong longitudinal vortices. [11].

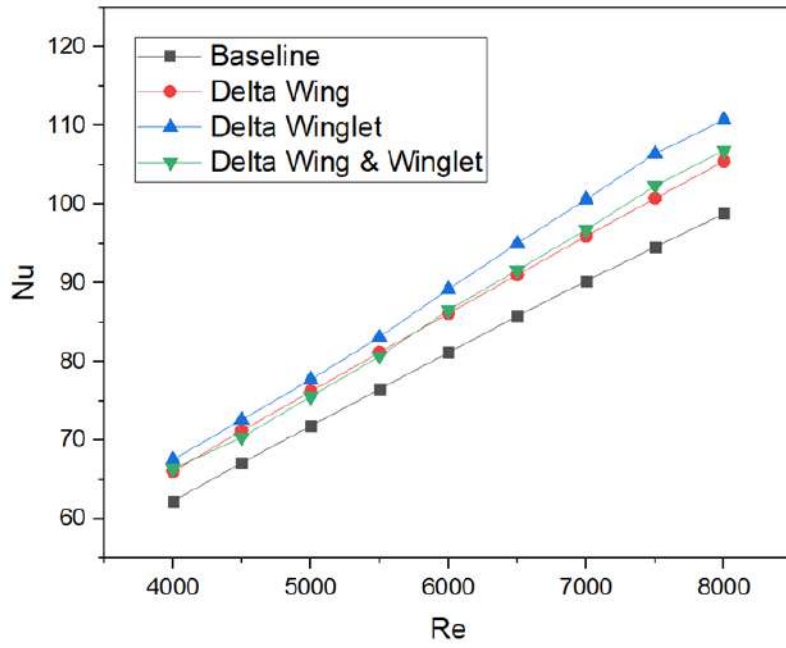


Figure 5. The effect of Nu (Nusselt Number) vs Reynold number (Re)

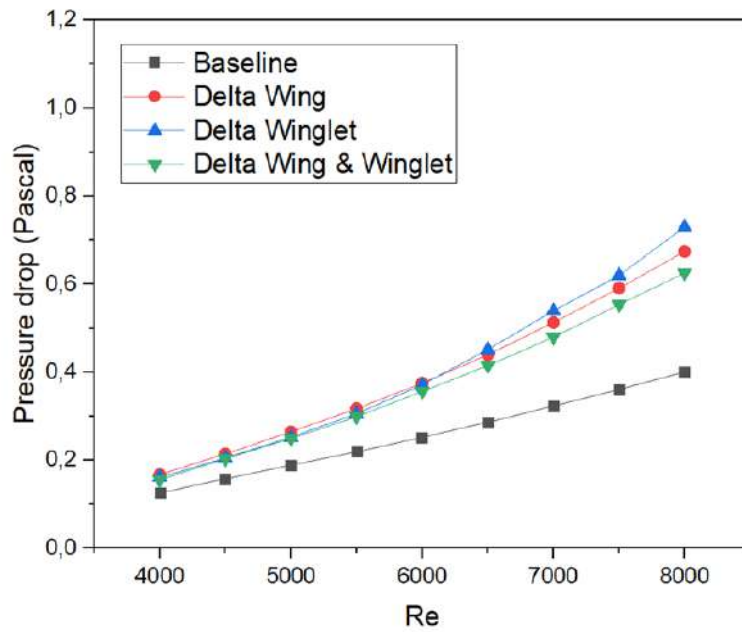


Figure 6. Effect of pressure drop vs Reynold's number

Fig. 6 shows that an increase in the Reynolds number leads to a rise in the pressure drop. This increase occurs because a higher Reynolds number enhances the frictional force between the fluid and the surface of the vortex generator, resulting in a higher pressure drop. [3]. The use of a vortex generator can improve heat transfer performance and also increase the pressure drop value. [11].

The average results from Fig. 6 show an increase in pressure drop for vortex generators with Reynolds number variations from 4000 to 8000, at intervals of 500, with increases of 33.55% - 68.32% for the delta wing vortex generator, 28.22% - 143.59% for the delta winglet vortex generator, and 24.34% - 56.18% for the combination of delta wing and winglet vortex generators, compared to the baseline. The overall average pressure drop increase from using vortex generators was 49.63% for the delta wing vortex generator, 65.04% for the delta winglet vortex generator, and 40.62% for the combined delta wing and winglet vortex generator, compared to the baseline. Therefore, it can be concluded that the delta winglet vortex generator produces the highest average pressure drop. This increase in pressure drop is caused by the resistance from fluid flow impacting the walls of the delta winglet vortex generator, and the larger surface area of the delta winglet vortex generator results in a higher pressure drop value. [12].

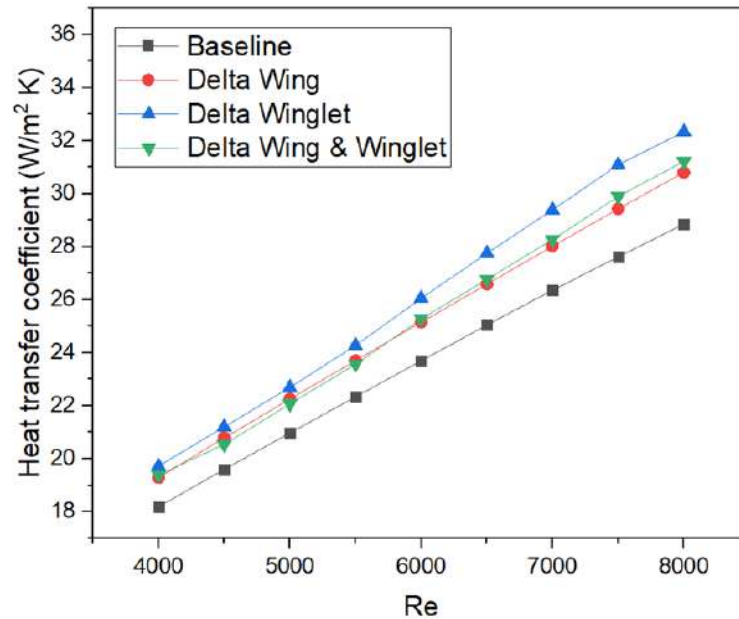


Figure 7. Effect of heat transfer coefficient vs Reynolds number with difference of vortex generator

Fig. 7 shows that using a vortex generator can enhance the heat transfer coefficient as the Reynolds number increases. A higher Reynolds number improves heat transfer performance due to increased turbulence intensity and flow vorticity. [12]. Fig.7 illustrates the rise in the heat transfer coefficient for vortex generators with Reynolds number variations from 4000 to 8000 at 500 intervals, resulting in increases of 6.04%, 6.09%, 6.11%, 6.10%, 6.15%, 6.12%, 6.31%, 6.57%, and 6.74% for the delta wing vortex generator; 8.45%, 8.18%, 8.20%, 8.69%, 9.92%, 10.79%, 11.51%, 12.57%, and 12.07% for the delta winglet vortex generator; and 6.62%, 4.83%, 5.23%, 5.48%, 6.68%, 6.84%, 7.24%, 8.25%, and 8.17% for the combined delta wing and winglet vortex generator, compared to the baseline. The overall average increase in the heat transfer coefficient for Reynolds numbers from 4000 to 8000 at 500 intervals was 6.25% for the delta wing vortex generator, 10.04% for the delta winglet vortex generator, and 6.59% for the combined delta wing and winglet vortex generator, compared to the baseline.

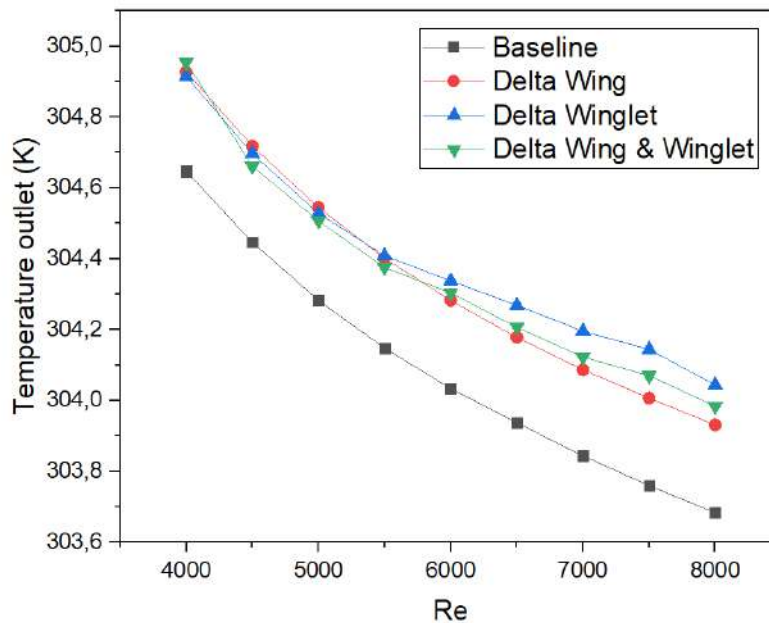


Figure 8. Temperature outlet distribution vs Reynold number with the difference of vortex generator.

The graph in Fig. 8 shows that with each increase in the Reynolds number, the outlet temperature decreases. It can be seen that the outlet temperature for Re 4000 with the delta wing vortex generator decreases by -0.33% compared to the outlet temperature at Re 8000. Similarly, the delta winglet vortex generator shows a temperature reduction of -0.29% from Re 4000 to Re 8000, and the combination of delta wing and winglet vortex generators also exhibits a temperature decrease of -0.32% from Re 4000 to Re 8000. The decrease in outlet temperature with higher Reynolds numbers is due to the high flow velocity, which limits effective heat absorption. Fig.8 also clearly shows that the use of vortex generators results in a higher outlet temperature than the baseline, due to the extensive contact of the fluid flow with the vortex generator surfaces, creating longitudinal vortices that enhance heat transfer performance. [4].

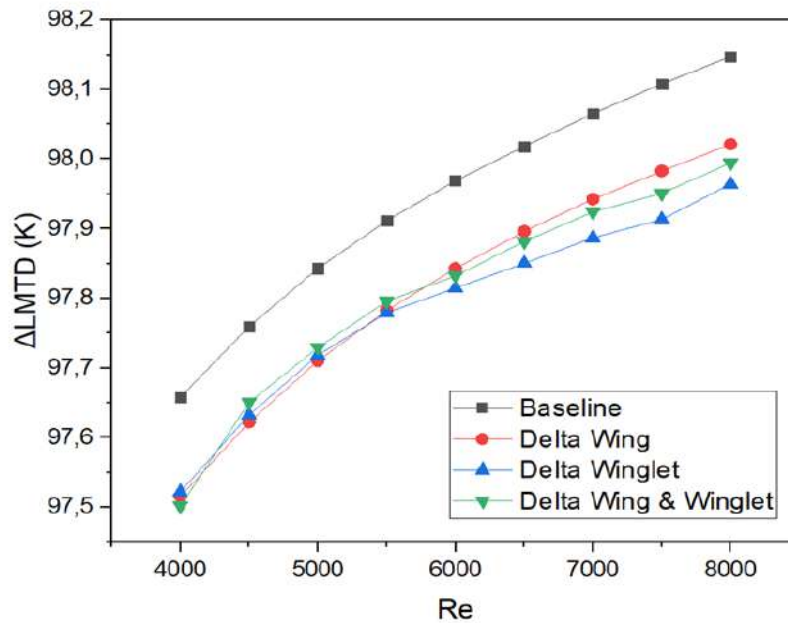


Figure 9. Effect of log mean temperature difference vs Reynold number with the difference of vortex generator

Fig. 9 shows that as the Reynolds number increases, the value of the logarithmic mean temperature difference (LMTD) also rises. This increase in LMTD indicates a greater amount of heat transfer, as the LMTD represents the average logarithmic difference between hot and cold temperatures at the outlet. [13]. The average increase in LMTD values for vortex generators from Re 4000 to Re 4500 up to Re 8000, at intervals of 500, is 0.11%, 0.20%, 0.27%, 0.34%, 0.39%, 0.44%, 0.48%, and 0.52% for the delta wing vortex generator; 0.11%, 0.20%, 0.26%, 0.30%, 0.34%, 0.37%, 0.40%, and 0.45% for the delta winglet vortex generator; and 0.15%, 0.23%, 0.30%, 0.34%, 0.39%, 0.43%, 0.46%, and 0.51% for the combination of delta wing and winglet.

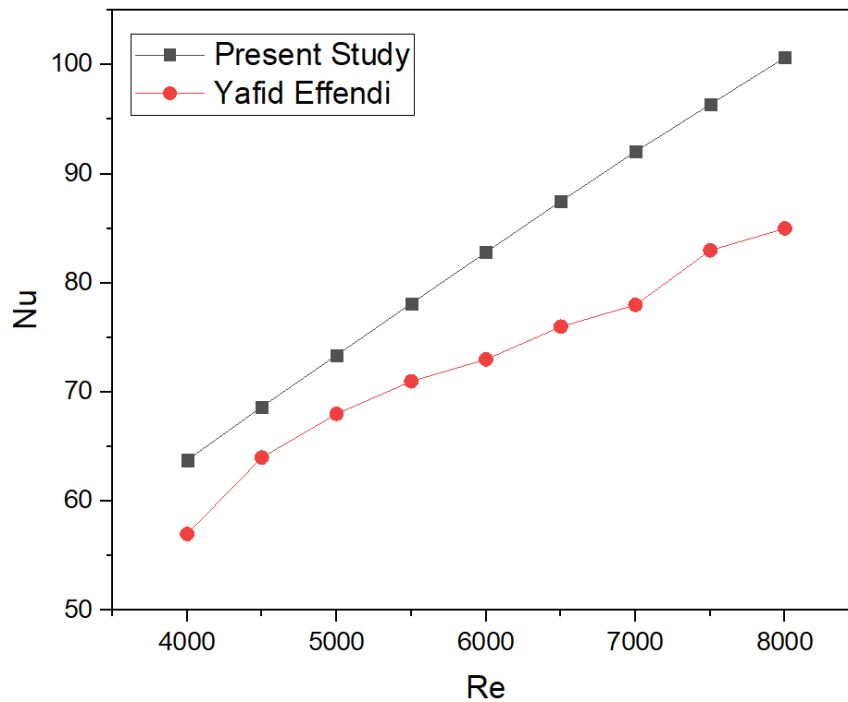


Figure 10. Comparison study for a correlation between Nusselt number vs Reynold number

In Fig. 10, the experiment conducted by Yafid Effendi will be used to validate the current study [12], ensuring the accuracy of the generated data. Validation will use the Nusselt number, as it is a dimensionless unit, along with a plain fin and tube heat exchanger and Reynolds numbers ranging from 4000 to 8000 in intervals of 500. Figure 4.34 shows a percentage difference of 13.14% between Yafid Efendi's study and the current study, likely due to methodological differences. Yafid Efendi's study used an experimental approach, while the current study employs a simulation method.

4 Conclusions

This study aims to improve the heat transfer performance of heat exchangers through additional vortex generators such as plain, wing, winglet, and a combination of

wing and winglet vortex generators, which can be drawn from this paper. The summary of this study is as follows;

1. The use of a vortex generator as a principle can improve the heat transfer coefficient and Nusselt number by around 12% compared to without a vortex generator. For delta winglets, it can augment better than a delta winglet vortex generator.
2. The phenomenon of fluid flow, which affected the wake region behind the tube, was seen by pressure drop. The higher the pressure drop value, the more the primary fluid was mixed with the secondary fluid, which enhanced the heat transfer process.

References

- [1] T. Kuppan, *Heat Exchanger Design*. 2000.
- [2] C. Xie *et al.*, “Flow and heat transfer optimization of a fin-tube heat exchanger with vortex generators using Response Surface Methodology and Artificial Neural Network,” *Case Stud. Therm. Eng.*, vol. 39, no. September, p. 102445, 2022, doi: 10.1016/j.csite.2022.102445.
- [3] Syaiful, H. Nabilah, M. S. K. T. Suryo Utomo, A. Suprihanto, and M. F. Soetanto, “Numerical simulation of heat transfer enhancement from tubes surface to airflow using concave delta winglet vortex generators,” *Results Eng.*, vol. 16, no. August, p. 100710, 2022, doi: 10.1016/j.rineng.2022.100710.
- [4] P. Saini, A. Dhar, and S. Powar, “International Journal of Heat and Mass Transfer Performance enhancement of fin and tube heat exchanger employing curved trapezoidal winglet vortex generator with circular punched holes,” *Int. J. Heat Mass Transf.*, vol. 209, p. 124142, 2023, doi: 10.1016/j.ijheatmasstransfer.2023.124142.
- [5] J. Xie and H. M. Lee, “Flow and heat transfer performances of directly printed curved-rectangular vortex generators in a compact fin-tube heat exchanger,” *Appl. Therm. Eng.*, vol. 180, p. 115830, 2020, doi: 10.1016/j.applthermaleng.2020.115830.

-
- [6] Y. Liu, X. Ma, X. Ye, Y. Chen, Y. Cheng, and Z. Lan, "Heat transfer enhancement of annular finned tube exchanger using vortex generators : The effect of oriented functional circumferential arrangement," *Therm. Sci. Eng. Prog.*, vol. 10, no. April 2018, pp. 27–35, 2019, doi 10.1016/j.tsep.2018.12.010.
- [7] L. Garelli, G. Ríos Rodriguez, J. J. Dorella, and M. A. Storti, "Heat transfer enhancement in panel type radiators using delta-wing vortex generators," *Int. J. Therm. Sci.*, vol. 137, no. October 2018, pp. 64–74, 2019, doi 10.1016/j.ijthermalsci.2018.10.037.
- [8] M. Fiebig, A. Valencia, and N. K. Mitra, "Wing-type vortex generators for fin-and-tube heat exchangers," *Exp. Therm. Fluid Sci.*, vol. 7, no. 4, pp. 287–295, 1993, doi: 10.1016/0894-1777(93)90052-K.
- [9] K. W. Song, Z. P. Xi, M. Su, L. C. Wang, X. Wu, and L. B. Wang, "Effect of geometric size of curved delta winglet vortex generators and tube pitch on heat transfer characteristics of the fin-tube heat exchanger," *Exp. Therm. Fluid Sci.*, vol. 82, pp. 8–18, 2017, doi: 10.1016/j.expthermflusci.2016.11.002.
- [10] S. B. Kharge, N. C. Ghuge, and V. S. Daund, "Experimentation using delta winglet type vortex generator attached on tube surface of the tube in tube heat exchanger for heat transfer augmentation," *Int. J. Curr. Eng. Technol.*, vol. 5, no. 5, pp. 398–402, 2016, doi: 10.14741/ijcet/22774106/spl.5.6.2016.74.
- [11] M. J. Li, W. J. Zhou, J. F. Zhang, J. F. Fan, Y. L. He, and W. Q. Tao, "Heat transfer and pressure performance of a plain fin with radiantly arranged winglets around each tube in fin-and-tube heat transfer surface," *Int. J. Heat Mass Transf.*, vol. 70, pp. 734–744, 2014, doi: 10.1016/j.ijheatmasstransfer.2013.11.024.
- [12] Y. Effendi, A. Prayogo, Syaiful, M. Djaeni, and E. Yohana, "Effect of perforated concave delta winglet vortex generators on heat transfer and flow resistance through the heated tubes in the channel," *Exp. Heat Transf.*, vol. 35, no. 5, pp. 553–576, 2022, doi: 10.1080/08916152.2021.1919245.
- [13] Azwinur and Zulkifli, "Kaji Eksperimental Pengaruh Baffle Pada Alat," *SINTEK J. J. Ilm. Tek. Mesin*, vol. 13, no. 1, pp. 8–14, 2019.

AUTHOR GUIDELINES

Author guidelines are available at the journal website:
<http://e-journal.usd.ac.id/index.php/IJASST/about/submissions#authorGuidelines>

This page intentionally left blank